MODELLING OF KNITTED FABRIC DEFORMATION

ANDREY U. LOGINOV

Ph.D. 2000

MODELLING OF KNITTED FABRIC DEFORMATION

By

Andrey U. Loginov

The thesis submitted in partial fulfilment of the requirements for the degree of Doctor of Philosophy

De Montfort University

December, 2000

MODELLING OF KNITTED FABRIC DEFORMATION

Contents

List of Figures

Abstract

The objective of this study was to investigate new models for the mechanical behaviour of knitted fabrics in quasi-static deformation from an initially relaxed state to the extended state. In order to do so a mechanism for plain knitted structure deformation in plane was proposed, implemented and tested on a range of real samples. The problem of extension of a knitted structure is complicated by the combination of non-linear properties derived from both the characteristics of the knitted structure and the properties of the yarn. To obtain a solution to this problem a finite-element technique was used to evaluate the proposed model.

The proposed model of mechanical behaviour of knitted fabrics is an analogue of the thin membrane problem in mechanics. The model developed is applicable to a wide range of mechanical problems where it is possible to assume that fabric is a thin membrane with zero bending rigidity.

To facilitate the mechanical properties of the proposed model, standard dimensional parameters of fabric and yarn combined with the mechanical properties have been used.

With the purpose of obtaining important yarn characteristics for the subsequent evaluation of the model, an advanced analysis of the yarn path in plain knitted fabric was performed. An algorithm for loop geometry from the given fabric dimensions in course and wale directions and yarn properties were developed.

In order to implement the algorithms developed during this investigation complex software was written. This software allows simulation of the mechanical behaviour of different plain knitted structures under various loading and boundary conditions.

At the approval stage of the model, a number of fabric samples were produced and tested; models of real samples have been simulated and compared with experimental data.

The model used could be developed further to extend the application to tackle complex 3D deformation and to simulate a range of different knitted structures.

Acknowledgements

I am very grateful to the following people for their help and advice during this work:

At De Montfort University:

Prof. R.J. Harwood, for providing an opportunity to study at De Montfort University and support throughout this work;

Dr. S.A. Grishanov, for his supervision, and discussions.

The special thanks to all security officers, who support me at *out of hours* time at De Montfort.

At Unilever Research Laboratory:
For kind permission to accomplish experimental work on KES-F Bending Tester, and for help throughout experiment.

At St. Petersburg State University of Technology and Design:
Prof. N.N. Truevtsev, for support and advice.
Dr. S.V.Lomov, for useful discussions, help and inspiration.
Dr. E.B. Belov, for his kind help and participation in experimental work on measurement of yarn torsion rigidity, helpful discussions on various subjects.

At St. Petersburg Technical University:
Dr. E.I. Mansirev for his supervision, useful discussions on various subjects related to this work.

My deepest gratitude for my wife and son for their love and patience.

Nomenclature

- To simplify formulation and arguments the following denotations are accepted further.

$t=[n1:n2]$ $\Leftrightarrow$ Variable t attains an integer values from $n1$ to $n2$ continuously.
$t=\{n1,...,n2\}$ $\Leftrightarrow$ Variable t attains whole numbers from $n1$ to $n2$.
$\underline{A}$ $\Leftrightarrow$ Vector A.
$\{A\}$ or $\{A_i\}$ $\Leftrightarrow$ Row of components of vector A.
$\underline{\underline{B}}$ $\Leftrightarrow$ Second-order tensor B.
$\{B\}$ or $\{B_{i,j}\}$ $\Leftrightarrow$ Matrix of components of tensor B.
The following operands are accepted:
$\underline{a}\cdot\underline{b}$ $\Leftrightarrow$ Scalar product of two vectors $\underline{a}$ and $\underline{b}$.
$\underline{a}\times\underline{b}$ $\Leftrightarrow$ Vector product of two vectors $\underline{a}$ and $\underline{b}$.
Δa $\Leftrightarrow$ Increment in a.
$\dim(\underline{a})$ $\Leftrightarrow$ Dimension of vector $\underline{a}$.

$\frac{\partial}{\partial \underline{a}}=\sum_{i=1}^{\dim(a)}\frac{\partial}{\partial a_i}\underline{e_i}$ $\Leftrightarrow$ Gradient operand.

- The most of dimensional values are expressed in SI system where main units are:

$[N]$: Newton.
$[m]$: Meter.
$[s]$: Second.

- The list of other dimensional units is represented below:

[mm] : Millimetre.
[tex] : Tex.
[cm] centimetre.

CHAPTER 1. Introduction

1.1 General

The work presented here is primarily concentrated on the application of an advanced structural analysis methods to the tensile behaviour of fabrics. This is an important property of fabric and consequently one of principle theoretical problems in textile mechanics. The importance of the problem is reflected in the large amount of work published on this subject over the years.

The tensile properties of woven fabrics, together with other mechanical properties such as behaviour in bending and shear, are of considerable importance in determining how the fabric will perform in use. The applications of woven fabrics vary widely. In apparel end-uses, the tensile strains that are likely to be encountered in normal wear will usually be relatively small, but in some industrial applications, the strains involved may be quite large.

The tensile properties of fabrics are determined, among other things by the tensile and bending behaviour of the yarns composing the fabric. Taking into account that the yarn bending rigidity is normally quite small in comparison with yarn tensile rigidity it is possible to consider yarn bending and tension separately. It is usually assumed that the constitutive equations for tensile and bending modes of yarn deformation are uncoupled even for the large yarn displacement [21].

Any theoretical analysis of the tensile behaviour of fabric requires a starting point, *i.e.* a model of the unstrained fabric. The models usually used are those provided by Peirce [55]. Both models suggested by Peirce assumed that the cross-sections of the yarn in the fabric are circular. The first model also assumed that the yarns are flexible, *i.e.* their bending rigidity is zero. This leads to the model in which the yarn path is composed of circular arcs and straight lines.

The assumption of circular yarn cross-sections in the fabric is, of course, quite unrealistic since yarns are easily compressible by lateral forces imposed on them at the points of yarn interaction. This assumption cannot be used for the fabric subjected to

tensile load as the compression forces increase dramatically in the tensed fabric and that leads to considerable displacements arising from the mutual compression of yarns.

Konopasek [20] has classified the textile structures as it is shown in Table 1.1. The field of the present research is represented in the boxes 2.2 and 3.2. If the fabric is assumed to behave as a continuum, the problems in boxes 2.2, 3.2 and 3.3 are represented in the general case by sets of unmanageable non-linear partial differential equations as opposed to other problems represented in Table 1.1, where the problem may be formulated in terms of a set of ordinary differential equations, which may be solved by standard numerical procedures.

Table 1.1

<table>
<tr><td colspan="3">Number of independent geom. variables</td><td colspan="2" rowspan="2"></td></tr>
<tr><td>1</td><td>2</td><td>3</td></tr>
<tr><td rowspan="3">1.1
Tensile or torsion deformation of fibres and yarns.</td><td rowspan="2">2.1
In plane deformations of fibres and yarns.</td><td>3.1
Bending and torsion deformations of fibres and yarns in the 3D space.</td><td>3</td><td rowspan="4">Number of independent geom. variables</td></tr>
<tr><td rowspan="2">2.2
In plane tensile and shear deformations of sheets (fabrics).</td><td>3.2
Tensile, shear and bending deformations of sheets (fabrics) in 3D space</td><td>2</td></tr>
<tr><td>3.3
Complex deformations of fibres and fibre assemblies in 3D space</td><td>3</td></tr>
</table>

The present research is aimed at formulating the mechanical problems 2.2, 3.2 and 3.3 in Table 1.1 as a pseudo-continuum problem. Namely, the aim is to define the mechanical properties of continuum that would be equivalent to a discrete structure. To illustrate these we consider a simple problem of tensioning of a system of initially straight yarns as shown in Figure 1.1. Here the yarn direction is parallel to the load direction and the yarn's ends are clamped.

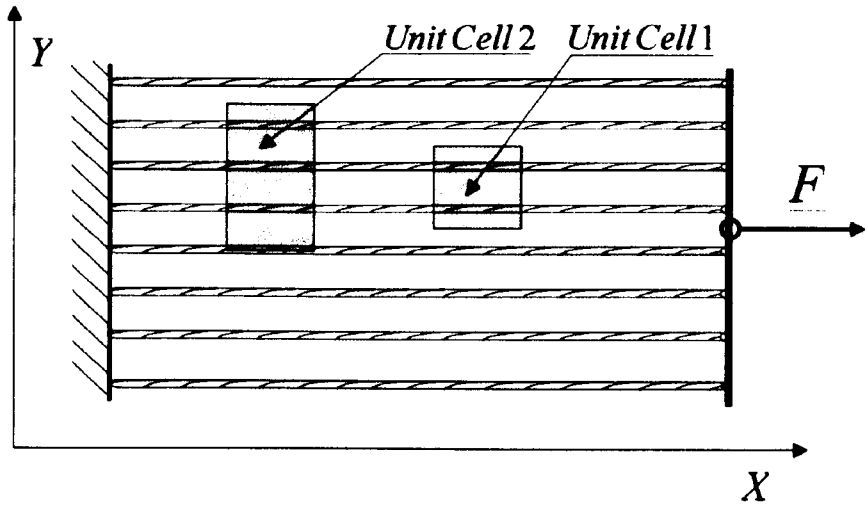

Figure 1.1 ***Extension of the system of straight yarns.***

Extension of eight yarns ($N_{yarns}^{sample}=8$) by the force F in the OX direction is represented in Figure 1.1. The *unit cell 1* in Figure 1.1 consists of two yarns ($N_{yarns}^{cell}=2$) and, hence, the stress-strain relationship for this cell can be expressed as:

$$f_{cell}=2D_{yarn}\,\varepsilon_{cell}$$

where $f_{cell}=F\dfrac{N_{yarns}^{cell}}{N_{yarns}^{sample}}$ is tensile force acting at the unit cell;

ε_{cell} is relative deformation of the unit cell;

D_{yarn} is rigidity modulus of a single yarn.

The *unit cell 2* in Figure 1.1 consists of approximately three and a half yarns and hence the stress-strain relationship for this cell can be expressed as:

$$f_{cell}=3.5D_{yarn}\,\varepsilon_{cell}\,.$$

Although the physical sense of the unit cell containing a fractional number of yarns is not clear, it is formally possible to define a unit cell of any size. That makes it possible to formulate the continuum mechanical problem (2.2, 3.2 and 3.3 in Table) in the terms of ordinary differential equations. This in turn enables the solution to be simplified, and discrete properties of structure to be considered.

The classification of the mechanical problems according to the type of fabric deformation was represented by Lloyd [21]. These types are briefly represented in Table 1.2 in order of increasing complexity of the problem.

Table 1.2

N	Types of deformation	Description
1.	*Planar deformation*	An initially flat sheet is deformed in its own plane. The strains developed in the plain of the sheet are known as membrane strains.
2.	*Tension membranes*	Transverse displacements occur, but the fabric has negligible bending rigidity, and the boundary conditions are such that the fabric is every-where in tension.
3.	*Plate and shell deformation*	A fabric with significant bending rigidity which is subjected to complex (incl. transverse) displacements.
4.	*Buckling deformation*	Buckling of fabric due to the non-linear properties of system.
5.	*Post-buckling deformation*	After buckling occurred the problem transformed into shell-type problem. Pre-tensed condition of that shall adds to the complexity of the problem.

According to the classification represented in Table 1.2 the area of the present research is limited by the first and the second type of fabric deformation. Although the model developed is probably applicable to consider buckling and post-buckling behaviour, these types of deformation are not considered.

The main emphasis of the present research is made on defining the mechanical properties of knitted structures from the mechanical properties of constituent yarns and the structure geometry. To validate the model proposed the planar deformation of knitted structure was considered.

The ultimate goal of this work is to be able to predict behaviour of *knitted* fabric theoretically, when yarn properties and dimension properties of manufactured fabric are given. This is not a single task but a series of inter-connected problems, of which the main ones are:

- prediction of fabric advanced structural-geometric properties based on fabric parameters and yarn properties;
- modelling the fabric deformation mechanism, *i.e.* prediction of mechanical properties of an elementary cell, prediction of the mechanical properties of a system of elementary cells restricted by boundary conditions;

- numerical evaluation of the model developed against experimental data.

Fabric is a structure, consists of perhaps many thousands of yarns with a consequent vast number of mutual contact points Figure 1.2 (c). Each yarn, in turn, is normally a collection of a filaments or fibres Figure 1.2 (b). Each filament or fibre is a 3D body with a complex shape Figure 1.2 (a).

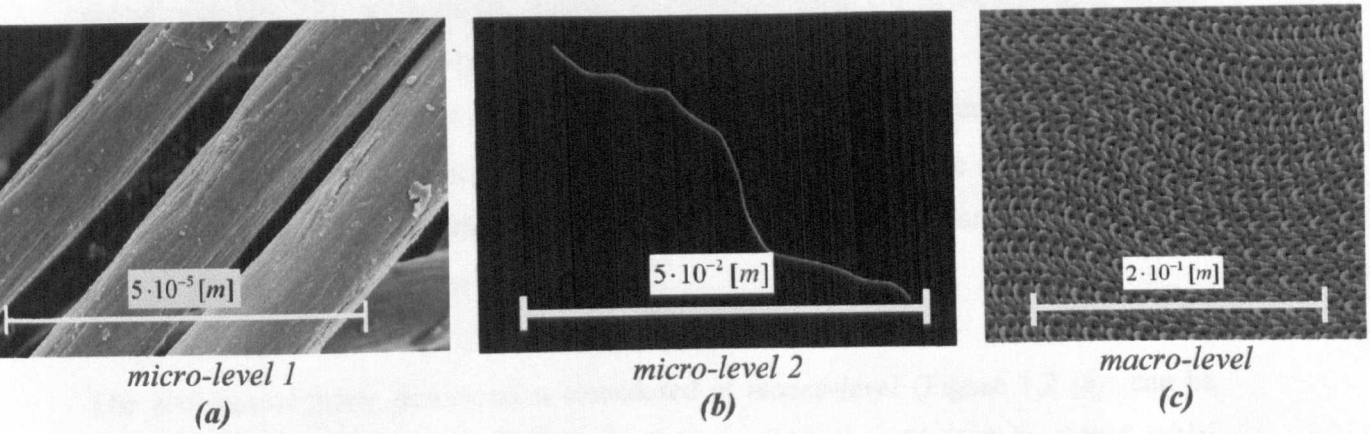

micro-level 1 ***(a)*** *micro-level 2* ***(b)*** *macro-level* ***(c)***

Figure 1.2 ***Different scales of the textile mechanics.***
Fibres under the microscope (micro-level 1) – (a); computer generated image of wool fibre (micro-level 2) – (b); computer generated image of fabric (macro-level) – (c).

The fabric mechanics can be studied at three different levels of complexity according to three different zooming levels of textile materials represented in Figure 1.2 (a, b, c). Modelling a fabric at the *micro-level 1* implies consideration of each fibre as a complex 3D body, Figure 1.2 (a). The huge number of fibres leads to an impossibly large number of complex differential equations and makes the problem virtually irresolvable, even for modern computers. Only the simplest problems of fabric deformation can be studied at *micro-level 1* [19].

The next zooming level – *micro-level 2* (Figure 1.2 (b)) implies known mechanical properties of the constituent yarn. Namely, each constituent yarn is considered as a one-, two-, or three-dimensional continuum with known mechanical properties. Modelling of fabric as such a collection of yarns requires considerable computation effort and, thought it is still impossible to resolve the general *boundary-value* problem at this level of complexity even using modern computers [21, 22]. A number of attempts have been made by the researchers to simulate fabric deformation assuming yarn as a one-dimensional continuum [17, 18, 20, 21, 22, 24, 25, 35, 36, 65]. The yarn

is normally simulated by so called *elastica* curve. *Elastica* is a material line with an imaginary cross section, which remains unchanged and orthogonal to the line during the line deformation. The initial form and boundary conditions for the *elastica* are assumed following the yarn initial geometry and the assumed conditions of yarn-to-yarn interaction at the contact points. In some special cases, it is possible to resolve the problem of *elastica* deformation and hence to simulate the fabric behaviour analytically [20, 22], however the general problem for large *elastica* deflections cannot be resolved analytically [15]. A number of numerical techniques were proposed to approach the problem [20, 21, 22, 23], however all of them were focused on simulating for some special cases of fabric deformation (pure bending or fabric drape [43, 44, 45, 46, 47]; tension in one direction or shear deformation of infinitely large sheets [26, 32, 33, 34, 35, 36, 37, 68, 69]; *etc.*).

The problem of fabric deformation considered at *macro-level* (Figure 1.2 (c)) can be classified as a membrane-, plate- or shell-type problem, subjected to fabric initial shape, loading and boundary conditions (see Table 1.2). Fabric in this case is normally assumed to behave as a 2D continuum. For this level of analysis, a full boundary value problem of fabric deformation can be resolved following to the developed apparatus for the Elasticity Theory [13, 14]. The specific applications of general theoretical and numerical methods of Elasticity Theory to textile materials are discussed elsewhere [21]. The disadvantage of such an analysis applied to fabric deformation is that the mechanical properties of discrete fabric structure are replaced with some effective properties, which are equivalent to that of the discrete structure only for some limited types of loading and boundary conditions.

The model of fabric deformation presented in this work is a combination of *micro-level 2* (Figure 1.2 (b)) and *macro-level* (Figure 1.2 (c)) analysis. Thus, a fabric unit cell introduced here is a discrete collection of yarns and it is possible to consider any small unit cell by formal replacing an integer yarns number in basic unit cell (loop for knitted structure) by a fractional number of yarns. Decreasing the unit cell size down the infinitely small value will give the element of some hypothetic continuum, which would have the same mechanical properties as a parent discrete structure.

The mechanical behaviour of fabric is determined by the mechanical properties of the constituent fibres, yarn structure, fabric structural properties and the manufacturing parameters of fabric production. We do not consider the manufacturing process and assume some given geometrical properties of fabric and geometrical/mechanical properties of yarn. There is relatively little information available in published literature on the mechanical properties of knitted fabrics. Mechanical property information is mainly available from direct measurement but some useful information is provided by previous theoretical/experimental research. In this particular investigation, the input parameters required for the model developed are listed in Table 1.3.

Table 1.3

Property	Description	References
A_{kn} and B_{kn} $[mm]$	Dimension of plain knitted fabric in course and wale directions. Measured as a specified length divided by number of loops in respective directions.	Figure 2.1
D_{yarn} $[m]$	Yarn diameter	
B_{yarn} $[N\,m^2]$	Yarn bending rigidity. Measured experimentally on Kawabata bending tester.	Section 4.2
T_{yarn} $[N]$	Yarn tensile rigidity function. Measured experimentally on Instron testing machine.	Section 4.4
Φ_{yarn}	Yarn torsion rigidity coefficient. Measured experimentally on torsion balance rig.	Section 4.3; [75]
$K0_{yarn}$	Initial value of yarn compression rigidity	[1, 2]
K_{yarn}	Non-linear function of yarn compression rigidity	[1, 2]

A method described here was devised to predict fabric extensional properties by means of mechanical/geometrical properties of yarn/fabric listed in Table 1.3. Some of these properties can be easily obtained from experimental observation; others had been described in relevant literature [1, 2, 4, 75].

Mechanical properties of fabrics are greatly influenced by the mechanical properties of yarns. Yarn mechanics investigation could be traced back to the work of Hearle on developing the yarn mechanical model [16]. A number of improvements have been made to the model over the years. We consider only the effective properties of the yarn, which could be derived from experiment or predicted by some model, *i.e.* the micro-mechanism of yarn deformation is not a subject of study in the present work. Yarn is assumed to behave as an elastic rod with linear bending and torsion properties and non-linear, time-independent tensile properties.

The model of knitted structure proposed in the present work simulates tensile behaviour of a knitted structure subjected to some external load and restricted by some boundary conditions. Although the model probably could be extended to tackle a complex 3D problem of fabric deformation, only the behaviour of fabric *in plane* is considered. To verify the model a number of strip samples were tested by means of a uni-axial tensile test on an Instron testing machine (section 4.5).

The first part of the work presented here in section 2.1 of CHAPTER 2 is concentrated on evaluation of yarn geometry when fabric is initially relaxed and 'set'. Loop form is evaluated with respect to geometrical parameters of yarn/fabric listed above in Table 1.3. Although a number of models of relaxed plain knit had been developed over the years, a new one is proposed, which is based on geometrical assumptions, and provide all data, in a format required for subsequent analysis and algorithm implementation. Assumptions are made to define the parts of loop involved in mutual contact with other loops and geometrical parameters of loop sections (contact zones and free zones).

The mechanism of knitted fabric deformation is discussed in section 2.2. After qualitative discussion of this subject, the unit cell is defined as a set of elementary parts of loop and interlacing regions (*contact zones*). Qualitative analysis of different boundary conditions is represented here.

Application of *Lagrange Principle of Energy Minimisation* to the elementary parts of a loop (*constitutive elements*) is represented in section 2.3. The potential energy of each constitutional element is derived as a function of introduced virtual co-ordinates

following the assumptions. The total energy of the unit element is derived with respect to link conditions. The final formulas in components required for subsequent numerical analysis are represented in Appendix B (1 – 6).

Micro-mechanical model of boundary conditions for constitutive elements in the unit cell is considered in section 2.4; a rheologic scheme of unit cell is proposed and boundary conditions for unit cells in the whole system are also discussed.

In CHAPTER 3 a numerical evaluation of the proposed model by means of the finite-element method is discussed; the main finite-element relationships are given in section 3.2. Evaluation of rigidity matrixes for the whole system and the problems related to method stability and convergence are discussed in the later sections of CHAPTER 3. To illustrate the model properties a qualitative analysis of simple testing structures is given. Deformation of a number of samples was numerically simulated and load-extension curves were obtained for the model verification.

Experimental procedures required for evaluation of input parameters and model verification are represented in CHAPTER 4. These include yarn tensile, bending and torsion tests and fabric uni-axial extension tests.

Discussion of the results obtained and possible applications of the proposed model for solving more complex problems than that of *in plane* deformation of the plain knitted fabric are outlined in CHAPTER 5.

1.2 Textile Materials; woven and noon-woven structure

Textile materials have been manufactured and used since the early stages of human evolution. Manufacturing process arose due to man's intuition at the very beginning of human civilisation. From that time until our days, it is being developed on the base of inherited experience.

Increasing industrial competition demands more and more from textile designers and they in turn demand better knowledge of their material. As the industry works with a

wider range of yarns and with different fabric structures, the need for a solution to this problem becomes pressing, for there is little practical experience which is based on theoretical models to guide the manufacturer. The development of new methods of investigating fabric mechanical properties is therefore very critical. The quest for better understanding of the problem is also motivated by the more academic desire for research to increase the knowledge of subject.

For apparel and industrial applications, designing textile fabrics with specific mechanical properties is important. One of the most fundamental of these properties is the load-extension behaviour, which is determined by the properties of the constituent yarns, and fabric dimensional properties (*i.e.* yarn path, fabric thickness *etc.*). Predicting tensile properties for a woven fabric has received much attention from scientists around the world [24, 25, 26, 27, 28, 29, 30, 71, 72].

Kawabata *et al* [24, 25, 26] presented a non-linear theory of predicting the bi-axial tensile property of the plain weave fabric in 1973, and the theory was improved to introduce the effect of yarn bending stiffness into the theory [27, 28]. Investigation of more complex structure of fabric (tri-axial-weave fabric) is represented elsewhere [29]. Although the structure of woven fabric could differ significantly from that of an ordinary plain-weave fabric, it is basically the same weave structure, and the theory of the plain weave may be applicable to the wide range of different structures with some modifications. A paper published by Reumann in 1990 [30] used Kawabata's approach to estimate uniaxial load-extension characteristics for any weave. While this should represent an advance over the previous work, the paper does not consider important practical features, including prediction with the bi-axial mode of loading. A more general model had been proposed by Fangning Sun *et al* in 1997 [31].

Several theoretical analyses [26, 32, 33, 34, 35, 36, 37] reported in scientific literature have dealt with shear properties of fabric. Grosberg and Park [32] based their calculations on a two-dimension model of fabric shear in which slippage between the yarns at cross-over regions (contact zones) increases gradually from zero slippage length of the contact region up to the length of the whole contact region. Olofsson [33] assumed that the fabric shear hysteresis results from the complete mutual rotation of threads at cross-over points. Kawabata *et al.* [26] related the experimental torque

necessary to rotate two sets of threads relative to each other to the fabric shear hysteresis by using experimentally determined constants. Skelton [34] used geometrical considerations to calculate the maximum shear angle for a woven fabric.

More recently, Postle *et al.* [36, 37] and de Jong [35] used an energy method of analysis to study the mechanical properties of textile structures. This analysis had been applied in the case of continuous contact between threads in cross-over regions by Sinoimeri *et al* in 1996 [38].

A macroscopic approach to dealing with *multi-axial warp knitted* fabric structure under uni-axial tensile deformation is represented in [39]. *Multi-axial warp knitted* fabric system normally consists of five yarn systems, four for inserting yarns (namely warp, weft and bias yarns), which are held together by the fifth, the stitching system (chain or tricot loops) through the thickness of fabric. The properties of stitching system are neglected here.

Fabrics are well known for their property-direction dependence or property anisotropy. Kilby [40] was one of the early researches to deal with the mechanical anisotropy of a woven fabric. He derived the so-called generalized modulus of a fabric, expressing the fabric tensile modulus in relation to the test direction. Fabric shear strength was examined by Pan *et al* [41]. Fabric shear strength is predicted here from measured uni-axial tensile strength of the fabric at the principle and off-axial directions. A harmonic expression is adopted here to approximate the experimental results.

During draping, fabric undergoes large deformations under small applied forces. In order to describe drape phenomenon fabric is normally assumed to be an elastic continuum with some anisotropy. The pioneering work in the area of numerical simulation of fabric drape was the use of catenary curves to model fabric developed by Weil [42] in 1986. This work led to a number of computer graphic-based fabric modelling works, including some commercial software. However, most of the early models did not account for the physical properties of fabric in a comprehensive way.

Some recent works show modelling of fabric drape using finite-element methods. Coiler *at al* [43] studied draping behaviour of fabrics by using a non-linear finite-

element method based on classical non-linear plate theory. While a fabric goes through small strain and large rotation during draping, with the maximum deflection of the fabric being of order of hundreds of times the fabric thickness, the solution of a classical plate theory only agree closely with experiment data up to the deflection-to-thickness ratio of six because of approximate calculation of the bending curvature. Eischen and Kim [44] established a fabric model by using a large deformation beam theory. They focused primarily on simulating fabric-bending behaviour with a symmetry that allows the 3D fabric draping problem to be analysed in 2D. A shear flexible shell theory was used to predict the drape of fabric by Bijan Chen [45]. Kang *et al* [46] considered draped fabric as a thin plate using non-linear relationships for the curvature coefficients.

An attempt to model dynamic deformation properties of textiles had been made by Postle [48] in 1999. The solution obtained here enables complicated fabric profiles to be predicted. Furthermore, it makes it possible to consider the evaluation in real time of 3D fabric profile or the dynamic behaviour of draped fabrics during deformation.

The phenomenon of buckling of flexible sheets under tension had been studied using the continuum mechanics theory by Amirbayat [49]. Opposite to the fabric drape phenomenon, bulking occurs when fabric undergoes large deformation having been subjected to considerable load. The paper discusses the factors affecting the buckling of flexible sheets under tension that occurs when the external loads are not uniformly distributed. It goes further to analyse the energy of the system and gives the criteria for sheet instability in terms of dimensionless quantities formed from material properties and sheet dimensions.

Nonwoven fabrics are normally assumed as a web, which is made up of a number of fibres. Fibres in the web are oriented at various directions following random or some known statistical distribution [53]. The fabric is treated as built up of *unit cells*, which experience the same strain as applied to the fabric. The unit cells are assumed large enough to allow each fibre to have a number of bonds in order to avoid any local variation in strain [54].

Knitted fabrics differ significantly from woven and nonwoven fabrics in structural and mechanical properties, however it is the same sheet material. Thus, all fabrics undergo large deformation under small applied forces during bending (draping). Having been extended they can withstand considerable load.

1.3 Knitted Structure

The papers outlined in previous section dealt mostly with woven and non-woven fabrics. Although a knitted structure is used as a stitching system in *multi-axial warp knitted* fabric the influence of stitching yarns on fabric behaviour are normally neglected [39].

There is much less literature available, which considers the mechanical properties of knitted fabrics. A number of researches Peirce [56], Shin [57], Doyle [58], Leaf and Glaskin [59], Postle and Munden [60], De Jong and Postle [71, 72], Grosberg [63, 64] have all made attempts to define geometrically the configuration of the unit cell of a plain knitted fabric i.e. initial geometry of the relaxed loop. These parameters were then fitted to give experimentally observed values of the fabric parameters.

In attempts to study knitted fabric subjected to external load a force analysis approach had been preferred by most of researches Peirce [60], Shanahan and Postle [62], Hepworth and Leaf [65], Konopasek [66], Olofsson [67], Hepworth [18, 69, 70]. To analyse the fabric by means of force analysis, the yarn should be divided into segments at whose ends forces and (or) couples may act.

The force analysis of a knitted structure implies the resolution of a complex system of non-linear equilibrium equations, especially when yarn is treated as an elastic rod (i.e. couples are taken into account). It is for this reason the researches have had to make simplifying assumptions, which however restricts the models' application.

Hepworth *et al* [68] considered an idealized knit structure constructed from naturally straight, inextensible and incompressible yarns. The model of relaxed plain knitted fabric proposed here gives the initial shape of the loop. The solution is obtained by numerical resolution of the equilibrium equations of the loop segment, which is subjected to external forces. These forces arise due to assumed loop segmentation (the reaction forces at cut edges) and external loads which arise from yarn-to-yarn compression at the contact zones and jamming between courses. The same equilibrium equations, which had been used for evaluation of the relaxed state of the fabric, have

been applied to the problem of fabric extension in wale and course directions [69]. The solution gives load-extension curves for plain knitted fabric with various ratios of yarn diameter to loop length. One of the basic assumptions in the Hepworth's model [68, 69, 70] is that during fabric deformation the contact points of yarns are located at the same places as in the initially relaxed fabric. Although yarns are assumed incompressible, and, hence it is possible to impose kinematical constraints to restrict yarn movement in the points of contact and consider the whole quarter of the loop, the equivalent force was introduced to simulate the reaction force which acts in contact point and the quarter of the loop was subdivided into sections. That is formally correct however it makes it difficult to follow the argument. The solution is represented here in the form of load-extension curves in both course and wale directions. The curves were obtained for plain knitted fabric with different tightnesses (ratio of yarn diameter to length of yarn involved in loop). The shape of load-extension curves represented in [69] qualitatively agrees with that observed in experiments, except for a few curves which represent course contraction of the fabric loaded in wale direction. Thus, for tight fabric the model predicts the fabric extension in the course direction when it is subjected to extension in the wale direction. Although the magnitude of predicted extension in course direction is relatively low, it is in obvious disagreement with experiment.

An energy minimisation technique was applied to the problem of plain knitted fabric under low tension by De Jong and Postle [71, 72]. The basic equilibrium equations and the boundary conditions for plain knitted fabric are derived here without assuming any detailed pre-conditions related to loop interlocking. A continuous region of contact between the yarns in fabric is introduced to simulate yarn-to-yarn compression in the interlacing region, this is a refinement on Hepworth's approach as she assumed yarn to be incompressible.

It is worth saying that results obtained by Hepworth, De Jong and Postle [68, 69, 71, 72] are represented in a form which is not suitable for subsequent investigation. Neither full theoretical equations are written nor experimental validation of the obtained results is represented. The biased scientific discussion of the subject [73, 74] does not make the situation clear.

In all of the work mentioned on studying knitted fabric mechanics the internal couples acting in the loop are taken into account. During the first stages of the present project, attempts were made to use a similar approach to that represented by Hepworth, De Jong and Postle [69, 70] for modelling the tensile properties of knitted structures. The yarn was assumed to behave as an elastic rod with tensile and bending properties derived from experiments on yarns. Yarn-to yarn contact had been replaced by the kinematical boundary conditions at contact points. A typical example of deformed knitted structure obtained with assumptions outlined above is represented in Figure 1.3. The blue curves represent the initial position of the yarn and red curves represent the deformed state of knit with the external load applied in the course direction. The author strongly believes that lateral contraction of fabric predicted by Hepworth [69] for loose fabric structure and re-predicted in Figure 1.3 comes from internal couples which occurred at the contact points. The couples in turn occur because yarn bending rigidity had been taken into account. It is worth noting that bending rigidity of yarn is of extremely small magnitude and it is doubtful that such couples have considerable influence on the fabric behaviour.

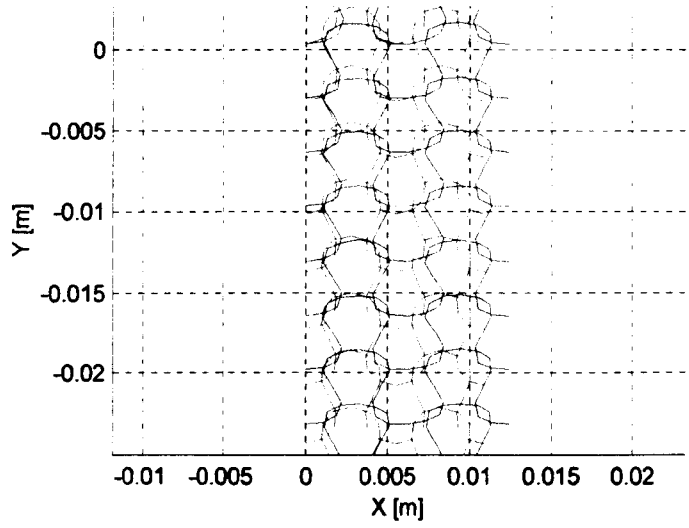

Figure 1.3 ***Extension of knitted structure simulated by the system of elastic rods fixed in contact points.***

The argument represented in Appendix B.7 makes it possible to neglect internal couples in tensed fabric, which in turn simplifies the model considerably and enables the factors particularly neglected by previous authors [60, 69], i.e. yarn-to-yarn compression, jamming and length redistribution, to be taken into account.

Kawabata [80]developed a theoretical method to calculate the bi-axial tensile properties of plain knitted fabrics. The unit model of plain knitted fabrics is assumed to be elongated to such an imaginary degree that the yarn has no tension. The tensile force is calculated from the bending region and stretching region.

More recently, Wei-Liang *et al* 1994 [81] proposed a model of fabric deformation which is based on geometrical structure of plain knitted fabric. Knitted fabric is considered here as a set of the hexagonal elements (Figure 1.4(a)) joint as shown in Figure 1.4 (b). To define the equilibrium position of the system of joint unit cells the forces acting at each point (vertex) of the unit cell were balanced. To fit the theory to the experimental data the mechanical properties of the unit cell were defined from the same experiment by means of the least squares method (it would probably be the same if average characteristics were used). To remove the difference between the experimental and the theoretical load-extension curves the model was improved further to introduce the slippage effect in the cross over regions (contact zones). The load extension curves obtained with the improved model show good agreement with the theory at low applied load for the uni-axial extension and for relatively high load for the strip elongation. To avoid the method diverging the slippage is restricted here by introducing a 'potential force' in the form:

$$\begin{cases} \Delta l = 0 & F \le F_c \\ F = K_f \Delta l & F \succ F_c \end{cases} \qquad (1.1)$$

where Δl is a length of unstressed yarn slipped from the cross over point;

F is resultant withdrawal force acting at the cross over point;

K_f is a coefficient, which is defined by error method;

F_c is the maximum static frictional force, which is in turn defined as follows:

$$F_c = \mu \ N$$

where μ is static friction coefficient and N is a resultant force in cross over point.

It is obvious that for initially relaxed state the resultant force $N=0$, and, hence, following the equation (1.1) the slippage restriction force is defined by the value of coefficient K. Namely, if value of K is high enough the slippage will occur from the first stages of deformation and $F = K_f \ \Delta l$, for the lower value of K no slippage will

occur. Thus, the introduced slippage is an additional parameter which is used for better fit of the theory with the experiment. Note that force F is the only one factor which restricts extended system of the unit cells from being collapsed into one line and the value of K was matched to provide the method stability and to fit the experimental results [81].

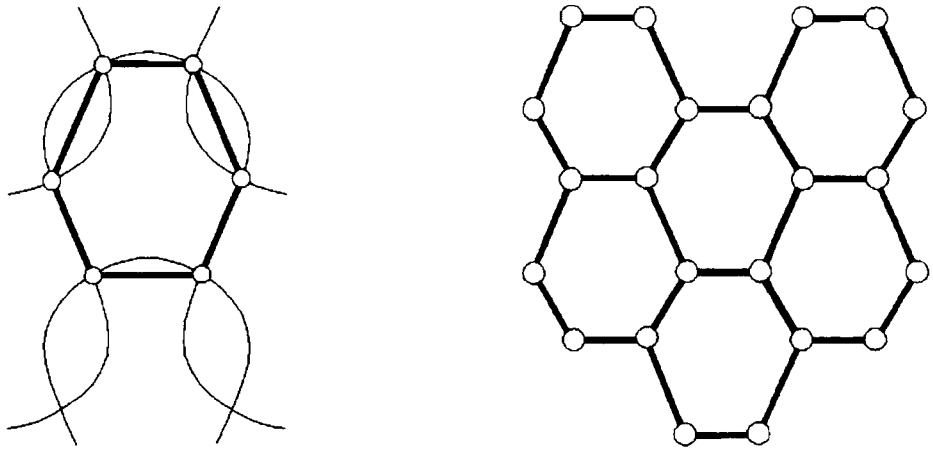

(a) *(b)*

Figure 1.4 (a, b) ***The hexagonal unit cells.***

The investigation recorded in this thesis has no direct parallel with any other reported work. The closest work was undertaken by Wei-Liang [81] but the model proposed therein is based on a unit cell whose mechanical properties can not be defined from the mechanical properties of the yarn and the loop geometry. The model developed by Wei-Liang leads to predictions of the fabric mechanical properties which deviate significantly from the properties of real fabrics. Therefore, arbitrary constants were introduced as correction factors to improve the outcome; the introduction of correction factors has not been necessary in the model proposed in this thesis. The approach described in this thesis makes its possible to define the fabric deformation mechanism from its discrete properties and allows fabric mechanical properties to be predicted from the cell geometry and the mechanical properties of the yarn.

Since the application of textile fabrics has expanded into industrial and composite areas, aspects of industrial application of fabrics have been presented in a number of publications during the last decade [50, 51, 52, 78, 79]. Hearle and Du [78] presented

an overview of modern textile technology from the point of interaction with the composite industry. It was pointed out that an understanding of textile solutions can be beneficial to the composite engineers and conversely, composites provide an opportunity for textile researches.

During the last few decades, a number of approaches have been developed to deal with fabric deformation. Most of the researchers made detailed assumptions on the initial geometry of the knitted structure and, unfortunately, unrealistic assumptions about the fabric deformation mechanism. Their models were restricted either by the fabric structure (plain knitted fabric) or by the loading conditions (extension in course direction [71]; bi-axial elongation of an infinitely large sheet of fabric [69], in-plane deformation *etc.*). An increasing interest in more precise modelling of fabric deformation requires a full boundary-value analysis of complex fabric deformation to be performed. That in turn requires definition of the complex deformation of a small part of fabric or the *unit cell.* The *unit cell* proposed in the present work enables simulation of any complex deformation of each elementary part of fabric sheet subjected to various loading and boundary conditions. As oppose to the pure continuum approach [21] the recent model defines the hypothetical continuum with mechanical properties inherited from the discrete fabric structure.

A number of researches have attempted the problem considering deformation of each yarn within the fabric structure [68, 71]. This kind of analysis is restricted, among the other things, by the impossibility to subdivide the whole problem into a series of problems for the smaller elements. The finite element, introduced here as a system of unit cells, allows consideration of a larger finite element for faster solution and smaller elements for higher precision.

CHAPTER 2. Theoretical model

2.1 Geometrical Parameters of Knitted Fabric, 3D model of plain knitted loop

An algorithm for evaluation of yarn path in plain knitted fabric is presented. Mechanical properties of yarn are neglected. Yarn path is approximated by parametric spline curve. Knot points for spline curve are obtained with regards to fabric dimension and yarn diameter. Further assumptions are made to determine the parts of loop involved in mutual contact. Input data are chosen that could be obtained from direct measurement of fabric dimensions.

The first step in analysis of mechanical properties of fabric is evaluation of the initial form of the yarn loop. Yarn in knitted fabric follows a complicated 3D path, which is affected by a number of factors. Determination of the exact loop form requires rigorous analysis of manufacturing parameters and mechanical properties of both yarn and fabric. In the present work, the simplest approach for evaluation of the 3D form of the plain knitted loop is used.

Plain-knitted fabric is illustrated in Figure 2.1 (a, b), where a 3D image of fabric and the projection of the central axis of yarn onto plane XY are represented. Right-hand Cartesian co-ordinate system is used like that in Figure 2.1 (b). The same co-ordinate system is used further for description of an initially flat fabric. According to textile terminology, the 0X-direction is called 'course' direction; the 0Y-direction is called 'wale' direction.

Parameters A_{kn} and $B_{kn} = (b1 + b2)/2$ represent fabric loop dimensions in the wale and course directions; fabric thickness is in the *0Z* direction. The values of A_{kn} and B_{kn} are considered to be the main periods of the knitted structure. Thus, shifting any loop in Figure 2.1 towards wale or course direction by A_{kn} or B_{kn} will give the next neighbour loop of the system. Values of A_{kn} and B_{kn} can be evaluated as the number of loops per

10 [cm] in course and wale directions, whereas loop dimension H_y, Figure 2.1 requires direct measurement of individual loops.

Note that value of *b1* and *b2* are different in real fabrics however, it is not possible to measure *b1* and *b2* separately and it is assumed further that

$$b1 = b2 = B_{kn}. \tag{2.1}$$

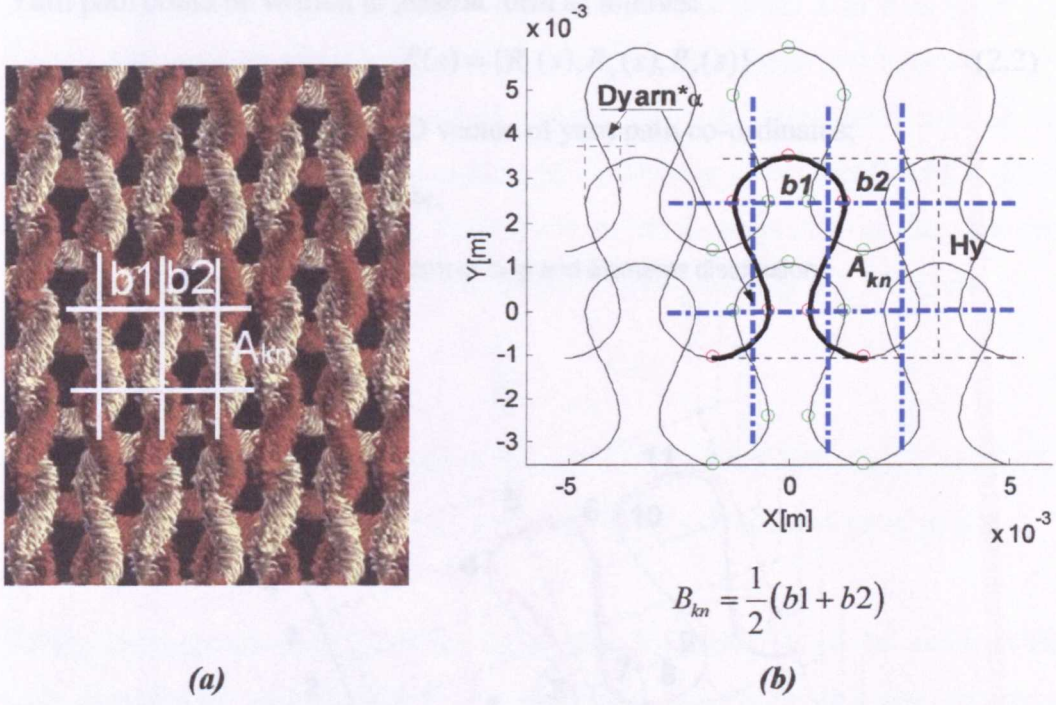

$$B_{kn} = \frac{1}{2}(b1 + b2)$$

(a) *(b)*

Figure 2.1 (a, b) ***Fabric dimension.***

numerically generated image — (a); loop projection onto XY plane — (b).

The length of the yarn involved in loop and the yarn diameter are important parameters of knitted loop structure. A number attempts had been made to find out the relationship between loop dimensions *a* and *b*, yarn diameter D_{yarn} and loop length [56, 57, 58, 59, 60, 61, 62]. However, we assume all mentioned parameters to be independent. In the present work, we use loop length as an input parameter for the model. Loop length could be estimated from a prior formula [3]* or measured for any individual fabric.

---

* $L_{loop} = \frac{50\pi}{P_C} + \frac{200}{P_W} + \pi D_{yarn}$, *where* L_{loop} *is loop length [mm];* D_{yarn} *is yarn diameter [mm];* P_C *and* P_W *are number of loops per 100 [mm] in coarse and wale directions respectively.*

Parameters A_{kn} and B_{kn}, in Figure 2.1, with yarn diameter and loop length form a set of main fabric properties. The present approach is aimed at determining a reasonably accurate approximation of yarn path by using only the parameters as mentioned above and listed in Table 1.3.

One of possible paths of the yarn axis (*yarn path*) in a loop is represented in Figure 2.2. Yarn path could be written in general form as follows:

$$\underline{R}(s) = \{R_x(s), R_y(s), R_z(s)\} \tag{2.2}$$

where $\underline{R} = \{R_x, R_y, R_z\}$ is the 3D vector of yarn path co-ordinates;

s is arc length co-ordinate.

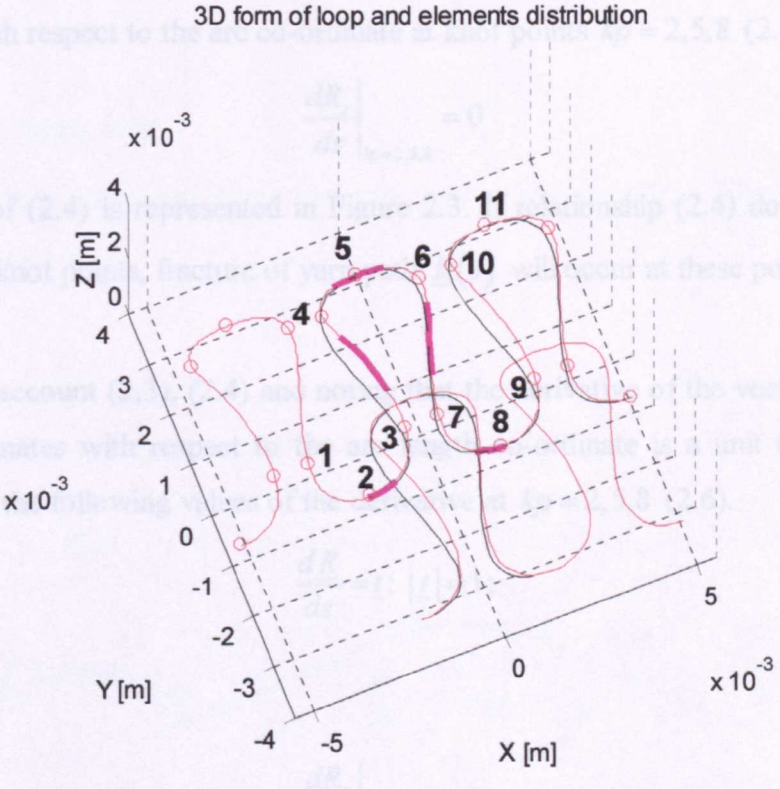

Figure 2.2 ***3D view of knitted structure.***

3D loop form (red); numbered knot points (1-9); parts of the loop not involved in contact (magenta curves)

We define knot points (red circles in Figure 2.2) such that the value of the derivative of at least one component of $\underline{R}(s)$ with respect to the arc length s is equal to zero at the

knot point. Thus, for knot points numbered from 2 to 8 the following relationships can be written:

$$\left.\frac{dR_y}{ds}\right|_{kp=2} = 0; \left.\frac{dR_x}{ds}\right|_{kp=3} = 0; \left.\frac{dR_x}{ds}\right|_{kp=4} = 0; \left.\frac{dR_y}{ds}\right|_{kp=5} = 0; \cdots\cdots; \left.\frac{dR_y}{ds}\right|_{kp=8} = 0 \qquad (2.3)$$

where *kp* is a knot point numbered according to the Figure 2.2.

There is arbitrariness in loop definition. Thus, it is possible to define a loop in two different ways: passing through knot points numbered from 2 to 8 or from 5 to 11. Taking into account (2.1) it is possible to assume that these two loop definitions are equivalent except that the second is flipped about the horizontal axis of the first defined loop. The mentioned symmetry and periodicity of structure make it possible to derive additional conditions for derivatives of the z component of the yarn path co-ordinates with respect to the arc co-ordinate at knot points $kp = 2,5,8$ (2.4).

$$\left.\frac{dR_z}{ds}\right|_{kp=2,5,8} = 0 \qquad (2.4)$$

Illustration of (2.4) is represented in Figure 2.3. If relationship (2.4) does not hold at some of the knot points, fracture of yarn path $\underline{R}(s)$ will occur at these points.

Taking into account (2.3), (2.4) and noting that the derivative of the vector of the yarn path co-ordinates with respect to the arc length co-ordinate is a unit tangent vector (2.5) we get the following values of the derivative at $kp = 2,5,8$ (2.6).

$$\frac{d\underline{R}}{ds} = \underline{t}; \ |\underline{t}| = 1; \qquad (2.5)$$

$$\left.\frac{dR_x}{ds}\right|_{kp=2,5,8} = 1. \qquad (2.6)$$

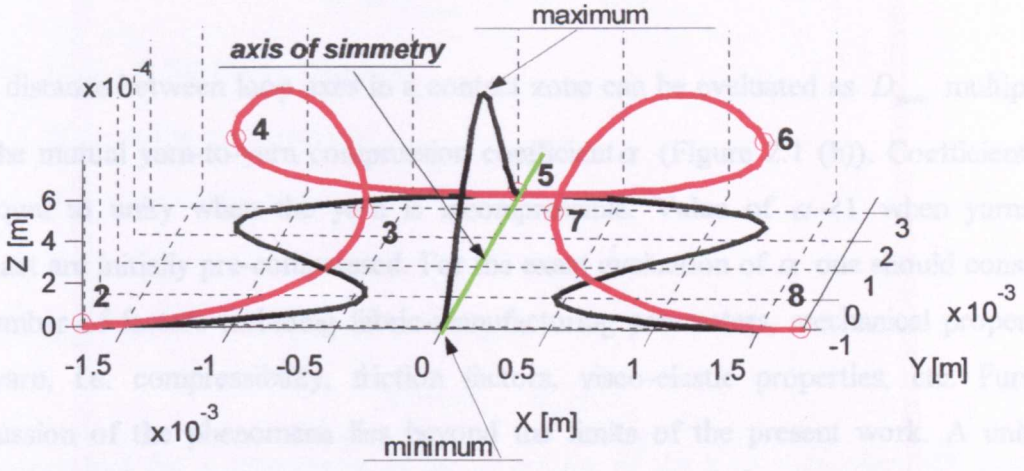

Figure 2.3 ***A single loop.***

3D view of single loop - red, projection onto plane (XY) and (ZY) – black, knot points numbered from 2 to 8.

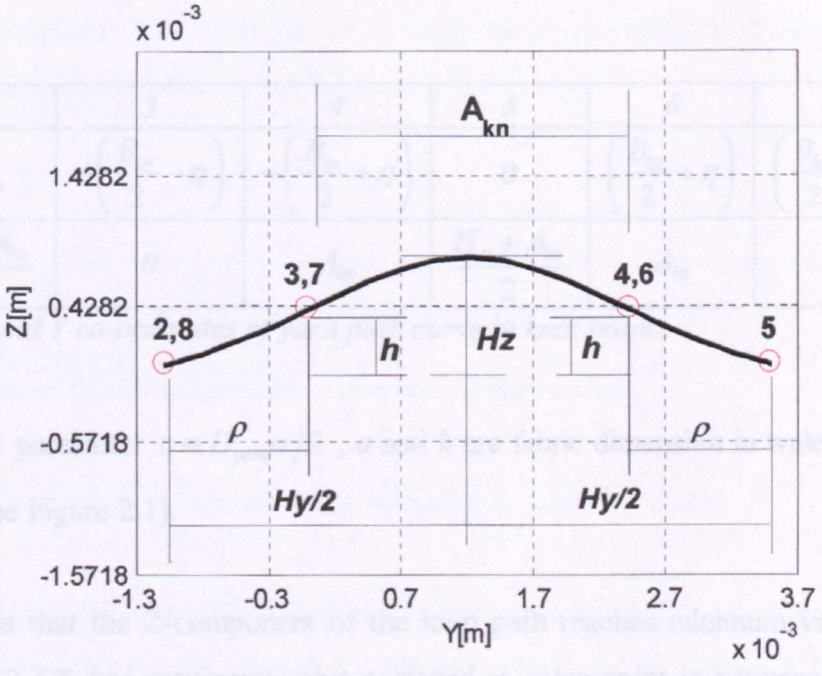

Figure 2.4 ***Projection of loop onto (YZ) plane with mapped knot points.***

Some parts of the loop are involved in contacts with neighbouring loops (*contact zone*). The rest of yarn in the loop is free of contact (*free zone*). The distribution of free zones along the loop length is represented in Figure 2.2 (magenta curves).

The distance between loop axes in a contact zone can be evaluated as D_{yarn} multiplied by the mutual yarn-to-yarn compression coefficient α (Figure 2.1 (b)). Coefficient α is equal to unity when the yarn is incompressible. Value of $\alpha \prec 1$ when yarns in contact are initially pre-compressed. For the exact evaluation of α one should consider a number of factors including fabric-manufacturing parameters, mechanical properties of yarn, i.e. compressibility, friction factors, visco-elastic properties, etc. Further discussion of the phenomena lies beyond the limits of the present work. A unitary value of α is assumed for further calculations.

To obtain co-ordinates of knot points we assume a known wale dimension of the loop H_y (Figure 2.1 (b)). According to the abovementioned symmetry and periodicity of fabric it is possible to derive X and Y co-ordinates of knot points for a single loop as shown in Table 2.1.

Table 2.1

kp	2	3	4	5	6	7	8
$R_x\|_{kp}$	$-B_{kn}$	$-\left(\frac{B_{kn}}{2}-\eta\right)$	$-\left(\frac{B_{kn}}{2}+\eta\right)$	0	$\left(\frac{B_{kn}}{2}+\eta\right)$	$\left(\frac{B_{kn}}{2}-\eta\right)$	B_{kn}
$R_y\|_{kp}$	$\frac{H_y-A_{kn}}{2}$	0	A_{kn}	$\frac{H_y+A_{kn}}{2}$	A_{kn}	0	$\frac{H_y-A_{kn}}{2}$

Value of X and Y co-ordinates of yarn path curve in knot points.

In Table 2.1 parameter $\eta \equiv D_{yarn}\alpha/2$, a and b are fabric dimension in wale and course direction (see Figure 2.1).

It is obvious that the Z-component of the loop path reaches minimum value at knot points $kp = 2,5,8$ and maximum value achieved at some point in between $kp = [3:4]$ and $kp = [6:7]$ (Figure 2.3 and Figure 2.4). Assuming that yarns are not compressed in the contact zone ($\alpha = 1$) and fabric is not compressed in the Z direction it is possible to

assume that fabric thickness H_{fabric} is equal to double the yarn diameter. The maximum Z-dimension of the loop axis H_z could be expressed as follows:

$$H_z = H_{fabric} - 2 \cdot R_{yarn} = D_{yarn} \tag{2.7}$$

where H_{fabric} is the fabric thickness;

R_{yarn} is the yarn radii and

D_{yarn} is the yarn diameter.

Due to loop symmetry, parameter ρ in Figure 2.4 can be expressed as follows:

$$\rho = \left(H_y - A_{kn}\right)/2 . \tag{2.8}$$

Assuming that the Z component of the projection of the loop onto plane ZY linearly increases from zero to the maximum value and then linearly decreases from maximum to zero, gives the following value of h (Figure 2.4):

$$h = 2^{H_z}\!/_{H_y} \cdot \rho \tag{2.9}$$

Parameter h in Figure 2.4 gives the value of Z co-ordinates at knot points $kp = \{3,7\},\{4,6\}$.

Taking into account (2.7), (2.8) and (2.9) yields the Z co-ordinates of the yarn path at the knot points are as shown in Table 2.2.

Table 2.2

kp	2	3	4	5	6	7	8
$R_z\|_{kp}$	0	h	h	0	h	h	0

Value of Z co-ordinates of the yarn path curve at knot points.

In Table 2.2 parameter h is determined according to equation (2.9).

The selection of an approximation function for the loop, which led to an acceptable loop form, can be accomplished in different ways [12]. One of the possible approximation functions is a cubic spline. Cubic splines provide continuity of curve of the second order (continuity of derivatives up to the first degree).

It is not possible to construct a simple polynomial spline in the form $y = Spl(x)$ due to multi-valued shape of the loop, *i.e.* the Y co-ordinate of the loop can attain different values for the same value of X co-ordinate. Parametric splines were chosen to overcome the problem. Additional knot points from the neighbouring loops in a row, with numbers 1 and 9 as shown in Figure 2.2, were used for more even loop form approximation. Finally, we assume that loop form is approximated at the interval $kp = \{2:8\}$. Curves lie in between knot points $kp = \{1,2\}$ and $kp = \{8,9\}$ are subsidiary.

The value of the arc co-ordinate s in knot points cannot be determined until the curve is defined. For parametric curve evaluation, an independent continuous parameter t_{kp} was chosen in such a way that:

$$t_{kp} = [1:9] \text{ for } kp = \{1,...,9\}.$$

The derivatives in expressions (2.3) to (2.6) are all defined with respect to the arc length s, which is unknown. To construct the spline these derivatives should be rewritten with respect to the new parameter t_{kp} according to the following relationship:

$$\frac{d\,Spl_{x,y,z}}{dt_{kp}} = \frac{d\,Spl_{x,y,z}}{ds}\,\frac{ds}{dt_{kp}} \tag{2.10}$$

The loop shape is defined at knot points $kp = \{2,...,8\}$, and it is assumed that the derivative of the arc co-ordinate with respect to chosen parameter t_{kp} is constant:

$$\frac{ds}{dt_{kp}} = \frac{L_{loop}}{2-8} = \frac{L_{loop}}{6} \tag{2.11}$$

where L_{loop} is the known length of the loop.

Relationships (2.10) and (2.11) make it possible to recalculate derivatives of the yarn path with respect to the new parameter t_{kp} and evaluate the 3D spline which approximates the loop form (Figure 2.2 and Figure 2.3). Finally, the curve defined yarn path can be expressed in the form of equation (2.2). Knot point co-ordinates and derivatives of the yarn path, which are required for evaluation of spline functions, are summarised in Table 2.3.

Table 2.3

kp	1	2	3	4	5	6	7	8	9
R_x	$-\left(\frac{3B_{kn}}{2}+\eta\right)$	$-B_{kn}$	$-\left(\frac{B_{kn}}{2}-\eta\right)$	$-\left(\frac{B_{kn}}{2}+\eta\right)$	0	$\left(\frac{B_{kn}}{2}+\eta\right)$	$\left(\frac{B_{kn}}{2}-\eta\right)$	B_{kn}	$\left(\frac{3B_{kn}}{2}+\eta\right)$
$\frac{dR_x}{dt_{kp}}$	0	1/6	0	0	1/6	0	0	1/6	0
R_y	0	$\frac{H_y - A_{kn}}{2}$	0	A_{kn}	$\frac{H_y + A_{kn}}{2}$	A_{kn}	0	$\frac{H_y - A_{kn}}{2}$	0
$\frac{dR_y}{dt_{kp}}$	1/6	0	1/6	1/6	0	1/6	1/6	0	1/6
R_z	--	0	h	h	0	h	h	0	--
$\frac{dR_z}{dt_{kp}}$	--	0	--	--	0	--	--	0	-

Knot point co-ordinates and derivatives of the yarn path defined at knot points

To determine the unknown value of the loop dimension in the Y direction H_y, we consider a set of loops with the Y dimension varied from $A_{kn}+\delta 1$ to $A_{kn}+\delta 2$ (Figure 2.5). Searching for the loop with the required arc length yields an estimate of the unknown value of H_y.

Values of $\delta 1$ and $\delta 2$ are determined automatically while searching iterations are executed. For a standard loop shape, the values of $\delta 1 = 0.1 A_{kn}$ and of $\delta 2 = 0.5 A_{kn}$ are accepted.

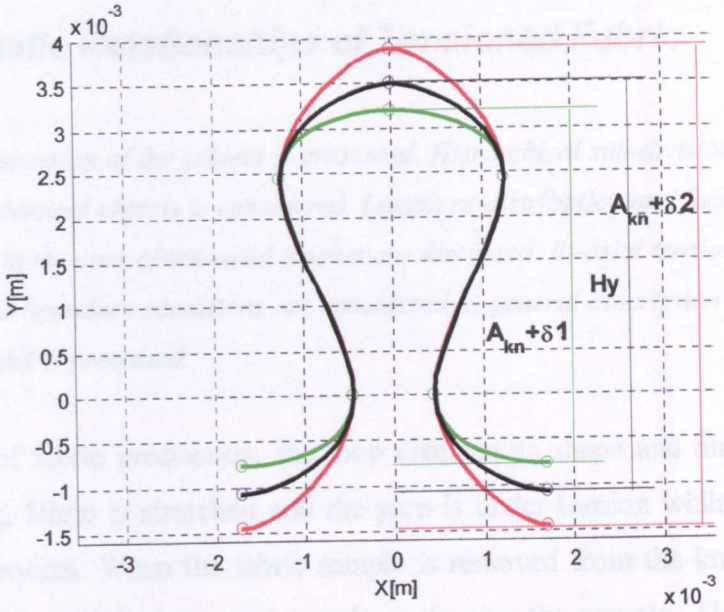

Figure 2.5 ***Variation of the loop form.***

loop with pre-set length (black), loop with increased length (red), loop with decreased length (green).

Note that the 3D length of the loop is considered while the loop with appropriate length is searching.

For subsequent modelling of mechanical properties of the fabric, it is important to define where the yarn is in contact with neighbouring yarns and where it is free (Figure 2.2). Due to yarn unevenness in a real fabric it is difficult to determine whether yarn is in contact or not. To simplify the model we assume that two neighbouring yarns are in contact when their projections onto plane *XY* intersect.

2.2 Kinematic Relationships of Tensioned Fabric

A qualitative discussion of the subject is presented. Hierarchical sub-division of the fabric into elementary mechanical objects is considered. Length re-distribution and factors restricting fabric collapse in the case of uni-axial tension are discussed. Bi-axial tension, shear deformation and boundary conditions are considered. A general description of the fabric mechanical model is presented.

At the stage of fabric production, the loop changes its shape and dimensions. During manufacturing, fabric is stretched and the yarn is under tension while it is involved in the knitting process. When the fabric sample is removed from the knitting machine, it relaxes but some residual stresses remain acting on the sample. This residual stress causes fabric instability *in plane*, i.e. the sample normally does not remain flat without external constraint. Normally, flat knitted samples transform into a cylindrical shape tending to curl around some axis from edges towards the centre. The process of total strain relaxation in a fabric may take up to several weeks. During this period the fabric sample changes its shape and dimension in three directions and becomes a more or less stable structure. Due to the time-dependent mechanical properties of yarns, stress in a fabric tends to be balanced with internal friction. A 'set' sample is balanced as a whole system, however when a new cut edge is introduced the system becomes unstable again. Studying this kind of phenomena is particularly important for garment prototyping when cut samples change dimension compared to the designed pattern. In the present work, we study tensile properties of set fabric. Moreover, we assume that all yarns are slack and, hence, no friction force acts in an initially slack fabric.

The present work is aimed at defining a micro-mechanical model of fabric deformation. The behaviour of yarns in loops, yarn-to-yarn interactions and change of loop parameters during fabric tension are the main subjects for further analysis.

The basic feature of knitted structure (particularly of plain knitted and 1+1 rib fabric) is that subjected to strain in one direction it achieves considerable lateral contraction in the other in-plane dimension. The same phenomena could be observed when a sample made from *isotropic* continua materials (copper, steel, etc.) is stretched. However, the

mechanism of the phenomena is entirely different in fabric than in a continuous sheet material. Firstly, lateral contraction of a continuous sheet sample is generally much less when compared to knitted structures. Visible changing of cross section can be observed when a continuum sample is subjected to a force comparable to breaking point force. Normally, behaviour of any material is considerably non-linear when the material is close to break point. Fabric in turn, achieves considerable lateral contraction from the early stages of loading, when working in the linear zone and approaching the break point the lateral dimension tends towards a minimum possible value.

Secondly, continuum materials considerably resist volume changes (except porous materials). The ratio of axial relative deformation ε_l to corresponding transverse deformation ε_n is constant for an individual material. The Poison ratio ν for a linear isotropic material can be expressed as follows:

$$\varepsilon_n = -\nu\varepsilon_l . \tag{2.12}$$

The maximum possible value of Poison's ratio for continuous material is ½. A value of ½ is characteristic of an incompressible material. A Poisson's ratio higher a ½ corresponds to a hypothetical material with a negative *relative volume deformation* (2.13).

$$\frac{\Delta V}{V} \approx 2\varepsilon_n + \varepsilon_l = \varepsilon_l(1-2\nu) \tag{2.13}$$

Here V is volume and ΔV is change of volume of a small element.

The Poison's ratio for knitted structure, calculated experimentally according to relationship (2.12), could be up to 0.6. That means that the fabric behaviour could be classified as close to that of an incompressible *isotropic* material. On the other hand, the fabric is soft (weak) enough to allow considerable volume change.

The phenomena could be explained by assuming a physical relationship between axial and transversal strains. To illustrate these we consider deformation of a loop when fabric is stretched in the course direction. The projection of the yarn in the knitted fabric follows a path which is represented schematically in Figure 2.6 (a, b) (see also Figure 2.1 and Figure 2.2).

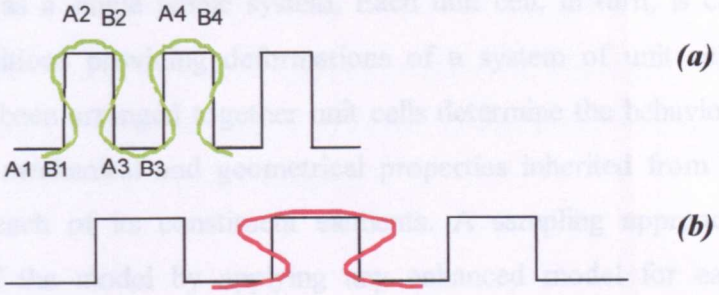

Figure 2.6 (a, b) ***A schematic representation of the yarn path projection onto plane XY.***

initial state of fabric with slack loops – (a), fabric stretched in the course direction – (b).

Having been stretched, horizontal parts of the loop (A1B1, A2B2 in Figure 2.6 or the corresponding magenta curves in Figure 2.2) transfer tension to vertical parts of the loop (B1A2, B2A3 in Figure 2.6) via contact zones. This argument leads to the assumption that during axial tension lateral pressure acts in the sample. It is also possible to assume a functional dependence of tension in the horizontal part of loop and tension in the vertical part.

It is possible to assume some special anisotropy to describe the phenomena; however studying the internal kinematic relationship is still essential. It was decided to consider a discontinuous model of fabric rather then a complicated anisotropy applied to a continuum.

To describe the micro mechanism of fabric deformation we consider a hierarchical sub-division of fabric into a series of elements. The surface of the fabric is sub-divided into elementary cells (*unit cells*) and each cell in turn is considered as a system of elementary elements (*constituting elements*). (For subsequent numerical implementation of the algorithm a finite element is considered, which consists of a number of unitary cells, this is discussed further in CHAPTER 3). Sampling analysis allows dividing the unit cell into several elements and definition of properties for each element separately. That is, we consider the properties of the horizontal and vertical parts of the loop, contact zones, etc. separately. Each element of the unit cell is considered with respect to kinematics and force conditions, which determine behaviour

of the unit cell as a single whole system. Each unit cell, in turn, is considered with respect to conditions providing deformations of a system of unit cells as a whole sample. Having been arranged together unit cells determine the behaviour of a sample with integrated mechanical and geometrical properties inherited from the single unit cell and from each of its constituent elements. A sampling approach allows easy improvement of the model by applying any enhanced model for each constituent element.

To simplify arguments we consider fabric, which lies in a plane before it is subjected to tension. This enables us to assume that the Z co-ordinates are identical for each loop (Figure 2.2). Although *in plane* deformations are considered further, the model proposed is not restricted to 2D. Transformation of model to 3D deformation is discussed in section 5.2 below.

Yarn in fabric follows a periodical path, so that all loops have identical form. The co-ordinates of each loop in the plane (XY) could be expressed as:

$$\begin{cases} \{X^i\}_{n,k} = \{X^i\}_{0,0} + nb & n = \{...-1,0,1,...\} \\ \{Y^i\}_{n,k} = \{Y^i\}_{0,0} + ka & k = \{...-1,0,1,...\} \end{cases}, \qquad (2.14)$$

where $\{X^i\}_{0,0}$, $\{Y^i\}_{0,0}$ and $\{X^i\}_{n,k}$, $\{Y^i\}_{n,k}$ are sets of X and Y co-ordinates of a basic loop and of any arbitrary repeating loop in the structure respectively.

Loop path co-ordinates $\{X^i\}_{0,0}$ and $\{Y^i\}_{0,0}$ can be evaluated according to Table 2.3.

From the mechanical point of view, a single loop does not represent the mechanical properties of an elementary cell. Namely, deformation of loop in a real fabric is restricted considerably by neighbouring loops. Thus the effective rigidity of contacting loops relating to that of a single loop subjected to tensile force in the course direction could be as much as 10^3. This makes it necessary to take into account the influence of neighbouring loops on the behaviour of a single loop.

Taking into account (2.14) it is reasonable to sub-divide fabric into unit cells as shown in Figure 2.7 (a, b). The unit cell has dimensions in X and Y directions that are equal to

corresponding course and wale dimensions of the fabric (B_{kn} and A_{kn} in Figure 2.1). In Figure 2.7 (a), numeration of loops is used as presented in equation (2.14). Numeration of elementary cells is developed further as shown in Figure 2.7(b) (from the upper-left corner to bottom-right corner of the sample).

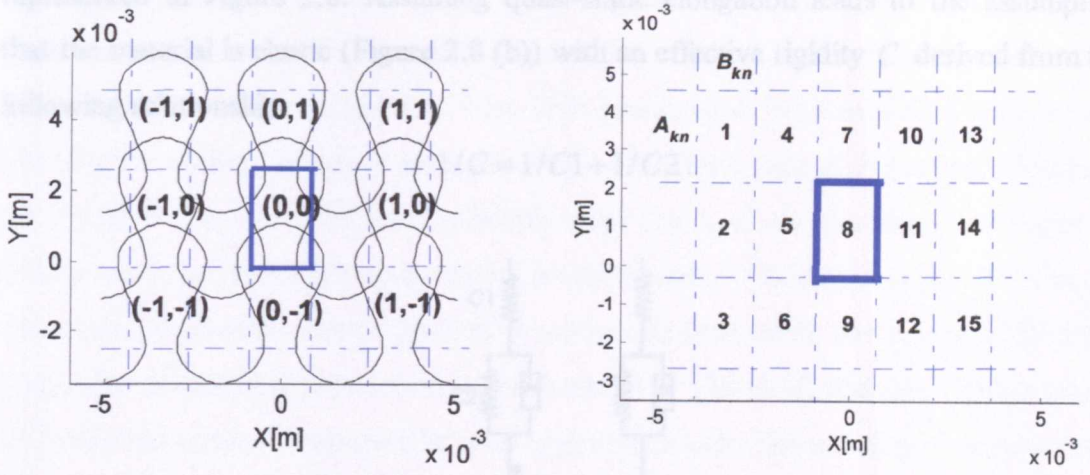

(a) *(b)*

Figure 2.7 (a, b) ***Sub-division of fabric sample into elementary cells.***

numbered loops – (a), numbered cells – (b).

Following to proposed sub-division of fabric, unit cell number 8 in Figure 2.7 (b) includes the following parts of loops (constituent elements):

- ✓ four contact zones of loop (0,1) and (0,-1) with loop (0,0);
- ✓ three free parts of loop (0,0);
- ✓ one free part of loop (0,-1).

Note that the unit cell defined as shown in Figure 2.7 (a, b) does not contain all of the elements to make up one whole loop.

Taking into account symmetry of the plain knit structure discussed in the previous section and equation (2.1), all unit cells can be assumed to have the same mechanical and geometrical properties. Unit cell number *11*, for instance, is equivalent to cell number *8* with a horizontal axis flip; they can be assumed to have the same properties.

Transmission of axial force from the horizontal part of loop to the vertical is restricted by yarn-to-yarn friction in the contact zones. However, the work done by friction forces is assumed to be negligibly small in comparison with the work done by other forces acting in stretched fabric. The assumption above enables to the creep flow of fabric to be neglected. One of the possible rheologic models of fabric material is represented in Figure 2.8. Assuming quasi-static elongation leads to the assumption that the material is elastic (Figure 2.8 (b)) with an effective rigidity C derived from the following relationship:

$$1/C = 1/C1 + 1/C2.$$

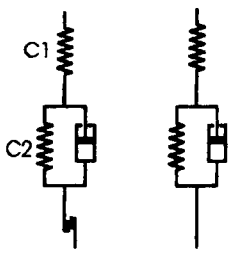

(a) *(b)*

Figure 2.8 (a, b) ***Possible rheological models of hereditarily elastic material.***

with creep flow – (a); without creep deformation – (b).

To prove that the assumption above is valid, extensive experimental research is required. We limit discussion with simple qualitative arguments. The value of the creep flow of the fabric ε_c could be up to 10-15% while full stress ε_{full} is approximately 150-200%*. Thus, ε_c comprises some 5-10% of the total stress. In fact, creep flow of oil-proof rubber achieves up to 17% of the total deformation [5].

If it is assumed that no friction force acts in the zones of mutual contact of yarns, yarn is free to slide from one part of the loop to another (from horizontal free part to vertical free part Figure 2.2). If in turn yarn is treated as an elastic rod with zero thickness this will cause the cell to collapse into one line when a small force is applied to the cell element (Figure 2.9). One of the factors which prevents cells (loops) from collapsing is yarn-to-yarn compression. Assuming yarn cross sections with known compression

rigidity makes it possible to depict the cell as shown in Figure 2.9. The unit cell is represented here as a closed yarn loop (blue and red curves), which is carried by pulleys. The centre of each pulley is free to move in the 2D plane XY. Springs in Figure 2.9 represent yarn-to-yarn compression.

Normally, yarn compression rigidity is a non-linear function of lateral contraction. Uncompressed yarn has low initial compression rigidity, however having been pre-compressed it resists considerably. Van Wyk proposed in [4] a model of compression of a fibre assembly, which is used widely for describing yarn compression. However, his model is acceptable only for relatively small levels of compression. In a paper by Grishanov *et al* [1] an improved model is represented. This model takes into account the minimum possible area of yarn cross section. In both cases, compression rigidity is a singular function of yarn's lateral contraction. In Van Wyk's model, rigidity grows infinitely when yarn cross section area approaches zero (he considered a *volume* of fibre assembly, which is presumably the same as the yarn cross-section area when one of the dimensions remains constant) and in the model proposed in [1] it tends to infinity when the yarn cross section area approaches to some minimum value. Further discussion of yarn compression rigidity is represented in section 2.3 below.

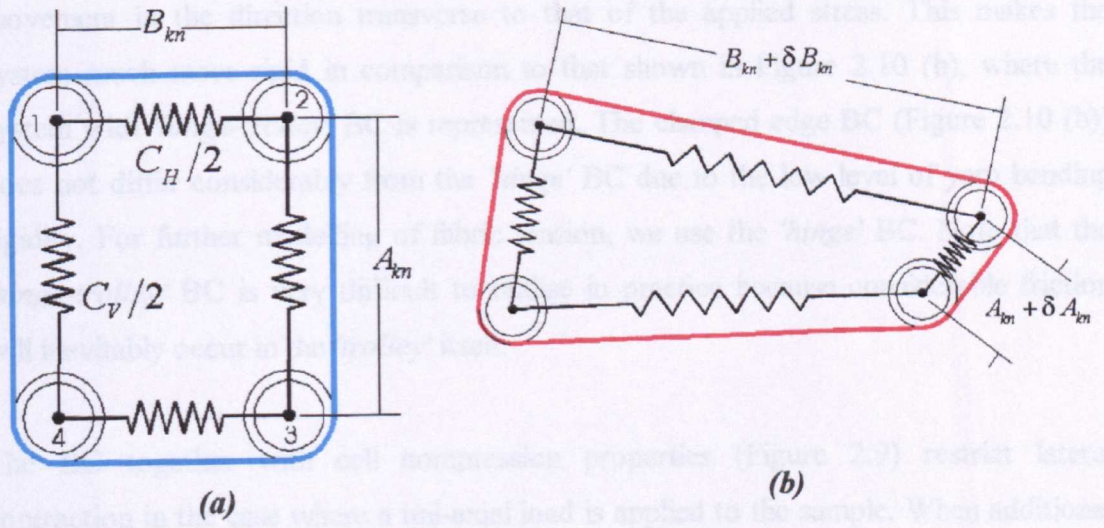

(a) *(b)*

Figure 2.9 (a, b) ***Rheologic scheme of cell element.***

initial state of unit cell — (a), in plane deformation of the unit cell— (b); blue curve – initially slack yarn; red curve – deformed yarn.

---

* *These data were estimated during tensile testing of fabric (see CHAPTER 4)*

Yarn is free to slide over the 'pulley' and, hence yarn length re-distribution occurs in the deformed cell. It is possible to describe yarn in the cell as a closed polygon (as shown in Figure 2.9), however we consider yarn as a set of yarn sections touching at the polygon vertexes. Each yarn is assumed to have an additional variable, which is used for yarn slippage (redistribution) description. Further discussion of this subject follows in section 2.3 below.

As opposed to the continuum mechanics, the cell represented in Figure 2.9 could not be sub-divided further into smaller cells. Rather it is possible to consider any size of cell, however a cell which is smaller than a loop dimension, has no physical sense. Moreover, it is not possible to consider one cell as a stable structure. In reality, fabric samples only remain stable when they have enough (about 10 by 10) loops in course and wale direction. Sample consisted of a small number of loops is unstable as it would tend to de-knit when subjected to a small force. This make it's necessary to consider fabric tension with regard to the sample dimension.

Boundary conditions (BC) are also very important when large displacements are considered. Thus, *'hinge'* BC in Figure 2.10 (c) restricts the edge points from movement in the direction transverse to that of the applied stress. This makes the system much more rigid in comparison to that shown in Figure 2.10 (b), where the system with *'hinge-trolley'* BC is represented. The clamped edge BC (Figure 2.10 (b)) does not differ considerably from the *'hinge'* BC due to the low level of yarn bending rigidity. For further modelling of fabric tension, we use the *'hinge'* BC. Note that the *'hinge-trolley'* BC is very difficult to realise in practice because considerable friction will inevitably occur in the *'trolley'* itself.

The BC together with cell compression properties (Figure 2.9) restrict lateral contraction in the case where a uni-axial load is applied to the sample. When additional extension forces act in the transverse direction each cell is subjected to stress in that direction. If the value of the transverse force is high enough cells could achieve extension in both directions.

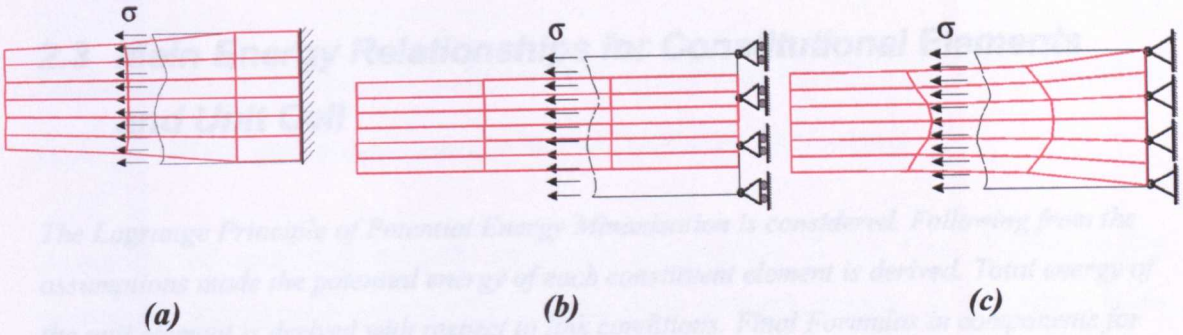

Figure 2.10. (a, b, c) ***Modal analysis of different boundary conditions for one-axial extension of fabric sample.***

clamped edge — (a), hinged-trolley edge — (b), hinged edge — (c).

The proposed model for fabric is similar to that which might be used for a thin membrane. Thus, the fabric can be considered to have zero bending rigidity. The scope of the problem is then restricted by consideration fabric in an extended condition.

Qualitative analysis of simple cell structures is represented in section 3.9.

2.3 Main Energy Relationships for Constitutional Elements and Unit Cell

The Lagrange Principle of Potential Energy Minimisation is considered. Following from the assumptions made the potential energy of each constituent element is derived. Total energy of the unit element is derived with respect to link conditions. Final Formulas in components for subsequent numerical analysis are represented in Appendix B 2-5.

The scalar functional $\mathrm{E}(\underline{q})$ gives the *total potential energy* of the mechanical system. It can be expressed through the vector of virtual external forces $\underline{F}$ and co-ordinates $\underline{q}$ of the system as:

$$\mathrm{E}(\underline{q}) = \Pi\left(\underline{q}\right) - \underline{F} \cdot \underline{q} \tag{2.15}$$

where $\Pi(\underline{q})$ defines the potential energy of the system.

Note that system co-ordinates (components of $\underline{q}$) are independent and determine the position of the system unambiguously.

The Lagrange principle points out that on real values of displacements the variation

$$\delta\left(\mathrm{E}(\underline{q})\right) = 0 \tag{2.16}$$

and the functional $\mathrm{E}(\underline{q})$ assumes its local minimum.

The sum on right side of equation (2.15) is the work done by external forces $\underline{F}$ with corresponding displacements $\underline{q}$ of the system.

Assuming a system of equations, which restricts deformation of the system in the form $\underline{\xi}\left(\underline{q}\right) = \underline{0}$ it is possible to reformulate the Lagrange principle by introducing a new function for total energy E_c:

$$\mathrm{E}_c\left(\underline{q}, \underline{\lambda}\right) = \mathrm{E}\left(\underline{q}\right) + \underline{\xi}\left(\underline{q}\right) \cdot \underline{\lambda} \tag{2.17}$$

where E is the total energy of the system free of constraints;

$\underline{\lambda}$ is a vector of additional co-ordinates, the so called Lagrange multipliers.

Replacing $E(\underline{q})$ in equation (2.16) with $E_c(\underline{q},\underline{\lambda})$ from equation (2.17) the Lagrange principle for the mechanical system with constraints can be obtained.

A number of numerical methods are based on equation (2.16). One of the possible numerical algorithms based on (2.16) is the finite element method. To provide a basis for the work in this thesis the concepts of the finite-element method and its application to the problem is discussed briefly in CHAPTER 3. Potential energy of complicated mechanical systems can be expanded into terms, where each term represents the potential energy of an element of the system. The potential energy of each part of system is derived below.

2.3.1 Effective Rigidity Modulus of pre-bent yarn

Replacing of a pre-bent yarn by a non-linear spring with corresponding effective rigidity modulus

To obtain the mechanical properties of a unit cell (Figure 2.9) it is necessary to determine the effective properties of each element. Namely, each part of the cell should be replaced by an element with the same mechanical properties. Thus, a contact zone is emulated by a *'helix'* element, which is considered below; the free part of a yarn loop can be replaced by a spring with some non-linear properties. Effective related deformation ε_E and corresponding effective rigidity D_E (see Figure 2.11) define the mechanical properties of the spring. Effective deformation ε_E can be defined as the relative deformation of a chord connected to the two ends of the element.

The part of the loop, which is not involved in mutual contact (*free zone*), follows a 3D path, which is normally not straight. The mechanical properties of the free zone could be represented as the stretching of pre-bent rod. When subjected to a relatively small tensile force it straightens. Bending is dominant during the initial deformation. When the rod approaches to straight line, tensile deformation starts to affect behaviour of the system. Taking into account that bending rigidity of a yarn is very small in comparison with tensile rigidity, it is possible to divide the process of pre-bent yarn deformation

into two phases: *straightening* and *tension* (Figure 2.11 (a, b, c)). We assume that during the *straightening* phase, only bending deformation takes place in the yarn and during *tensioning,* only tensile deformation takes place in yarn.

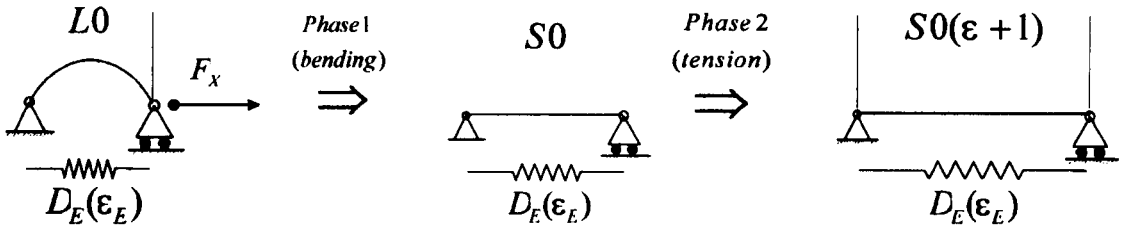

(a) *(b)* *(c)*

Figure 2.11 (a, b ,c) ***Two phases of deformation of initially bent rod subjected to force*** F_X.

initially bent rod — (a), straighten rod — (b), extended rod —(c).

We assume a known relationship for the tensile rigidity D as a function of the relative deformation of a straight rod/yarn ε. In the present work, tensile curves of yarns were obtained experimentally (section 4.4). No limitations are imposed on the tensile properties of the yarn; it is formally possible to take into account time-dependent properties of yarns.

Effective deformation of yarn ε_E during second phase of deformation can be expressed as following (Figure 2.11 (c)):

$$\varepsilon_E = \frac{S0(\varepsilon+1) - L0}{L0} \tag{2.18}$$

where ε is relative deformation of straight yarn,

$L0$ is length of chord connected yarn ends,

$S0$ is initial arc length of yarn.

Taking into account that $D\varepsilon = D_E \varepsilon_E \equiv F_X$ and (2.18) yields the following expression for effective rigidity D_E:

$$D_E = D\varphi(\varepsilon) \tag{2.19}$$

where $\varphi(\varepsilon) = \dfrac{L0}{\left(1+1/\varepsilon\right)S0 - L0/\varepsilon}$.

Maximum value of effective rigidity D_E is limited by the value of D_E^{∞}:

$$D_E^{\infty} = D\lim_{\varepsilon\to\infty}\varphi(\varepsilon) = D\frac{L0}{S0}.$$

For evaluation of the effective rigidity modulus D_E for the first phase of deformation, a *non-linear problem of rod straightening* needs to be resolved. To approach the problem a finite-element model of the pre-bent rod subjected to a tensile force F_X with boundary conditions as shown in Figure 2.11 (a, b, c) has been implemented (Figure 2.12). To simplify the problem only *in plane* deformation of the rod was considered. The initial form of rod's axis is assumed to be circular arc with arc length and chord equal to that of a *'real'* curve. The shape of *'real'* curve had been obtained according to the algorithm considered in section 2.1 above. Bending and tensile rigidities of rod/yarn were obtained experimentally (sections 4.2 and 4.4).

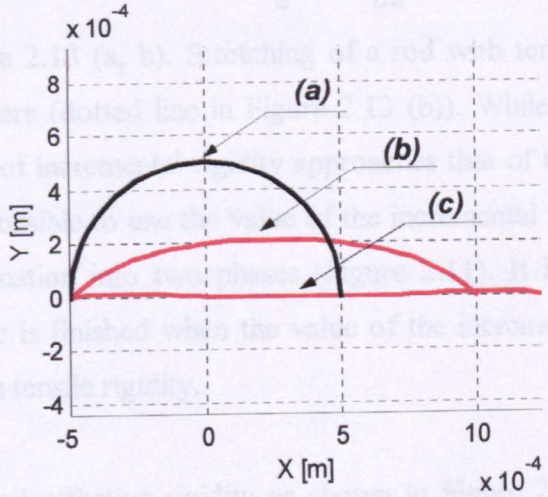

Figure 2.12 ***A typical example of stretching of pre-bent rod with conditions as shown in Figure 2.11***

black curve – initial position – (a), red curves – deformed rod (intermediate – (b) and final position – (c)).

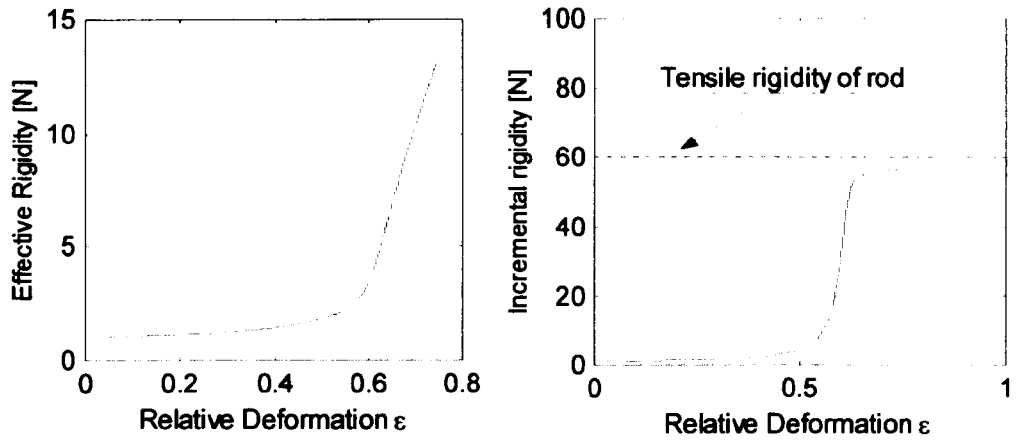

(a) *(b)*

Figure 2.13 (a, b) ***Effective and incremental rigidity of pre-bent rod.***

effective rigidity of the rod as a function of ε – (a), incremental rigidity of the rod as a function of ε and tensile rigidity of straight rod (dotted line) – (b).

The effective and incremental rigidity of a stretched rod undergoing extension as illustrated in Figure 2.12 is defined as $\frac{F}{\varepsilon}$ and $\frac{\partial F}{\partial \varepsilon}$ respectively. These rigidities are represented in Figure 2.13 (a, b). Stretching of a rod with tensile rigidity equal to 60 [N] is considered there (dotted line in Figure 2.13 (b)). While deformation of the rod increases, the value of incremental rigidity approaches that of the tensile rigidity of the rod. This makes it possible to use the value of the incremental rigidity as a criterion for separation of deformation into two phases (Figure 2.11). It is assumed that the first (straightening) phase is finished when the value of the incremental rigidity reaches the level of 99% of rod's tensile rigidity.

Numerically evaluated effective rigidity as shown in Figure 2.13 and equation (2.19) make it possible to obtain piece-wise function for effective rigidity for the range of all possible yarn deformations. Finally, it is possible to express effective rigidity in the form $D_E = D_E(\varepsilon_E)$. We omit subscript 'E' in further argument, assuming ε to be the effective deformation of the element.

2.3.2 Model of Free Yarn in Loop ('Thread' Element)

The potential energy of an element with variable initial length is considered

We consider a straight elastic rod with effective mechanical properties as obtained above. The rod has initial length a_0 and tensile rigidity can be written in the form: $D = D(\varepsilon)$ (note that subscript *'E'* is omitted here and following, as the 'effective' characteristics are considered), where ε is relative deformation of the rod. The components of the vector of virtual co-ordinates $\underline{q}$ (equation (2.15)) are chosen as $\{a, as\}$, where a is the current distance between the ends of rod and $(as + a_0)$ is current initial length of the rod. Relative deformation of the rod can be expressed as follows:

$$\varepsilon = \frac{a - (a_0 + as)}{(a_0 + as)}. \tag{2.20}$$

Potential energy Π can be expressed as the curvilinear $\{a, as\}$ integral from initial to deformed position:

$$\Pi = \int_{A \to B} D(\varepsilon)\varepsilon\big(da - d\big((\varepsilon + 1)as\big)\big) \tag{2.21}$$

where A and B are points on the plane $\{a, as\}$ with co-ordinates $\{a_0, 0\}$ and $\{a, as\}$ respectively.

Substituting (2.20) into (2.21) yields the following relationship for potential energy:

$$\Pi(\{a, as\}) = \int_{A \to B} D(\varepsilon)\big(Q_{as}(a, as)\,das + Q_a(a, as)\,da\big) \tag{2.22}$$

where $Q_{as}(a, as) = -\varepsilon\dfrac{a_0 a}{(a_0 + as)^2}$, $Q_a = \varepsilon\dfrac{a_0}{a_0 + as}$.

It is possible to show that integral (2.22) is independent of path and, hence, function $\Pi(\{a, as\}) = U(B) - U(A)$, where $U(\{a, as\})$ is some function. To show that, one can make sure that one of following relationships ((2.23) or (2.24)) holds:

$$\frac{\partial\big(D(\varepsilon)Q_a(a, as)\big)}{\partial as} \equiv \frac{\partial\big(D(\varepsilon)Q_{as}(a, as)\big)}{\partial a} \tag{2.23}$$

Relationship (2.23) could be expanded as following:

$$D(\varepsilon)\frac{\partial Q_a}{\partial as}+Q_a\frac{\partial D(\varepsilon)}{\partial \varepsilon}\frac{\partial \varepsilon}{\partial as}\equiv D(\varepsilon)\frac{\partial Q_{as}}{\partial a}+Q_{as}\frac{\partial D(\varepsilon)}{\partial \varepsilon}\frac{\partial \varepsilon}{\partial a}. \qquad (2.24)$$

For evaluation of potential energy Π any curve with ends at points A and B could be chosen. Potential energy, hence, can be expressed as follows:

$$\Pi(a,as)=\int_{a_0}^{a} D\big(\varepsilon(a,0)\big)Q_a(a,0)\,da+\int_{0}^{as} D\big(\varepsilon(a,as)\big)Q_{as}(a,as)\,das. \qquad (2.25)$$

Introducing Cartesian co-ordinate system XYZ and taking into account that

$$\begin{cases} a_0=\sqrt{(x0_2-x0_1)^2+(y0_2-y0_1)^2+(z0_2-z0_1)^2} \\ a=\sqrt{(x_2-x_1)^2+(y_2-y_1)^2+(z_2-z_1)^2} \\ as=s_1+s_2 \end{cases} \qquad (2.26)$$

where $\{x0_1,x0_2,y0_1,...,z0_2\}$ are the initial co-ordinates of rod's ends,

$\{x_1,x_2,y_1,...,z_2\}$ are the current co-ordinates of rod's ends ,

$\{s_1,s_2\}$ are the change of initial length via rod's ends,

it is possible to obtain potential energy (2.25) in components. Full expression of potential energy is not represented here because of the size of the final formulae. Assuming that the Z component is zero in set of equations (2.26) the potential energy for *in plane* deformation can be derived.

A constituent element derived according to the arguments above will subsequently be called a *'thread element'*.

2.3.3 Model of Mutual Yarn Compression in Elementary Cells ('Side' and 'Height' elements)

The potential energy of two contacting yarns is derived. Compression rigidity of yarn is discussed. Mechanism of mutual yarn contact in the unit cell is discussed, two models are considered.

We consider here two yarns with compressible cross sections as shown in Figure 2.14. We denote the relative potential energy of compressed yarn per unit length of yarn as $\widetilde{\Pi}\equiv \Pi/L_{cont}$, where L_{cont} is the length of the contact zone. The relative potential energy is defined for each contacting yarn separately and can be written in the form:

$$\widetilde{\Pi}(a) = \int_{a_0}^{a} K\left(\frac{(a-a_0)}{2}\right)\frac{(a-a_0)}{2}da \qquad (2.27)$$

where K is the specific compression rigidity of the yarn related to the yarn length,

a_0 and a are initial and current distance between yarn's axes respectively.

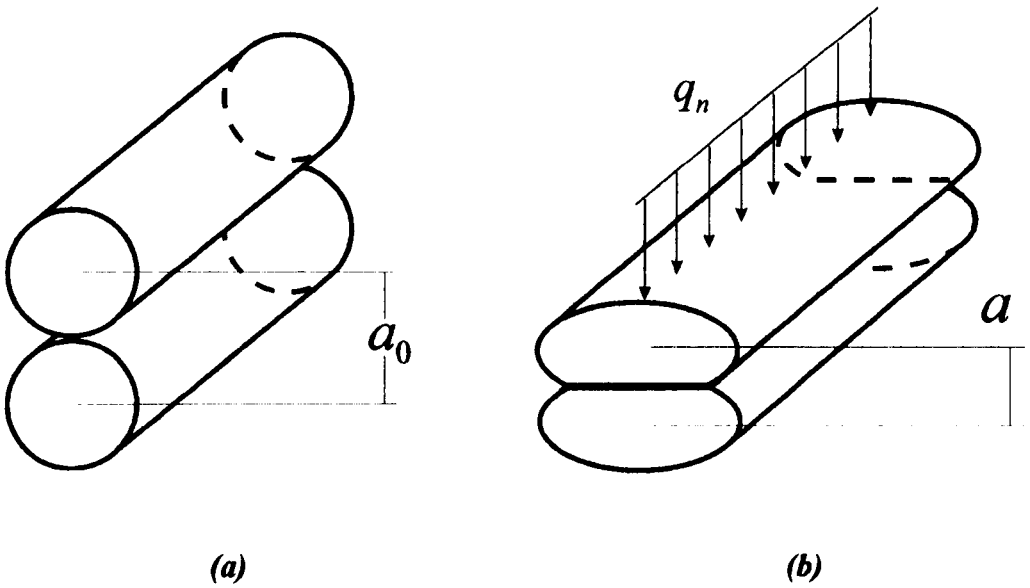

(a) *(b)*

Figure 2.14 (a, b) ***Mutual compression of two yarns.***

initial position – (a), deformed position – (b).

According to Grishanov *et al* [1] the function $K(z)$ can be determined as:

$$K(z) = K0\,L_{cont}\frac{(1-z_{\min})}{z(z-z_{\min})^3} \qquad (2.28)$$

where $z = a/2D_{yarn}$ (a is distance between yarn axes determined as shown in Figure 2.14, D_{yarn} is the yarn diameter);

L_{cont} is the length of yarn involved in contact;

$K0$ is the initial value of compression rigidity, which can be obtained from experiment;

$z_{\min}$ is minimum value of z ($z_{\min} = 0.2$ is used further as estimated by Grishanov *et al* [1]).

Introducing the Cartesian co-ordinate system, XYZ, and taking into account the first two relations from equation (2.26) makes it possible to express $\widetilde{\Pi}(a)$ in components.

Compression of two neighbouring yarns in the unit cell is much more complicated in nature than shown in Figure 2.14. Moreover, yarn from one cell could be involved in mutual contact with yarn from a neighbouring cell. A deformed unit cell could in turn have an arbitrarily shape with only one restriction that it remains a quadrilateral without self-intersections. At the same time, the level of mutual yarn compression in a unit cell depends upon the deformation of the cell. Thus, it is necessary to determine a measure of the mutual compression (a in equation (2.27)) with respect to unit cell deformation. It is possible to use the current length of the cell side as a measure of mutual compression, or adjust a with the current area, S, of unit cell (Figure 2.15 (b, c)). However, both approaches are not good enough. A cell subjected to deformation as shown in Figure 2.15 (b), changes its area, however all sides length remains constant. Thus, in this case it is not possible to use length of the side to obtain a measure of the mutual compression; otherwise, compression will not occur in deformed cell. It can be seen that, in the case of deformation of the unit cell as shown in Figure 2.15 (c), relating the compression with cell area S is also not acceptable.

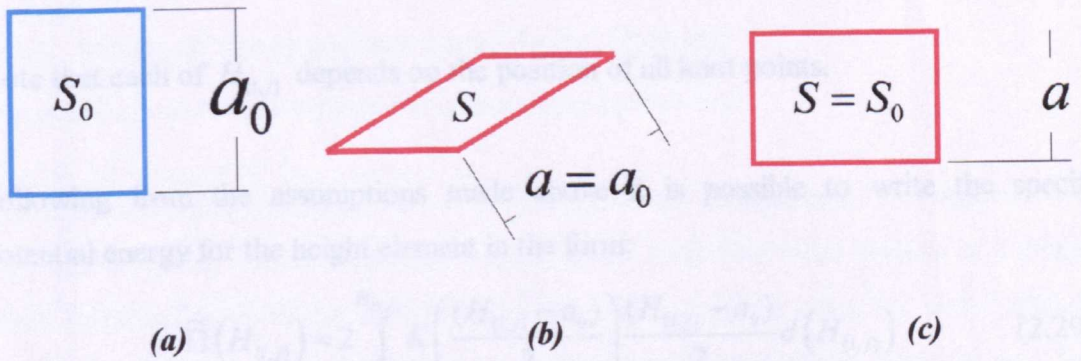

Figure 2.15 (a, b, c) ***Two possible shapes of deformed unit cell.***

initial shape of unit cell – (a), shear deformation with constant side length – (b), complex deformation with constant area of unit cell – (c).

In some special cases of fabric deformation, using side length to give a measure of compression gives good results. Respective constitutional element where the measure of compression is defined as a side length we will call *'side element'*. Using the *side*

element is very attractive due to its simplicity; however, in most cases it causes method instability or very slow convergence.

To approach the problem 'height element' is proposed below. The unit cell is subjected to arbitrary deformation as represented in Figure 2.16. Vertexes of the quadrilateral numbered from 1 to 4, represent knot points of the unit cell. We define the measure of compression $H_{\{1,4\}}$ as the average value of two heights $h1$ and $h2$. The same parameter $H_{\{i,j\}}$ could be defined for each couple of neighbouring points: $\{1,2\}$, $\{2,3\}$, $\{3,4\}$ as shown in Figure 2.16 for knot points $\{4,1\}$.

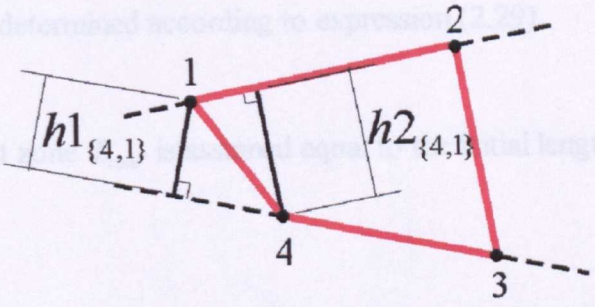

Figure 2.16 ***Arbitrary deformation of unit cell.***

knot points are numbered from 1 to 4.

Note that each of $H_{\{i,j\}}$ depends on the position of all knot points.

Following from the assumptions made above it is possible to write the specific potential energy for the height element in the form:

$$\widetilde{\Pi}\left(H_{\{i,j\}}\right)=2\int_{a_0}^{H_{\{i,j\}}} K\left(\frac{(H_{\{i,j\}}-a_0)}{2}\right)\frac{(H_{\{i,j\}}-a_0)}{2}d\left(H_{\{i,j\}}\right) \qquad (2.29)$$

where $\{i,j\}=\{1,2\},\{2,3\},\{3,4\},\{4,1\}$.

The integral in (2.29) is multiplied by 2 because two yarns are involved in the contact.

To derive the final expression for the potential energy for the *height element* we assume firstly that neighbouring sides of the unit cell are not involved in mutual compression. Thus sides $\{4,1\}$ and $\{1,2\}$ in Figure 2.16 do not interact, while sides

{1,2} and {3,4} are involved in mutual compression. Thus, only two pairs of opposite sides (yarns) of the unit cell (loop) are involved in mutual compression. At the same time, four *height elements* are defined according to relationship (2.29). We assume that one *height element* represents mutual compression of two half-lengths of opposite sides. Thus, element $H_{\{4,1\}}$ in Figure 2.16 represents compression of half of sides {1,2} and {3,4}. Finally, it is possible to express potential energy Π for the *height element* in the form:

$$\Pi\left(H_{\{i,j\}}\right) = \widetilde{\Pi}\left(H_{\{i,j\}}\right)\frac{L_{cont}}{2} \tag{2.30}$$

where L_{cont} is the length of the contact zone,

$\widetilde{\Pi}\left(H_{\{i,j\}}\right)$ is determined according to expression (2.29).

The length of contact zone L_{cont} is assumed equal to the initial length of the unit cell side.

Introducing the Cartesian co-ordinate system, *XYZ*, and taking into account the first two relations from (2.26) yields an expression for the potential energy in components.

2.3.4 Model of Yarns contact zone ('Helix' Element)

The model of two intersected yarns in contact zone is presented.

The behaviour of a yarn in contact with another is very complicated. Unevenness of the yarn cross-section makes it virtually impossible to determine exact bounds of a contact zone. Friction forces in the contact are cause additional difficulties for stress analysis. Assuming that a yarn has non-linear properties adds to the problem, which is very hard to resolve. To approach the problem we make the following assumptions.

1. Yarn has circular cross section with diameter equal to D_{yarn}.
2. The initial arc length L_h of each of the contact zones (Figure 2.2) is determined according to the algorithm described in section 2.1 above.
3. The 3D path of the yarn axis in the contact zone is approximated by a 3D helix with initial diameter equal to D_{yarn}.

4. The helix makes a half turn around its axis (azimuth angle φ equals to π, and remains constant during fabric deformation).
5. During deformation of the fabric, the 3D path of the yarn axis remains helical with the diameter changing due to compression of the yarns in contact zone.
6. During deformation of the fabric, the helix changes its arc length due to withdrawal force acting at the ends of the yarns involved in the contact.
7. Mechanical properties of contact zone are located at the unit cell vertexes, so that the orientation of the helix axis is not critical.
8. Two helixes, which represent two yarns in the contact zone both have identical form and differ by π in azimuth angle. An identical deformation of the both helixes is assumed.

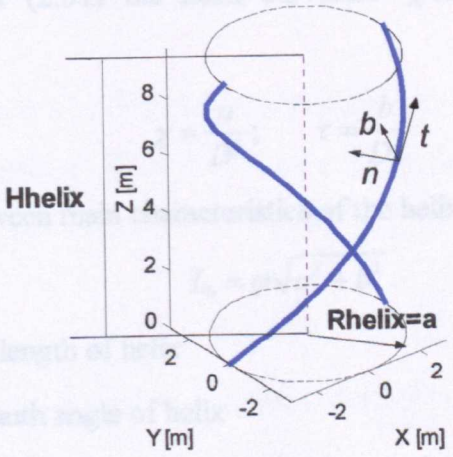

Figure 2.17 ***Model of the contact zone***

blue curves represent yarns axes, black curves represent projection of yarn axes onto a plane perpendicular to helix axis (doted line); unit vectors $\underline{t},\underline{n},\underline{b}$ *represent natural basis vectors of the helix (tangent, normal and bi-normal respectively).*

The constituent element, which represents the yarn in the contact zone will be referred as the *'helix element'*. The *helix element* is aimed to link length re-distribution co-ordinates $s1$ and $s2$ (see equation (2.26)) of two neighbouring *thread elements* (free parts of yarn in loop). The potential energy of the *helix element* is independent of its geometrical position, thus an external load only exerts work on length re-distribution co-ordinates. Having been arranged together with other constitutional elements, the

helix element is subjected to withdrawal forces, which tend to change the initial length of yarn involved in the contact.

The helix is defined by the following vector equation:

$$\underline{R} = a\cos\left(\frac{s}{D}\right)\underline{i} + a\sin\left(\frac{s}{D}\right)\underline{j} + b\frac{s}{D}\underline{k} \tag{2.31}$$

where a and b are helix radius and pitch respectably;

$D = \sqrt{a^2 + b^2}$;

s is arc length parameter of helix;

$\underline{i}, \underline{j}, \underline{k}$ are unit vectors in Cartesian co-ordinate system XYZ which define directions OX, OY, OZ respectively.

Taking into account (2.31) the helix curvature χ and helix torsion τ could be expressed as:

$$\chi = \frac{a}{D^2}; \qquad \tau = \frac{b}{D^2}. \tag{2.32}$$

The relationship between main characteristics of the helix may be written in form:

$$L_h = \varphi\sqrt{a^2 + b^2} \tag{2.33}$$

where L_h is the arc length of helix

φ is the azimuth angle of helix

a and b are the helix radius and pitch respectively.

The potential energy of **one** deformed helix can be expressed as:

$$\Pi = \int_{a_0}^{a} L_h K_c\, a\, da + \int_{h_0}^{h} L_h K_c \left(\frac{h}{2}\right) d\left(\frac{h}{2}\right) + \int_{\chi_0}^{\chi} K_\chi\, \chi\, d\chi + \int_{\tau_0}^{\tau} K_\tau\, \tau\, d\tau \tag{2.34}$$

where K_c is compression rigidity coefficient of yarn-to-yarn compression (see equation (2.28) and section 4.6);

K_χ is yarn bending rigidity coefficient (see section 4.2);

K_τ is yarn torsion rigidity coefficient (see section 4.3);

$h = \pi b$.

Substituting the above equations (2.32) and (2.33) into the expression for the potential energy (2.34), it is possible to express the potential energy of the deformed helix trough virtual co-ordinates a and b. Having been arranged together with the *thread element*, the *helix element* is subjected to external load, which tends to withdraw yarn from the contact zone. Thus, the external load does not exert any work on virtual co-ordinates $\{a,b\}$. To obtain the potential energy of the full system, additional virtual co-ordinates with corresponding constraint equations need to be introduced.

Assuming that two contacting yarns are deformed identically we introduce two additional parameters of length re-distribution (length withdrawal) $s1$ and $s2$ in the way that:

$$(s1+s2)=\Delta L_h \tag{2.35}$$

where ΔL_h is an increment of helix arc length.

It is possible to obtain a new expression for the potential energy with regard to the above constraint equation (2.35). If Lagrange multipliers technique is used the constraint equation (2.35) could be written in the form (see equation (2.17) in section 2.3 above):

$$\Pi_\lambda=((s1+s2)-\Delta L_h)\lambda$$

where λ is an additional virtual co-ordinate (Lagrange multiplier).

Finally, the potential energy of the system of two contacting helixes could be expressed through five virtual co-ordinates $\{a,b,s1,s2,\lambda\}$ in the form:

$$\Pi_{full}=\Pi_{a,b}+\Pi_\chi+\Pi_\tau+\Pi_\lambda \tag{2.36}$$

where $\Pi_{a,b}$ is the potential energy of yarn-to-yarn compression in the directions $\underline{n}$ and $\underline{b}$ (Figure 2.17);

Π_χ is the potential energy of yarn bending;

Π_τ is the potential energy of yarn torsion;

Π_λ is the potential due to the constraint equation (2.35).

Finally the potential energy of the *helix element* is expressed through five virtual co-ordinates: $\{a, b, s1, s2, \lambda\}$ helix radius, helix pitch, two length re-distribution parameters and an additional constraint parameter respectively.

In expression (2.36) yarn bending and torsion rigidity are taken into account. It is possible to neglect yarn bending, tension and torsion in contact zone. To show this we consider a testing example of the *helix element* subjected to an external withdrawal force. We assume that the external force exerts work on virtual co-ordinate $s2$ and co-ordinate $s1$ is restricted by an external potential Π_{ext}:

$$\Pi_{ext} = \int_0^{s1} K_c L_{cont}\, s1\, ds1. \tag{2.37}$$

The above expression for external potential simulates mutual yarn-to-yarn compression outside the contact zone (yarn-to-yarn compression of sides in the unit cell).

The potential energy of the testing system considered can be derived by adding an external potential energy term (2.37) into the expression for full energy of the *helix element* (2.36). The solution obtained with aid of (2.16) is represented in Figure 2.18. The black curve represents the total energy involved in yarn bending and torsion (Π_χ and Π_τ (2.36)). The red and green curves represent energy involved in yarn-to-yarn compression in $\underline{n}$ and $\underline{b}$ directions (Figure 2.17) within the contact zone ($\Pi_{a,b}$ respectively (2.36)). The magenta curve represents external energy (Π_{ext} (2.37)). The energy involved in torsion and bending comprises less then 0.1% of the total energy of the system. This makes it possible to neglect terms Π_χ and Π_τ in the expression for the full energy of the *helix element* (2.36).

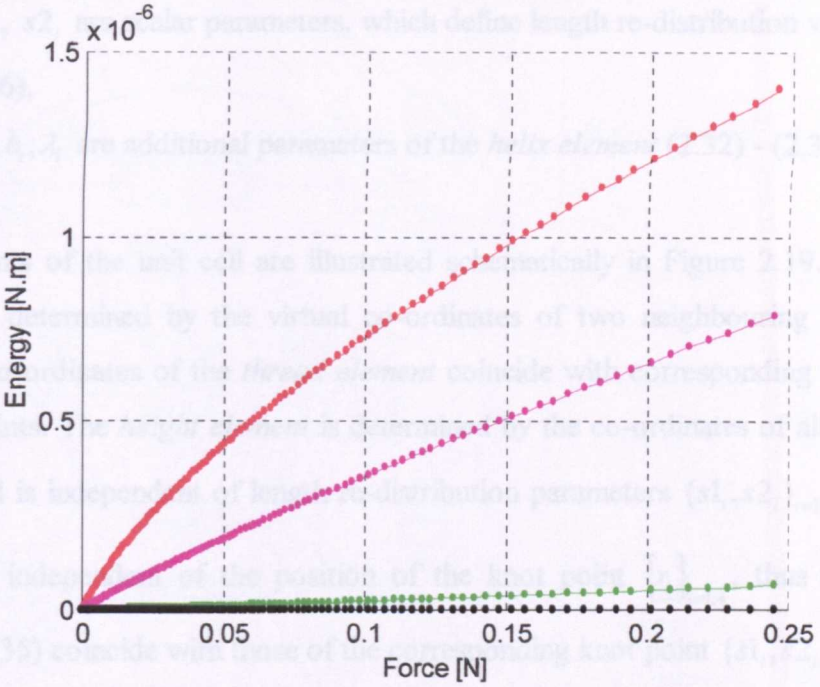

Figure 2.18 ***Energy distribution in deformed helix.***

yarn mutual compression in direction $\underline{n}$ — red curve, compression of neighbouring yarns in cell – magenta curve, yarn mutual compression in direction $\underline{b}$ — green curve, yarn bending, twisting plus torsion — black curve.

2.4 Boundary Conditions

The micro mechanical model of boundary conditions for constitutional elements in the unit cell is considered. Boundary conditions for the unit cell in whole system are discussed.

Constituent elements considered in 2.3 above are designed to simulate behaviour of corresponding parts of the unit cell. To simulate behaviour of the unit cell as a single whole the constituent elements should be arranged together with respect to some boundary conditions. We assume mutual contact of elements take place at knot points of the unit cell. To simplify further arguments, we define each knot point $i = \{1:4\}$ by a set of virtual co-ordinates $\{q_i\}$:

$$kp = i \underset{i=\{1:4\}}{\Rightarrow} \{q_i\} = \{\underline{r}_i, s1_i, s2_i, a_i, b_i, \lambda_i\} \tag{2.38}$$

where $\underline{r}_i$ is the position vector of the unit cell in 3D or in 2D,

$s1_i$, $s2_i$ are scalar parameters, which define length re-distribution via knot points (2.26),

a_i, b_i, λ_i are additional parameters of the *helix element* (2.32) - (2.35).

The elements of the unit cell are illustrated schematically in Figure 2.19. The *thread element* is determined by the virtual co-ordinates of two neighbouring knot points, thus, the co-ordinates of the *thread element* coincide with corresponding co-ordinates of knot points. The *height element* is determined by the co-ordinates of all knot points $\{\underline{r}_i\}_{i=1:4}$ and is independent of length re-distribution parameters $\{s1_i, s2_i\}_{i=1:4}$. The *helix element* is independent of the position of the knot point $\{\underline{r}_i\}_{i=1:4}$, thus co-ordinates $\{s1, s2\}$ (2.35) coincide with those of the corresponding knot point $\{s1_i, s2_i\}_{i=1:4}$.

Following on, from equation(2.38), the unit cell (k) is defined by a set of virtual co-ordinates $\{q_i\}_{i=1:4}^{(k)}$ Figure 2.20, where (k) is the number of the cells in the system. In the whole system, the neighbouring cells or some boundary conditions affect the deformation of each adjacent cell. We assume that contact of two neighbouring cells takes place only at the knot points. Assuming two cells (k) and (m) have joint knot points i and j respectively, yields virtual co-ordinates of cell (k): $\{q_i\}^{(k)}$ coincident with those of cell (m): $\{q_j\}^{(m)}$.

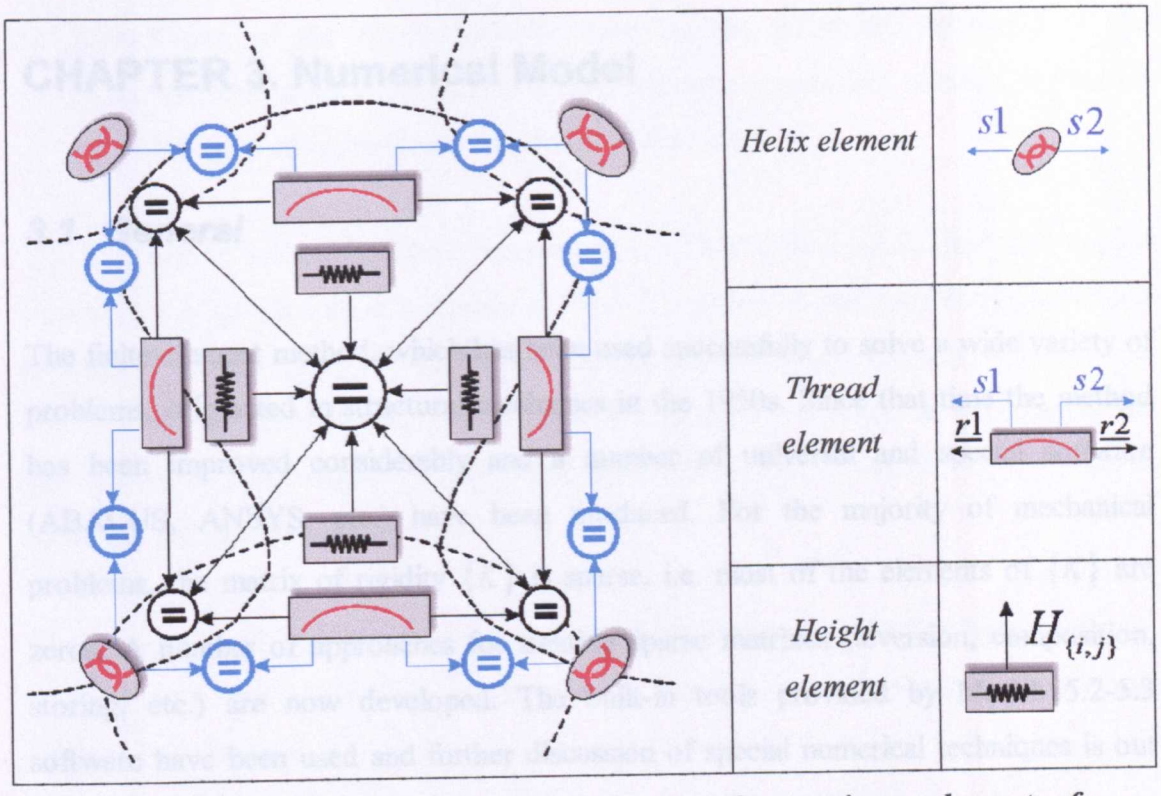

Figure 2.19 ***Schematic illustration of the rheology of a constituent elements of a unit cell.***

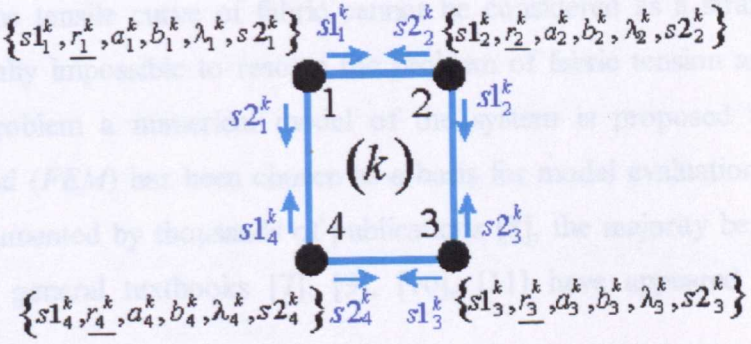

Figure 2.20 ***Virtual co-ordinates for unit cell.***

By restricting some co-ordinates at the knot points, different boundary conditions can be introduced. The main emphasis made here is on the study of uni-axial extension of a sample when two opposite edges are clamped. We assume that in a clamped knot point (i) an increment of virtual co-ordinates $\{s1_i, s2_i, a_i, b_i, \lambda_i\}$ is equal to zero. Additional kinematic relationships for the position of knot points subjected to different boundary conditions can be obtained following well-known logic applied to the general problem of shell (plate) deformation.

CHAPTER 3. Numerical Model

3.1 General

The finite-element method, which has been used successfully to solve a wide variety of problems, originated in structural mechanics in the 1950s. Since that time the method has been improved considerably and a number of universal and special software (ABACUS, ANSYS, etc.) have been produced. For the majority of mechanical problems, the matrix of rigidity $\{K\}$ is sparse, i.e. most of the elements of $\{K\}$ are zeros. A number of approaches for treating sparse matrixes (inversion, composition, storing, etc.) are now developed. The built-in tools provided by Matlab 5.2-5.3 software have been used and further discussion of special numerical techniques is out of scope of the present work.

The behaviour of fabrics is considerably non-linear. Even when subjected to relatively small forces the tensile curve of fabric cannot be considered as a straight line. This makes it virtually impossible to resolve the problem of fabric tension analytically. To resolve the problem a numerical model of the system is proposed below. Finite-element method (*FEM*) has been chosen as a basis for model evaluation. The FEM is now well documented by thousands of publications [8], the majority being specialised papers. More general textbooks [7], [9], [10], [11] have appeared during recent decades.

Although the formulation can differ significantly from problem to problem, FEM can be distinguished by the following principal features [6], [7].

1. The physical region of the problem is sub-divided by a mesh of imaginary lines or surfaces into sub-regions, the so-called finite-elements (*FE*).
2. One or more of the dependent variables is approximated in functional form over each element; the parameters of these shape functions become the unknowns of the problem.

3. Substitution of the above approximations in the governing equations of the problem yields a set of equations in the unknown parameters, which can then be solved to give an approximate solution to the problem.

The unit cell of knitted structure represented in CHAPTER 2 subdivides the physical region of the sample into sub-regions or FEs. A number of unit cells can be arranged together to form a larger FE. Constituent elements approximate deformation of the unit cell and virtual co-ordinates of the unit cell (Figure 2.20) are, in fact, unknown parameters of approximation. Governing equations can be obtained with regards to Lagrange principle (2.16).

The term *unit cell* introduced in CHAPTER 2 has the same meaning as the term *finite-element* used here. However, the term finite element is used where the numerical procedure is implied.

3.2 Main Finite-element Relationships

The potential energy Π of a system is a scalar function of the vector of virtual co-ordinates or virtual displacements $\underline{q}$ of a mechanical system (equation (2.15)). Components of $\underline{q}$ should be independent and determine unambiguously the position of the system. According to the Lagrange principle (2.16), the full energy of system $\mathrm{E}(\underline{q})$ attains a local minimum at real value of $\underline{q}$.

We consider a system in an equilibrium state with a vector of virtual co-ordinates $\underline{q}^0$ and external force $\underline{F}^0$. If the system is disturbed by an additional virtual force $\Delta\underline{F}$, the virtual co-ordinates will change by $\Delta\underline{q}$ so that the new position of the system becomes $\underline{q}^0 + \Delta\underline{q}$. If the value of $\Delta\underline{q}$ is 'small' enough, it is possible to assume that the minimum value of the total energy $\mathrm{E}(\underline{q})$ ***necessarily and sufficiently*** coincides with point where derivatives of $\mathrm{E}(\underline{q})$ with respect to virtual co-ordinates $\underline{q}$ is a zero-vector:

$$\mathrm{E}(\underline{q}^0 + \Delta\underline{q}) = \min\left\{\mathrm{E}(\underline{q})\right\} \Leftrightarrow \left.\frac{\partial \mathrm{E}}{\partial \underline{q}}\right|_{\underline{q}=\underline{q}^0+\Delta\underline{q}} = \underline{0}. \tag{3.1}$$

Note that the derivative of a scalar function with respect to a vector gives a vector. Vector $\underline{0}$ in the right part of logical relationship (3.1) has the same dimensions as the vector of the virtual co-ordinates $\underline{q}$. The second derivative of a scalar function with respect to a vector gives a tensor of second order.

Expanding the right part of logical relationship (3.1) into a Taylor series of the first order gives the following relationship:

$$\left.\frac{\partial \mathrm{E}(\underline{q})}{\partial \underline{q}}\right|_{\underline{q}=\underline{q}^0+\Delta\underline{q}} \approx \left(\left.\frac{\partial \mathrm{E}(\underline{q})}{\partial \underline{q}}\right|_{\underline{q}=\underline{q}^0}\right) + \left(\left.\frac{\partial^2 \mathrm{E}(\underline{q})}{\partial \underline{q}^2}\right|_{\underline{q}=\underline{q}^0}\right) \cdot \Delta\underline{q} = \underline{0}.$$

Taking into account that $\mathrm{E}(\underline{q}) = \Pi(\underline{q}) - \underline{F} \cdot \underline{q}$ and assuming that the virtual force $\underline{F} = \underline{F}^0 + \Delta\underline{F}$ is independent of the virtual co-ordinates $\underline{q} = \underline{q}^0 + \Delta\underline{q}$ the above expansion of relationship (3.1) could be re written in the form:

$$\underline{\underline{K}} \cdot \Delta\underline{q} = \underline{F} - \underline{R}_q \tag{3.2}$$

where $\underline{\underline{K}} \equiv \left(\left.\frac{\partial^2 \Pi}{\partial \underline{q}^2}\right|_{\underline{q}=\underline{q}^0}\right)$ and $\underline{R}_q = \left(\left.\frac{\partial \Pi}{\partial \underline{q}}\right|_{\underline{q}=\underline{q}^0}\right)$.

Substituting the approximation of potential energy in components into (3.2) it would be the same as rewriting (3.2) in matrix form:

$$\{K_{i,j}\}\{\Delta q_i\} = \{F_i\} - \{R_{q_i}\} \tag{3.3}$$

where $\{q_i\}$ are unknown parameters of approximation.

Relationship (3.3) gives a system of linear equations (governing equations). Matrix $\{K_{i,j}\}$ is called the rigidity matrix of the system, vector $\{R_{q_i}\}$, in fact, is the reaction force of the deformed system. In the case of an initially slack system, i.e. no internal force acts in the system; the reaction force $\{R_{q_i}\}$ is always equal to a zero-vector.

The potential energy of the system, Π, can be written in general form as follows:

$$\Pi = \sum_i \int_0^{q_i} C_i\left(\varphi\left(\{q_i\}\right)\right) P_i\left(\varphi\left(\{q_i\}\right)\right) dq_i$$

where C_i is the rigidity coefficient, which determines the physical properties of system;

P_i and φ are some function.

Substituting the above expression for potential energy into the governing equation, (3.3) can be written as:

$$\left(\left\{K_{i,j}^C\right\} + \left\{K_{i,j}^G\right\}\right)\{\Delta q_i\} = \{F_i\} - \left\{R_{q_i}\right\} \tag{3.4}$$

where $\left\{R_{q_i}\right\} = C_i\left(\varphi\left(\{q_i\}\right)\right) P_i\left(\varphi\left(\{q_i\}\right)\right)$;

$$\left\{K_{i,j}^C\right\} = \left\{\frac{\partial C_i}{\partial \varphi}\frac{\partial \varphi}{\partial q_j} P_i\right\};$$

$$\left\{K_{i,j}^G\right\} = \left\{\frac{\partial P_i}{\partial \varphi}\frac{\partial \varphi}{\partial q_j} C_i\right\}.$$

Matrix $\left\{K_{i,j}^C\right\}$ is the system rigidity matrix due to physical non-linearity of the system. Assuming that system is physically linear, i.e. $\{C_i\} \equiv const$, matrix $\left\{K_{i,j}^C\right\} = \{0\}$.

Matrix $\left\{K_{i,j}^G\right\}$ in (3.4) reflects the geometrical properties of system.

Governing equations in form (3.2), (3.3) or (3.4) lead to various iteration methods for evaluation of the current position of system $\{q_i\}$. It is convenient to use incremental methods, which solve the problem for a sequence of load steps. Incremental methods provide solutions for intermediate values of external load and show better agreement when large displacements are considered [7].

To simplify the description of the method we use the governing equation in vector form (3.2). It is assumed that a solution $\underline{q}^{k-1}$ is known at load $\underline{F}^{k-1}$ and that a solution $\underline{q}^k = \underline{q}^{k-1} + \Delta\underline{q}^k$ is desired at load $\underline{F}^k = \underline{F}^{k-1} + \Delta\underline{F}^k$.

Using equation (3.2) yields:

$$\Delta \underline{q}^k = \left(\underline{\underline{K}}\left(\underline{q}^{k-1}\right)\right)^{-1} \cdot \left(\underline{F}^k - \underline{R}_q\left(\underline{q}^{k-1}\right)\right) \tag{3.5}$$

This is the formulation for an ordinary incremental method. For better convergence it is reasonable to repeat iteration (3.5) several times (N) with the same load $\underline{F}^k$, recalculating the values of $\underline{\underline{K}}$ and $\underline{R}_q$ each time. Thus each step of load k is subdivided into n repeated iterations and $\Delta \underline{q}^k = \sum_{n=1}^{N} \Delta \underline{q}^{k,n}$ could be obtained as follows:

$$\Delta \underline{q}^{k,n} = \left(\underline{\underline{K}}\left(\underline{q}^{k-1} + \sum_{n=1}^{n} \Delta \underline{q}^{k,n}\right)\right)^{-1} \cdot \left(\underline{F}^k - \underline{R}_q\left(\underline{q}^{k-1} + \sum_{n=1}^{n} \Delta \underline{q}^{k,n}\right)\right). \tag{3.6}$$

Repeated iterations are executed until norm $\left\|\Delta \underline{q}^{k,n}\right\|$ is larger then some pre-determined value *eps*. We define the norm as $\left\|\Delta \underline{q}^{k,n}\right\| = \Delta \underline{q}^{k,n} \cdot \Delta \underline{q}^{k,n} \Big/ L\dim\left(\underline{q}\right)$, where L is the geometric dimension of the sample and $\dim\left(\underline{q}\right)$ is the dimension degree of vector $\underline{q}$.

This is the so-called self-correcting incremental method (3.6), which gives much better results in comparison with the ordinary incremental method (3.5).

3.3 Cell Composition, Full Boundary-Value Problem

Problems related to the cell and whole system composition are considered.

Execution of iteration (3.6) requires a value of the rigidity matrix $\{K\}$ to be recalculated at new position $\{\underline{q}\}$. That implies considerable computational effort and optimisation and unification of this procedure becomes very important. The full rigidity matrix is formed from arranged matrixes of finite elements, which in turn are obtained from rigidity matrixes of the constituent elements. Substituting the potential energy of each of the constitutive elements Π into (3.4) the rigidity matrixes for constituent elements can be obtained. The final expressions for the rigidity matrixes of

constituent elements for 2D deformation in components are shown in Appendix B.(1–6) respectively.

The finite-element can be composed from a number of unit cells. To simplify the implementation we only consider the case where finite-element consists of an equal number of unit cells in both Y and X directions. Potential energy for n constituent elements Π_n can be derived by multiplying the potential energy of one element by n.

Links between local numeration of co-ordinates of constituent elements and sub-global numeration of finite-elements are shown in Table 3.1 (a, b, c)

Table 3.1 (a, b, c)

(a)

Spiral element	*s1*	*a*	*b*	*λ*	*s2*
I	1	2	3	4	7
II	8	9	10	11	14
III	15	16	17	18	21
IV	22	23	24	25	28

(b)

Thread element	*x1*	*y1*	*s1*	*s2*	*x2*	*y2*
I	5	6	7	8	12	13
II	12	13	14	15	19	20
III	19	20	21	22	26	27
IV	26	27	28	1	5	6

(c)

Height element	*x1*	*y1*	*x2*	*y2*	*x3*	*y3*	*x4*	*y4*
I	26	27	5	6	12	13	19	20
II	5	6	12	13	19	20	26	27
III	12	13	19	20	26	27	5	6
IV	19	20	26	27	5	6	12	13

Deformation of a finite-element *in plane* is described by 28 components. Following the rule represented in Table 3.1 (a, b, c) and the scheme of the unit cell shown in Figure 2.19, the rigidity matrix for the finite element can be obtained. The full rigidity matrix for the system of finite-elements can be obtained by rearrangement of the finite-element matrixes.

To simplify implementation of the algorithm only uniform finite elements are considered. Namely, the mesh of the system consists of an orthogonal and equally spaced grid. That makes it possible to define rows and columns of finite elements. Global numeration of the finite elements is accepted as that shown for unit cells in Figure 2.7 (b).

Finally, the sequence of co-ordinates of the finite-element for each knot point is accepted as follows:

$$\{s1, a, b, \lambda, x, y, s2\}$$

where $\{x, y\}$ are co-ordinates of the finite element vertex (knot point);

$\{s1, s2\}$ are length redistribution parameters in/via knot point;

$\{a, b, \lambda\}$ are parameters of the *helix element* (section 2.3.4).

Co-ordinates $\{a, b, \lambda, x, y\}$ of the knot point coincide with the neighbour contacting point. Co-ordinates $\{s1, s2\}$ should be re-numbered as shown in Figure 3.1 to provide a unified procedure for arranging the finite elements into one system.

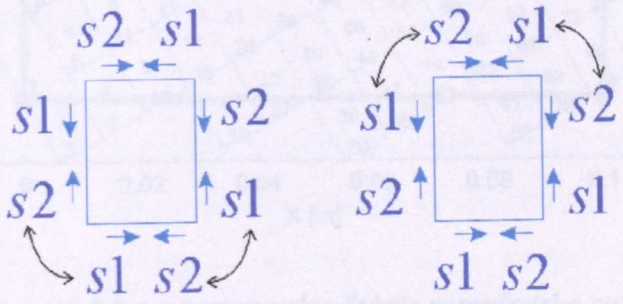

(a) *(b)*

Figure 3.1 (a, b) ***Re-numbering of finite-element co-ordinates***

re-numbering procedure for odd – (a) and even – (b) rows.

Thus, the virtual co-ordinates of finite-elements that belong to odd rows (for example elements numbered from 6 to 9 in Figure 3.2) are re-numbered according Figure 3.1 (a).

Finite elements should cover the physical region (area) of the fabric sample. Taking into account that the finite elements initially are uniform right-angled rectangles it is not possible to cover an arbitrary geometrical area by finite elements. Some of the knot points will inevitably be beyond the bounds of a given shape of sample. It is assumed that an element belongs to the sample if at least two of its knot points lie within the bounds of a real sample. The typical example of mesh for rectangle sample is represented in Figure 3.2. Here thick green lines represent the real bounds of the sample. Decreasing geometrical size of the finite-element infinitely makes it possible to approximate the real bound with any arbitrarily precision. The extension of different fabric samples, which have shapes like that shown in Figure 3.2 is considered later.

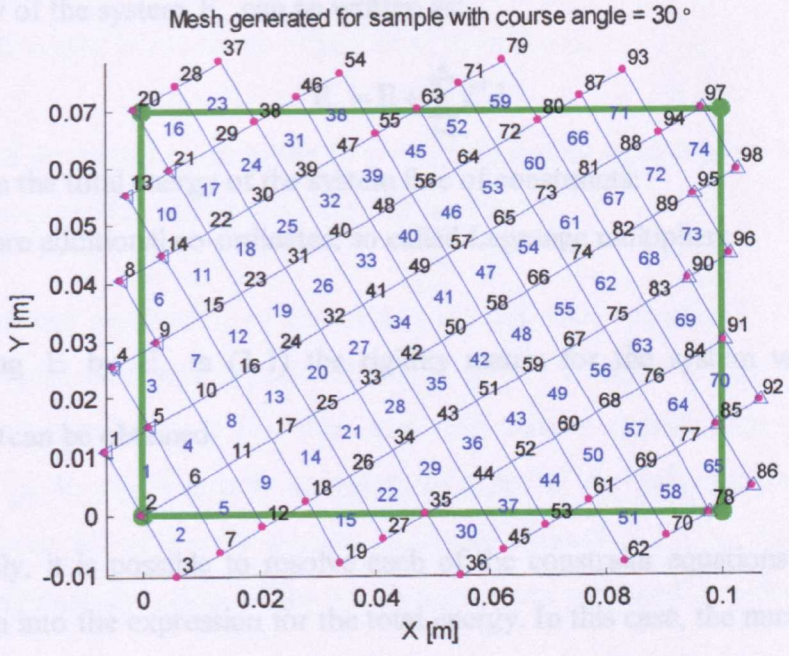

Figure 3.2 ***Mesh generated for a rectangular fabric sample (the course direction makes 30° with axis OX).***

real bounds of sample (green lines), finite elements (blue lines), global numeration of finite-elements in the system (blue numbers from 1 to 74), global numeration of

system's knot points (black numbers from 1 to 98), edge knot points (magenta points), edge points with given boundary conditions (magenta point inside a triangle).

Some of the knot points are subjected to boundary conditions. In Figure 3.2 the magenta points inside a triangle indicate points where boundary conditions are specified.

3.4 Different Types of System's Boundary Conditions, Lagrange multipliers techniques

Using of the Lagrange multiplier technique for different BC: 'fixed all'; 'slide all', 'fixed clamp', 'movable clamp'

Boundary conditions can be considered as additional constraint equations for virtual co-ordinates. Assuming n constraint equations in the form $\{\xi^i(\underline{q})\}=0,(i=1:n)$, the total energy of the system E_c can be written as:

$$E_c = E + \sum_{i=1}^{n} \xi^i \lambda_i \tag{3.7}$$

where E is the total energy of the system free of constraints;

λ_i are additional co-ordinates, so called Lagrange multipliers.

By replacing E by E_c in (3.1) the rigidity matrix for the system with constraints $\{\xi^i(\underline{q})\}=0$ can be obtained.

Theoretically, it is possible to resolve each of the constraint equations and substitute the solution into the expression for the total energy. In this case, the number degrees of freedom of the system will decrease. New co-ordinates λ_i increase the number degrees of freedom of whole system, which in turn causes a larger rigidity matrix and greater computational effort for matrix inversion. On the other hand, by using the Lagrange multiplier technique the algorithm of rigidity matrix evaluation is simplified and this leads to a more unified numerical implementation.

We assume that the boundary conditions are given only at the edge points of the system. During tensile tests opposite edges of a sample were clamped. One of the clamps is fixed during sample loading while the other is free to move towards the applied force. Thus, it is reasonable to introduce two types of clamps (*'fixed clamp'* and *'movable clamp'*). The clamp, which is moved *in plane* along one direction (without rotation) could be represented as an additional finite-element with one degree of freedom $\underline{q_{cl}^1}$. External tensile force F is applied to the clamp thus work done by the external force due to system deformation is equal to $\underline{F} \cdot \underline{q_{cl}^1}$.

Knot points where boundary conditions are given are connected to a corresponding type of clamp. There are several possible types of joint of knot points with a clamp:

- co-ordinates of these points could be inflexibly joined to the clamp (*'fixed all'*)
- points are free to slide along the clamp while the clamp moves in some direction (*'slide all'*)
- points are free to slide along the clamp except for one given point, which is inflexibly joined to the clamp (*'fixed first'*, *'fixed last'*).

Extension of the rigidity matrix due to constraints can be implemented for all boundary conditions considered with the aid of equation (3.7).

To illustrate the application of the mentioned boundary conditions we consider the problem of axial tension of a plane sample as shown in Figure 3.3 (a). Because of the reflection of sample about the horizontal and vertical middle lines (doted lines in Figure 3.3 (a, b, c)), it is only necessary to consider the deformation of half of the sample (Figure 3.3 (b)) or a quarter of sample (Figure 3.3 (c)). According to the specified terminology, edges of the whole sample are subjected to following boundary conditions:

- upper edge: *'fixed clamp'*, *'fixed all'* (clamp is fixed and all points are inflexibly jointed to the clamp)
- lower edge: *'movable clamp'*, *'fixed all'* (clamp is free to move in the direction of the applied force $\underline{F}$ and all points are inflexibly jointed to the clamp).
- side edges: no constraining conditions

For equivalent deformation of the half and the quarter of the sample, the lower edge is subjected to same boundary conditions as that for the whole sample. The boundary conditions for the upper edge for half of the sample can be expressed as *'fixed clamp'* and *'slide all'*. The boundary conditions for the upper edge of the quarter of sample can be expressed as *'fixed clamp'* and *'fixed first'* or *'fixed last'* (depends on the numbering of the knot points accepted for the system).

Although it is possible to reduce the system dimensions and consider deformation of half or quarter of the whole only the full sample has been considered in most cases, except low-dimension testing examples in section 3.9 below. This causes more computational effort but it simplifies the implementation of the algorithm.

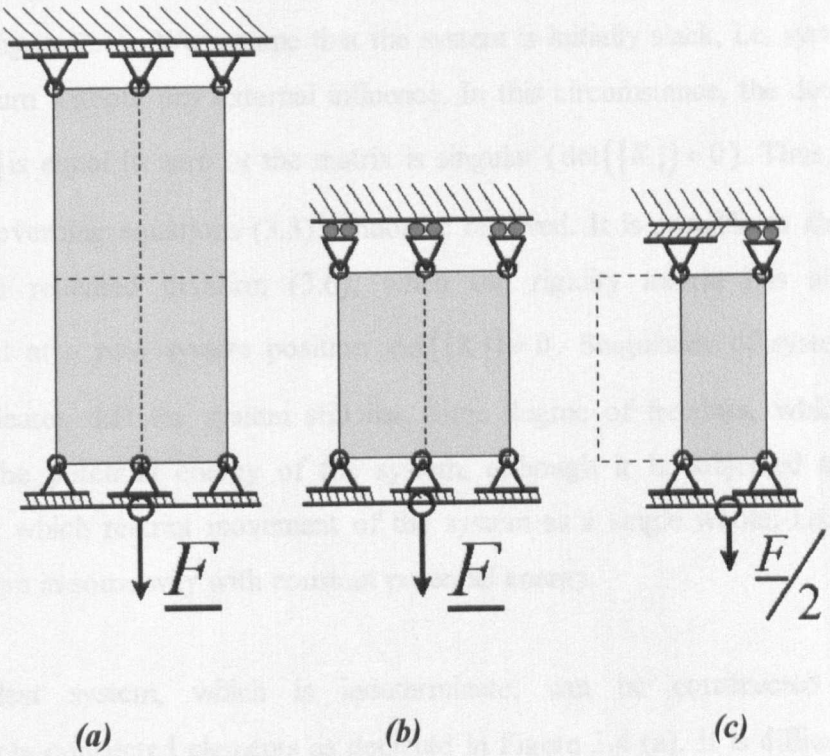

Figure 3.3 ***The problem of axial extension of a flat sample.***

the whole sample – (a), the equivalent problem for half of sample – (b), the equivalent problem for quarter of sample – (c).

3.5 Indeterminate Rigidity Matrix, Possible Solutions ('Diagonal' Element)

For a slack configuration the determinant of the rigidity matrix is equal to zero; two possible ways of getting a solution: either generation of some initial solution corresponding to the deformed state of the system or introducing a diagonal element, which affects the system behaviour only on the first steps when the determinant of the matrix is close to zero.

The full boundary value problem of extending a rectangular sample as shown in Figure 3.3 (a) is considered further. Imaginary lines subdivide the physical region of the sample into finite-elements as shown in Figure 3.2. The full rigidity matrix $\{K\}$ can be obtained with aid of equation (3.2) or (3.3) by following the established co-ordinate sequence as shown in Table 3.1 (a, b, c) and the scheme of unit cell (finite-element) shown in Figure 2.19. We assume that the system is initially slack, i.e. system remains at equilibrium without any external influence. In this circumstance, the determinant of matrix $\{K\}$is equal to zero or the matrix is singular ($\det(\{K\})=0$). Thus, the system of linear governing equations (3.3) cannot be resolved. It is possible to show that for the second repeated iteration (3.6), when the rigidity matrix has already been recalculated at a new system position $\det(\{K\})\neq 0$. Singularity of system's rigidity matrix indicates that the system still has some degree of freedom, which does not influence the potential energy of the system, although it is subjected to boundary conditions, which restrict movement of the system as a single whole; i.e. the system could deform in some way with constant potential energy.

The simplest system, which is indeterminate, can be constructed from two consecutively connected elements as depicted in Figure 3.4 (a). It is difficult to obtain an analytical expression for the determinant of the rigidity matrix for that system and virtually impossible to show that it is equal to zero. To illustrate the phenomena we consider a simplified problem of extension of a system of elastic springs hinged together as shown in Figure 3.4 (b). Identical springs with tensile rigidity D_a represent the *thread* constituent elements of the finite element. The spring with tensile rigidity equal to D_H represents the *height* constituent element. To show that the system of

springs in Figure 3.4 (b) has a singular rigidity matrix, it is enough to show that the simplified system shown in Figure 3.4 (c) also has a singular rigidity matrix.

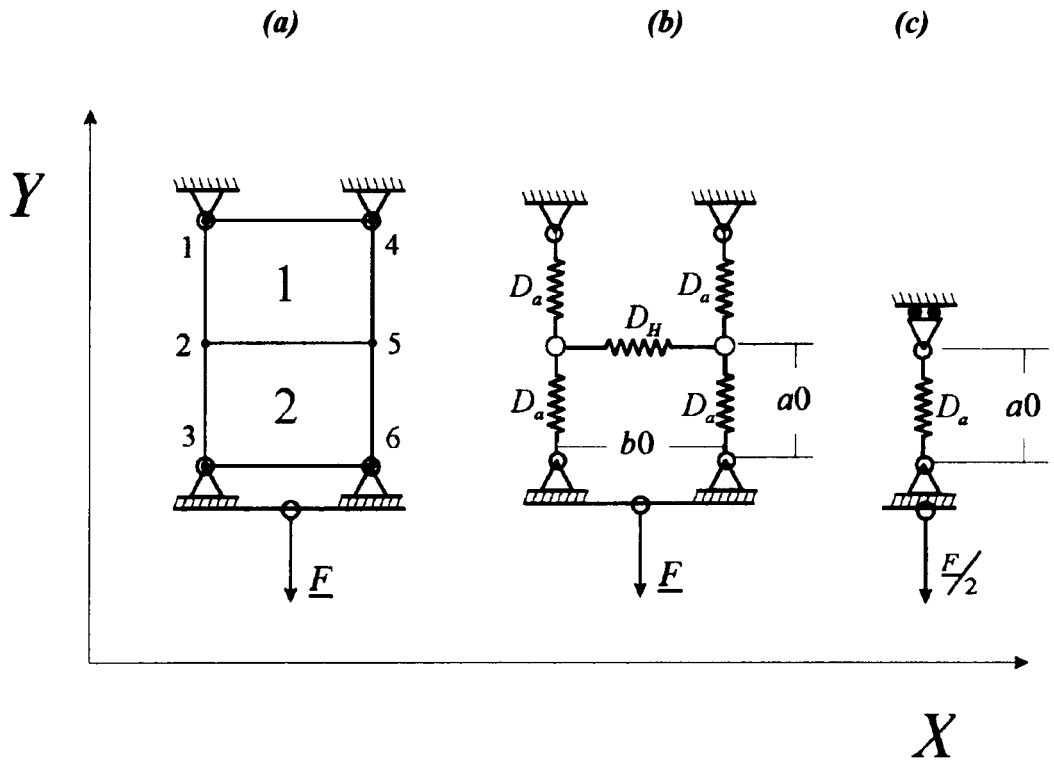

Figure 3.4 (a, b, c) ***The indeterminate systems.***

indeterminate system constructed from two finite-elements – (a); indeterminate system constructed from springs – (b);the simplest indeterminate system – (c).

The potential energy Π for the spring shown on right-hand picture of Figure 3.4 could be expressed as:

$$\Pi = D_a \frac{(a - a0)^2}{a0}$$

where $a0$ is the initial length of the spring;

a is the current length of the spring.

By introducing the Cartesian co-ordinate system, XY, the initial and current length of the spring can be expressed in components as:

$$a0 = \sqrt{(x0_2 - x0_1)^2 + (y0_2 - y0_1)^2}$$

$$a = \sqrt{(x0_2 - x0_1 + Ux_2 - Ux_1)^2 + (y0_2 - y0_1 + Uy_2 - Uy_1)^2}$$

where $x0_{\{1,2\}}; y0_{\{1,2\}}$ are the initial co-ordinates of the spring ends;

$Ux0_{\{1,2\}}; Uy0_{\{1,2\}}$ are displacements of the spring ends.

The rigidity matrix $\{K_{i,j}\}$ can be written as:

$$\{K_{i,j}\} = \left\{\frac{\partial^2 \Pi}{\partial q_i \partial q_j}\right\}$$

where $\{q_n\}_{n=\{1:4\}} = \{Ux_1, Uy_1, Ux_2, Uy_2\}$.

Taking into account the boundary conditions, it is possible to show that:

$$\det\left(\{\tilde{K}\}\right) = (D_a)^2\left(1 - \frac{a0}{a}\right)$$

where $\{\tilde{K}\}$ is the rigidity matrix of the spring with respect to the boundary conditions ($Ux_1 = 0, Uy_2 = 0$).

When the spring is initially slack $a = a0$ and, hence, $\det\left(\{\tilde{K}\}\right) = 0$.

The above arguments illustrate the phenomena of singularity of the finite-element. The problem can be approached from different directions. It is possible to generate some initial solution for the system and then recalculate the rigidity matrix for the given solution. In the case of a spring in a plane, which has four degrees of freedom, it is not difficult to generate some reasonable solution. In the case of a system of finite elements, which has up to 2000 degrees of freedom that is virtually impossible.

Another way to resolve the problem is the introduction of an additional constituent element (*diagonal element*), which restricts movement of diagonal knot points of the finite-element. The *diagonal element* represents the initial shear rigidity of the element. We assume that the rigidity of the *diagonal element* remains constant during element deformation and equal to the initial value of rigidity of the *height element.*

Introduction of the *diagonal element* allows the solution of the governing equations (3.3) for an initially slack system on the first iteration (3.6). It is possible to remove the *diagonal element* for subsequent calculations, however due to the relatively small rigidity of the *diagonal element* it does not exert considerable influence on the system behaviour under a small applied force and makes the system more stable when it is subjected to a considerable load. Thus, it is reasonable to use the diagonal element for all iterations (3.5) and (3.6).

3.6 Method Stability when the System is Close to Singular Points (High Load)

Discussion of the subject is presented. The singular terms in potential energy are considered. An approximation of a singular function of compression rigidity coefficient is proposed.

Yarn-to-yarn compression is the main factor, which prevents the finite-element from being collapsed into a line when subjected to external load. Due to singularity of the compression rigidity coefficient (2.28), the potential energy of yarn compression (2.29) grows infinitely when yarns approach the critical distance (when the value of z in equation (2.28) tends to $z_{\min}$). The system is also singular due to singularity of the *thread element*. One could see that the denominator of the expression for relative deformation of the *thread element* (2.20) could attain zero value.

Singularity of the system causes slow convergence of the method and in some cases entails method instability when the system is subjected to considerable load. A typical example of instable solution of the system is represented in Figure 3.5. When the system is subjected to a relatively low load, the method gives a stable solution. When the load approaches to some critical value the solution oscillates with a lower damping factor and finally, when the load attains some critical value the solution diverges. Due to the high non-linearity of the model, it is unclear how to estimate the value of that critical force. To obtain a convergence criterion it is necessary to perform complex asymptotic analysis of the method and model.

The value of the critical load normally leads to quite a high value of relative deformation of the sample (up to 100%). Thus, the shape of the sample immediately before method stability loss (when external load is approaching its critical value) is represented in Figure 3.6. If higher deformations are not required, it is possible to retain singular functions in the expression for potential energy of the system. To obtain a solution beyond the critical load the singular term should be replaced by some non-singular function.

During testing calculations, it was found that the main factor, which causes method instability, is the singularity of the yarn-to-yarn compression coefficient. It is assumed that it is possible to approximate the singular function of the compression coefficient $K(z)$ (2.28) by some non-singular function $\widetilde{K}(z)$. Function $\widetilde{K}(z)$ should adequately describe the real compression rigidity when $z \gg z_{\min}$. When z is close to the singular point, function $\widetilde{K}(z)$ should attain a high but finite value to prevent mutual yarn penetration and collapse of the finite element.

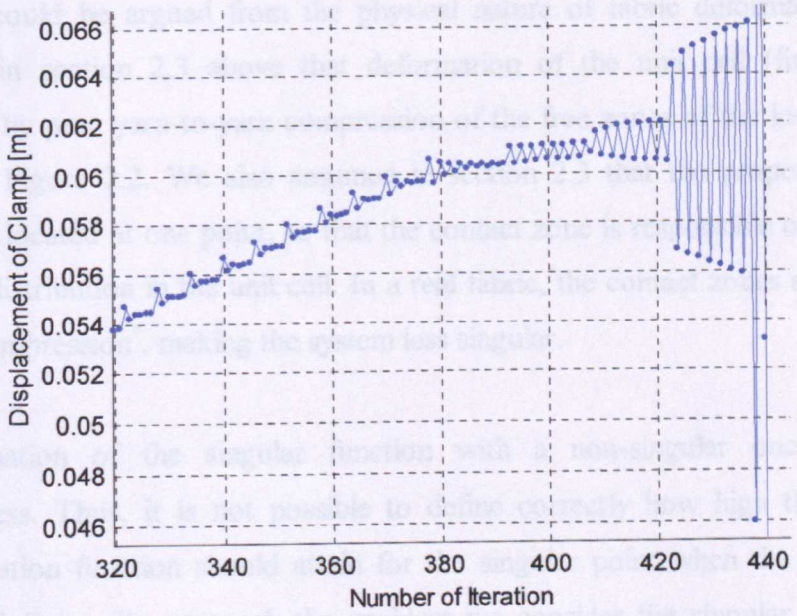

Figure 3.5 A *typical example of instable solution.*

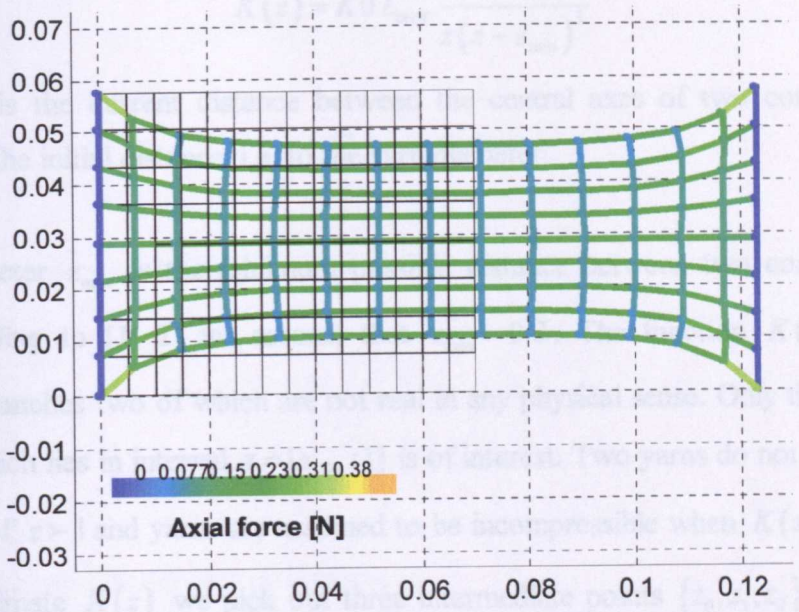

Figure 3.6 ***Shape of sample before solution diverge.***

relative deformation of sample here is 70% approx.

Approximation of the singular compression rigidity coefficient with a mildly sloping function could be argued from the physical nature of fabric deformation. Thus, we assumed in section 2.3 above that deformation of the unit cell (finite-element) is restricted by pure yarn-to-yarn compression of the free zones of the loop (sides of the unit cell) Figure 2.2. We also assumed in section 2.3 that the properties of contact zones are located at one point, so that the contact zone is responsible only for the yarn length redistribution in the unit cell. In a real fabric, the contact zones also take part in mutual compression*, making the system less singular.

Approximation of the singular function with a non-singular one implies some arbitrariness. Thus, it is not possible to define correctly how high the value of the approximation function should attain for the singular point when the real function is equal to infinity. To approach the problem we consider the singular function of the rigidity coefficient (the same one as in equation (2.28)):

* *And probably play an important role in loop contraction.*

$$K(z) = K0\, L_{cont} \frac{(1 - z_{\min})}{z(z - z_{\min})^3} \tag{3.8}$$

where z is the current distance between the central axes of two contacting yarns relative to the initial distance, i.e. to the yarn diameter.

The parameter $z_{\min}$ is the minimum possible distance between two contacting yarns and according to [1, 2] we assume that $z_{\min} = 0.2$. The function $K(z)$ has three separate branches two of which are not real in any physical sense. Only that part of the branch, which lies in interval $z = [z_{\min} : 1]$ is of interest. Two yarns do not interact when the value of $z \succ 1$ and yarns are assumed to be incompressible when $K(z) \xrightarrow[z \to 0.2]{} \infty$. To approximate $K(z)$ we pick out three intermediate points $\{z_0, z_1, z_2\} = \{0.4, 0.6, 1\}$. The following five types of approximation function $\widetilde{K}(z)$ were tested and implemented.

➢ ***Linear approximation.***

Approximation function

$$\widetilde{K}(z)=\begin{cases}0 & z\in[\infty,z_0]\\ P^1(z) & z\in[z_0,-\infty]\end{cases}$$

where linear polynomial $P^1(z)$ satisfies the following criteria:

$$\begin{cases}P^1(z_0)=K(z_0)\\ P^1(z_2)=K(z_2)\end{cases}.$$

➢ ***Piece-wise linear approximation.***

Approximation function

$$\widetilde{K}(z)=\begin{cases}0 & z\in[\infty,z_0]\\ P_1^1(z) & z\in[z_0,z_1]\\ P_2^1(z) & z\in[z_1,-\infty]\end{cases}$$

where linear polynomials $P_1^1(z)$ and $P_2^1(z)$ satisfies the following criteria:

$$\begin{cases}P_1^1(z_0)=K(z_0)\\ P_1^1(z_1)=K(z_1)=P_2^1(z_1).\\ P_2^1(z_2)=K(z_2)\end{cases}$$

➢ ***Quadratic polynomial approximation***

Approximation function

$$\widetilde{K}(z)=\begin{cases}0 & z\in[\infty,z_0]\\ P^2(z) & z\in[z_0,-\infty]\end{cases}$$

where quadratic polynomial $P^2(z)$ satisfies the following criteria:

$$\begin{cases}P^2(z_0)=K(z_0)\\ P^2(z_1)=K(z_1)\\ P^2(z_2)=K(z_2)\end{cases}.$$

➢ ***Piece-wise quadratic polynomial approximation.***

Approximation function

$$\widetilde{K}(z)=\begin{cases}0 & z\in[\infty,z_0]\\ P_1^2(z) & z\in[z_0,z_1]\\ P_2^2(z) & z\in[z_1,-\infty]\end{cases}$$

where quadratic polynomials $P_1^2(z)$ and $P_2^2(z)$ satisfy the following criteria:

$$\begin{cases}P_1^2(z_0)=K(z_0)\\ P_1^2(z_1)=K(z_1)=P_2^2(z_1)\\ \left.\dfrac{\partial P_1^2}{\partial z}\right|_{z=z_1}=\left.\dfrac{\partial K}{\partial z}\right|_{z=z_1}=\left.\dfrac{\partial P_2^2}{\partial z}\right|_{z=z_1}\\ P_2^2(z_2)=K(z_2)\end{cases}.$$

➢ ***Cubic spline approximation.***

Approximation function

$$\widetilde{K}(z)=\begin{cases}0 & z\in[\infty,z_0]\\ P_1^3(z) & z\in[z_0,z_1]\\ P_2^3(z) & z\in[z_1,-\infty]\end{cases}$$

where cubic polynomials $P_1^3(z)$ and $P_2^3(z)$ satisfy the following criteria:

$$\begin{cases}\\ P_1^3(z_0)=K(z_0)\\ P_1^3(z_1)=K(z_1)=P_2^3(z_1)\\ \left.\dfrac{\partial P_1^3}{\partial z}\right|_{z=z_1}=\left.\dfrac{\partial K}{\partial z}\right|_{z=z_1}=\left.\dfrac{\partial P_2^3}{\partial z}\right|_{z=z_1}\\ \left.\dfrac{\partial^2 P_1^3}{\partial z^2}\right|_{z=z_1}=\left.\dfrac{\partial^2 K}{\partial z^2}\right|_{z=z_1}=\left.\dfrac{\partial^2 P_2^3}{\partial z^2}\right|_{z=z_1}\\ P_2^3(z_2)=K(z_2)\end{cases}.$$

During testing calculations, it was found that the *quadratic piece-wise approximation* is a trade-off among the above types of approximation functions. It provides good approximation at points located far away from the singular value and prevents the system from been collapsed when a high level of compression occurs. At the same time, the *quadratic piece-wise approximation* function is mildly sloping enough to provide method stability at high levels of deformation. The *cubic spline approximation* gives approximation functions, which grows too fast near the singular point to provide the method stability.

3.7 Convergence Improvement

3.7.1 Length Restriction Element

In some cases, the system was unstable when subjected to considerable load. The discussion of the phenomena is presented. To provide a stable solution it was proposed to restrict a considerable difference of length redistribution in neighbouring node points

Length redistribution in the finite-element is restricted only at the knot points, which belong to sample edges where points are clamped and length redistribution is prohibited. The influence of boundary conditions on length redistribution in the finite-elements located far away from the edges of a sample is low. A system consisting of a large number of finite-elements becomes unstable when subjected to relatively high load. The mechanism of system instability can be illustrated as follows.

We consider a deformed finite-element as shown in Figure 3.7, which is located somewhere in the middle of the system. Each side of the finite element represents a corresponding *thread element*. Co-ordinates of corresponding knot points $\underline{r0}_i + \underline{U}_i\big|_{i=\{1:4\}}$ and length redistribution in/via the points $\{s1_i, s2_i\}_{i=\{1:4\}}$ determine the current position of the *thread elements*. Displacement of knot points is restricted additionally by height elements and diagonal elements, while length redistribution is restricted implicitly by the boundary conditions where length redistribution is prohibited. When a finite element is located far away from the clamped edge skewness of length redistribution for some of sides can appear. Namely, when a sample is

subjected to a relatively high load it appears that at some iteration co-ordinate $s2_2 \gg s1_3$; these leads to slow convergence, oscillation of the solution and, finally, to method instability, when the load is high.

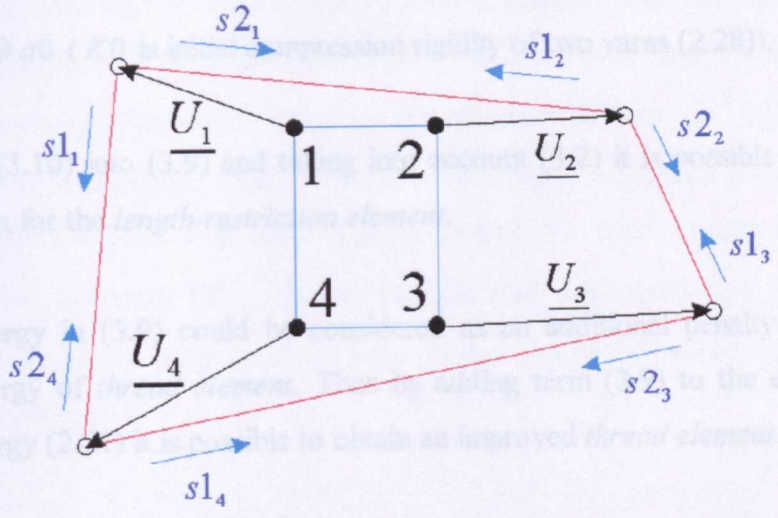

Figure 3.7 ***Deformed finite-element.***

The values of length redistribution for the thread elements are independent co-ordinates, however for small elements they should have one order of magnitude since it is essential that stress field is smooth for the finite-element. To approach the problem we introduce a new constituent element: *'length-restriction element'*, which constraints additionally length redistribution skewness.

Potential energy Π of the *length-restriction element* can be expressed as:

$$\Pi = \int_0^{bs} C_L(bs)\, bs\, d\, bs \tag{3.9}$$

where $bs = \left|s1_i - s2_j\right|, \{i,j\} = \{\{1,2\},\{2,3\},\{3,4\},\{4,1\}\}$;

C_L is the rigidity coefficient for the *length-restriction element.*

The *length-restriction element* should not influence the system behaviour when the value of bs is small, *i.e.* the level of skewness is low. To provide this the following expression for compression coefficient is assumed:

$$C_L = \frac{C0_L}{(z_{\min} - z)^2} \tag{3.10}$$

where $z = {bs}/{a0}$ ($a0$ is initial length of thread element (2.20));

$z_{\min} = 0.6^*$;

$C0_L = K0\, a0$ ($K0$ is initial compression rigidity of two yarns (2.28)).

Substituting (3.10) into (3.9) and taking into account (3.2) it is possible to obtain the rigidity matrix for the *length-restriction element.*

Potential energy in (3.9) could be considered as an additional penalty term for the potential energy of *thread element.* Thus by adding term (3.9) to the expression for potential energy (2.21) it is possible to obtain an improved *thread element.*

The *length restriction element* obtained according the above assumptions does not significantly influence the behaviour of the system when it is subjected to relatively low loads and provides method convergence at higher load where the calculation without the *length restriction element* failed.

3.7.2 Influence of derivatives of the 'Thread element'

Taking into account the derivatives of yarn tensile rigidity leads to faster convergence of the system.

The value of the potential energy of the thread element grows infinitely when the denominator in the expression for relative deformation of the *thread element* (2.20) approaches zero. The singularity order of the potential energy of the *thread element* is equal to $S_{thr} \sim \int_0^{const} \frac{1}{x}\, dx \sim \ln 0$ (see equation (2.21)), where *const* is some positive constant. The singularity order of the *spiral element* and the *height element* is equal to $S_{heigh} \sim \int_0^{const} \frac{1}{x^3}\xi(x)\, dx \sim {1}/{O^2}$, where $\xi(x)$ is some non-singular function on the

specified interval and O is infinitesimal (see relationship for the singular compression coefficient (2.27) and expressions for the potential energy for the *helix* and *height* elements (2.34), (2.29)).

Taking into account that the tensile rigidity is not a singular function (see Figure 2.13) it was decided initially to neglect derivatives of the tensile rigidity in the rigidity matrix of the *thread element*. Thus, it was assumed that term $\{K^C\}$ for the *thread element* in (3.4) is negligibly small. It was thought that convergence of 'more' singular elements requires a load step small enough to provide convergence of the *thread element* without the term $\{K^C\}$. It was thought that this would save computational effort. When singularity occurred due to the *thread element*, it would indicate that the load step is too large.

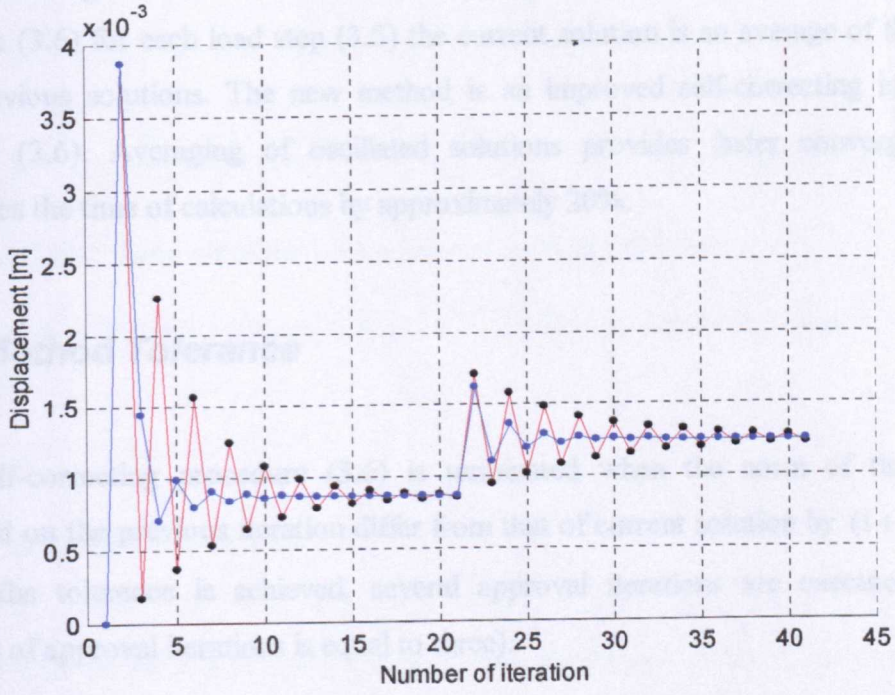

Figure 3.8 ***Method convergence with and without derivatives of yarn tensile rigidity.***

Method convergence with (blue curve) and without (red curve) derivatives of the thread element.

---

* *Obtained from numerical experiment with the model (see CHAPTER 4)*

During test calculations, however, the system showed much better convergence in the case where derivatives of tensile rigidity were taken into account. Thus, in Figure 3.8 displacement of the clamp is represented for two load steps (3.5) each consisted of 20 repeated iterations (3.6). The blue curve represents the system with derivatives of tensile rigidity and red curve represents the system without derivatives of tensile rigidity. Taking into account $\{K^C\}$ for the *thread element* improves the convergence of system and finally saves computational effort as it allows termination of the iterations much earlier.

3.7.3 Averaging of oscillated solution

Due to the self-correcting procedure (3.6) the solution of the system represents damped oscillations Figure 3.8. To increase the damping factor we accept that after the first iteration (3.6) for each load step (3.5) the current solution is an average of the current and previous solutions. The new method is an improved self-correcting incremental method (3.6). Averaging of oscillated solutions provides faster convergence and decreases the time of calculations by approximately 20%.

3.8 Method Tolerance

The self-correcting procedure (3.6) is terminated when the norm of the solution obtained on the previous iteration differ from that of current solution by $(1+\varepsilon)$ or less. When the tolerance is achieved, several approval iterations are executed (default number of approval iterations is equal to three).

The default value of the tolerance is $\varepsilon = 10^{-4}$. It approximates to 0.01% relative error at each iteration. So a high level of tolerance is required only for the more stable numerical procedure and helps to avoid summing up errors. Decreasing the tolerance causes method instability and in some cases even causes an increase in the calculation time because of higher solution oscillation.

In Figure 3.9 two solutions obtained at different value of tolerance ($\varepsilon = 10^{-4}$ and $\varepsilon = 10^{-3}$) are represented. When the tolerance is not high enough, the system becomes unstable and it is virtually impossible to obtain a solution at higher load when the system approaches singular points.

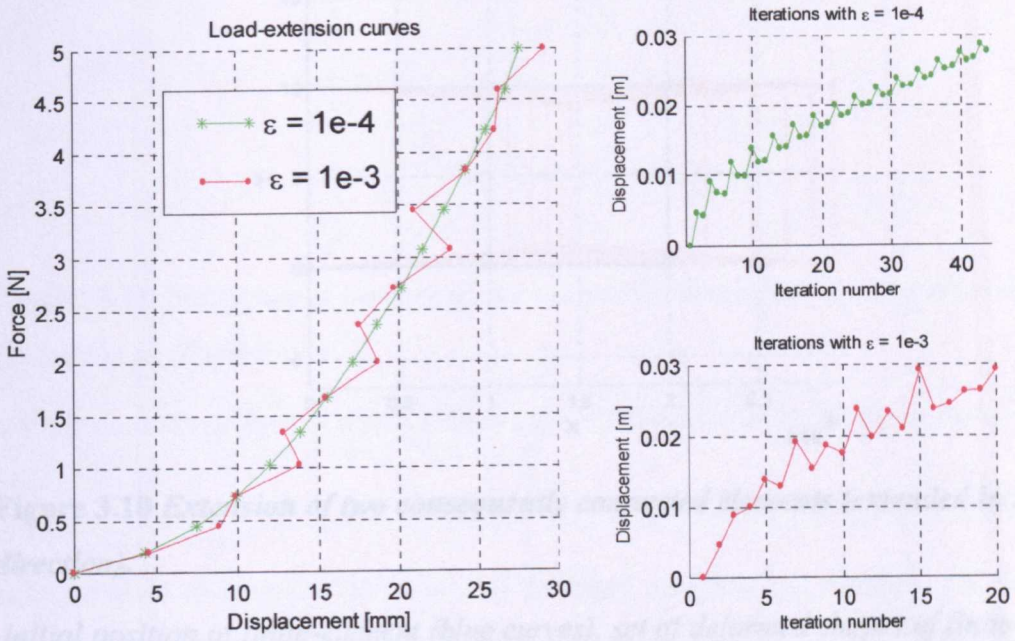

Figure 3.9 ***Solutions obtained with different method tolerance***

green curve represents solution with $\varepsilon = 10^{-4}$, *red curve represents solution with* $\varepsilon = 10^{-3}$.

3.9 Testing Examples

To illustrate the mechanical properties of the finite-element and outline possible fields of application of the proposed model, a number of test examples were examined. All of those samples considered here were based on average parameters of yarns and fabric. They were constructed for the qualitative analysis of the model and values of input parameters and loading conditions are not essential for further illustration.

Firstly, we consider a system of two finite elements subjected to boundary conditions and external load as shown in Figure 3.3 (a) (whole sample). The set of deformed shapes of the two elements at equally spaced loads is represented in Figure 3.10.

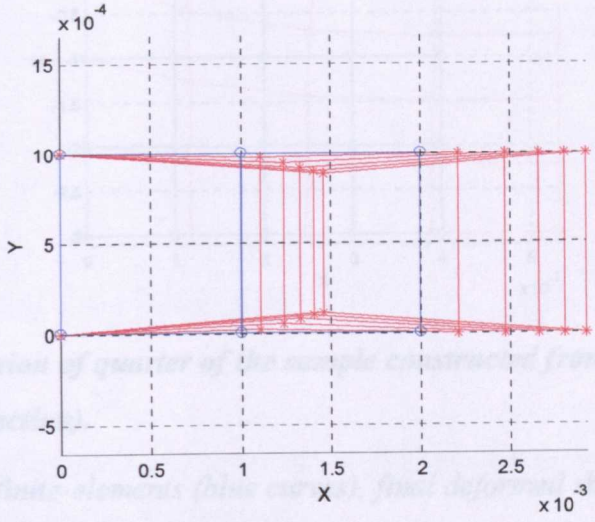

Figure 3.10 ***Extension of two consequently connected elements (extended in X direction).***

initial position of finite-element (blue curves), set of deformed shapes of finite-element (red curves)

Having been subjected to external load, the system displays lateral contraction in the direction transverse to the applied load. This qualitatively agrees with the phenomena as observed experimentally. To obtain a more even approximation of the deformed edge of the sample it needs to be subdivided into a greater number of finite elements.

The quarter sample subjected to load and boundary conditions as shown in Figure 3.3 (c) is represented in Figure 3.11. In this case, the whole sample is subdivided into 64 (8 by 8) finite elements. Because of the symmetry of the problem, it is possible to consider deformation of a quarter of the sample. In the case with a higher number of finite-elements, the model approximates the edges of the deformed sample more smoothly. Lateral contraction of the sample is restricted by both yarn-to-yarn compression and the clamped edge (left edge in Figure 3.11). The influence of the boundary conditions decreases at points located further from the clamped edge and, hence, a higher level of lateral contraction occurs there.

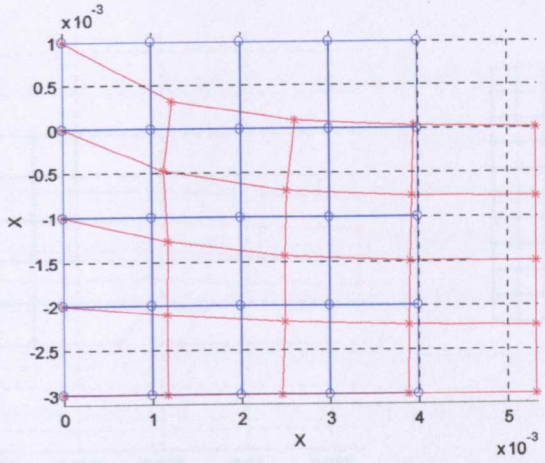

Figure 3.11 ***Extension of quarter of the sample constructed from 64 finite-elements (extended in X direction).***

initial position of finite-elements (blue curves), final deformed shape of finite-elements (red curves).

It is possible to simulate behaviour of damaged samples, i.e. samples with holes and cracks. We consider two samples with symmetric holes in the centre. To simulate a hole in a sample the corresponding finite-elements were removed from the system as shown in Figure 3.12 (b) and Figure 3.13 (b). Figure 3.12 (a) and Figure 3.13 (a) gives the shapes of the quarter of the sample at initial and deformed states.

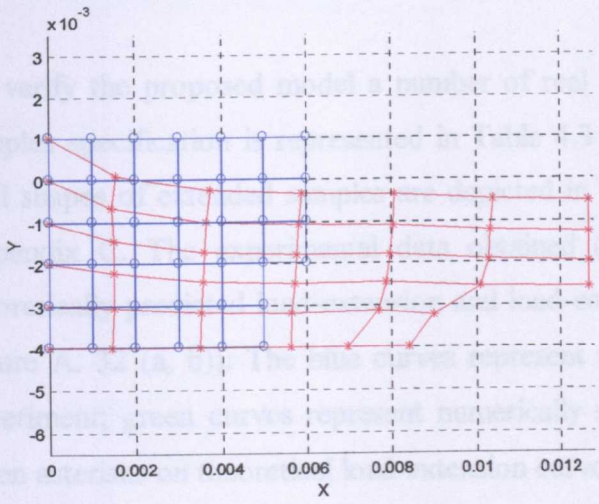

(a)

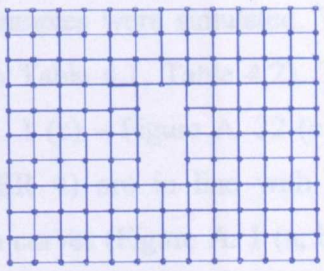

(Whole sample)

(b)

Figure 3.12 (a, b) ***Extension of quarter of sample constructed from 136 (12*12-2*4) finite-elements (extended in X direction).***

initial position of finite-elements (blue curves), final deformed shape of finite-elements (red curves).

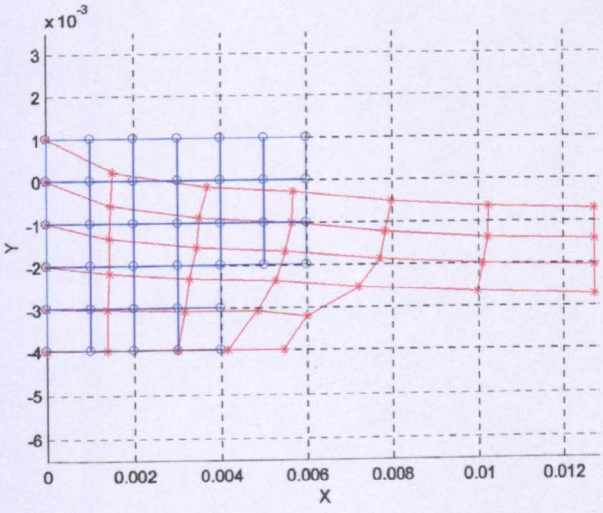

(a)

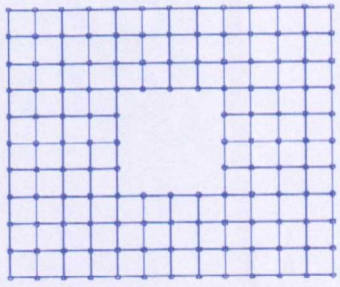

(Whole sample)

(b)

Figure 3.13 (a, b) ***Extension of quarter of sample with symmetric hole in centre constructed from 128 (12*12-4*4) finite-elements (extended in X direction)***

initial position of finite-elements (blue curves), final deformed shape of finite-elements (red curves).

3.10 Simulation of Extension of a Real Fabric

To verify the proposed model a number of real knitted samples were simulated. The samples specification is represented in Table 4.3 (see also Table 4.1, Table 4.2). The final shapes of extended samples are depicted in Figure A. 1 (c) – Figure A. 32 (c) in Appendix C. The experimental data obtained (CHAPTER 4) are in line with the theoretically predicted load-extension and load-contraction curves (Figure A. 1 (a, b) – Figure A. 32 (a, b)). The blue curves represent the load-extension curves obtained in experiment; green curves represent numerically simulated load-extension curves. The green asterisks on theoretical load-extension curves represent the load step.

A typical example of the load-extension and contraction curves plus final shape of the deformed sample is illustrated in Figure 3.14 (a, b, c); the sample shown (number 3) has a course angle $\alpha = 15^{o}$ (see Table 4.3, Table 4.2, Table 4.1 for details). The relative contraction curve represents relative contraction of the narrowest part of the sample.

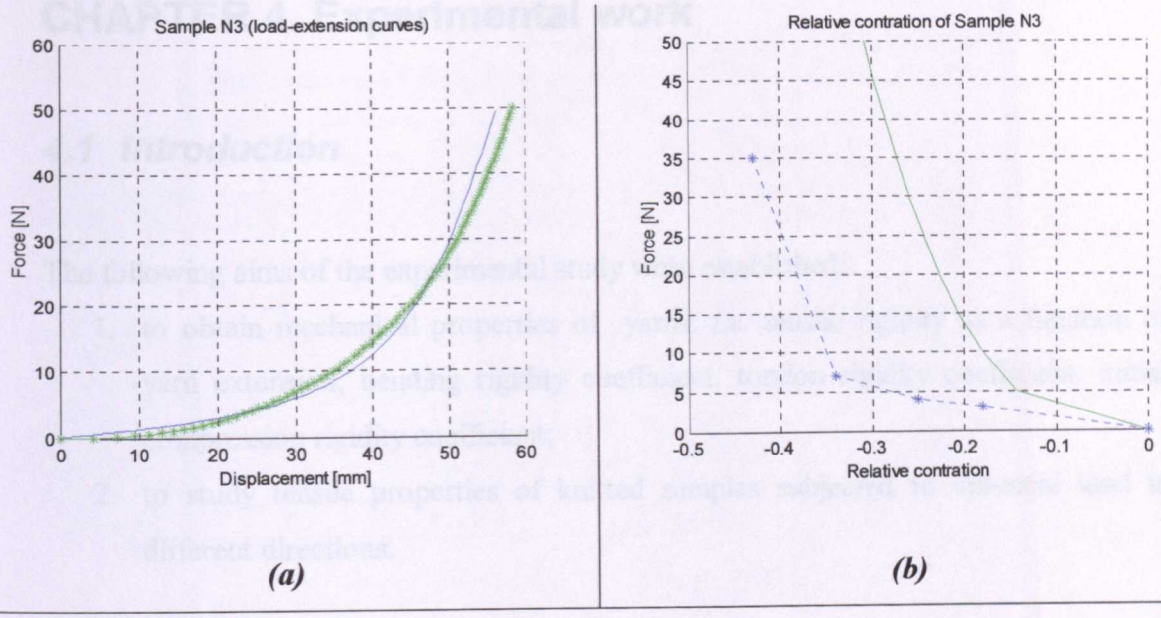

(a)

(b)

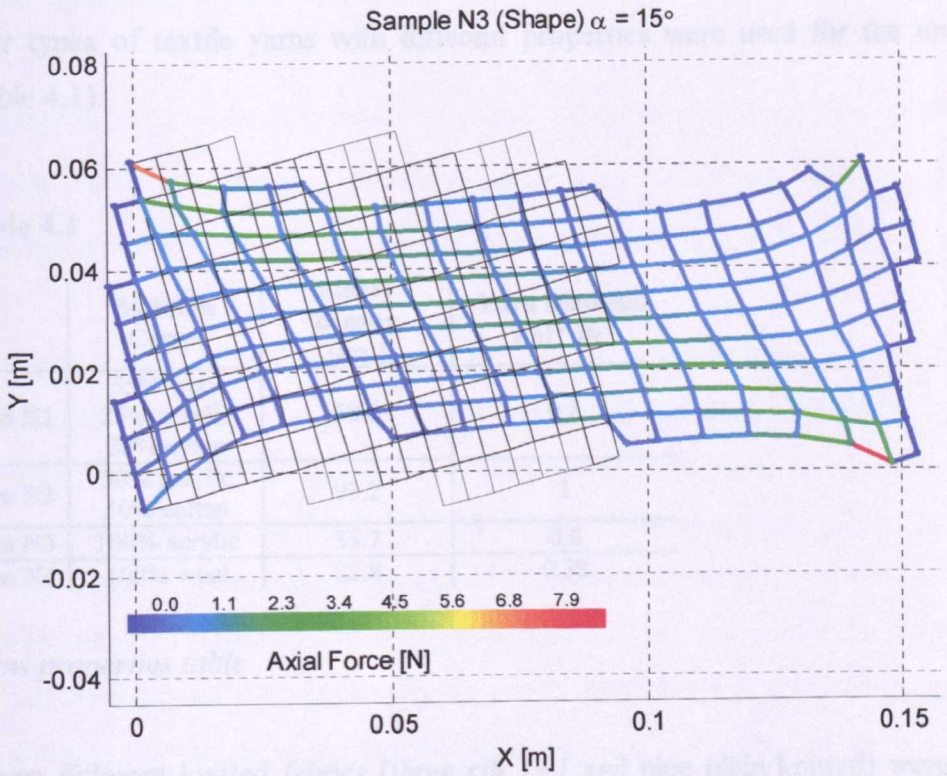

(c)

Figure 3.14 ***Sample number 3 (see Table 4.3).***

(a)-- load-extension curves; numerical model – green, experiment – blue ;

(b) – relative lateral contraction; numerical model – green, experiment – blue ;

(c) – Numerically simulated shape; initial state – black; final state –colour.

CHAPTER 4. Experimental work

4.1 Introduction

The following aims of the experimental study were established:

1. to obtain mechanical properties of yarns, *i.e.* tensile rigidity as a function of yarn extension, bending rigidity coefficient, torsion rigidity coefficient, initial compression rigidity coefficient;
2. to study tensile properties of knitted samples subjected to uni-axial load in different directions.

Four types of textile yarns with different properties were used for the investigation (Table 4.1).

Table 4.1

	% Fibre Comp.	Linear density [tex.]	Yarn Diameter [m]* 10^{-3}
Yarn N1	55% wool 25% acrylic 20% nylon	68.0	0.8
Yarn N2	50% acrylic 50% cotton	93.2	1
Yarn N3	100% acrylic	35.7	0.8
Yarn N4	100% wool	22.8	0.38

Yarns properties table

Eleven different knitted fabrics (three *rib 1+1* and nine plain knitted) were produced from yarns specified in Table 4.1 in the knitting laboratory of the Department of Textile Design and Production of De Montfort University. Fabrics were different in dimensional properties *a* and *b* (Figure 2.1). Fabrics properties are presented in Table 4.2.

Table 4.2

	Yarn Number	Fabric Type	Loop size in course direction (OX) [m] $*10^{-3}$	Loop size in wale direction (OY) [m] $*10^{-3}$
Fabric N1	YN 1	PLAIN	1.7($\pm$ 0.01)	2.45($\pm$ 0.02)
Fabric N2	YN 1	PLAIN	2.17($\pm$ 0.02)	3.55($\pm$ 0.02)
Fabric N3	YN 1	RIB 1+1	4.17($\pm$ 0.05)	2.63($\pm$ 0.04)
Fabric N4	YN 2	PLAIN	2.13($\pm$ 0.03)	2.29($\pm$ 0.03)
Fabric N5	YN 2	PLAIN	2.36($\pm$ 0.04)	3.49($\pm$ 0.02)
Fabric N6	YN 2	PLAIN	2.56($\pm$ 0.0)	3.85($\pm$ 0.03)
Fabric N7	YN 2	RIB 1+1	4.76($\pm$ 0.09)	2.98($\pm$ 0.05)
Fabric N8	YN 3	PLAIN	1.7($\pm$ 0.08)	2.43($\pm$ 0.02)
Fabric N9	YN 3	PLAIN	2.33($\pm$ 0.04)	3.39($\pm$ 0.03)
Fabric N10	3	RIB 1+1	4.6($\pm$ 0.05)	3.13($\pm$ 0.04)
Fabric N11	4	PLAIN	1.27($\pm$ 0.03)	1.94($\pm$ 0.03)
Fabric N12	4	PLAIN	1.35($\pm$ 0.03)	2.21($\pm$ 0.02)

Fabric properties Table

For each type of fabric parameters A_{kn} and B_{kn} were measured at least five times. An average value and standard deviation (*StD*) were calculated. The values of fabric dimensions are represented in Table 4.2 in the form: $a = a_{mean} \pm StD(a)$.

To verify the numerical model proposed above 42 different samples were cut from fabrics specified in Table 4.2. The samples cut from rib structure were tested, however the results have not been included into the present work because the numerical model for that structure had not been finished. Properties of the samples are listed in Table 4.3. All samples have a rectangle shape. Dimension of each of the samples is defined as dimension of designed pattern, which was initially drawn on the fabric surface. Having been cut out the samples changed their dimensions. The actual width of each of the samples after it had been clamped* is represented in brackets in respective columns in Table 4.3.

The samples and yarns were chosen to provide a range of knitted structures with different properties, *i.e.* tightness of structure and yarn mechanical properties.

* *Sample width in the narrowest part (see paragraph 4.5).*

Table 4.3

	Fabric Number	Length (X dir.) [m]*10^{-2}	Width (Y dir.) [m]*10^{-2}	Coarse angle	Fabric Type	Number of layers in sample	Direction of Force
Sample N1	FN 1	7	6 (4.5)	0°	PLAIN	2	X
Sample N2	FN 1	6 (5)	7	0° (90°)	PLAIN	2	Y (X)
Sample N3	FN 1	9	6 (4.5)	15°	PLAIN	2	X
Sample N4	FN 1	9	6 (5.5)	30°	PLAIN	2	X
Sample N5	FN 1	9	6 (6)	45°	PLAIN	2	X
Sample N6	FN 1	9	6 (5)	60°	PLAIN	2	X
Sample N7	FN 1	9	6 (5.3)	75°	PLAIN	2	X
Sample N8	FN 1	6	9 (5)	0° (90°)	PLAIN	2	Y (X)
Sample N9	FN 1	9	6 (3.8)	0°	PLAIN	2	X
Sample N10	FN 2	10	7 (3.5)	0°	PLAIN	2	X
Sample N11	FN 3	10	7 (6.5)	0°	RIB 1+1	1	X
Sample N12	FN 3	7 (7)	10	0° (90°)	RIB 1+1	1	Y (X)
Sample N13	FN 4	10	7 (6.5)	0°	PLAIN	2	X
Sample N14	FN 4	7 (5.5)	10	0° (90°)	PLAIN	2	Y (X)
Sample N14 (a)	FN 4	10	7 (6.8)	30°	PLAIN	2	X
Sample N15	FN 4	10	7 (6.9)	45°	PLAIN	2	X
Sample N16	FN 4	10	7 (7.1)	60°	PLAIN	2	X
Sample N17	FN 5	10	7 (5.5)	0°	PLAIN	2	X
Sample N18	FN 5	10	7 (5.9)	15°	PLAIN	2	X
Sample N19	FN 5	10	7 (6.5)	30°	PLAIN	2	X
Sample N20	FN 5	10	7 (6.4)	45°	PLAIN	2	X
Sample N21	FN 5	7 (5.5)	10	0° (90°)	PLAIN	2	Y (X)
Sample N22	FN 6	10	7 (5)	0°	PLAIN	2	X
Sample N23	FN 6	10	7 (6)	60°	PLAIN	2	X
Sample N24	FN 6	10	7 (6)	75°	PLAIN	2	X
Sample N25	FN 6	7 (6.4)	10	0° (90°)	PLAIN	2	Y (X)
Sample N26	FN 7	10	7 (6.5)	0°	RIB 1+1	1	X
Sample N27	FN 7	7 (6.5)	10	0° (90°)	RIB 1+1	1	Y (X)
Sample N28	FN 8	10	6 (4.8)	0°	PLAIN	2	X
Sample N29	FN 8	10	6 (5.3)	15°	PLAIN	2	X
Sample N30	FN 8	10	6 (5.8)	30°	PLAIN	2	X
Sample N31	FN 8	10	6 (6)	45°	PLAIN	2	X
Sample N32	FN 8	10	6 (5)	75°	PLAIN	2	X
Sample N33	FN 8	6 (4.9)	10	0° (90°)	PLAIN	2	Y (X)
Sample N34	FN 9	10	7 (4.5)	0°	PLAIN	2	X
Sample N35	FN 9	10	7 (6.5)	45°	PLAIN	2	X
Sample N36	FN 9	7 (6)	10	0° (90°)	PLAIN	2	Y (X)
Sample N37	FN 10	10	7 (6.6)	0°	RIB 1+1	1	X
Sample N38	FN 10	7 (6.8)	10	0° (90°)	RIB 1+1	1	Y (X)
Sample N39	FN 11	10	6 (3.6)	0°	PLAIN	2	X
Sample N40	FN 11	6 (3.7)	10	0° (90°)	PLAIN	2	Y (X)
Sample N41	FN 12	10	6 (3.8)	0°	PLAIN	2	X
Sample N42	FN 12	6 (3.4)	10	0° (90°)	PLAIN	2	Y (X)

Samples properties table

A brief description of equipment and experimental rigs are represented below.

4.2 Samples and Testing Equipment (Yarn Bending Rigidity test)

Yarn bending rigidity measurements were carried out on KES-F Pure Bending Tester (Kawabata 1980) under standard atmospheric conditions and according to the instruction manual. This equipment was originally intended for use with woven fabrics and the method used was adapted for yarns.

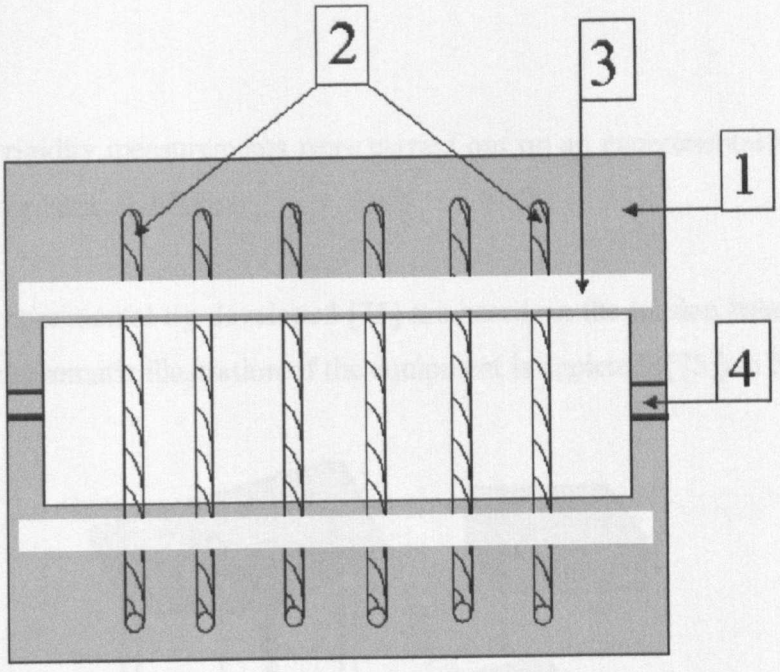

Figure 4.1 ***A schematic illustration of a sample for the bending tester.***

1 – the base of the sample (made from thin card);

2 –multiple samples of yarn (20 to 70 strands);

3 – sticky tape (used to attach yarn to the base of the sample);

4 – an approximate interval to cut out after the samples were mounted into the jaws of the tester.

Two samples consisting of 20-70 yarns for each type of yarn were prepared (see Figure 4.1) and tested.

The values obtained for the bending rigidity of the yarns are shown in Table 4.4.

Table 4.4

	Bending Rigidity [N*m^2]*10^{-8}
Yarn N1	3.6
Yarn N2	2.1
Yarn N3	4.2
Yarn N4	1.4

Bending rigidity coefficient for the tested yarns (see Table 4.1*)*

4.3 Samples and Testing Equipment (Yarn Torsion Rigidity test)

Yarn torsion rigidity measurements were carried out on an experimental rig [75] under standard atmospheric conditions.

The special experimental rig developed [75] are based on the torsion balance technique [76, 77]. The schematic illustration of the equipment is depicted ([75]) in Figure 4.2.

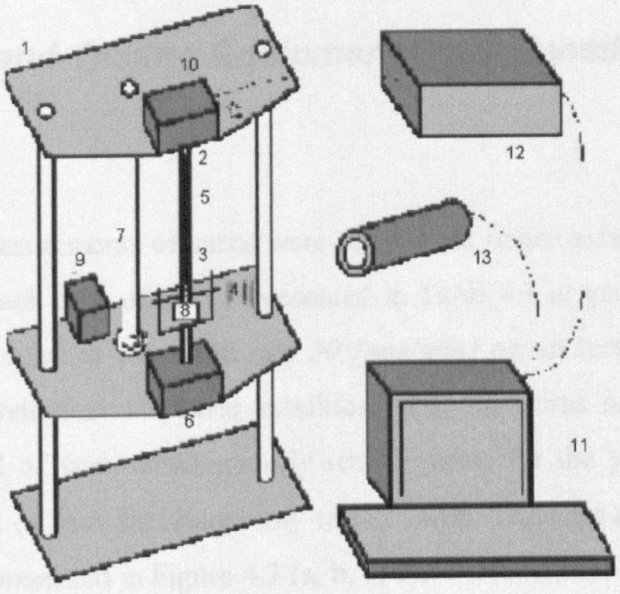

Figure 4.2 ***Experimental rig to study yarn twisting***

1 – support; 2 – upper clamp; 3 – lower clamp; 4 – Beam; 5 – sample; 6 – torquemeter; 7 – shorteningmeter; 8 – weight to tension the yarn; 9 –vibrodevice; 10 – stepper motor; 11 – PC to control yarn twisting; 12 – digital board to control stepper motor; 13 – CCD camera to register the yarn strain state.

The experimental sample *5* in Figure 4.2 is fixed in clamps *2* and *3*. The maximum gauge length in standard rig set is *200 [mm]*. The gauge length used for the testing was *100 [mm]*. The weight *8* is mounted to the lower end of the sample *3* to provide the desirable tension of the sample. The upper clamp *2* is connected to the axis of the stepper motor *10*. The stepper motor is controlled by the PC *11*. It is possible to choose the direction of twisting. The torsion rigidity was measured in both directions. An average value was adopted for further calculations. The values of initial torsion rigidity are represented in Table 4.5.

Table 4.5

	Torsion Rigidity $[N*m^2]*10^{-8}$
Yarn N1	1.4
Yarn N2	1.1
Yarn N3	2.7
Yarn N4	0.7

Torsion rigidity coefficient for the tested yarns (see Table 4.1*).*

4.4 Samples and Testing Equipment (Yarn Tensile Rigidity test)

Load-extension measurements of yarns were carried out under axial loading conditions on *2* samples for each type of yarn represented in Table 4.1 at gauge length *10 [cm]*. All samples were tested at extension rate *50 [mm/min]* on an Instron Tensile Testing machine under standard atmospheric conditions. For the yarns number *1, 2, 3* each specimen consisted of two simultaneously tested yarns; for the yarn number *4* each specimen consisted of four simultaneously tested yarns. The load-extension curves for tested yarns are represented in Figure 4.3 (a, b, c, d).

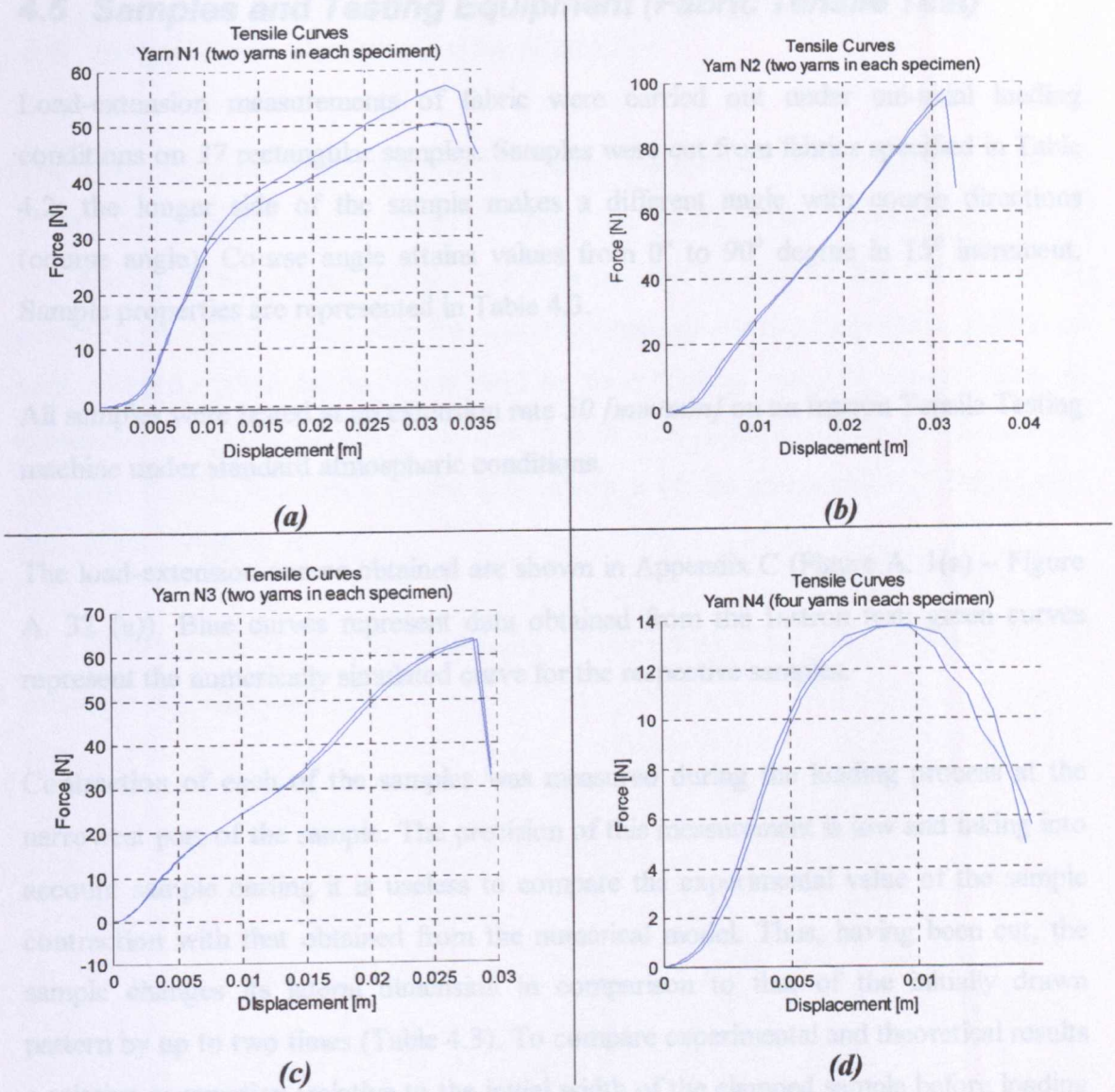

Figure 4.3 (a, b, c, d)

Experimental load-extension curves for the tested yarns (see Table 4.1*).*

4.5 Samples and Testing Equipment (Fabric Tensile Test)

Load-extension measurements of fabric were carried out under uni-axial loading conditions on *37* rectangular samples. Samples were cut from fabrics specified in Table 4.2; the longer side of the sample makes a different angle with course directions (course angle). Course angle attains values from 0^{o} to 90^{o} degree in 15^{o} increment. Sample properties are represented in Table 4.3.

All samples were tested at an extension rate *50 [mm/min]* on an Instron Tensile Testing machine under standard atmospheric conditions.

The load-extension curves obtained are shown in Appendix C (Figure A. 1(a) – Figure A. 32 (a)). Blue curves represent data obtained from the Instron test; green curves represent the numerically simulated curve for the respective samples.

Contraction of each of the samples was measured during the loading process at the narrowest part of the sample. The precision of this measurement is low and taking into account sample curling it is useless to compare the experimental value of the sample contraction with that obtained from the numerical model. Thus, having been cut, the sample changes its lateral dimension in comparison to that of the initially drawn pattern by up to two times (Table 4.3). To compare experimental and theoretical results a relative contraction (relative to the initial width of the clamped sample before loading for experiment and to the designed width of the sample pattern for the theoretical model) was calculated. The relative contraction curves are represented in Appendix C (Figure A. 1(b) – Figure A. 32 (b)). Blue curves represent data obtained from experiments; green curves represent numerically simulated curves for the respective samples.

4.6 Initial Yarn Compression Rigidity

The value of initial yarn compression rigidity (coefficient $K0$ in equation (3.8) or (2.28)) is estimated as $K0 = 15000\,[N\,m/m]$ for all of tested yarns. During testing calculations, it was found that the model is not too sensitive to the value of initial compression rigidity and hence the specified value of initial compression coefficient was adopted. When fabric is subjected to an extension load, the current value of compression rigidity increases very fast due to fast decrease of the denominator in equation (2.28). This leads to the low influence of the initial value of the current compression rigidity K.

The experimental routine for evaluation of the initial compression rigidity $K0$ is described elsewhere in [1, 2].

CHAPTER 5. Comparison and Discussion

5.1 Comparison of Experimental Data with Numerical Calculated Data

The work presented here is concentrated on the development of a physical-mathematical model of a knitted structure under tension with the main emphasis made on theoretical and numerical formulation of the problem and application to the plain knitted structure subjected to uni-axial extension. The experimental investigation presented here is not comprehensive enough to make a quantitative analysis of the model. Thus, it is not correct to state that the model proposed predicts the behaviour of any knitted structure. For this level of analysis of the model, many more of different structures should be covered by experimental investigation. Moreover, each of the samples should be tested several times* to evaluate the data confidence interval. For the quantitative analysis and comparison of the numerical model with the experimental data, it is particularly important to evaluate model sensitivity to the input data variation, which in turn appears due to the tolerance of the evaluation of the input data; that will give a confidence interval of the model response due to variation of input parameters. For the quantitative analysis of the model, it is necessary to compare the confidence intervals of experimental data with that of the model. Although some quantitative conclusions are made below, further analysis remains of a qualitative nature.

The uni-axial tensile test is used for the evaluation of the important parameters of fabrics. It is normally assumed that a tested sample is long enough to minimize the influence of the boundary conditions (clamps). In the case of woven fabric, which has much more stable structure in comparison with plain knit, it is possible to test a long sample with length-to-width ratio say up to six. The plain knit sample of that dimension is very unstable due to curling of the sample edges; thus, it is necessary to test a shorter sample, which increases the influence of the boundary conditions. It is

* *Due to residual strains it is probably not correct to test the same sample several times, on the other hand a similar sample will inevitably differ from the origin in it's properties.*

therefore more correct to study plain knit behaviour when all edges of the sample are restricted with some boundary conditions, which could be a bi-axial extension test for instance.

The model proposed gives a much more stable solution when the fabric is subjected to tensile force in both directions. When only the axial load is acting, each of the finite elements tends to extend in the direction parallel to the applied force and contract in the transverse direction. The yarn-to-yarn compression is the only factor restricting the finite element from collapsing. The yarn-to-yarn compression rigidity increases very fast when the yarns (sides of the finite-element) approach each other; that in turn leads to an unstable response of the system (Figure 3.5). In the case of bi-axial extension of the sample, each of the finite elements would be subjected to extension in both directions, and the system will give a much more stable response in this case. It should be noted that uni-axial extension of the plain knit, when some of the sample edges are free from any constraints, is probably the most complicated problem as oppose to the situation where all of the sample's edges are restricted by some boundary conditions.

A comparison of the experimental data with that obtained numerically yields the conclusion that the model satisfactorily describes the behaviour of the plain knit subjected to uni-axial load. An appreciable discrepancy between theory and experiment still exists; especially at higher extensions but the general shape of the theoretically predicted curves agrees well with that of the experimentally obtained curves.

The numerically predicted shape of the extended samples qualitatively agrees with that observed in the experiment (Figure A. 1(c) – Figure A. 32 (c)). Thus, the narrowest part of the sample is located in the middle, and there is an interval in the middle of the sample where width remains virtually the same. Approaching the clamps, the sample width increases rapidly and reaches the value of the initial sample width at the clamped edges.

When the plain knit sample was subjected to high loads, slippage of yarn from the clamps occurred. The process normally begins at the outermost points of the clamp. That could be attributed to stress concentration at these locations. The theoretically predicted distribution of axial force acting in yarns in extended samples is illustrated

by colour gradation of axial force (from blue to red) in Figure A. 1(c) – Figure A. 32 (c). It is seen that the maximum load is exerted near the end of the clamped edge which is qualitatively agrees with what happened in reality.

The evaluation of the simulated sample contraction during loading also agrees qualitatively with that obtained experimentally. The value of the sample contraction in the narrowest part (see for example Figure 3.14 (b)) relative to the initial sample width is represented in Figure A. 1(b) – Figure A. 32 (b). The sample width reduces rapidly during the initial stages of loading and tends to some constant value at higher loads.

Predicted and experimental load-extension curves are represented in Figure A. 1(a) – Figure A. 32 (a). In the worst case, which is the case of the sample number 14 represented in Figure A. 11(a, b, c), the discrepancy between the predicted and experimental elongation is equal to $\Delta = 10[mm]$ at load *20 [N]*, while the initial sample length $L_s^0 = 100[mm]$ and the final length of the sample (from experiment), at load *20 [N]*, $L_s = 115[mm]$. Thus, the maximum value of the relative value of the discrepancy over all tested samples can be estimated as $eps = \frac{\Delta}{L_s^0} \approx 0.1$, or as $\widetilde{eps} = \frac{\Delta}{L_s} \approx 0.087$.

5.2 Further extension of the Model

5.2.1 Transformation from 2D to 3D Deformation

Although the problem of fabric extension *in plane* is considered the model is not restricted by 2D. Extension of the model to 3D requires complicated routine work for implementation of the model, however the idea is quite simple.

To consider an out of plane deformation it is necessary to obtain a corresponding rigidity matrix of the system, which incorporates an additional block with regards to additional co-ordinate Z (four additional degrees of freedom $Z_i\,(i = 1:4)$ one for each of the knot points of the finite-element). The essential improvements of the constitutive

elements (see section 2.3), required for the model extension from 2D to 3D are outlined below.

- **Thread constitutive element**

To obtain the potential energy with respect to the additional co-ordinate it is enough to keep variable z_1 and z_2 in equation (2.26). The rigidity matrix for 3D *thread element* can be obtained then according to equation (3.2) or (3.3).

- **Helix constitutive element**

The potential energy of the *helix element* is independent of its geometrical position and an external load only exerts work on length re-distribution co-ordinates, which are scalars. Thus, it is possible to use the *helix element* for the 3D without any changes.

- **Height constitutive element**

The *height* and *side elements* were introduced to describe the unit cell/finite-element resistance to compression. The physical sense of those elements is to simulate yarn-to-yarn interaction in the deformed fabric. It was assumed that compressibility of the plain knit is determined by the mutual interaction/compression of the opposite sides of the unit cell/finite-element. That implies that interaction of the others yarns except the neighbour is not taken into account. That is a reasonable assumption for the *in plane* deformation of the flat sample when the out-of-plane deflection Z is prohibited. Considering the general 3D deformation of a fabric, it is probably not correct to keep the same assumption as that made for the 2D deformation because any two or more yarns could interact due to possible shape of fabric surface in the deformed state. To approach the general 3D problem it is necessary to define some effective characteristics of the measure of the deformed fabric state. That can be for example a volume V_f of some figure circumscribed over the fabric surface. The potential energy of the system in this case can be written in a general form as:

$$\Pi = \Pi_{system}\left(\underline{q}\right) + \Pi_V\left(V_f\right)$$

where Π is the total potential energy of a system;

$\Pi_V\left(V_f\right)$ is the potential energy of yarn-to-yarn interaction as a function of the introduced volume;

$\Pi_{system}\left(\underline{q}\right)$ is the potential energy of the system as a function of the virtual co-ordinate vector $\underline{q}$.

The volume V_f can be considered as an independent parameter which constraints deformation of the whole system. To obtain a corresponding rigidity matrix it is then enough to calculate only one derivative: $\frac{\partial \Pi_V}{\partial V_f}$. Although an implementation of this approach is very simple, it is very hard to write a reasonable expression for the function $\Pi_V\left(V_f\right)$. Moreover, the term $\Pi_V\left(V_f\right)$ gives an integral constraint of the sample compression and do not provide a reasonable shape of deformed fabric. Thus, self-intersections of the deformed surface of the fabric may occur during deformation.

Another way to approach the problem is to consider all possible yarn-to-yarn interactions in a deformed fabric. It is worth stating that this kind of approach is very complicated. Taking into account that at each step of fabric deformation it is necessary to take control of all possible contacts of 3D yarns in 3D, makes the problem virtually irresolvable.

Despite the above arguments, there is a wide range of 3D problems which can be tackled by the model. For example, the problem of deflection of the initially flat sample with all clamped edges subjected to located or dislocated force F acting orthogonal to the initial fabric surface direction as shown in Figure 5.1. In this case, it is possible to accept the assumptions, which were used for the 2D problem. To extend the *height* or *side elements* to 3D it is necessary to include Z-components in the expression for the side length (variable a in equation (2.27)) or define a similar to $H_{i,j}$ (equation (2.29)) *height* parameter for a 3D quadrilateral unit cell. The *height* parameter, for example could be defined as the height of a projection of the 3D unit cell onto some mean plane Ψ. It is possible to assume for example that Ψ minimise the following sum:

$$\sum_{i=1}^{4} R_n^i$$

where R_n^i is a distance from the knot point i of the unit cell to the plane Ψ.

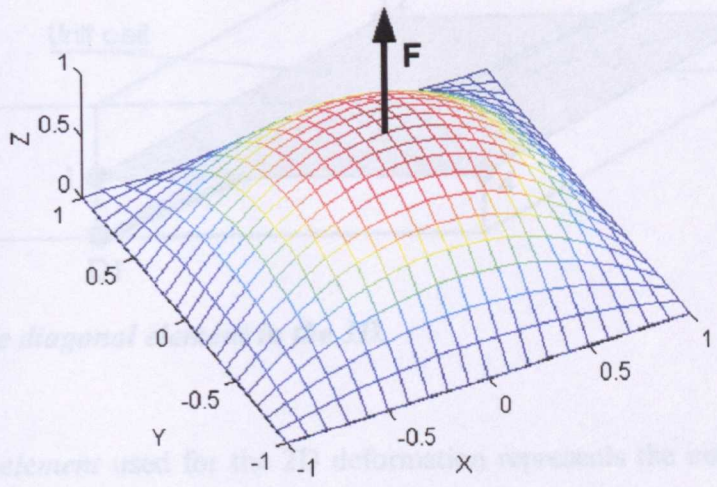

Figure 5.1 ***Deflection of the initially flat sample with all clamped edges subjected to located or dislocated force*** F ***acting in orthogonal to the initial fabric surface direction.***

- **Diagonal element.**

The *diagonal* element, introduced in section 3.5 is used to provide a definable rigidity matrix for the system. To obtain a definable rigidity matrix for the 3D deformation of the unit cell it is possible to consider the same diagonal element, which connects the vertexes D1 and D3 of the imaginary prism as shown in Figure 5.2. The *diagonal element* for the 2D deformation connects knot point 1 and 3 of the unit cell. The height of the imaginary prism T can be considered as a thickness of the fabric.

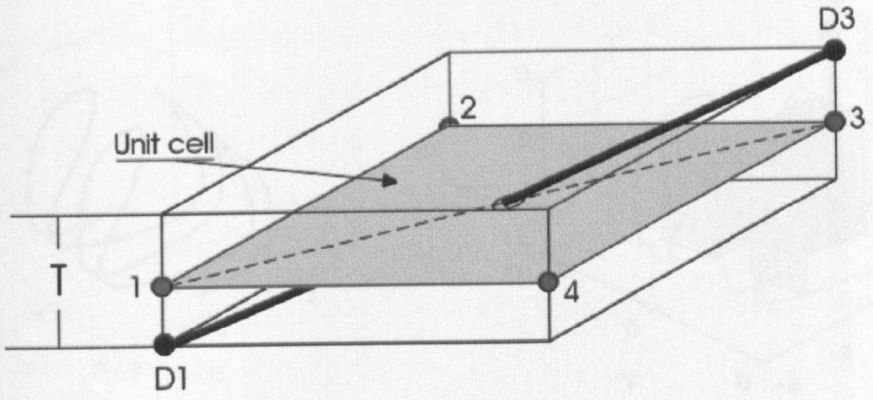

Figure 5.2 ***The diagonal element in the 3D.***

The *diagonal element* used for the 2D deformation represents the initial shear rigidity of the unit cell. The introduced 3D *diagonal element* simulates both the shear rigidity and bending rigidity of the unit cell.

5.2.2 1+1 Rib Fabric

The typical example of the 3D yarn path in 1+1 rib structure is represented in Figure 5.3 (a). Although the structure of 1+1 rib differs form that of the plain knit fabric, it is probably possible to use virtually the same approach to study deformation of the 1+1 rib fabric. The unit cells for 1+1 rib structure can be defined as shown in Figure 5.3 (b). Defined in this way the unit cell forms a 3D profile which is determined by the fabric thickness and fabric dimensions A_{rib} and B_{rib} which are similar to that of the plain knit fabric shown in Figure 2.1 (a, b).

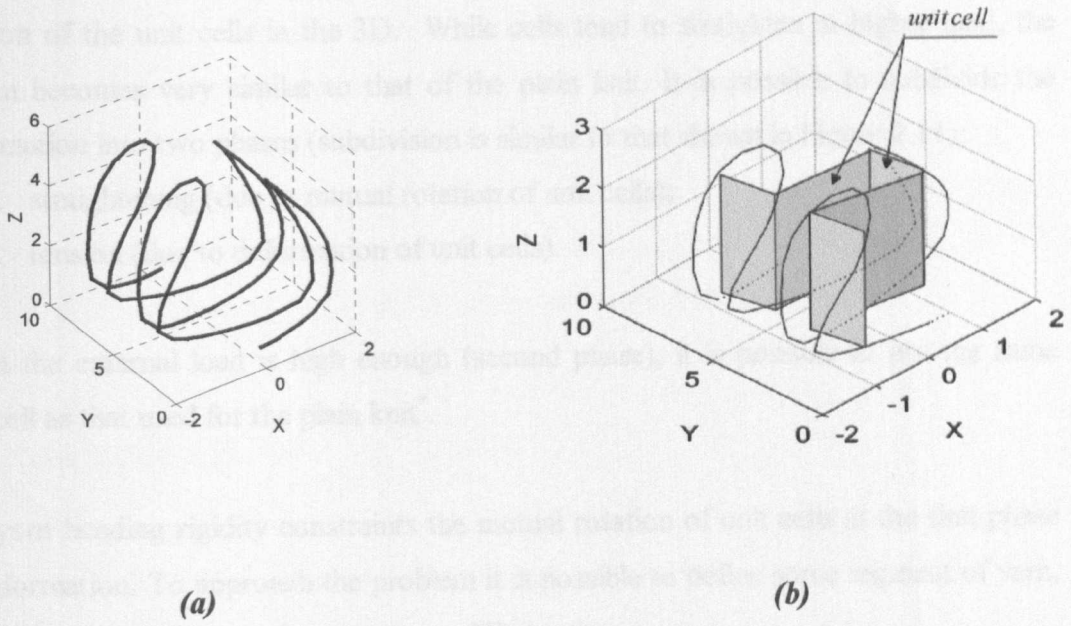

Figure 5.3 (a, b). ***The 1+1 rib fabric.***

typical example of the yarn path — (a);

schematic illustration of the unit cells (grey quadrilaterals) — (b);

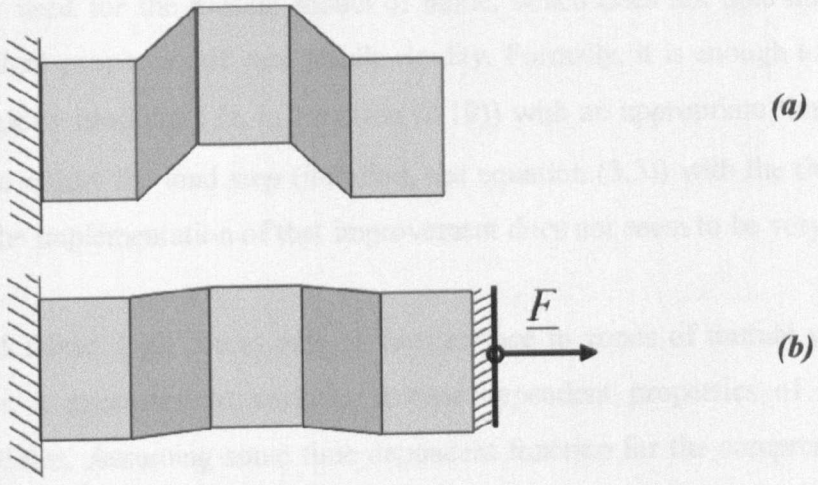

Figure 5.4 ***Deformation of unit cells for 1+1 rib fabric.***

initial position – (a); deformed state – (b).

Deformation of the unit cells subjected to external force $\underline{F}$ is illustrated in Figure 5.4. When external force $\underline{F}$ is small deformation of the structure is determined by mutual

rotation of the unit cells in the 3D. While cells tend to straighten at higher load, the system becomes very similar to that of the plain knit. It is possible to subdivide the deformation into two phases (subdivision is similar to that shown in Figure 2.11):

1. straightening (due to mutual rotation of unit cells);
2. tension (due to deformation of unit cells).

When the external load is high enough (second phase), it is possible to use the same unit cell as that used for the plain knit*.

The yarn bending rigidity constraints the mutual rotation of unit cells at the first phase of deformation. To approach the problem it is possible to define some segment of yarn, which is responsible for cell resistance to 3D rotation.

5.2.3 Recommendations for Further Work

Although the model proposed describes fabric mechanical properties it should be noted that a large amount of work yet should be done. Namely, the simplest model of yarn extension is used for the present model of fabric, which does not take into account a time dependent properties of yarn tensile rigidity. Formally, it is enough to replace the effective rigidity modulus (D_E in equation (2.19)) with an appropriate time dependent function and adjust the load step (iteration, see equation (3.5)) with the time intervals. However, the implementation of that improvement does not seem to be very easy.

In extended fabric, high forces acts at yarn surface in zones of mutual yarn contact. That makes it necessary to consider a time dependent properties of compression rigidity modulus. Assuming some time dependent function for the compression rigidity coefficient ($K(z)$ in equation (2.28)) it is possible to implement an algorithm, which takes into account time dependent properties of compression.

* *The properties of the unit cell for rib structure will differ considerably from that of the plain knit due to different geometric properties of constitutive elements.*

The algorithm itself requires some improvements. Thus, in reality having been subjected to considerable extension fabric does not assume any further significant contraction. It is probably reasonable to introduce a locking of the finite-element. When compression exceeds some pre-determined limit, it is possible to restrict further contraction. However developing the locking criteria requires an additional analysis to be made. The implementation of lockable finite-element is also not obvious.

5.3 Conclusions

1. To define initial dimensional properties of the plain knitted fabric from its known dimensions and yarn properties a geometrical approach was developed and implemented. With the aid of the developed algorithm and software, it is possible to define important characteristics of fabric for the subsequent use as input parameters for the theoretical model.
2. An experimental investigation of fabric extension was carried out. Yarn mechanical properties were obtained in experiment.
3. The model of the static extension of the plain knit fabric was developed, implemented and tested. The results show that the model describes adequately the real phenomena. Although an appreciable discrepancy between theory and experiment still exists, especially at higher extensions the general shape of the theoretically predicted curves agrees well with that of the experimentally obtained curves.
4. Complex software for computer modelling and visualisation of plain knitted fabric deformation was developed. This software allows simulation of *in plane* extension of an arbitrary fabric sample under various loading conditions. An appropriate format of input data was developed; a suitable graphic user interface is provided.
5. Possible application of the model to more complex problems (*i.e.* studying of different knitted structures, 3D deformation of fabric) is outlined.

References

1. Grishanov, S.A., Lomov, S.V., Harwood, R.J., Cassidy,T. and Farrer, C., 'The Simulation of the Geometry of Two Component Yarns. P. I: The Mechanics of Strand Compression: Simulation Yarn Cross Section Shape', *J. Textile Inst.*, Vol. 88, pp. 118-131, (1997).

2. Harwood, R.J., Grishanov, S.A., Lomov, S.V., Cassidy, T., 'Modelling of Two Component Yarns. Part I: The Compressibility of Yarns', *J. Textile Inst.*, Vol. 88, pp. 373-384, (1977).

3. Davidovich, A.S. 'The Basic Theory of Knitting', Legkaya Industria, Moscow, (1970).

4. Van Wyk, C.M. 'Note on Compressibility of Wool', *J. Textile Inst.*,37,T285-92, (1946).

5. Spravochn. Mashinostroit. GNTI ML Moskva 1952 Vol.2 p.223-237

6. Norrie, D.H. and de Vries, G., 'An Introduction to Finite Element Analysis', New York, Academic Press, (1978).

7. Postnov,V.A., Harhurim,I., 'The Finite Element Method. Application to the Naval Architecture Mechanics.', Sudostroenie, Leningrad, (1974).

8. Norrie, D.H. and de Vries, G., 'A Finite Element Bibliography', New York, Plenum Press, (1973).

9. Zienkiewicz, O.C. 'The Finite Element Method in Engineering Science', London, McGraw-Hill, 2nd ed., 1971.

10. Obraszov, I.F., Savel'ev, L.M., Hazanov,H.S., 'The Finite Element Method. Application to Aircraft Mechanics', Moscow, High School Press, (1985).

11. Shabrov, N.N. 'The Finite Element Method. Application to Heat-engine Mechanics.', Leningrad, Machinery Society, (1983).

12. Choong-Gyoo Lim, 'A Universal Parameterisation in B-spline Curve and Surface interpolation', *Computer Aided Geometric Design*, 16, pp.407-422, (1999).

13. Novozilov, V.V., 'Thin Shell Theory', P. Noordhoff, Groningen, (1964).

14. Love, A.E.H., 'A Treatise on the Mathematical Theory of Elasticity', Dover Publications, New York, (1944)

15. Eliseev,V.V., 'Mechanics of Elastic Rod', S-Petersburg Technical University, (1994).

16. Hearle, J.W.S., 'The Mechanics of Twisted Yarns: the Influence of Transversal Forces on Tensile Behaviour.' *J. Text. Inst.*, vol. 49; 1958.

17. Leaf,G.A.V., 'Woven Fabric Tensile Mechanics', *Mechanics of Flexible Fibre Assembles,* NATO Advanced Study Institute Ser. E: Applied Science N. 38, Sjthooff and Noordhoff, The Netherlands, pp 143-157, (1980).

18. Hepworth, R.B., 'Some Aspects of Mechanics of a Model of Plain Weft-knitting', *Mechanics of Flexible Fibre Assembles,* NATO Advanced Study Institute Ser. E: Applied Science N. 38, Sjthooff and Noordhoff, The Netherlands, pp 175-196 (1980).

19. Grosberg,P., 'The Bending of Yarns and Plain Woven Fabrics', *Mechanics of Flexible Fibre Assembles,* NATO Advanced Study Institute Ser. E: Applied Science N. 38, Sjthooff and Noordhoff, The Netherlands, pp 197-209, (1980).

20. Konopasek, M, 'Classical Elastica Theory and its Applications', *Mechanics of Flexible Fibre Assembles,* NATO Advanced Study Institute Ser. E: Applied Science N. 38, Sjthooff and Noordhoff, The Netherlands, pp 255-274, (1980).

21. Lloyd, D.W., 'The analysis of Complex Fabric Deformation', *Mechanics of Flexible Fibre Assembles,* NATO Advanced Study Institute Ser. E: Applied Science N. 38, Sjthooff and Noordhoff, The Netherlands, pp 311-342, (1980).

22. Lloyd, D.W., 'An Integrated Approach to the Mechanical Modelling of One, Two and Tree-dimensional Textile Structures', *The Application of Mathematics and Physics in the Wool Industry,* Wool Research Organisation of New Zealand (Inc) and the Textile Institute New Zealand Section, Christchurch, New Zealand, pp 21-42, (1988).

23. Buckley,C.P., Lloyd, D.W., Konopasek,M., 'On the Deformation of Slender Filaments with Planar Crimp: Theory, Numerical Solution and Applications to Tendon Collagen and Textile Materials', *Proceedings of the Royal Society of London*, SeriesA, 372, pp 33-64, (1980).

24. Kawabata, S., Niwa, M. and Kawai ,H. 'The Finite Deformation Theory of Plane-weave Fabrics, Part I: The Bi-axial Deformation Theory', *J. Textile Inst.* , Vol. 64 (2), pp. 21-46, (1973).

25. Kawabata, S., Niwa, M. and Kawai ,H. 'The Finite Deformation Theory of Plane-weave Fabrics, Part II: The Uni-axial Deformation Theory', *J. Textile Inst.* , Vol. 64 (2), pp. 47-61, (1973).

26. Kawabata, S., Niwa, M. and Kawai ,H. 'The Finite Deformation Theory of Plane-weave Fabrics, Part III: Shear Deformation Theory', *J. Textile Inst.* , Vol. 64 (2), pp. 61-72, (1973).

27. Kawabata, S., 'Proceedings of 14th Textile Research Symposium at Mount Fuji, 1984', the Textile Machinery Society of Japan, Osaka, p.1., (1984).
28. Kawabata, S., 'Textile Structural Composites', Elsevier, Amsterdam, p.79, (1989).
29. Kawabata, S., Mari Inoue and Masako Niwa, 'Non-linear Theory of the Bi-axial Deformation of a Triaxial-weave Fabric', *J. Textile Inst.*, Vol. 83 (1), pp.104-119, (1992).
30. Reunmann, R.D., 'CAD Method for the Predetermination of the Weave-Related Load-Extension Characteristics of Woven Fabrics', *Melliand Textilber*, 11, E386-E388, (1990).
31. Fangning Sun, Abdelfatan, M., Seyam and B.S. Gupta, 'A Generalized Model for Prediction Load-Extension Properties of Woven Fabrics', *Textile Res. J.*, Vol. 67 (9). pp. 654-664. (1997).
32. Grosberg, P. and Park, B.J., 'The Mechanical Properties of Woven Fabrics. Part V: The Initial Modulus and the Frictional Restraint in Shearing of Plane-weave Fabrics', *Textile Res. J.*, Vol. 36, pp.420-431, (1966).
33. Olofsson, B., 'A Study of Inelastic Deformation of Textile Fabrics', *J. Textile Inst.*, Vol. 58, pp.224-241, (1967).
34. Skelton, J., 'Fundamentals of Fabric Shear', *Textile Res. J.*, Vol. 46, pp. 862-869, (1976).
35. de Jong, S., 'A Study of Fabric Mechanics Using Energy Methods of Analysis', Ph.D. Thesis, University of New South Wales, (1976).
36. de Jong, S. and Postle, R., 'A General Energy Analysis of Fabric Mechanics , Using Optimal-Control Theory', *Textile Res. J.*, Vol. 48,pp. 127-135 , (1978).
37. Postle, R., Carnaby, G.A. and S. de Jong, 'The Mechanics of Wool Structures', Ellis Horwood, Chinchester, West Sussex, England, pp. 195-207, (1988).
38. Sinoimeri, A., and Drean,. J.Y., 'A study of the Mechanical Behaviour of the Plane-Weave Structure by using Energy Methods: Fabric Shear', *J. Textile Inst.*, Vol. 87 (1,P.I), pp. 120-128, (1996).
39. Hu Jinlian, Jiang Yaming, Ko Frank, 'Modelling Uni-axial Tensile Properties of Multi-axial Warp Knitted Fabrics', *Textile Res. J.*, Vol.68 (11) ,pp. 828-834, (1998).
40. Kilby, W.F., 'Plannar Stress-Strain Relationship in Woven Fabrics', *J. Textile Inst.*, Vol. 54 (T9) , (1963).
41. Pan, N. and Mee-Young Yoon, 'Structural Anisotropy, Failure Criterion, and Shear Strength of Woven Fabrics', *Textile Res. J.*, Vol. 66 (4) ,pp. 238-244 , (1996).

42. Weil.,J., 'The Synthesis of Cloth Objects', *Comput. Graph.*. 20 (4), p. 49, (1986)
43. Collier, J.R. and Collier, B.J., 'Drape Prediction by Means of Finite-Element Method', *J. Textile Inst.*, Vol. 82 (1), pp. 96-107, (1991).
44. Eischen, J.W. and Kim, Y.G., *Int. J. Cloth. Sci. Technol.*, 5 (3), p. 69, (1993).
45. Bijan Chen and Muthu Govidaraj, 'A Physically Based Model of Fabric Drape Using Flexible Shell Theory', *Textile Res. J.*, Vol.65 (6) ,pp. 324-330, (1995).
46. Kang, T.J. and Yu, W.R., 'Drape simulation of Woven Fabric by using the Finite-Element Method', *J. Textile Inst.*, Vol. 86 (4) ,pp. 635-648, (1995).
47. Lloyd,D.W., Norton,A.N., Postle,R., 'Approaches to Modelling the Mechanical Properties of Fabrics and the Representation of Fabrics as Flexible Surfaces using Differential Geometry', *The Mathematics and Computation of Deforming Surfaces*, Clarendon Press, Oxford, pp 19-32, (1996).
48. Postle, J.R. and Postle, R., 'The dynamics of Fabric Drape', *Textile Res. J.*, Vol.69 (9) ,pp. , (1999).
49. Amirbayat, J., 'The Buckling of Flexible Sheets under Tension. Part I: Theoretical Analysis.', *J. Textile Inst.*, Vol. 82 (1) ,pp. 71-77, (1991).
50. Fujita Akihiro, Hamada Hiroyuki, Maekawa Zenichiro, Ohno , 'Mechanical properties of textile composites. 1st Report: Knitted Fabric Composite', Nihon Kikai Gakkai Ronbunshu, A Trans. Jap. Soc. Mech. Eng. A., 59 (566), pp.2323-2330, (1993).
51. Bannister, M., K., Herszberg, I., 'Textile Preforms for Composite structures', Inst. Eng., Austral., 93/6 (Pt. 2), pp. 357-362, (1993).
52. Boisse, P., Cherouat, A., Gelin, J.,C., Sabhi, H., 'Experimental Study and FEM Simulation of Glass Fiber Fabric Shaping Process', *Polymer Composites*, 16 (1), pp. 83-95, (1995).
53. Hearle, J.W.S. and Stevenson, P.I., *Textile Res. J.*, Vol.30 ,pp.704 , (1960).
54. Bais-Singh, S. and Goswam,B.C., 'Theoretical Determination of Mechanical Response of Spun-bonded Nonwovens', *J. Textile Inst.*, Vol.86 (2) ,pp. 271-288, (1995).
55. Peirce, F.T., *J. Textile Inst.*, Vol.28 ,pp. T45-T96, (1937)
56. Peirce, F.T., 'Geometrical Principles applied to Design of Functional Fabrics', *Textile Res. J.*, Vol.17, p. 123, (1947).
57. Shin, W.E., 'An Engineering Approach to Jersey Fabric Construction', *Textile Res. J.*, Vol.25, p. 250, (1955).

58. Doyle, P.J., 'Fundamental Aspects of the Design of Knitted Fabrics', *J. Textile Inst.*, Vol. 44, p. 561, (1953).

59. Leaf, G.A.V. and Glaskin, A.J., 'The Geometry of Plain knitted Loop', *J. Textile Inst.*, Vol. 46, p. 587, (1955).

60. Postle, R. and Munden, D.L., 'Analysis of the Dry Relaxed Knitted Loop Configuration', *J. Textile Inst.*, Vol. 58, p. T352 , (1967).

61. Shanahan, W.J. and Postle, R., 'A Theoretical Analysis of the Plain Knitted Structure', *Textile Res. J.*, Vol.40, pp. 656-665, (1970).

62. Shanahan, W.J. and Postle, R., 'Jamming of Knitted Structures', *Textile Res. J.*, Vol. 43, pp. 532-538, (1973).

63. Grosberg,P., 'The Geometry of Warp-knitted Fabrics', *J. Textile Inst.*, Vol. 51 ,pp. T39-T48, (1960).

64. Grosberg,P., 'The Geometrical Properties of Simple Warp-knit fabrics', *J. Textile Inst.*, Vol 55. ,pp.T18-T30 , (1964).

65. Hepworth, B. and Leaf, G.A.V., 'The Shape of Loops in an Undeformed Plain Knit Structure', *Studies in Modern Fabrics*, Text. Inst. Conf., pp 181-196, (1970).

66. Konopasek, M., 'Improved Procedure for Calculating the Mechanical Properties of Textile structures', Ph.D. Thesis, UMIST, Manchester, (1970).

67. Olofsson, B., 'A General Model of a Fabric as Geometric-Mechanical Structure', *J. Textile Inst.*, Vol. 55, pp. 541-557, (1964).

68. Hepworth, R.B., Leaf,G.A., 'The Mechanics of an Idealized Weft-knitted Structure', *J. Textile Inst.*, Vol. 67 (8) ,pp. 241-248, (1976).

69. Hepworth, R.B., 'The bi-axial Load-Extension Behaviour of a Model of Plain Weft Knitting. Part I', *J. Textile Inst.*, Vol. 69, p. 101, (1978).

70. Hepworth, R.B., 'The Dimensional and Mechanical Properties of Plain Weft Knits', *Knitting International*, p. 33, (Jan. 1982).

71. De Jong,S. and Postle,R., 'Energy Analysis of Knitted Fabric Mechanics by means of Optimal Control Theory. Part I. The Nature of Loop Interlocking in the Plain Knitted Structure.' *J. Textile Inst.*, Vol. 68 (10) ,pp. 307-315, (1977).

72. De Jong,S. and Postle,R., 'Energy Analysis of Knitted Fabric Mechanics by means of Optimal Control Theory. Part II. Relaxed Fabric Dimensions and Tensile Properties of the Plain Knitted Structure', *J. Textile Inst.*, Vol. 68 (10) ,pp. 316-323, (1977).

73. Hepworth, R.B., 'The Load-extension Properties of the Weft Knitted Structure', *J. Textile Inst.*, Vol.65 (10) ,pp. 561-562 , (1974).

74. Shanahan,W.J., Postle,R., 'The Load-extension Properties of the Weft Knitted Structure_Reply', *J. Textile Inst.*, Vol.65 (10) ,pp. 562-563 , (1974).
75. Belov,E.B.,'Investigation into Mechanics of Yarn Subject to the High Level of Axial Torsion' Ph.D. Thesis, De Montfort University, (1999).
76. Morton, W.E., Permanyer, F.J., 'The Measurement of Torsional Relaxation in Textile Fibres', *J. Textile Inst.*, Vol. 38, T 54 , (1947).
77. Dhingra, R.C., Postle, R.,'The Bending and Recovery Properties of Continuous-Filament and Staple-Fibre Yarns', *J. Textile Inst.*, Vol. 67 (12), pp. 426-433, (1976).
78.Herle,J.W.C., Du,G.W., 'Forming Rigid Fibre Assemblies: The Interaction of Textile Technology and Composites Engineering', *J. Textile Inst.*, Vol. 81 (4), pp. 360-383, (1990).
79. Ramakrishna,S., Huang,Z.M., Teoh,S.H., Tay,A.A.O. and Chew,C.L., 'Application of the Model of Leaf and Glaskin to Estimating the 3D Elastic Properties of Knitted-fabric-reinforced Composites', *J. Textile Inst.*, Vol. 91 Part 1 (1) ,pp. 132-151, (2000).
80. Kawabata,S., Niwa,M.,Nanashima,Y., *J. Text. Mach. Soc. of Japan*, 1970, 23, p T223
81. Wei-Liang Wu, Hiroyuko,H., Maekawa, 'Computer Simulation of the Deformation of Weft-Knitted Fabrics for Composite Materials', *J. Textile Inst.*, Vol. 85 ,pp.198-214 , (1994).

Appendix A. Overview of Software Development

The model calculation module was developed using MATLAB. The module is a set of scripts. It allows

1. to input initial model data
2. to simulate extension of the specified sample
3. to display/recalculate calculated/saved data.

The program provides the operator with the user interface to specify input files and control calculation processes.

The program flowchart is represented at the end of Appendix A. Blue blocks represent the processes, which are implied implementation of a complex algorithm. The description of the processes is tabulated below.

Process	Description	Main Functions
CALCULATION	Calculate rigidity matrixes and load vector for each of constitutive elements — CEM — (section 2.3).	system_matrix_nonl_1.m
	Arrange the CEMs to form rigidity matrix of the finite-element —FEM — (Figure 2.19).	system_matrix_nonl_1.m
	Arrange the FEMs to form rigidity matrix of the whole system	system_matrix_nonl_1.m
	Define the boundary conditions	ini_Clamp.m ini_boundary_Link.m
	Solve the system of governing equations (3.2) iteratively at increasing load steps (equations (3.5) and (3.6)).	main_fabric.m
Display calculated data	Process saved/calculated data. Define initial co-ordinates of each finite-element Define axial force for each side of each finite-element. Define the colour for visualisation of axial force distribution. Plot shape of the sample in deformed and initial states. Plot load-extension curve.	post_processor_fabric.m
Hold on the choosen experimental curve	Read the specified file with experimental data (ASCII file. format) Hold the experimental load-extension curve on the theoretical curve.	post_processor_fabric.m
define loop geometry plot specified graphics	Calculate 3D path of the loop. Define contact and free zones of the loop. Plot the yarn path in the 3D (Figure 2.2).	calculate_loop_geometry.m draw_loop.m
Calculate effective properties of arc elements of yarn	Define load-extension curve for pre-bent yarn from known geometry of free zones (Figure 2.2) and load-extension curves of straight yarn obtained from yarn testing (Figure 4.3).	calculate_tension_fast.m calculate_tension.m geometry_rod_2d_fabric.m processor_rod_2d_fabric.m post_processor_rod_2d_fabric. rig_mx_rod_2d_fabric.m
Calculate mesh plot mesh plot boundary points	Divide the specified rectangular area into rectangular finite-elements. Plot the mesh (Figure 3.2). Process and save the specified clamped points.	form_mesh.m

The format of input data files was developed to input the model initial data. The list of file types and data format description are represented below.

- ***Fabric properties file***

Format: ***ASCII file.***
Extension: ****.model.***
Example:

```
$ FABRIC PROPERTIES FILE:begin $  %do not change this string!!!!!!!

1. Fabric dimension :X and Y direction ([m])
X_size:   [ 1.7  ]*1e-3;
Y_size:   [ 2.45  ]*1e-3;

2. Yarn Diameter ([m])
D_yarn:   [ 1 ]*1e-3;

3. Length of the loop ([m]) set 0 for estimation from X_size and Y_size
L3D_loop:   [ 12.382 ]*1e-3;
4. Jamming coeffisient "% of X_size ,0- no jumming, value ]0, 1[
jamm:   [ 1 ];

5. Fabric type ( [plane] or [rib] )
fabric_type:   [ plane ];

6. Plot loop form? - Y N
   y;

$ FABRIC PROPERTIES FILE:end $  %do not change this string!!!!!!!
```

The values in square brackets should be specified by user.

- ***Yarn properties file***

Format: ***ASCII file.***
Extension: ****.model.***
Example:

```
$ YARN PROPERTIES FILE:begin $  %do not change this string!!!!!!!

1. Yarn Bending Rigidity ([N*m^2]):
 [ 0.2e-8  ]*1e0;

2. Yarn Tensile Rigidity - Force ([N]) and Displacement ([m]):
   Force:
 Force:   [  0.1678 0.3356 1.3423  3.0201   6.7114   28.8591   43.6242 ] 2;

   Displacement:
 Displ:   [ 1 2 3 4 5 10 20  ]*1e-3;

3.Length of Tested Sample  ([m]):
  L_sample:   [ 0.1 ]*1;

4. Yarn initial Compression Rigidity ([N]):
  Kompr0:   [ 15000 ];

5. Yarn Diameter  ([M])
  D_yarn:   [ 1 ]*1.e-3;

6. Plot Tensile Curves? - Y N
   y;

$ YARN PROPERTIES FILE:end $  %do not change this string!!!!!!!
```

The values in square brackets should be specified by user.

- ***Sample dimensions and mesh properties file***

Format: *text document.*
Extension: **.mesh.*
Example:

```
S MESH PROPERTIES FILE begin S  %do not change this string!!!!!!!

1. Sample dimension [m]
   X direction:   [ 0.07 ]*1;
   Y direction:   [ 0.06 ]*1;

2.  Desirable number of loops in element (N*N)
   N:    [ 3.2 ]*1;

3.  Coarse angel:
  alfa:   [ 0 ]*1;

 S MESH PROPERTIES FILE end S  %do not change this string!!!!!!!
```

The values in square brackets should be specified by user.

The above files can be prepared either before calculation from external text editor program or during calculations. According to specified data files, a *report* file is generated, which contains all input data and links to respective files where calculated data are stored.

To start the program it is necessary to type '*main_fabric('calc')*' in Matlab command window and then follow the dialog interface.

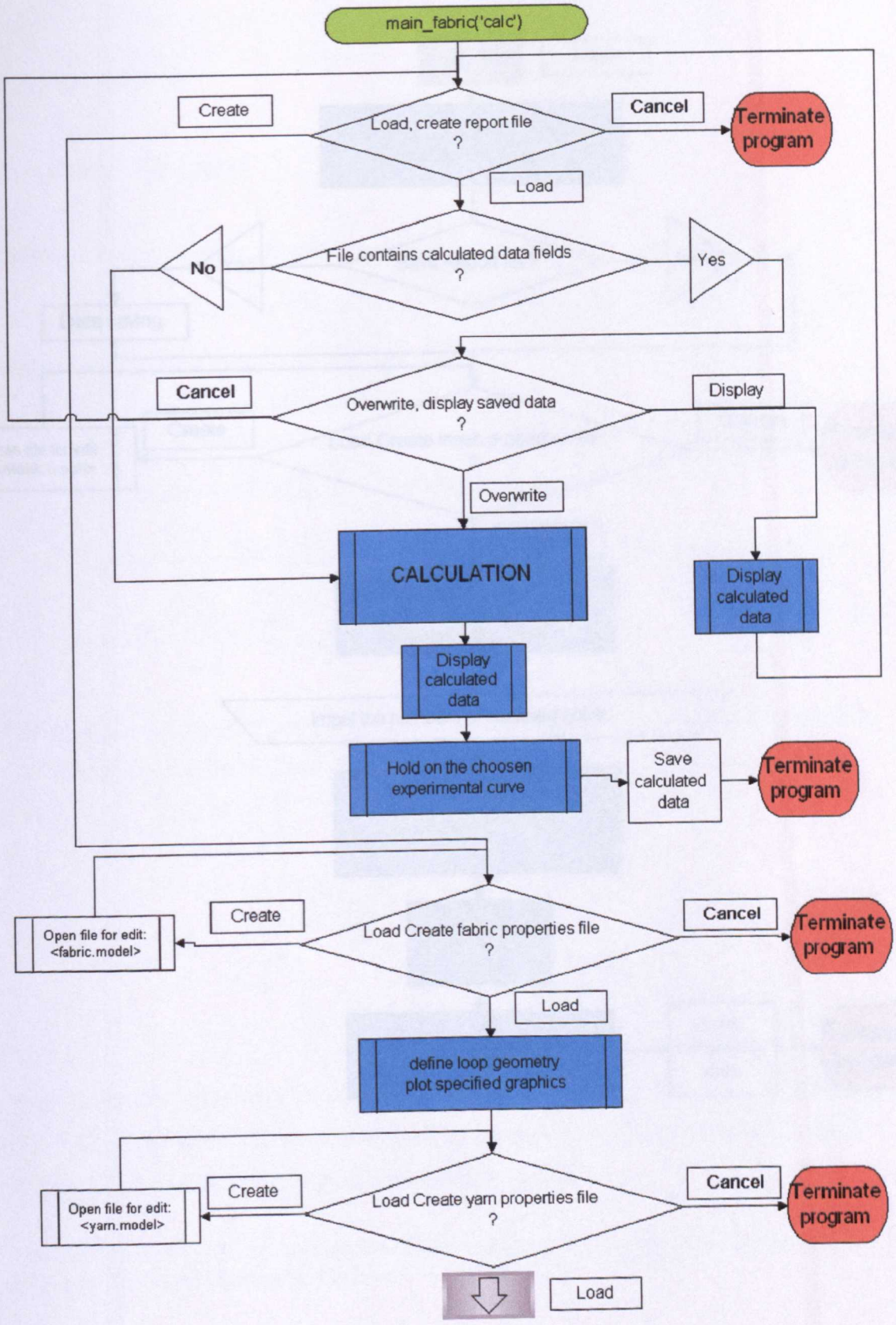
main_fabric('calc')
Create
Load, create report file ?
Cancel
Terminate program
Load
No
File contains calculated data fields ?
Yes
Cancel
Overwrite, display saved data ?
Display
Overwrite
CALCULATION
Display calculated data
Display calculated data
Hold on the choosen experimental curve
Save calculated data
Terminate program
Open file for edit: <fabric.model>
Create
Load Create fabric properties file ?
Cancel
Terminate program
Load
define loop geometry plot specified graphics
Open file for edit: <yarn.model>
Create
Load Create yarn properties file ?
Cancel
Terminate program
Load

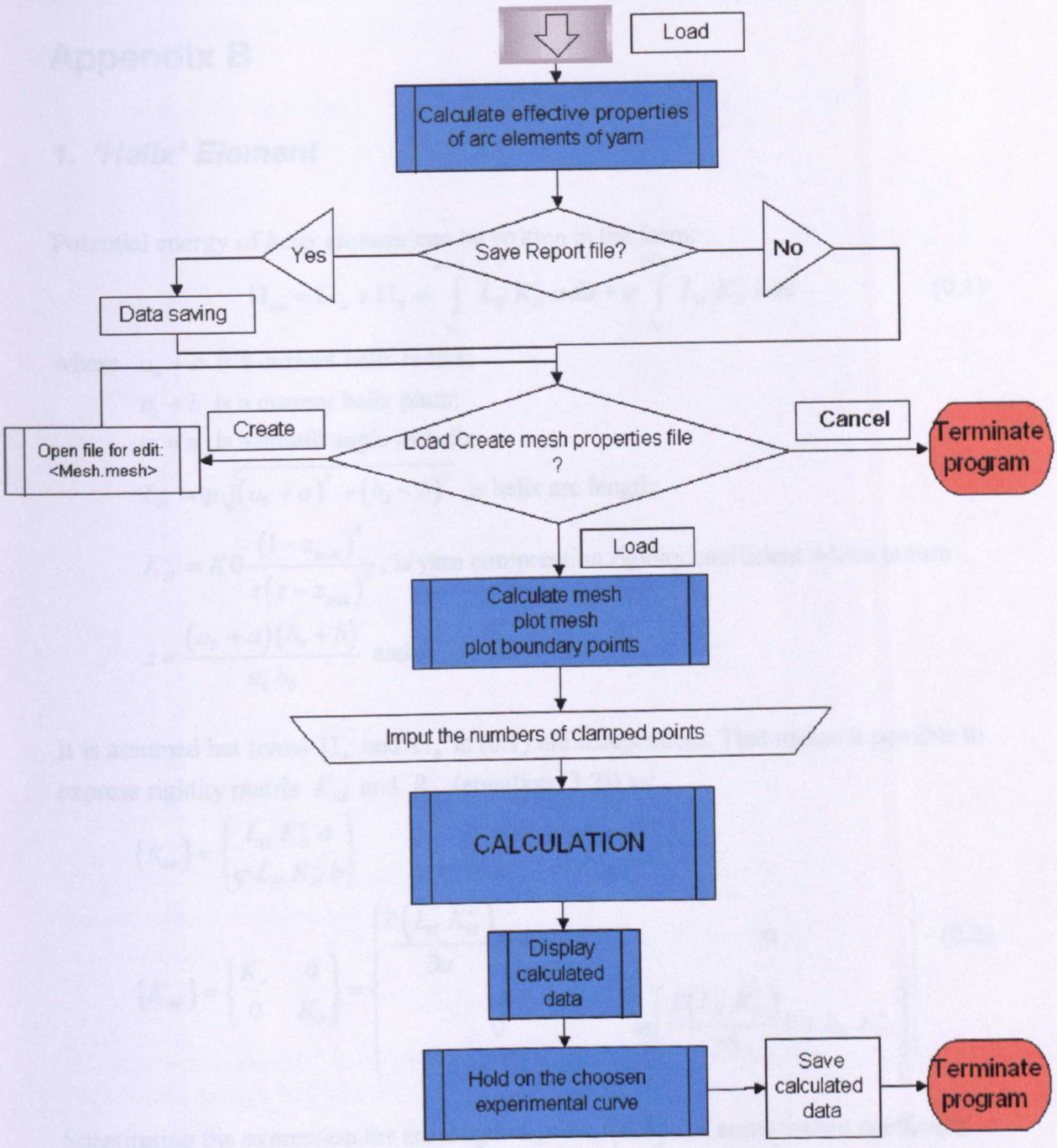
Load
Calculate effective properties of arc elements of yarn
Save Report file?
Yes
No
Data saving
Load Create mesh properties file ?
Create
Open file for edit: <Mesh.mesh>
Cancel
Terminate program
Load
Calculate mesh
plot mesh
plot boundary points
Imput the numbers of clamped points
CALCULATION
Display calculated data
Hold on the choosen experimental curve
Save calculated data
Terminate program

Appendix B

1. 'Helix' Element

Potential energy of *helix element* can be written in the form:

$$\Pi_{ab} = \Pi_a + \Pi_b = \int_{a_0}^{a+a_0} L_H K_H^c \, a \, da + \varphi \int_{b_0}^{b+b_0} L_H K_H^c \, b \, db \qquad (0.1)$$

where $a_0 + a$ is a current helix radius;

$b_0 + b$ is a current helix pitch;

$\varphi = \pi$ is azimuth angle of helix

$L_H = \varphi\sqrt{(a_0 + a)^2 + (b_0 + b)^2}$ is helix arc length;

$K_H^c = K0\dfrac{(1 - z_{\min})^3}{z(z - z_{\min})^3}$, is yarn compression rigidity coefficient where in turn

$z = \dfrac{(a_0 + a)(b_0 + b)}{a_0 b_0}$ and $z_{\min} = 0.2$.

It is assumed hat terms Π_a and Π_b in (0.1) are independent. That makes it possible to express rigidity matrix K_{ab} and R_{ab} (equation (3.2)) as:

$$\{R_{ab}\} = \begin{Bmatrix} L_H K_H^c \, a \\ \varphi L_H K_H^c \, b \end{Bmatrix}$$

$$\{K_{ab}\} = \begin{Bmatrix} K_a & 0 \\ 0 & K_b \end{Bmatrix} = \begin{Bmatrix} \dfrac{\partial(L_H K_H^c)}{\partial a} a + L_H K_H^c & 0 \\ 0 & \varphi\left(\dfrac{\partial(L_H K_H^c)}{\partial b} b + L_H K_H^c\right) \end{Bmatrix} \qquad (0.2)$$

Substituting the expression for arc length $L_H = L_H(a,b)$ and compression coefficient $K_H^c = K_H^c(a,b)$ into (0.2) it is not difficult to obtain expression for vector $\{R_{ab}\}$ and matrix $\{K_{ab}\}$ as function of virtual co-ordinates a and b.

The rigidity matrix *Klink* and vector *Rlink* due to constraint equation *link* = 0 (see equation (2.35)) is represented below.

RIGIDITY MATRIX and ini - VECTOR of LOAD for SPIRAL ELEMENT

(LINK, non - LINEAR)

$$link = 2 * (s1 + s2) \quad + \varphi * \left(\sqrt{(a0 + a)^2 + (b0 + b)^2} - \sqrt{a0^2 + b0^2}\right);$$

$$Pot\lambda = link * \lambda$$

$$Klink = \begin{pmatrix} 0 & 0 & 0 & 2 & 0 \\ 0 & -\frac{(a+a0)^2 \lambda \varphi}{Lh^3} + \frac{\lambda \varphi}{Lh} & -\frac{(a+a0)(b+b0) \lambda \varphi}{Lh^3} & \frac{(a+a0) \varphi}{Lh} & 0 \\ 0 & -\frac{(a+a0)(b+b0) \lambda \varphi}{Lh^3} & -\frac{(b+b0)^2 \lambda \varphi}{Lh^3} + \frac{\lambda \varphi}{Lh} & \frac{(b+b0) \varphi}{Lh} & 0 \\ 2 & \frac{(a+a0) \varphi}{Lh} & \frac{(b+b0) \varphi}{Lh} & 0 & 2 \\ 0 & 0 & 0 & 2 & 0 \end{pmatrix}$$

$$Rlink = \begin{pmatrix} 2 \lambda \\ \frac{(a+a0) \lambda \varphi}{Lh} \\ \frac{(b+b0) \lambda \varphi}{Lh} \\ 2 (s1 + s2) + (Lh - Lh0) \varphi \\ 2 \lambda \end{pmatrix}$$

Lh0	$\sqrt{a0^2 + b0^2}$
Lh	$\sqrt{(a0 + a)^2 + (b0 + b)^2}$

%%%v

Sequence of variables :

{1 ; 2 ; 3 ; 4 ; 5} → { s1 ; a ; b ; λ ; s2}

It is possible to consider a simplified expression for the constrain equation *link* = 0. The rigidity matrix and load vector can be written as follows.

RIGIDITY MATRIX and ini - VECTOR of LOAD for SPIRAL ELEMENT
(LINK , LINEAR)

$$\mathbf{link} = 2*(s1+s2) \quad +\varphi*\left(\sqrt{(a0+a)^2+(b0+b)^2}-\sqrt{a0^2+b0^2}\right) \approx$$
$$2*(s1+s2) + \varphi*\partial_a\left(\left(\sqrt{(a0+a)^2+(b0+b)^2}-\sqrt{a0^2+b0^2}\right)\right)\Delta a +$$
$$\varphi*\partial_b\left(\left(\sqrt{(a0+a)^2+(b0+b)^2}-\sqrt{a0^2+b0^2}\right)\right)\Delta b \quad ;$$

$\mathbf{Pot\lambda} \approx \mathbf{link}*\lambda$

Klink =

0	0	0	2	0
0	0	0	$\frac{\varphi*(a+a0)}{Lh}$	0
0	0	0	$\frac{\varphi*(b+b0)}{Lh}$	0
2	$\frac{\varphi*(a+a0)}{Lh}$	$\frac{\varphi*(b+b0)}{Lh}$	0	2
0	0	0	2	0

Rlink =

0
0
0
0
0

Lh	$\sqrt{(a0+a)^2+(b0+b)^2}$

%% v

Sequence of variables :

{ 1 ; 2 ; 3 ; 4 ; 5} → { s1 ; a ; b ; λ ; s2}

Finally, rigidity matrix $\{K_{Helix}\}$ and load vector $\{R_{Helix}\}$ can be obtained as:

$$\{K_{Helix}\} = \begin{Bmatrix} 0 & 0 & 0 & 0 & 0 \\ 0 & K_a & 0 & 0 & 0 \\ 0 & 0 & K_b & 0 & 0 \\ 0 & 0 & 0 & 0 & 0 \\ 0 & 0 & 0 & 0 & 0 \end{Bmatrix} + \{Klink\}$$

$$\{R_{Helix}\} = \begin{Bmatrix} 0 \\ R_a \\ R_b \\ 0 \\ 0 \end{Bmatrix} + \{Rlink\}$$

2. 'Thread' Element

RIGIDITY MATRIX FOR ' THREAD ' ELEMENT
(Plus T ension Derivatives)

Sequence of variables : {uX1, uY1, s1 , s2, uX2, uY2} as = (s1 + s2)

$$\Pi = C\int_{A->B}\frac{a-(a0+as)}{a0+as}\left(da-d\left(\frac{as\,a}{a0+as}\right)\right) = C\int_{A->B}Qa[a,as]\,da+Qas[a,as]\,das =$$

$$C\left(\int_{a0}^{a}Qa[a,0]\,da+\int_{0}^{as}Qas[a,as]\,das\right) = C\left(\int_{0}^{as}Qas[a0,as]\,das+\int_{a0}^{a}Qa[a,as]\,da\right)$$

$$Qa = \frac{a-(a0+as)}{a0+as}\left(1-\frac{as}{a0+as}\right)\;;\quad Qas = -\frac{a-(a0+as)}{a0+as}\,\frac{a0\,a}{(a0+as)^2}\;;$$

$$\frac{\partial\,Qa}{\partial\,as} = \frac{-2\,a\,a0+a0^2+a0\,as}{(a0+as)^3} = \frac{\partial\,Qas}{\partial\,a} \Rightarrow \Pi = \Pi[B]-\Pi[A]$$

$$Ra = \left(\frac{a\,a0-a0^2-a0\,as}{(a0+as)^2}\right)\;;\qquad Ras = \left(\frac{-a^2\,a0+a\,a0^2+a\,a0\,as}{(a0+as)^3}\right)\;;$$

$$KK[i,j] = \partial_{q_i}\partial_{q_j}\Pi[\{q_k\}] = \partial_{q_i}C[\{q_k\}]*R_j[\{q_k\}] = \frac{\partial C[\{q_k\}]}{\partial q_k}R_j[\{q_k\}]+C\frac{\partial R_j[\{q_k\}]}{\partial q_k} =$$

KK_lin + KK_nonl;

$$K\_lin = \frac{C}{(a0+as)}*\begin{pmatrix} \frac{Fx}{a^3(a0+as)} & \frac{a0\,dX\,dY}{a^3} & -\frac{Gx}{a(a0+as)^2} & -\frac{Gx}{a(a0+as)^2} & -\frac{Fx}{a^3(a0+as)} & -\frac{a0\,dX\,dY}{a^3} \\ \frac{a0\,dX\,dY}{a^3} & \frac{Fy}{a^3(a0+as)} & -\frac{Gy}{a(a0+as)^2} & -\frac{Gy}{a(a0+as)^2} & -\frac{a0\,dX\,dY}{a^3} & -\frac{Fy}{a^3(a0+as)} \\ -\frac{Gx}{a(a0+as)^2} & -\frac{Gy}{a(a0+as)^2} & \frac{Ks}{(a0+as)^3} & \frac{Ks}{(a0+as)^3} & \frac{Gx}{a(a0+as)^2} & \frac{Gy}{a(a0+as)^2} \\ -\frac{Gx}{a(a0+as)^2} & -\frac{Gy}{a(a0+as)^2} & \frac{Ks}{(a0+as)^3} & \frac{Ks}{(a0+as)^3} & \frac{Gx}{a(a0+as)^2} & \frac{Gy}{a(a0+as)^2} \\ -\frac{Fx}{a^3(a0+as)} & -\frac{a0\,dX\,dY}{a^3} & \frac{Gx}{a(a0+as)^2} & \frac{Gx}{a(a0+as)^2} & \frac{Fx}{a^3(a0+as)} & \frac{a0\,dX\,dY}{a^3} \\ -\frac{a0\,dX\,dY}{a^3} & -\frac{Fy}{a^3(a0+as)} & \frac{Gy}{a(a0+as)^2} & \frac{Gy}{a(a0+as)^2} & \frac{a0\,dX\,dY}{a^3} & \frac{Fy}{a^3(a0+as)} \end{pmatrix};$$

Ks	(a0 (3 a^2 - 2 a (a0 + as)))
Fx	(a0 (a^3 - a^2 (a0 + as) + (a0 + as) dX^2))
Fy	(a0 (a^3 - a^2 (a0 + as) + (a0 + as) dY^2))
Gx	(a0 (- 2 a + a0 + as) dX)
Gy	(a0 (- 2 a + a0 + as) dY)
dX	(- uX1 + uX2 - x01 + x02)
dY	(- uY1 + uY2 - y01 + y02)
a0	$\sqrt{((x02-x01)^2+(y02-y01)^2)}$
a	$\sqrt{(-uX1+uX2-x01+x02)^2+(-uY1+uY2-y01+y02)^2}$
as	(s1 + s2) !!!

INITIAL LOAD VECTOR FOR DEFORMED STATE & MATRIX non - LINEAR COMPONENT (ELEMENT THREAD)

$$K\_nonl = \frac{\partial C}{\partial eps} * \begin{pmatrix} \frac{\partial eps}{\partial a}\frac{dX^2\,Ra}{a^2} & \frac{\partial eps}{\partial a}\frac{dX dY\,Ra}{a^2} & -\frac{\partial eps}{\partial a}\frac{dX\,Ras}{a} & -\frac{\partial eps}{\partial a}\frac{dX\,Ras}{a} & -\frac{\partial eps}{\partial a}\frac{dX^2\,Ra}{a^2} & -\frac{\partial eps}{\partial a}\frac{dX dY\,Ra}{a^2} \\ \frac{\partial eps}{\partial a}\frac{dEpsa\,dX dY\,Ra}{a^2} & \frac{\partial eps}{\partial a}\frac{dY^2\,Ra}{a^2} & -\frac{\partial eps}{\partial a}\frac{dY\,Ras}{a} & -\frac{\partial eps}{\partial a}\frac{dY\,Ras}{a} & -\frac{\partial eps}{\partial a}\frac{dX dY\,Ra}{a^2} & -\frac{\partial eps}{\partial a}\frac{dY^2\,Ra}{a^2} \\ -\frac{\partial eps}{\partial as}\frac{dX\,Ra}{a} & -\frac{\partial eps}{\partial as}\frac{dY\,Ra}{a} & \frac{\partial eps}{\partial as}Ras & \frac{\partial eps}{\partial as}Ras & \frac{\partial eps}{\partial as}\frac{dX\,Ra}{a} & \frac{\partial eps}{\partial as}\frac{dY\,Ra}{a} \\ -\frac{\partial eps}{\partial as}\frac{dX\,Ra}{a} & -\frac{\partial eps}{\partial as}\frac{dY\,Ra}{a} & \frac{\partial eps}{\partial as}Ras & \frac{\partial eps}{\partial as}Ras & \frac{\partial eps}{\partial as}\frac{dX\,Ra}{a} & \frac{\partial eps}{\partial as}\frac{dY\,Ra}{a} \\ -\frac{\partial eps}{\partial a}\frac{dX^2\,Ra}{a^2} & -\frac{\partial eps}{\partial a}\frac{dX dY\,Ra}{a^2} & \frac{\partial eps}{\partial a}\frac{dX\,Ras}{a} & \frac{\partial eps}{\partial a}\frac{dX\,Ras}{a} & \frac{\partial eps}{\partial a}\frac{dX^2\,Ra}{a^2} & \frac{\partial eps}{\partial a}\frac{dX dY\,Ra}{a^2} \\ -\frac{\partial eps}{\partial a}\frac{dX dY\,Ra}{a^2} & -\frac{\partial eps}{\partial a}\frac{dY^2\,Ra}{a^2} & \frac{\partial eps}{\partial a}\frac{dY\,Ras}{a} & \frac{\partial eps}{\partial a}\frac{dY\,Ras}{a} & \frac{\partial eps}{\partial a}\frac{dX dY\,Ra}{a^2} & \frac{\partial eps}{\partial a}\frac{dY^2\,Ra}{a^2} \end{pmatrix};$$

$$Rful = C* \begin{pmatrix} -\frac{dX}{a} * Ra \\ -\frac{dY}{a} * Ra \\ 1 * Ras \\ 1 * Ras \\ \frac{dX}{a} * Ra \\ \frac{dY}{a} * Ra \end{pmatrix}$$

$\frac{\partial eps}{\partial a}$	$\frac{1}{a0+as}$
$\frac{\partial eps}{\partial as}$	$-\frac{a}{(a0+as)^2}$
Ra	$\frac{a\,a0-a0^2-a0\,as}{(a0+as)^2}$
Ras	$\frac{-a^2 a0+a\,a0^2+a\,a0\,as}{(a0+as)^3}$
dX	(-uX1 + uX2 - x01 + x02)
dY	(-uY1 + uY2 - y01 + y02)
a0	$\sqrt{((x02 - x01)^2 + (y02 - y01)^2)}$
a	$\sqrt{(-uX1 + uX2 - x01 + x02)^2 + (-uY1 + uY2 - y01 + y02)^2}$
as	(s1 + s2) !!!

3. Length Restricted' Element

Rigidity ' THREAD ' Element

Rigidity Matrix and Load Vector (length restriction)

$$Pot = \int_0^{bs} Kc * (bs)\, dbs;$$

$$bs = (s1 - s2);$$

$$CL = C01 * \frac{1}{\left(\frac{bs}{a0} - 0.6\right)^2};$$

$$Rbs = CL * bs;$$

$$Rbs = \begin{pmatrix} Rs1 \\ Rs2 \end{pmatrix} = Kc * bs \begin{pmatrix} 1 \\ -1 \end{pmatrix};$$

$$KK = \begin{pmatrix} D[Rs1, s1] & D[Rs1, s2] \\ D[Rs2, s1] & D[Rs2, s2] \end{pmatrix} = Kc \begin{pmatrix} 1 & -1 \\ -1 & 1 \end{pmatrix}$$

4. 'Side' Element

Rigidity 'Side' for CELL Element
Rigidity Matrix and Load Vector

$$\Pi = \int_{a0}^{a} K\,(a - a0)\,da$$

$$R_i = \partial_{q_i}\Pi = K\,(a - a0)\,\frac{\partial a}{\partial q_i}\;;\quad Ra = K*(a - a0)\;;$$

$$K_{i,j} = \partial_{q_j} R_i = K\frac{\partial}{\partial q_j}\left((a - a0)\,\frac{\partial a}{\partial q_i}\right) + \frac{\partial K}{\partial a}\,\frac{\partial a}{\partial q_j}\left((a - a0)\,\frac{\partial a}{\partial q_i}\right) = KL_{i,j} + KN_{i,j}$$

$$Ra = K*(a - a0)\;;$$

$$K = Z\_cont * K_0\,\frac{(1 - 0.2)^3}{\frac{a}{D_{yarn}}\left(\frac{a}{D_{yarn}} - 0.2\right)^3}\;;\quad \frac{\partial K}{\partial a} = -\,Z\_cont * K_0 * \frac{(1 - 0.2)^3\,D_{yarn}^4\,(4a - 0.2\,D_{yarn})}{a^2\,(a - 0.2\,D_{yarn})^4}\;;$$

$$KL = K*\frac{1}{a^3} * \begin{pmatrix} fX & a0\,dX\,dY & -fX & -a0\,dX\,dY \\ a0\,dX\,dY & fY & -a0\,dX\,dY & -fY \\ -fX & -a0\,dX\,dY & fX & a0\,dX\,dY \\ -a0\,dX\,dY & -fY & a0\,dX\,dY & fY \end{pmatrix};$$

$$KN = \frac{\partial K}{\partial a}\,(a - a0) * \frac{1}{a^2} * \begin{pmatrix} dX^2 & dX\,dY & -dX^2 & -dX\,dY \\ dX\,dY & dY^2 & -dX\,dY & -dY^2 \\ -dX^2 & -dX\,dY & dX^2 & dX\,dY \\ -dX\,dY & -dY^2 & dX\,dY & dY^2 \end{pmatrix}$$

$$R = K*\frac{1}{a} * \begin{pmatrix} -(a - a0)\,dX \\ -(a - a0)\,dY \\ (a - a0)\,dX \\ (a - a0)\,dY \end{pmatrix};$$

fX	$(a^3 - a^2\,a0 + a0\,dX^2)$
fY	$(a^3 - a^2\,a0 + a0\,dY^2)$
dX	$(-uX1 + uX2 - x01 + x02)$
dY	$(-uY1 + uY2 - y01 + y02)$
a0	$\sqrt{((x02 - x01)^2 + (y02 - y01)^2)}$
a	$\sqrt{(-uX1 + uX2 - x01 + x02)^2 + (-uY1 + uY2 - y01 + y02)^2}$

5. 'Height' Element

Rigidity 'Height - FULL' for CELL Element

Rigidity Matrix and Load Vector

$$\Pi = \int_{a0}^{h} C\,(h - a0)\,dh$$

$$R_i = \partial_{q_i}\Pi = C\,(h - a0)\,\frac{\partial h}{\partial q_i}\;; \quad Ra = C*(h - a0)\;;$$

$$KK_{i,j} = \partial_{q_j} R_i = C\,\frac{\partial}{\partial q_J}\left((h - a0)\,\frac{\partial h}{\partial q_i}\right) + \frac{\partial C}{\partial h}\,\frac{\partial h}{\partial q_J}\left((h - a0)\,\frac{\partial h}{\partial q_i}\right) =$$

$$\frac{\partial C}{\partial h}\,(h - a0) * \left(\frac{\partial h}{\partial q_J}\,\frac{\partial h}{\partial q_i}\right) + C*\left(\frac{\partial h}{\partial q_J}\,\frac{\partial h}{\partial q_i}\right) + C\,(h - a0) * \left(\frac{\partial^2 h}{\partial q_J\,\partial q_i}\right) =$$

$$\left(\frac{\partial C}{\partial h}\,(h - a0) + C\right) * K1 + C\,(h - a0) * K2$$

$$C = Z\_cont * K_0\,\frac{(1 - 0.2)^3}{\frac{h}{D_{yarn}}\left(\frac{h}{D_{yarn}} - 0.2\right)^3}\;;$$

$$\frac{\partial C}{\partial h} = -\,Z\_cont * K_0 * \frac{(1 - 0.2)^3\,D_{yarn}^4\,(4h - 0.2\,D_{yarn})}{h^2\,(h - 0.2\,D_{yarn})^4}\;;$$

$\frac{(bl^2\,dr23\cdot dk12\,s1)^2}{4\,bl^6}$	$-\frac{(bl^2\,dr23\cdot dk12\,s1)\,(bl^2\,dk23\cdot dr12\,s1)}{4\,bl^6}$	$\frac{(bl^2\,dr23\cdot dk12\,s1)\,(-bl^2\,b2\,dk13\cdot bl^3\,dk34\cdot b2\,dk12\,s1)}{4\,bl^6\,b2}$	$-\frac{(bl^2\,dr23\cdot dk12\,s1)\,(-bl^2\,b2\,dk13\cdot bl^3\,dk34\cdot b2\,dr12\,s1)}{4\,bl^6\,b2}$
$-\frac{(bl^2\,dr23\cdot dk12\,s1)\,(bl^2\,dk23\cdot dr12\,s1)}{4\,bl^6}$	$\frac{(bl^2\,dk23\cdot dr12\,s1)^2}{4\,bl^6}$	$\frac{\left(\frac{dr13}{bl}-\frac{dr34}{b2}+\frac{dk12\,s1}{bl^3}\right)(bl^2\,dk23\cdot dr12\,s1)}{4\,bl^3}$	$\frac{(bl^2\,dk23\cdot dr12\,s1)\,(-bl^2\,b2\,dk13\cdot bl^3\,dk34\cdot b2\,dk12\,s1)}{4\,bl^6\,b2}$
$\frac{(bl^2\,dr23\cdot dk12\,s1)\,(-bl^2\,b2\,dk13\cdot bl^3\,dk34\cdot b2\,dk12\,s1)}{4\,bl^6\,b2}$	$\frac{\left(\frac{dr13}{bl}-\frac{dr34}{b2}+\frac{dk12\,s1}{bl^3}\right)(bl^2\,dk23\cdot dr12\,s1)}{4\,bl^3}$	$\frac{1}{4}\left(\frac{dr13}{bl}-\frac{dr34}{b2}+\frac{dk12\,s1}{bl^3}\right)^2$	$\frac{1}{4}\left(\frac{dr13}{bl}-\frac{dr34}{b2}+\frac{dk12\,s1}{bl^3}\right)\left(-\frac{dk13}{bl}+\frac{dk34}{b2}+\frac{dr12\,s1}{bl^3}\right)$
$-\frac{(bl^2\,dr23\cdot dk12\,s1)\,(-bl^2\,b2\,dk13\cdot bl^3\,dk34\cdot b2\,dr12\,s1)}{4\,bl^6\,b2}$	$\frac{(bl^2\,dk23\cdot dr12\,s1)\,(-bl^2\,b2\,dk13\cdot bl^3\,dk34\cdot b2\,dr12\,s1)}{4\,bl^6\,b2}$	$\frac{1}{4}\left(\frac{dr13}{bl}-\frac{dr34}{b2}+\frac{dk12\,s1}{bl^3}\right)\left(-\frac{dk13}{bl}+\frac{dk34}{b2}+\frac{dr12\,s1}{bl^3}\right)$	$\frac{1}{4}\left(-\frac{dk13}{bl}+\frac{dk34}{b2}+\frac{dr12\,s1}{bl^3}\right)^2$
$-\frac{(bl^2\,dr23\cdot dk12\,s1)\,(-b2^3\,dr12\cdot bl\,b2^2\,dr24\cdot bl\,dr34\,s2)}{4\,bl^4\,b2^3}$	$\frac{(bl^2\,dk23\cdot dr12\,s1)\,(-b2^3\,dr12\cdot bl\,b2^2\,dr24\cdot bl\,dr34\,s2)}{4\,bl^4\,b2^3}$	$\frac{1}{4}\left(\frac{dr13}{bl}-\frac{dr34}{b2}+\frac{dk12\,s1}{bl^3}\right)\left(-\frac{dr12}{bl}+\frac{dr24}{b2}-\frac{dk34\,s2}{b2^3}\right)$	$\frac{(-bl^2\,b2\,dk13\cdot bl^3\,dk34\cdot b2\,dr12\,s1)\,(-b2^3\,dr12\cdot bl\,b2^2\,dr24\cdot bl\,dk34\,s2)}{4\,bl^4\,b2^4}$
$\frac{(bl^2\,dr23\cdot dk12\,s1)\,(-b2^3\,dr12\cdot bl\,b2^2\,dr24\cdot bl\,dr34\,s2)}{4\,bl^4\,b2^3}$	$-\frac{(bl^2\,dk23\cdot dr12\,s1)\,(-b2^3\,dr12\cdot bl\,b2^2\,dr24\cdot bl\,dr34\,s2)}{4\,bl^4\,b2^3}$	$\frac{(-bl^2\,b2\,dk13\cdot bl^3\,dk34\cdot b2\,dk12\,s1)\,(-b2^3\,dr12\cdot bl\,b2^2\,dr24\cdot bl\,dr34\,s2)}{4\,bl^4\,b2^4}$	$-\frac{(-bl^2\,b2\,dk13\cdot bl^3\,dk34\cdot b2\,dr12\,s1)\,(-b2^3\,dr12\cdot bl\,b2^2\,dr24\cdot bl\,dr34\,s2)}{4\,bl^4\,b2^4}$
$\frac{(bl^2\,dr23\cdot dk12\,s1)\,(b2^2\,dr23\cdot dr34\,s2)}{4\,bl^3\,b2^3}$	$-\frac{(bl^2\,dk23\cdot dr12\,s1)\,(b2^2\,dr23\cdot dr34\,s2)}{4\,bl^3\,b2^3}$	$\frac{\left(\frac{dr13}{bl}-\frac{dr34}{b2}+\frac{dk12\,s1}{bl^3}\right)(-b2^2\,dr23\cdot dr34\,s2)}{4\,b2^3}$	$-\frac{(-bl^2\,b2\,dk13\cdot bl^3\,dk34\cdot b2\,dr12\,s1)\,(b2^2\,dr23\cdot dr34\,s2)}{4\,bl^3\,b2^4}$
$-\frac{(bl^2\,dr23\cdot dk12\,s1)\,(b2^2\,dr23\cdot dr34\,s2)}{4\,bl^3\,b2^3}$	$\frac{(bl^2\,dk23\cdot dr12\,s1)\,(b2^2\,dr23\cdot dr34\,s2)}{4\,bl^3\,b2^3}$	$\frac{(bl^2\,b2\,dr13\cdot bl^3\,dr34\cdot b2\,dk12\,s1)\,(b2^2\,dr23\cdot dr34\,s2)}{4\,bl^3\,b2^4}$	$\frac{(-bl^2\,b2\,dk13\cdot bl^3\,dk34\cdot b2\,dr12\,s1)\,(b2^2\,dr23\cdot dr34\,s2)}{4\,bl^3\,b2^4}$

$-\frac{(bl^2\,dr23\cdot dk12\,s1)\,(-b2^3\,dr12\cdot bl\,b2^2\,dr24\cdot bl\,dr34\,s2)}{4\,bl^4\,b2^3}$	$\frac{(bl^2\,dr23\cdot dk12\,s1)\,(-b2^3\,dr12\cdot bl\,b2^2\,dr24\cdot bl\,dr34\,s2)}{4\,bl^4\,b2^3}$	$\frac{(bl^2\,dr23\cdot dk12\,s1)\,(b2^2\,dr23\cdot dk34\,s2)}{4\,bl^3\,b2^3}$	$-\frac{(bl^2\,dr23\cdot dk12\,s1)\,(b2^2\,dr23\cdot dr34\,s2)}{4\,bl^3\,b2^3}$
$\frac{(bl^2\,dr23\cdot dr12\,s1)\,(-b2^3\,dr12\cdot bl\,b2^2\,dr24\cdot bl\,dr34\,s2)}{4\,bl^4\,b2^3}$	$-\frac{(bl^2\,dk23\cdot dr12\,s1)\,(-b2^3\,dr12\cdot bl\,b2^2\,dr24\cdot bl\,dr34\,s2)}{4\,bl^4\,b2^3}$	$-\frac{(bl^2\,dr23\cdot dk12\,s1)\,(b2^2\,dr23\cdot dk34\,s2)}{4\,bl^3\,b2^3}$	$\frac{(bl^2\,dk23\cdot dr12\,s1)\,(b2^2\,dk23\cdot dr34\,s2)}{4\,bl^3\,b2^3}$
$\frac{1}{4}\left(\frac{dr13}{bl}-\frac{dr34}{b2}+\frac{dk12\,s1}{bl^3}\right)\left(-\frac{dr12}{bl}+\frac{dr24}{b2}-\frac{dk34\,s2}{b2^3}\right)$	$\frac{(-bl^2\,b2\,dr13\cdot bl^3\,dr34\cdot b2\,dk12\,s1)\,(-b2^3\,dk12\cdot bl\,b2^2\,dr24\cdot bl\,dr34\,s2)}{4\,bl^4\,b2^4}$	$\frac{\left(\frac{dr13}{bl}-\frac{dr34}{b2}+\frac{dk12\,s1}{bl^3}\right)(-b2^2\,dr23\cdot dk34\,s2)}{4\,b2^3}$	$\frac{(bl^2\,b2\,dr13\cdot bl^3\,dr34\cdot b2\,dk12\,s1)\,(b2^2\,dr23\cdot dr34\,s2}{4\,bl^3\,b2^4}$
$\frac{(-bl^2\,b2\,dk13\cdot bl^3\,dk34\cdot b2\,dr12\,s1)\,(-b2^3\,dk12\cdot bl\,b2^2\,dr24\cdot bl\,dr34\,s2)}{4\,bl^4\,b2^4}$	$-\frac{(-bl^2\,b2\,dk13\cdot bl^3\,dk34\cdot b2\,dr12\,s1)\,(-b2^3\,dk12\cdot bl\,b2^2\,dr24\cdot bl\,dr34\,s2)}{4\,bl^4\,b2^4}$	$-\frac{(-bl^2\,b2\,dk13\cdot bl^3\,dk34\cdot b2\,dr12\,s1)\,(b2^2\,dr23\cdot dk34\,s2)}{4\,bl^3\,b2^4}$	$\frac{(-bl^2\,b2\,dk13\cdot bl^3\,dk34\cdot b2\,dr12\,s1)\,(b2^2\,dr23\cdot dr34\,s2}{4\,bl^3\,b2^4}$
$\frac{1}{4}\left(\frac{dr12}{bl}-\frac{dr24}{b2}+\frac{dk34\,s2}{b2^3}\right)^2$	$-\frac{(-b2^3\,dr12\cdot bl\,b2^2\,dr24\cdot bl\,dk34\,s2)\,(-b2^3\,dk12\cdot bl\,b2^2\,dr24\cdot bl\,dr34\,s2)}{4\,bl^2\,b2^6}$	$\frac{(b2^2\,dr23\cdot dk34\,s2)\,(b2^3\,dr12\cdot bl\,b2^2\,dr24\cdot bl\,dk34\,s2)}{4\,bl\,b2^6}$	$-\frac{(b2^3\,dr12\cdot bl\,b2^2\,dr24\cdot bl\,dk34\,s2)\,(b2^2\,dr23\cdot dr34\,s2}{4\,bl\,b2^6}$
$-\frac{(-b2^3\,dr12\cdot bl\,b2^2\,dr24\cdot bl\,dr34\,s2)\,(-b2^3\,dk12\cdot bl\,b2^2\,dr24\cdot bl\,dr34\,s2)}{4\,bl^2\,b2^6}$	$\frac{1}{4}\left(\frac{dk12}{bl}-\frac{b2^2\,dr24\cdot dr34\,s2}{b2^3}\right)^2$	$-\frac{(b2^2\,dr23\cdot dk34\,s2)\,(b2^3\,dk12\cdot bl\,b2^2\,dr24\cdot bl\,dr34\,s2)}{4\,bl\,b2^6}$	$-\frac{(b2^2\,dr23\cdot dr34\,s2)\,(-b2^3\,dk12\cdot bl\,b2^2\,dr24\cdot bl\,dr34\,s$
$\frac{(b2^2\,dr23\cdot dk34\,s2)\,(b2^3\,dr12\cdot bl\,b2^2\,dr24\cdot bl\,dk34\,s2)}{4\,bl\,b2^6}$	$-\frac{(b2^2\,dr23\cdot dk34\,s2)\,(b2^3\,dk12\cdot bl\,b2^2\,dr24\cdot bl\,dr34\,s2)}{4\,bl\,b2^6}$	$\frac{(b2^2\,dr23\cdot dk34\,s2)^2}{4\,b2^6}$	$-\frac{(b2^2\,dr23\cdot dk34\,s2)\,(b2^2\,dr23\cdot dr34\,s2)}{4\,b2^6}$
$-\frac{(b2^3\,dr12\cdot bl\,b2^2\,dr24\cdot bl\,dk34\,s2)\,(b2^2\,dr23\cdot dr34\,s2)}{4\,bl\,b2^6}$	$-\frac{(b2^2\,dr23\cdot dr34\,s2)\,(-b2^3\,dk12\cdot bl\,b2^2\,dr24\cdot bl\,dr34\,s2)}{4\,bl\,b2^6}$	$-\frac{(b2^2\,dr23\cdot dk34\,s2)\,(b2^2\,dr23\cdot dr34\,s2)}{4\,b2^6}$	$\frac{(b2^2\,dr23\cdot dr34\,s2)^2}{4\,b2^6}$

K2 =

$\frac{b1^2\,(2\,dx12\,dx23 - s1) + 3\,dx12^2\,s1}{2\,b1^5}$	$\frac{b1^2\,(-dx12\,dx23 + dr12\,dr23) + 3\,dx12\,dr12\,s1}{2\,b1^5}$	$\frac{-3\,dx12^2\,s1 + b1^2\,(-dx12\,(dr13 + dr23) + s1)}{2\,b1^5}$	$-\frac{b1^4 + b1^2\,(-dx12\,dx13 + dr12\,dr23) + 3\,dx12\,dr12\,s1}{2\,b1^5}$
$\frac{b1^2\,(-dx12\,dx23 + dr12\,dr23) + 3\,dx12\,dr12\,s1}{2\,b1^5}$	$\frac{3\,dr12^2\,s1 - b1^2\,(2\,dx23\,dr12 + s1)}{2\,b1^5}$	$\frac{b1^4 + b1^2\,(dx12\,dx23 - dr12\,dr13) - 3\,dx12\,dr12\,s1}{2\,b1^5}$	$\frac{-3\,dr12^2\,s1 + b1^2\,(dx13\,dr12 + dx23\,dr12 + s1)}{2\,b1^5}$
$\frac{-3\,dx12^2\,s1 + b1^2\,(-dx12\,(dr13 + dr23) + s1)}{2\,b1^5}$	$\frac{b1^4 + b1^2\,(dx12\,dx23 - dr12\,dr13) - 3\,dx12\,dr12\,s1}{2\,b1^5}$	$\frac{b1^2\,(2\,dx12\,dr13 - s1) + 3\,dx12^2\,s1}{2\,b1^5}$	$\frac{b1^2\,(-dx12\,dx13 + dr12\,dr13) + 3\,dx12\,dr12\,s1}{2\,b1^5}$
$-\frac{b1^4 + b1^2\,(-dx12\,dx13 + dr12\,dr23) + 3\,dx12\,dr12\,s1}{2\,b1^5}$	$\frac{-3\,dr12^2\,s1 + b1^2\,(dx13\,dr12 + dx23\,dr12 + s1)}{2\,b1^5}$	$\frac{b1^2\,(-dx12\,dx13 + dr12\,dr13) + 3\,dx12\,dr12\,s1}{2\,b1^5}$	$\frac{3\,dr12^2\,s1 - b1^2\,(2\,dx13\,dr12 + s1)}{2\,b1^5}$
$\frac{dx12\,dr12}{2\,b1^3}$	$\frac{-b1^2 + dr12^2}{2\,b1^3}$	$\frac{1}{2}\left(-\frac{dx12\,dr12}{b1^3} + \frac{dx34\,dr34}{b2^3}\right)$	$\frac{1}{2}\left(\frac{1}{b1} + \frac{1}{b2} - \frac{dx34^2}{b2^3} - \frac{dr12^2}{b1^3}\right)$
$\frac{b1^2 - dx12^2}{2\,b1^3}$	$-\frac{dx12\,dr12}{2\,b1^3}$	$\frac{1}{2}\left(-\frac{1}{b1} + \frac{dx12^2}{b1^3} + \frac{-b2^2 + dr34^2}{b2^3}\right)$	$\frac{1}{2}\left(\frac{dx12\,dr12}{b1^3} - \frac{dx34\,dr34}{b2^3}\right)$
0	0	$-\frac{dx34\,dr34}{2\,b2^3}$	$\frac{-b2^2 + dx34^2}{2\,b2^3}$
0	0	$\frac{b2^2 - dr34^2}{2\,b2^3}$	$\frac{dx34\,dr34}{2\,b2^3}$

$\frac{dx12\,dr12}{2\,b1^3}$	$\frac{b1^2 - dx12^2}{2\,b1^3}$	0	0
$\frac{-b1^2 + dr12^2}{2\,b1^3}$	$-\frac{dx12\,dr12}{2\,b1^3}$	0	0
$\frac{1}{2}\left(-\frac{dx12\,dr12}{b1^3} + \frac{dx34\,dr34}{b2^3}\right)$	$\frac{1}{2}\left(-\frac{1}{b1} + \frac{dx12^2}{b1^3} + \frac{-b2^2 + dr34^2}{b2^3}\right)$	$-\frac{dx34\,dr34}{2\,b2^3}$	$\frac{b2^2 - dr34^2}{2\,b2^3}$
$\frac{1}{2}\left(\frac{1}{b1} + \frac{1}{b2} - \frac{dx34^2}{b2^3} - \frac{dr12^2}{b1^3}\right)$	$\frac{1}{2}\left(\frac{dx12\,dr12}{b1^3} - \frac{dx34\,dr34}{b2^3}\right)$	$\frac{-b2^2 + dx34^2}{2\,b2^3}$	$\frac{dx34\,dr34}{2\,b2^3}$
$\frac{3\,dx34^2\,s2 - b2^2\,(2\,dx34\,dr24 + s2)}{2\,b2^5}$	$\frac{b2^2\,(dx24\,dx34 - dr24\,dr34) + 3\,dx34\,dr34\,s2}{2\,b2^5}$	$\frac{-3\,dx34^2\,s2 + b2^2\,(dx34\,(dr23 + dr24) + s2)}{2\,b2^5}$	$-\frac{b2^4 + b2^2\,(dx23\,dx34 - dr24\,dr34) + 3\,dx34\,dr34\,s2}{2\,b2^5}$
$\frac{b2^2\,(dx24\,dx34 - dr24\,dr34) + 3\,dx34\,dr34\,s2}{2\,b2^5}$	$\frac{b2^2\,(2\,dx24\,dr34 - s2) + 3\,dr34^2\,s2}{2\,b2^5}$	$\frac{b2^4 + b2^2\,(-dx24\,dx34 + dr23\,dr34) - 3\,dx34\,dr34\,s2}{2\,b2^5}$	$\frac{-3\,dr34^2\,s2 + b2^2\,(-dx23\,dr34 - dx24\,dr34 + s2)}{2\,b2^5}$
$\frac{-3\,dx34^2\,s2 + b2^2\,(dx34\,(dr23 + dr24) + s2)}{2\,b2^5}$	$\frac{b2^4 + b2^2\,(-dx24\,dx34 + dr23\,dr34) - 3\,dx34\,dr34\,s2}{2\,b2^5}$	$\frac{3\,dx34^2\,s2 - b2^2\,(2\,dx34\,dr23 + s2)}{2\,b2^5}$	$\frac{b2^2\,(dx23\,dx34 - dr23\,dr34) + 3\,dx34\,dr34\,s2}{2\,b2^5}$
$-\frac{b2^4 + b2^2\,(dx23\,dx34 - dr24\,dr34) + 3\,dx34\,dr34\,s2}{2\,b2^5}$	$\frac{-3\,dr34^2\,s2 + b2^2\,(-dx23\,dr34 - dx24\,dr34 + s2)}{2\,b2^5}$	$\frac{b2^2\,(dx23\,dx34 - dr23\,dr34) + 3\,dx34\,dr34\,s2}{2\,b2^5}$	$\frac{b2^2\,(2\,dx23\,dr34 - s2) + 3\,dr34^2\,s2}{2\,b2^5}$

$$R = C* \begin{pmatrix} \frac{(b1^2\, dY23 - dX12\, S1)\ (2\, a0\, b1\, b2 - b2\, S1 - b1\, S2)}{4\, b1^4\, b2} \\ -\frac{(b1^2\, dX23 - dY12\, S1)\ (2\, a0\, b1\, b2 - b2\, S1 - b1\, S2)}{4\, b1^4\, b2} \\ \frac{(-b1^2\, b2\, dY13 + b1^3\, dY34 - b2\, dX12\, S1)\ (2\, a0\, b1\, b2 - b2\, S1 - b1\, S2)}{4\, b1^4\, b2^2} \\ -\frac{(-b1^2\, b2\, dX13 + b1^3\, dX34 + b2\, dY12\, S1)\ (2\, a0\, b1\, b2 - b2\, S1 - b1\, S2)}{4\, b1^4\, b2^2} \\ -\frac{(2\, a0\, b1\, b2 - b2\, S1 - b1\, S2)\ (-b2^3\, dY12 + b1\, b2^2\, dY24 - b1\, dX34\, S2)}{4\, b1^2\, b2^4} \\ \frac{(2\, a0\, b1\, b2 - b2\, S1 - b1\, S2)\ (-b2^3\, dX12 + b1\, b2^2\, dX24 + b1\, dY34\, S2)}{4\, b1^2\, b2^4} \\ \frac{(2\, a0\, b1\, b2 - b2\, S1 - b1\, S2)\ (b2^2\, dY23 - dX34\, S2)}{4\, b1\, b2^4} \\ -\frac{(2\, a0\, b1\, b2 - b2\, S1 - b1\, S2)\ (b2^2\, dX23 + dY34\, S2)}{4\, b1\, b2^4} \end{pmatrix};$$

H	$\frac{1}{2}\left(\frac{S1}{b1} + \frac{S2}{b2}\right)$
S1	$(-uX1 + uX2 - x01 + x02)\ (uY1 + uY2 + y01 + y02) + (uX1 - uX3 + x01 - x03)\ (uY1 + uY3 + y01 + y03) + (-uX2 + uX3 - x02 + x03)\ (uY2 + uY3 + y02 + y03)$
S2	$(-uX2 + uX3 - x02 + x03)\ (uY2 + uY3 + y02 + y03) + (uX2 - uX4 + x02 - x04)\ (uY2 + uY4 + y02 + y04) + (-uX3 + uX4 - x03 + x04)\ (uY3 + uY4 + y03 + y04)$
b1	$\left(\sqrt{dX12^2 + dY12^2}\right)$
b2	$\left(\sqrt{dX34^2 + dY34^2}\right)$
a0	$\sqrt{((x02 - x01)^2 + (y02 - y01)^2)}$
dX12	$(uX1 - uX2 + x01 - x02)$
dY12	$(uY1 - uY2 + y01 - y02)$
dX23	$(uX2 - uX3 + x02 - x03)$
dY23	$(uY2 - uY3 + y02 - y03)$
dX34	$(uX3 - uX4 + x03 - x04)$
dY34	$(uY3 - uY4 + y03 - y04)$
dX13	$(uX1 - uX3 + x01 - x03)$
dY13	$(uY1 - uY3 + y01 - y03)$
dX24	$(uX2 - uX4 + x02 - x04)$
dY24	$(uY2 - uY4 + y02 - y04)$

6. 'Diagonal' Element

Rigidity matrix for *diagonal element* is the same as for *side element* Appendix B.4.

7. Contribution of Internal Couples on Fabric Behaviour

To estimate the possible contribution of couples on fabric extension behaviour we consider a segment of loop as a circular arc of radius R and central angle α. The initial curvature of the arc can be expressed as $\chi_0 = 1/R$. The maximum moment occurred when the arc is straightened and, hence current curvature $\chi = 0$. The potential energy of straightened arc could be expressed as:

$$\Pi = \frac{1}{2} B |\Delta\chi| \alpha \tag{0.3}$$

where B is the bending rigidity of yarn/rod;

$|\Delta\chi| = |\chi - \chi_0| = 1/R$.

The value of bending rigidity of an average cotton or wool yarn can be estimated as $B \approx 3 \cdot 10^{-8}\ [N m^2]$ and if the arc represents the upper part of the loop which lies between the contact points (Figure 2.2) the central angle could be estimated as $\alpha \approx \pi/4$ and radius $R \approx 2 \cdot 10^{-3}\ [m]$. Substituting the above quantities into (0.3) potential energy of straighten arc can be estimated as $\Pi \approx 4 \cdot 10^{-6}\ [N m]$.

We consider then an average sample of fabric knitted from yarn with the specified bending rigidity. Assume sample is formed by 20 courses ($n_C = 20$) and is subjected to external load $F_{ext} = 2\ [N]$ in course direction. This force is normally enough to exert relative deformation of sample up to $\varepsilon = 0.15$. To strengthen the arguments we assume that $\varepsilon = 0.1$. The work done by the external force related to one loop could be written as:

$$W \approx \frac{F_{ext}\, \varepsilon\, B_{kn}}{n_C} \tag{0.4}$$

where B_{kn} is the fabric dimension in the course direction (Figure 2.1).

Assuming $B_{kn} = 3 \cdot 10^{-3}\ [m]$ and substituting respective quantities into (0.4) gives approximation of the work done by external force as $W \approx 3 \cdot 10^{-5}\ [N m]$.

Comparison of magnitude of potential energy due to internal couples with that of work of external load ($W/\Pi \approx 8$) leads to conclusion that internal couples do not contribute significantly into fabric behaviour. The internal couples affect the behaviour of fabric only at low stresses when the yarns straighten. When fabric withstands higher stresses

the value of W in (0.4) can be hundred times more. The value of Π in (0.3) represent the maximum energy involved in yarn bending so that ratio W/Π can be up to thousand at higher stresses.

Appendix C. Experimental and Theoretical curves for fabric samples, Shapes of Tensed Samples

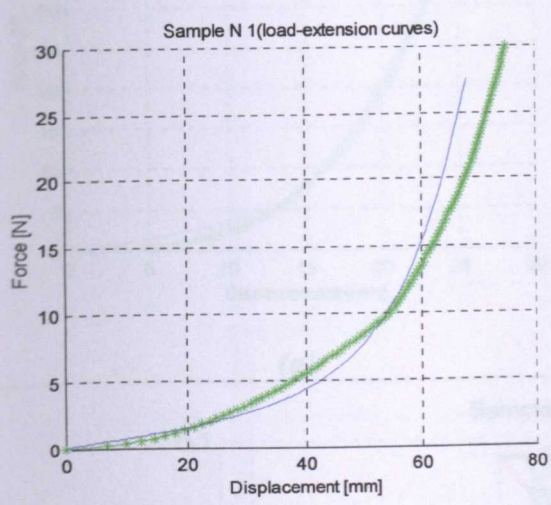

(a)

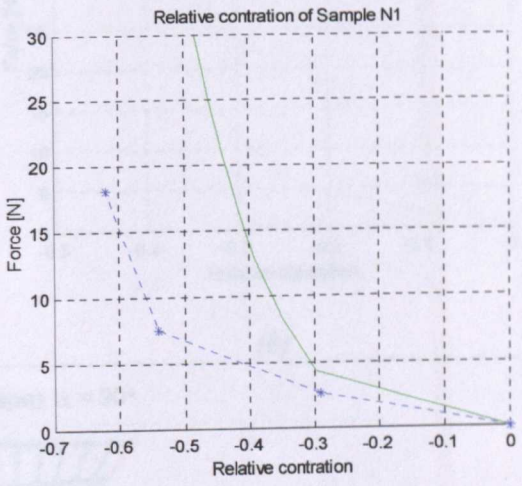

(b)

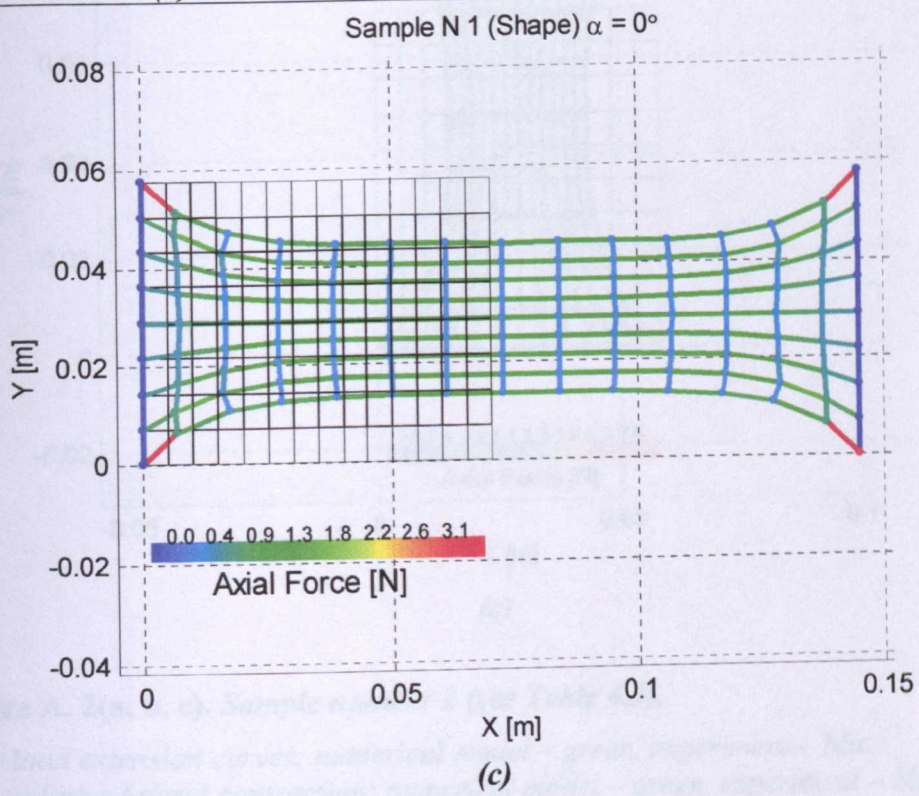

(c)

Figure A. 1(a, b, c). ***Sample number 1 (see Table 4.3).***

(a) – load extension curves; numerical model – green, experiment – blue ;
(b) – relative lateral contraction; numerical model – green, experiment – blue ;
(c) – Numerically simulated shape; initial state – black

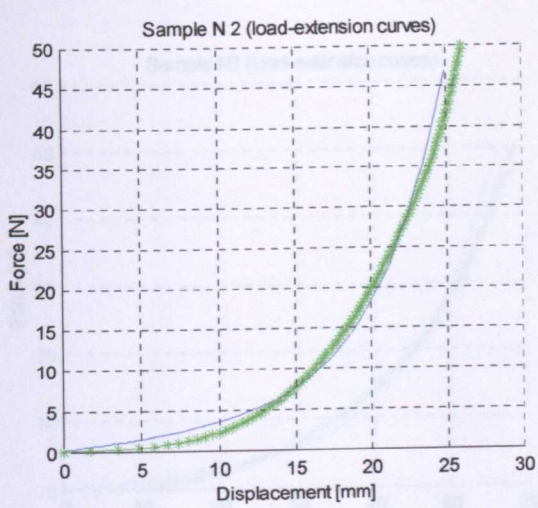

(a)

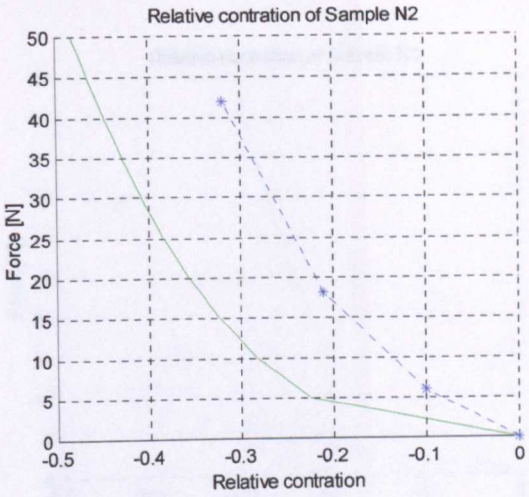

(b)

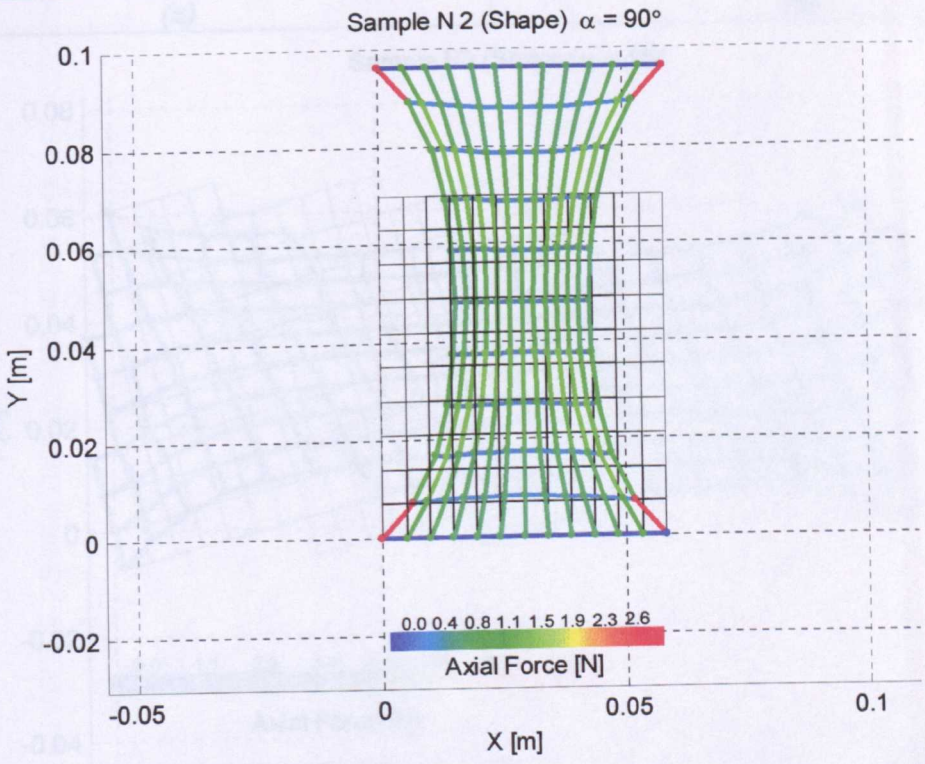

(c)

Figure A. 2(a, b, c). ***Sample number 2 (see Table 4.3).***

(a) – load extension curves; numerical model – green, experiment – blue ;
(b) – relative lateral contraction; numerical model – green, experiment – blue;
(c) – Numerically simulated shape; initial state – black

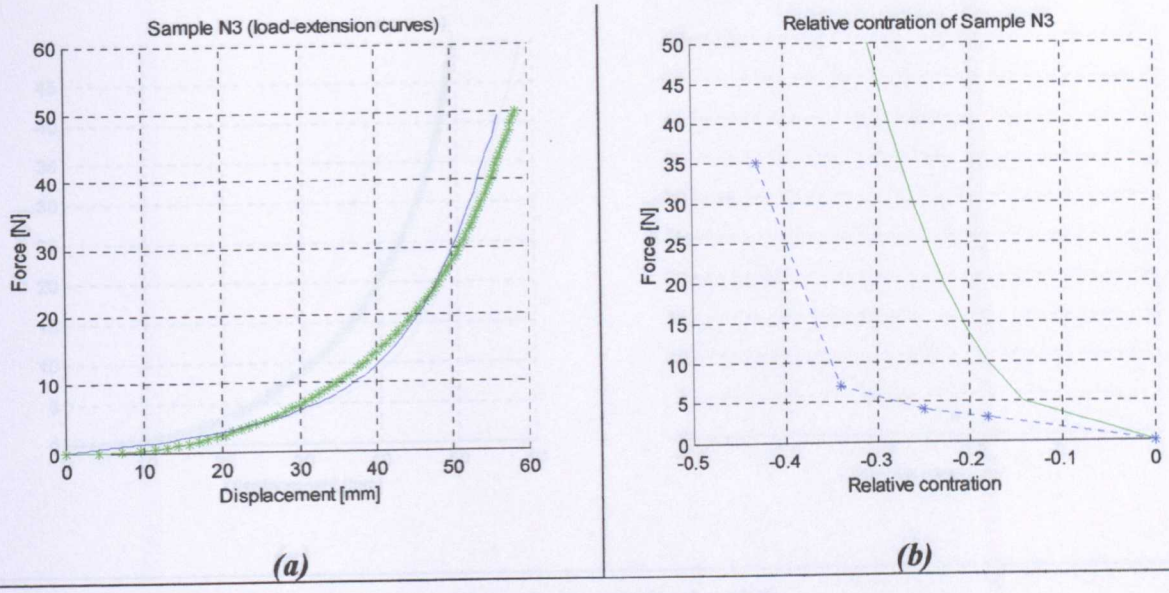

(a)

(b)

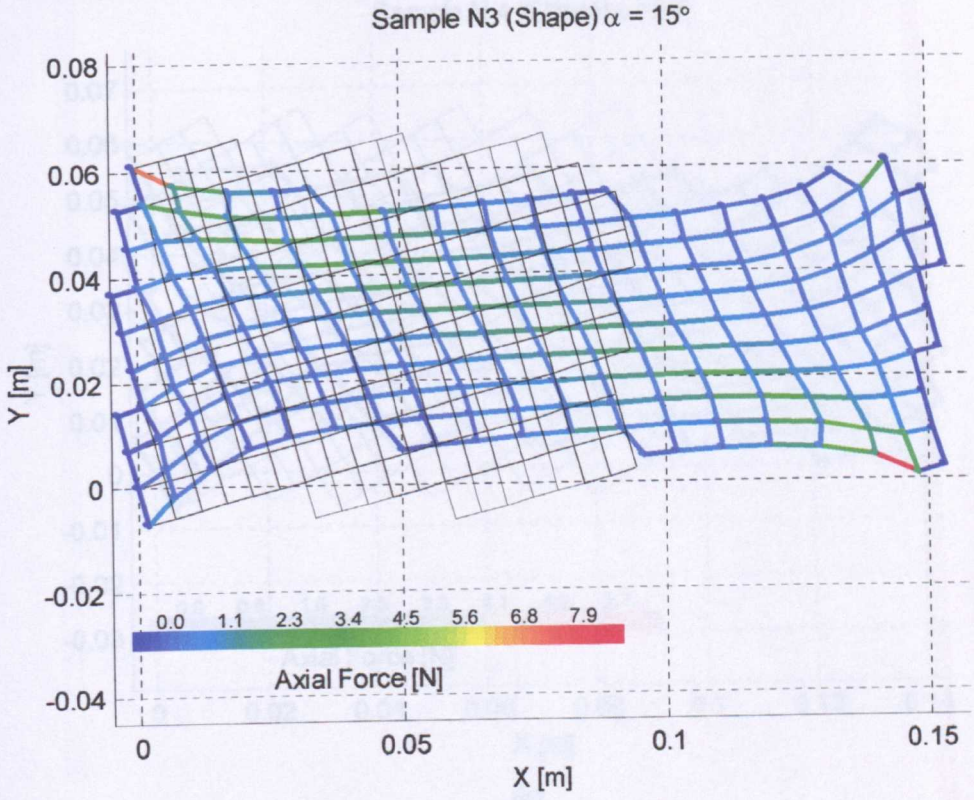

(c)

Figure A. 3(a, b, c). ***Sample number 3 (see Table 4.3).***

(a) – load extension curves; numerical model – green, experiment – blue ;
(b) – relative lateral contraction; numerical model – green, experiment – blue ;
(c) – Numerically simulated shape; initial state – black

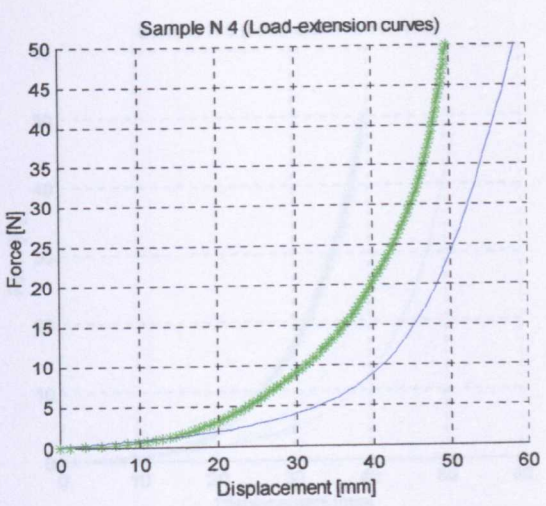

(a)

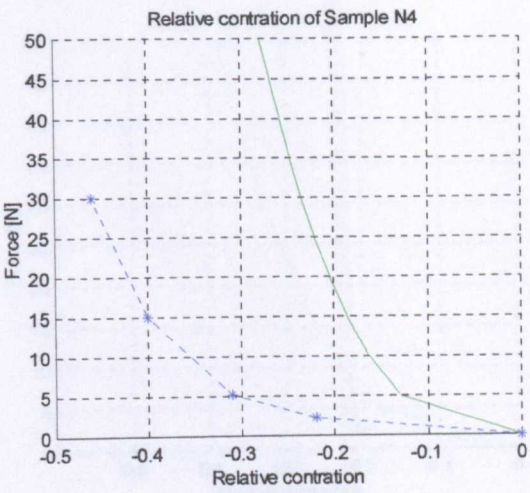

(b)

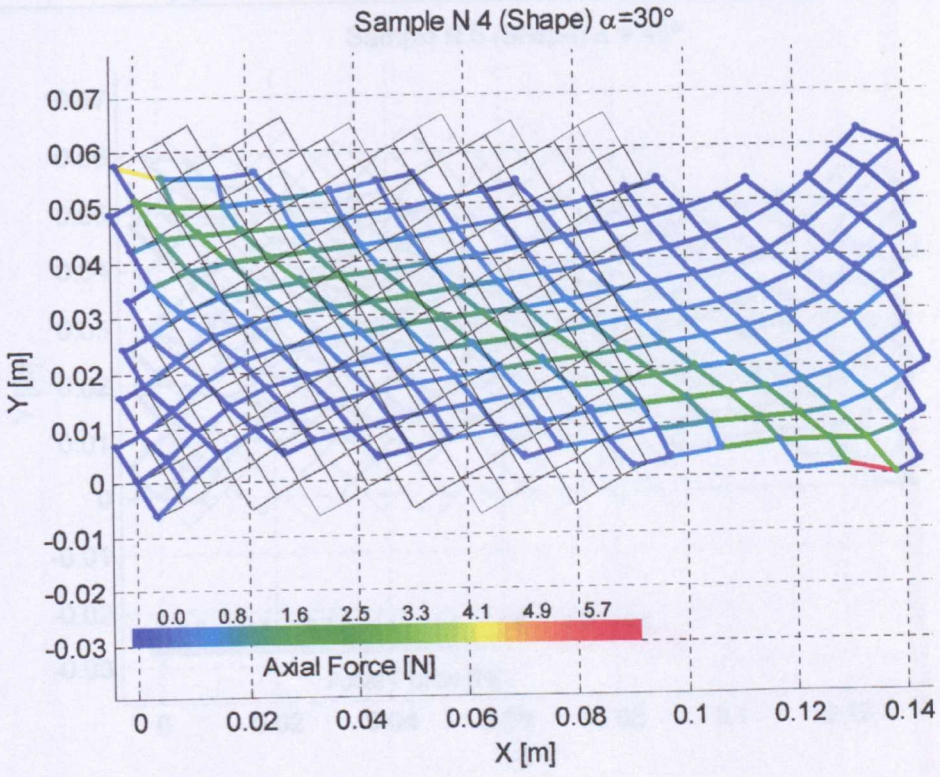

(c)

Figure A. 4(a, b, c). ***Sample number 4 (see Table 4.3).***

(a) – load extension curves; numerical model – green, experiment – blue ;
(b) – relative lateral contraction; numerical model – green, experiment – blue;
(c) – Numerically simulated shape; initial state – black

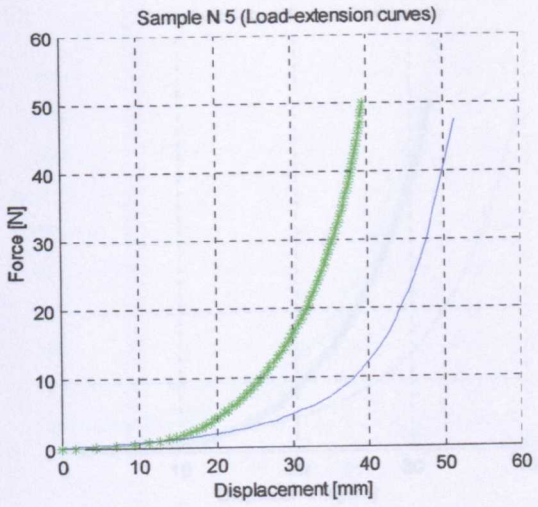

(a)

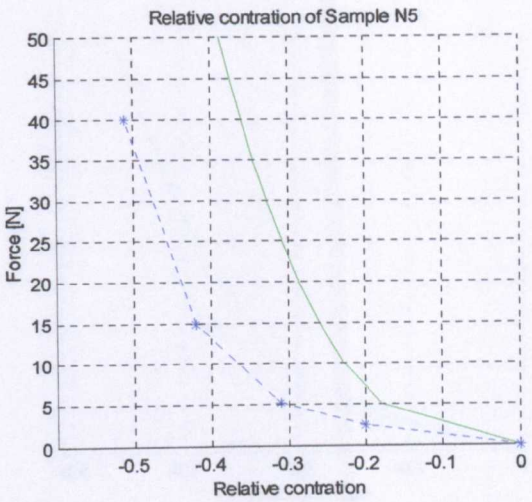

(b)

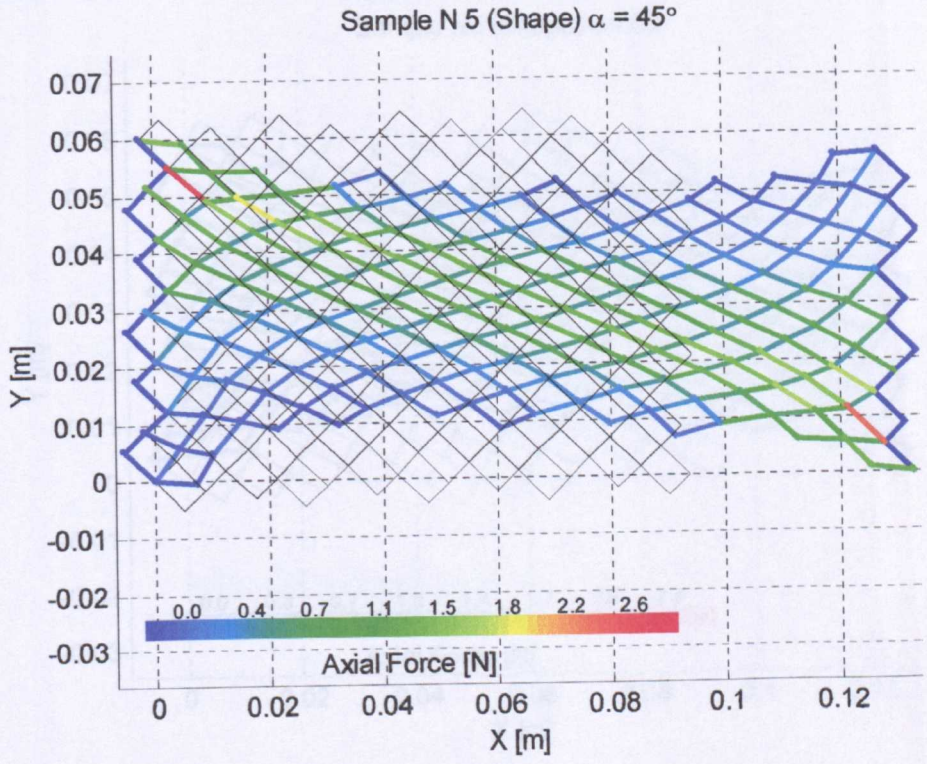

(c)

Figure A. 5(a, b, c). ***Sample number 5 (see Table 4.3).***

(a) – load extension curves; numerical model – green, experiment – blue ;
(b) – relative lateral contraction; numerical model – green, experiment – blue;
(c) – Numerically simulated shape; initial state – black

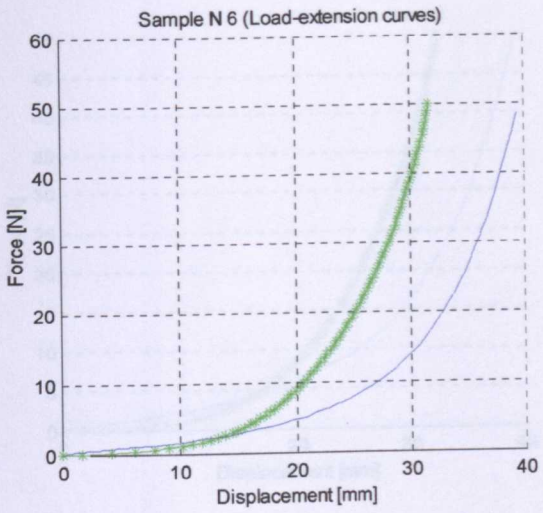

(a)

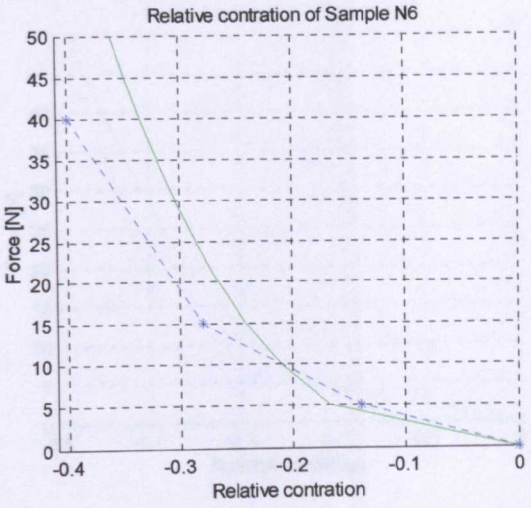

(b)

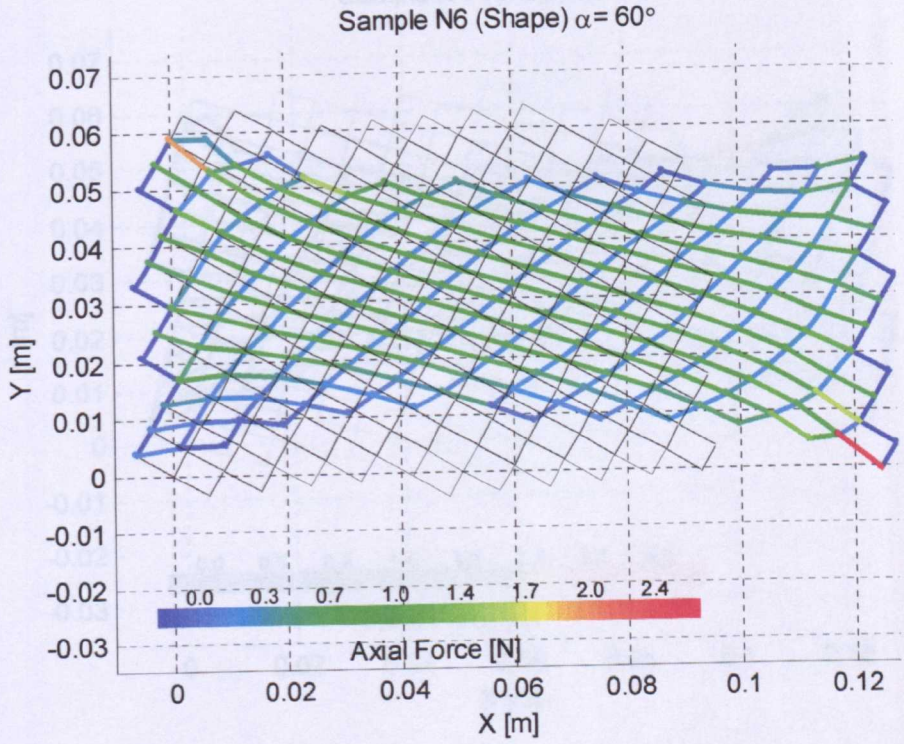

(c)

Figure A. 6(a, b, c). ***Sample number 6 (see Table 4.3).***

(a) – load extension curves; numerical model – green, experiment – blue ;
(b) – relative lateral contraction; numerical model – green, experiment – blue;
(c) – Numerically simulated shape; initial state – black

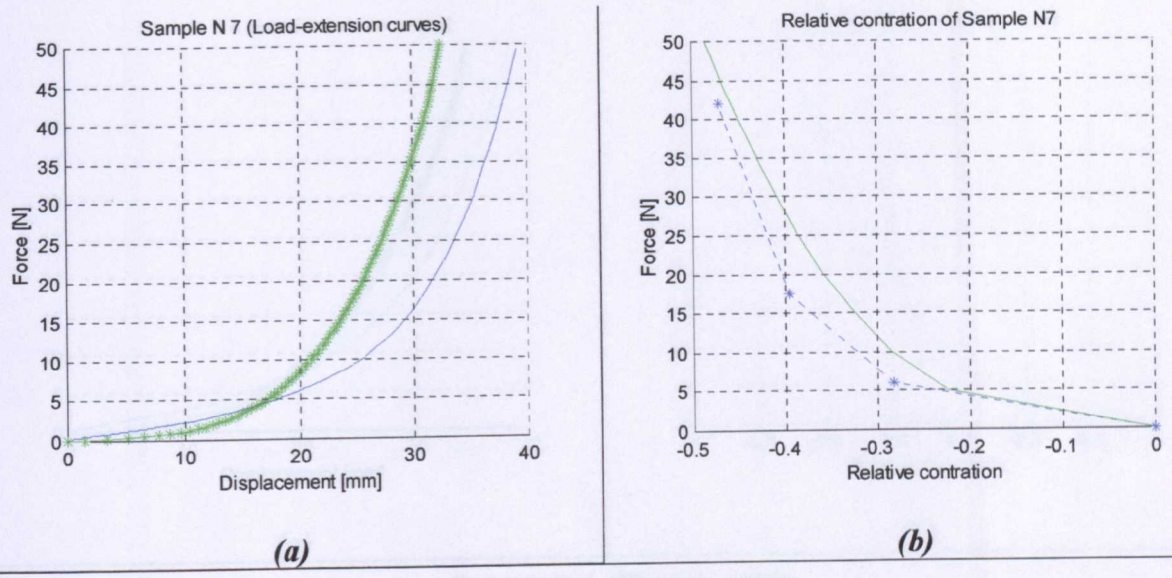

(a)

(b)

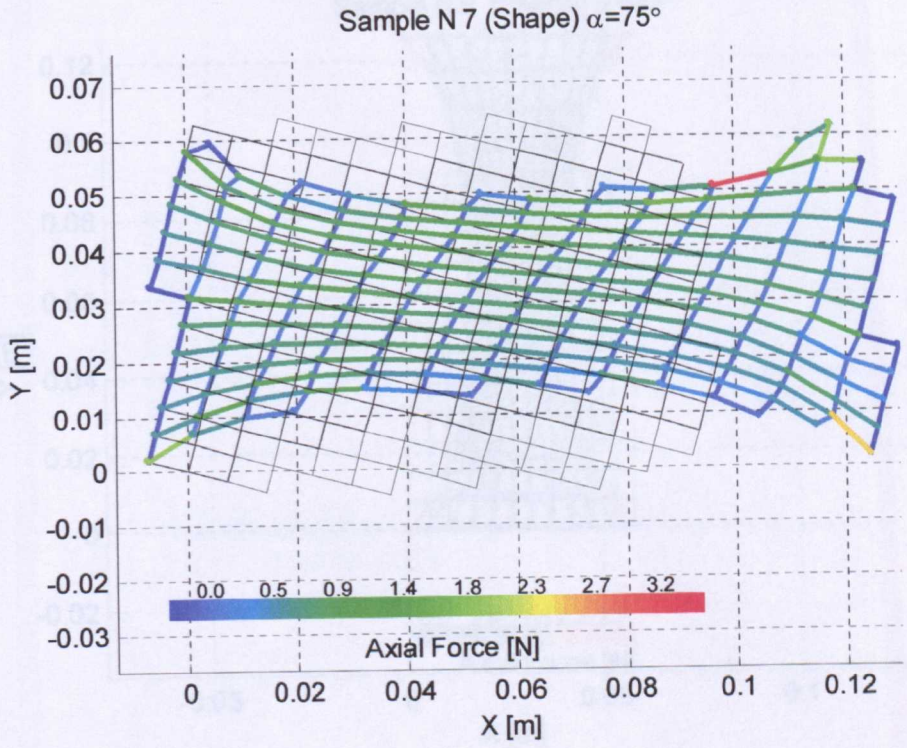

(c)

Figure A. 7(a, b, c). ***Sample number 7 (see Table 4.3).***

(a) – load extension curves; numerical model – green, experiment – blue ;
(b) – relative lateral contraction; numerical model – green, experiment – blue;
(c) – Numerically simulated shape; initial state – black

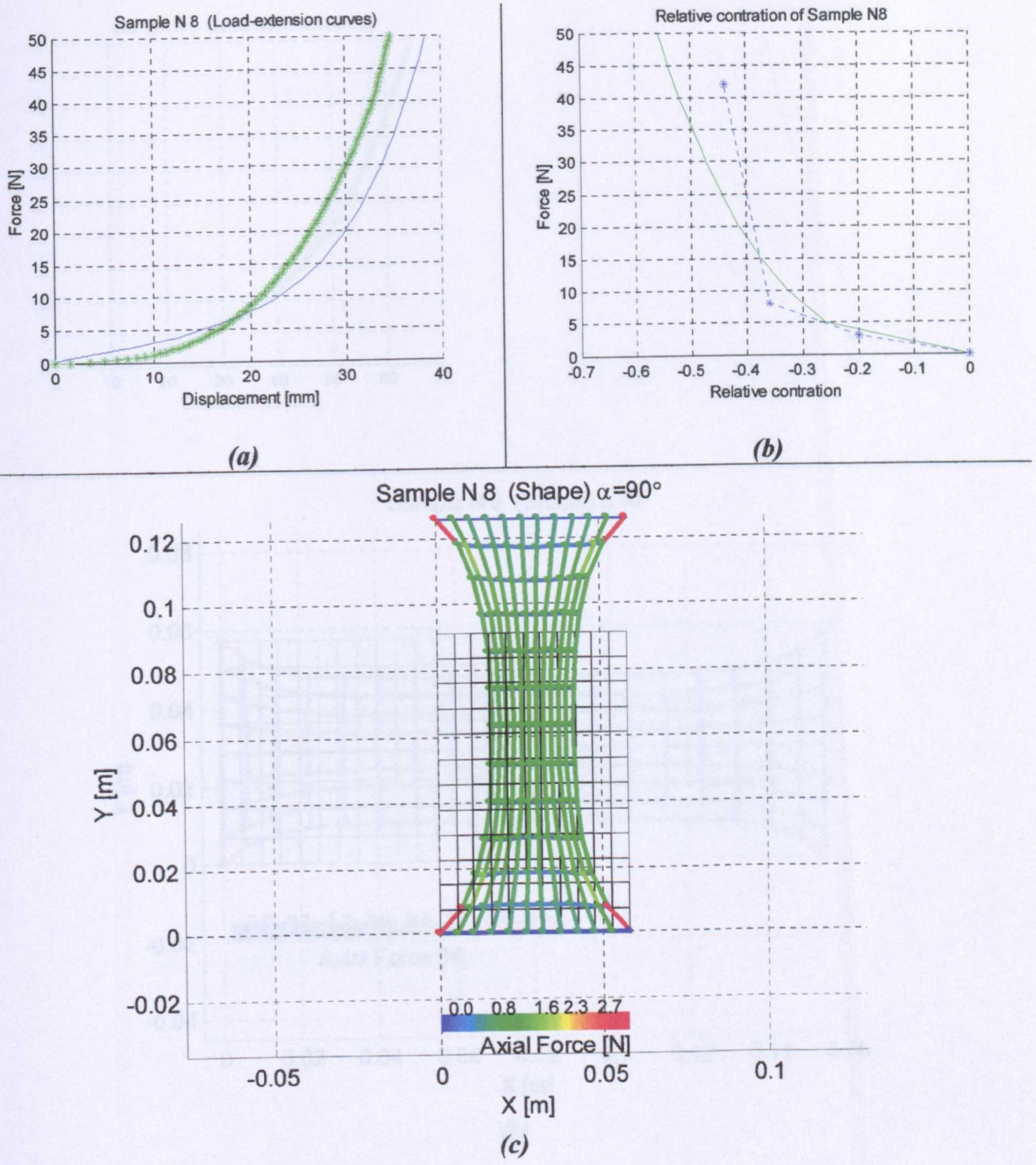

Figure A. 8(a, b, c). ***Sample number 8 (see Table 4.3).***

(a) – load extension curves; numerical model – green, experiment – blue ;
(b) – relative lateral contraction; numerical model – green, experiment – blue;
(c) – Numerically simulated shape; initial state – black

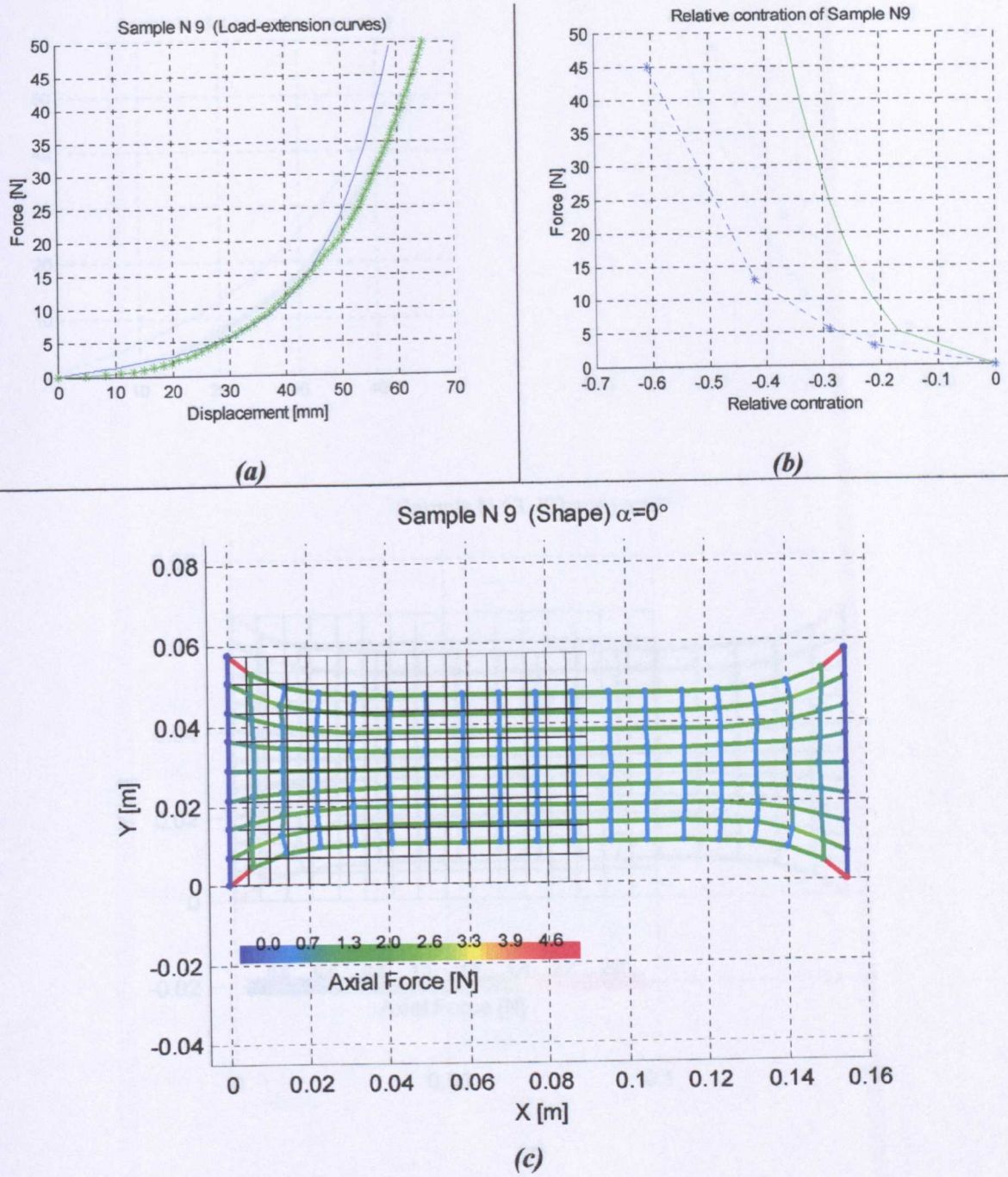

Figure A. 9(a, b, c). ***Sample number 9 (see Table 4.3).***

(a) – load extension curves; numerical model – green, experiment – blue ;
(b) – relative lateral contraction; numerical model – green, experiment – blue;
(c) – Numerically simulated shape; initial state – black

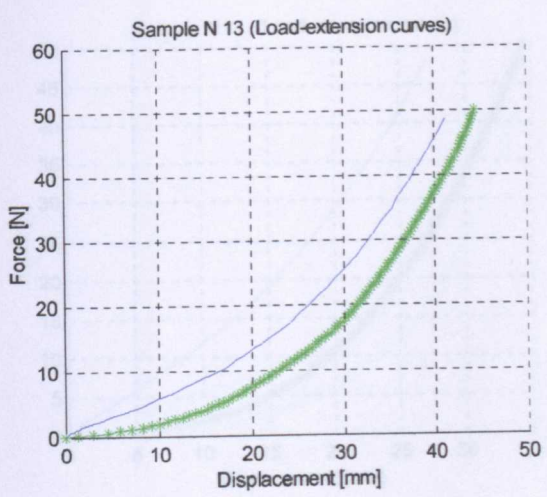

(a)

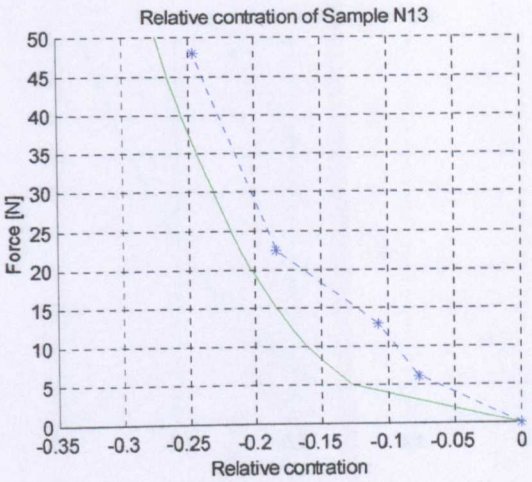

(b)

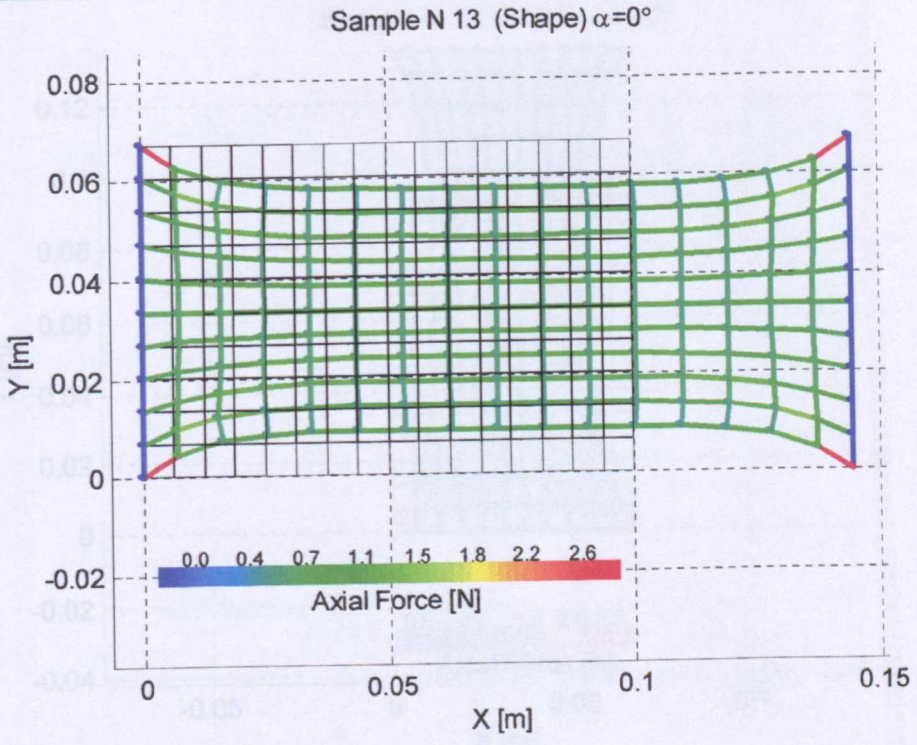

(c)

Figure A. 10(a, b, c). ***Sample number 13 (see Table 4.3).***

(a) – load extension curves; numerical model – green, experiment – blue ;
(b) – relative lateral contraction; numerical model – green, experiment – blue;
(c) – Numerically simulated shape; initial state – black

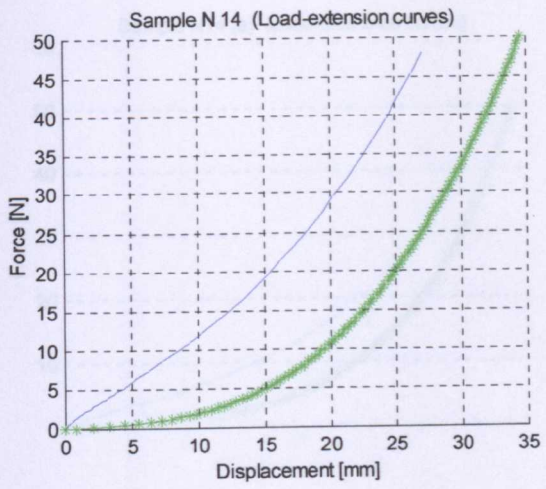

(a)

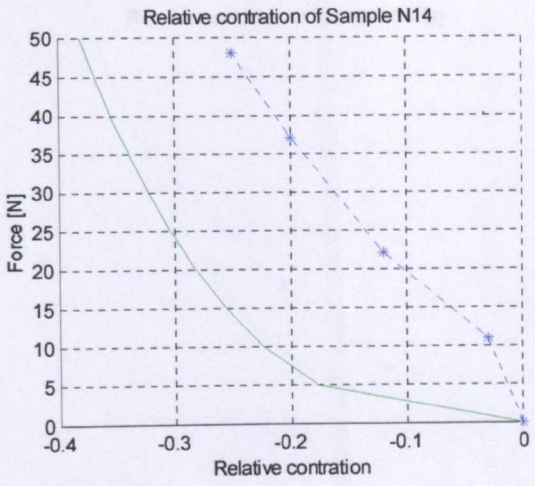

(b)

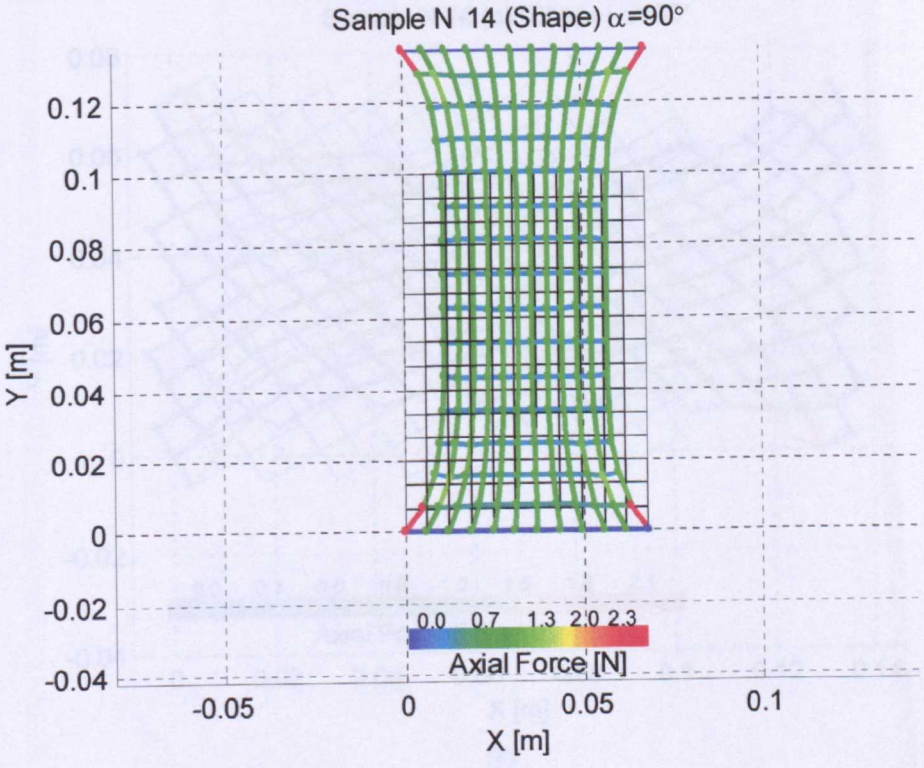

(c)

Figure A. 11(a, b, c). ***Sample number 14 (see Table 4.3).***

(a) – load extension curves; numerical model – green, experiment – blue ;
(b) – relative lateral contraction; numerical model – green, experiment – blue;
(c) – Numerically simulated shape; initial state – black

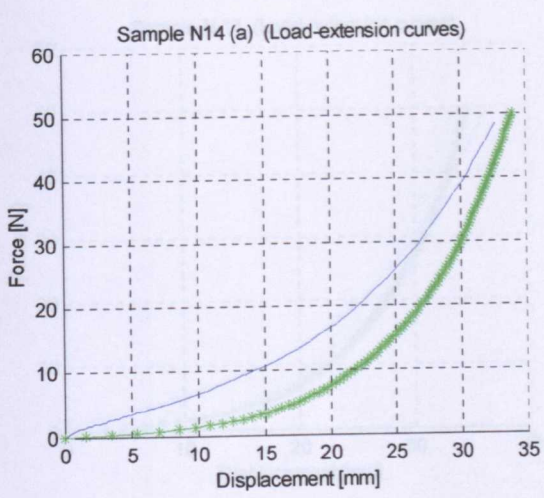

(a)

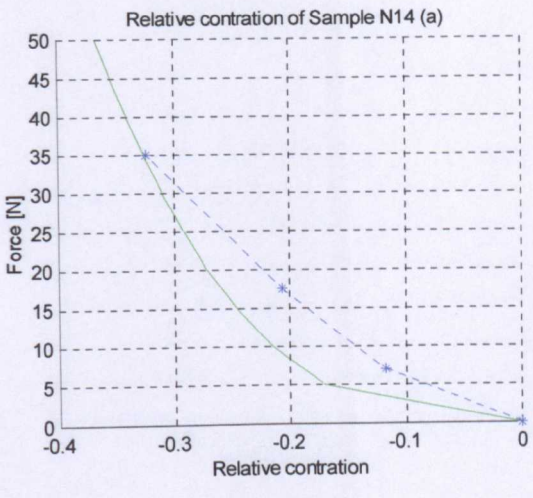

(b)

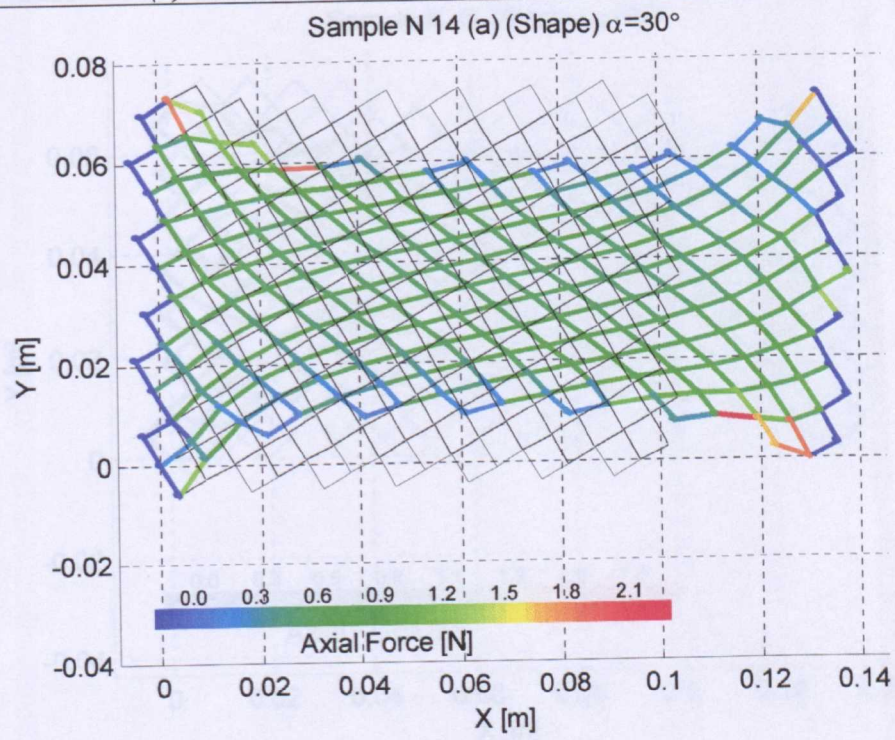

(c)

Figure A. 12(a, b, c). ***Sample number 14 a (see Table 4.3).***

(a) – load extension curves; numerical model – green, experiment – blue ;
(b) – relative lateral contraction; numerical model – green, experiment – blue;
(c) – Numerically simulated shape; initial state – black

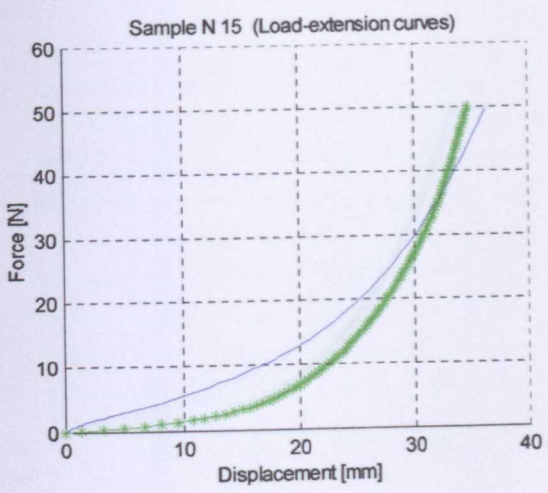

(a)

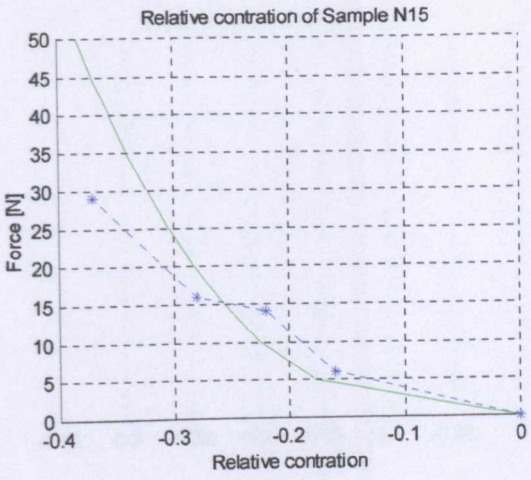

(b)

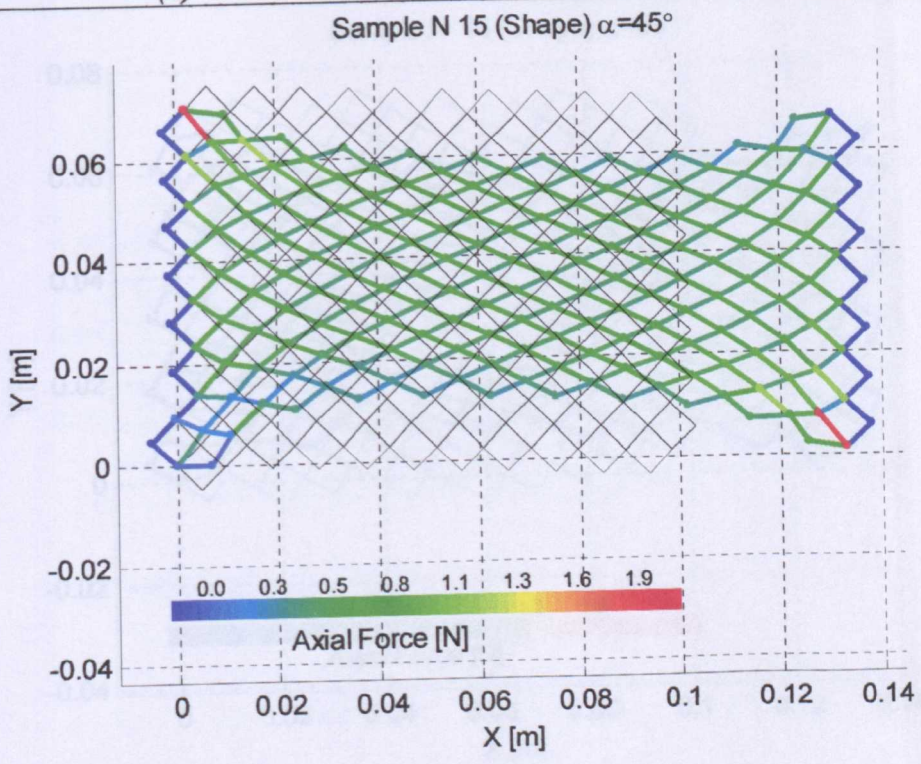

(c)

Figure A. 13(a, b, c). ***Sample number 15 (see Table 4.3).***

(a) – load extension curves; numerical model – green, experiment – blue ;
(b) – relative lateral contraction; numerical model – green, experiment – blue;
(c) – Numerically simulated shape; initial state – black

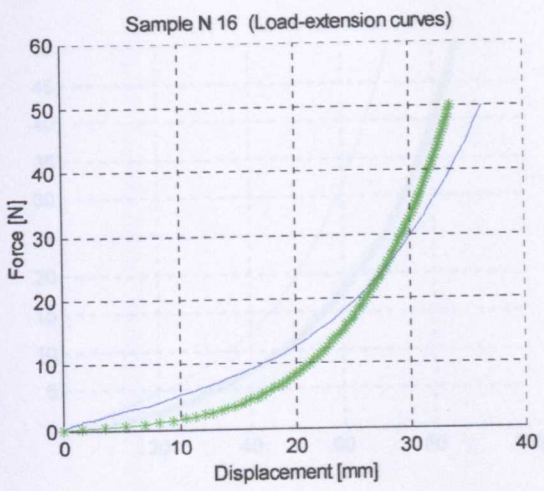

(a)

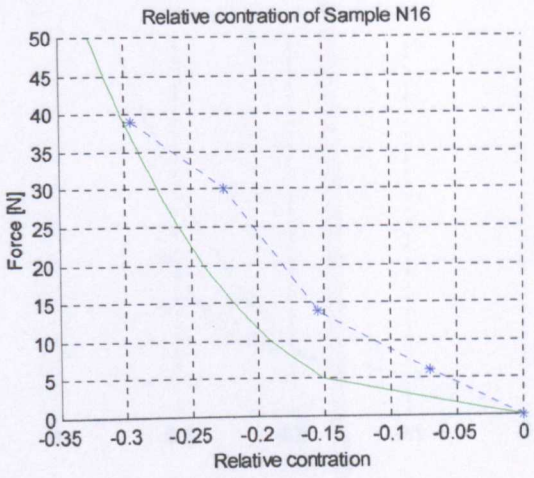

(b)

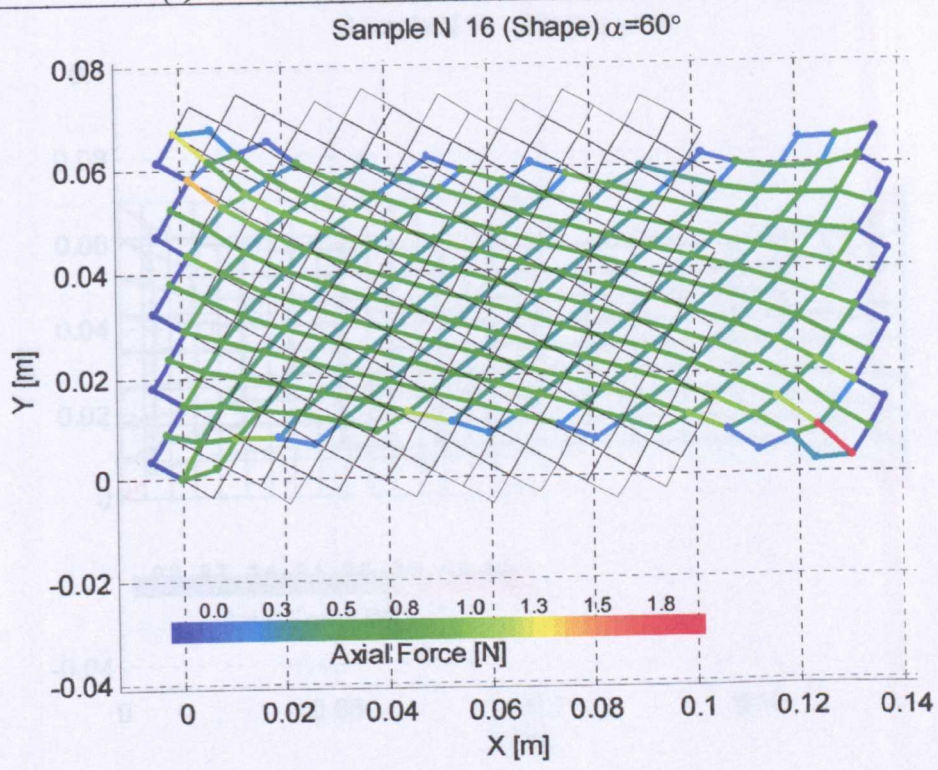

(c)

Figure A. 14(a, b, c). ***Sample number 16 (see Table 4.3).***

(a) – load extension curves; numerical model – green, experiment – blue ;
(b) – relative lateral contraction; numerical model – green, experiment – blue;
(c) – Numerically simulated shape; initial state – black

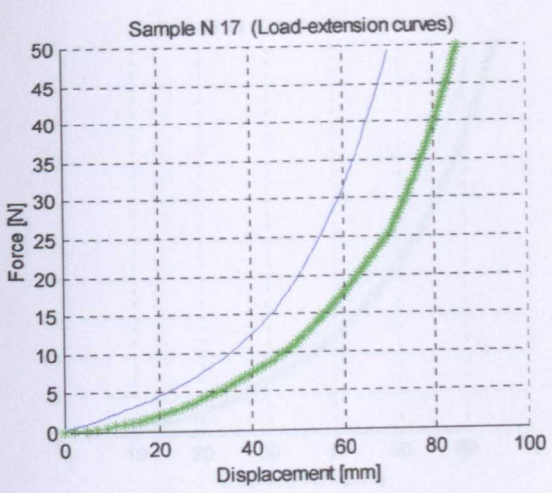

(a)

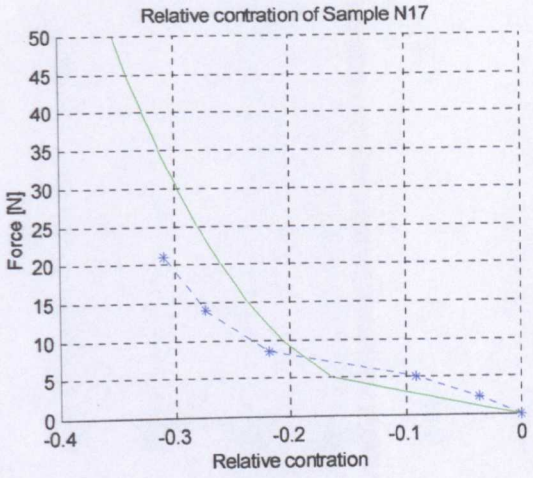

(b)

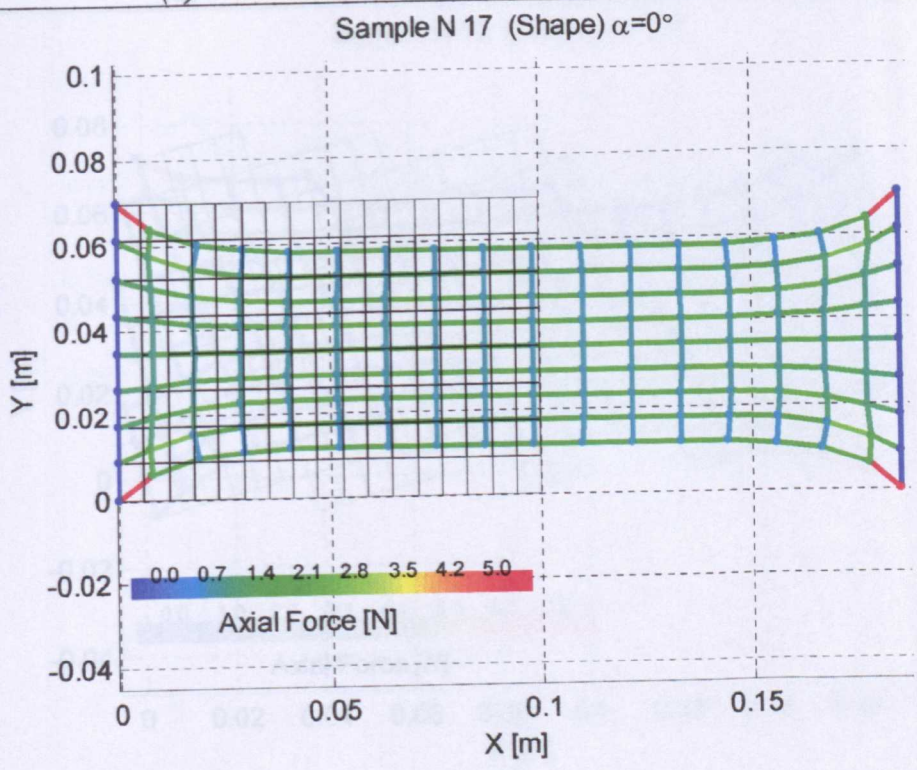

(c)

Figure A. 15(a, b, c). ***Sample number 17 (see Table 4.3).***

(a) – load extension curves; numerical model – green, experiment – blue ;
(b) – relative lateral contraction; numerical model – green, experiment – blue;
(c) – Numerically simulated shape; initial state – black

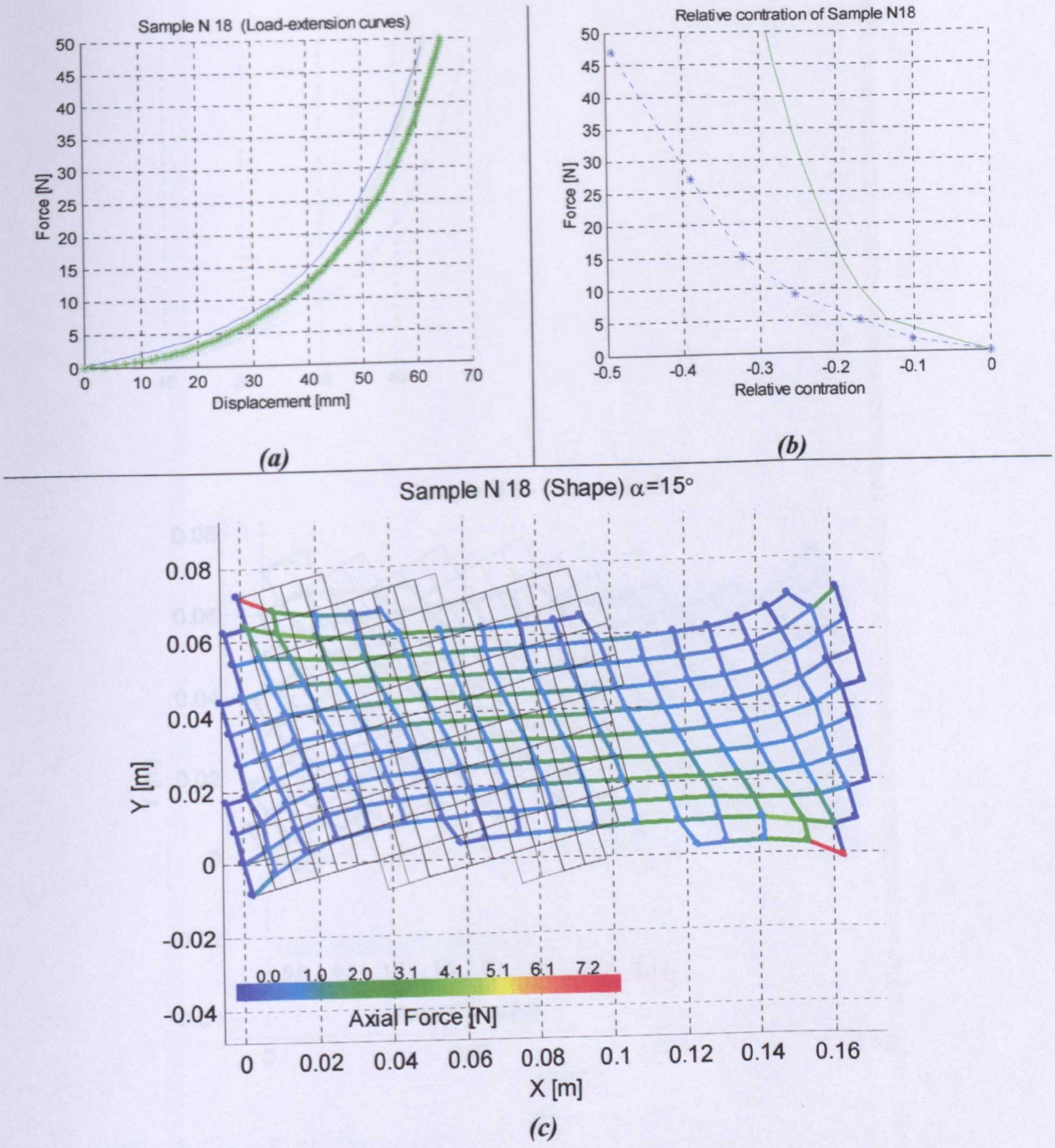

Figure A. 16(a, b, c). ***Sample number 18 (see Table 4.3).***

(a) – load extension curves; numerical model – green, experiment – blue ;
(b) – relative lateral contraction; numerical model – green, experiment – blue;
(c) – Numerically simulated shape; initial state – black

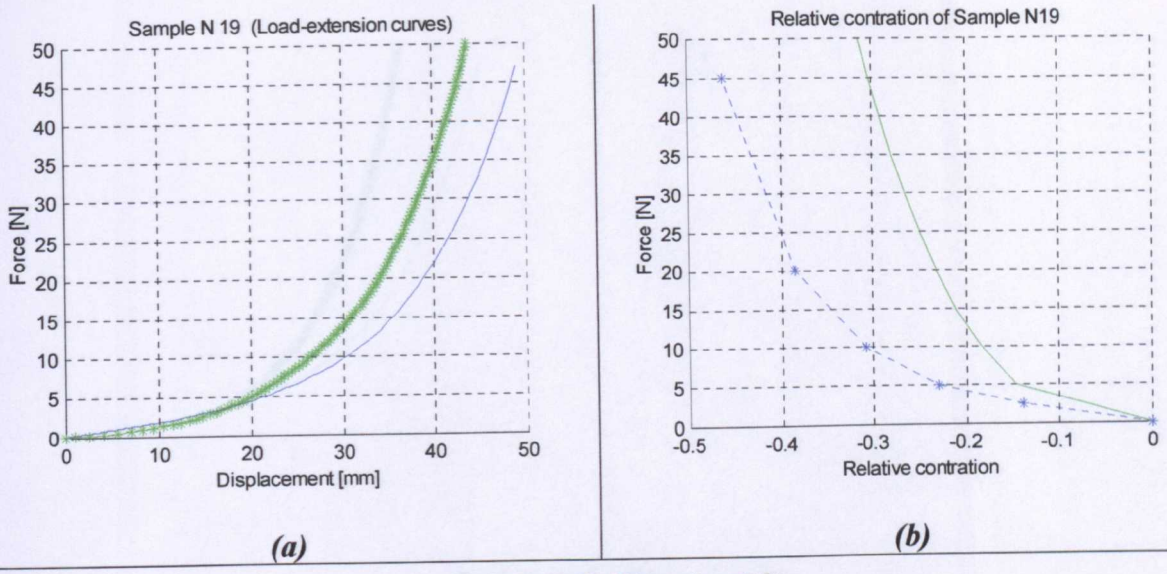

(a)

(b)

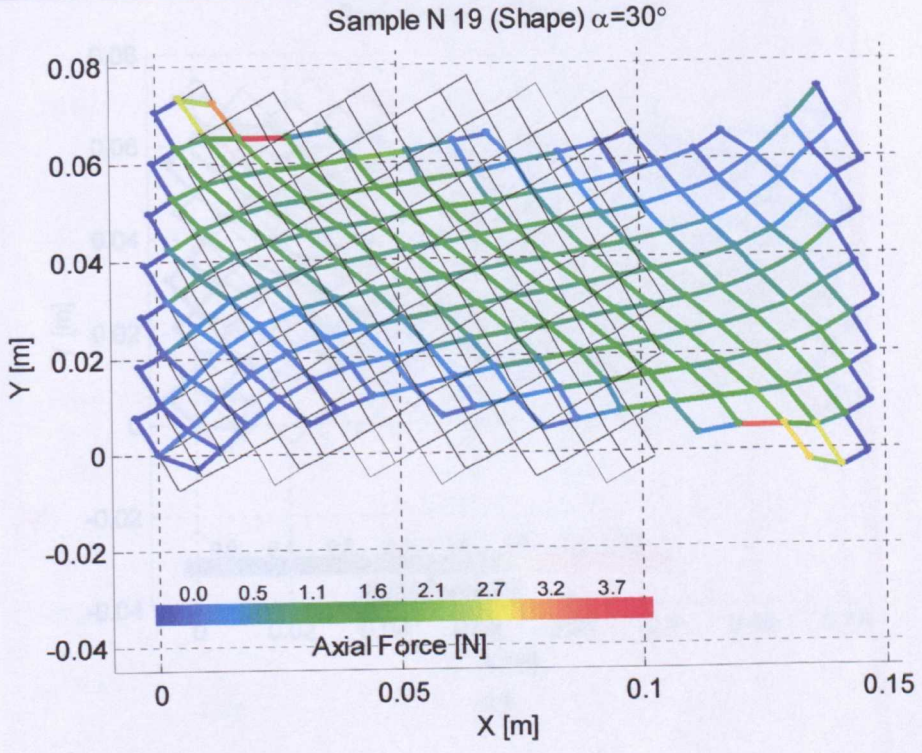

(c)

Figure A. 17(a, b, c). ***Sample number 19 (see Table 4.3).***

(a) – load extension curves; numerical model – green, experiment – blue ;
(b) – relative lateral contraction; numerical model – green, experiment – blue;
(c) – Numerically simulated shape; initial state – black

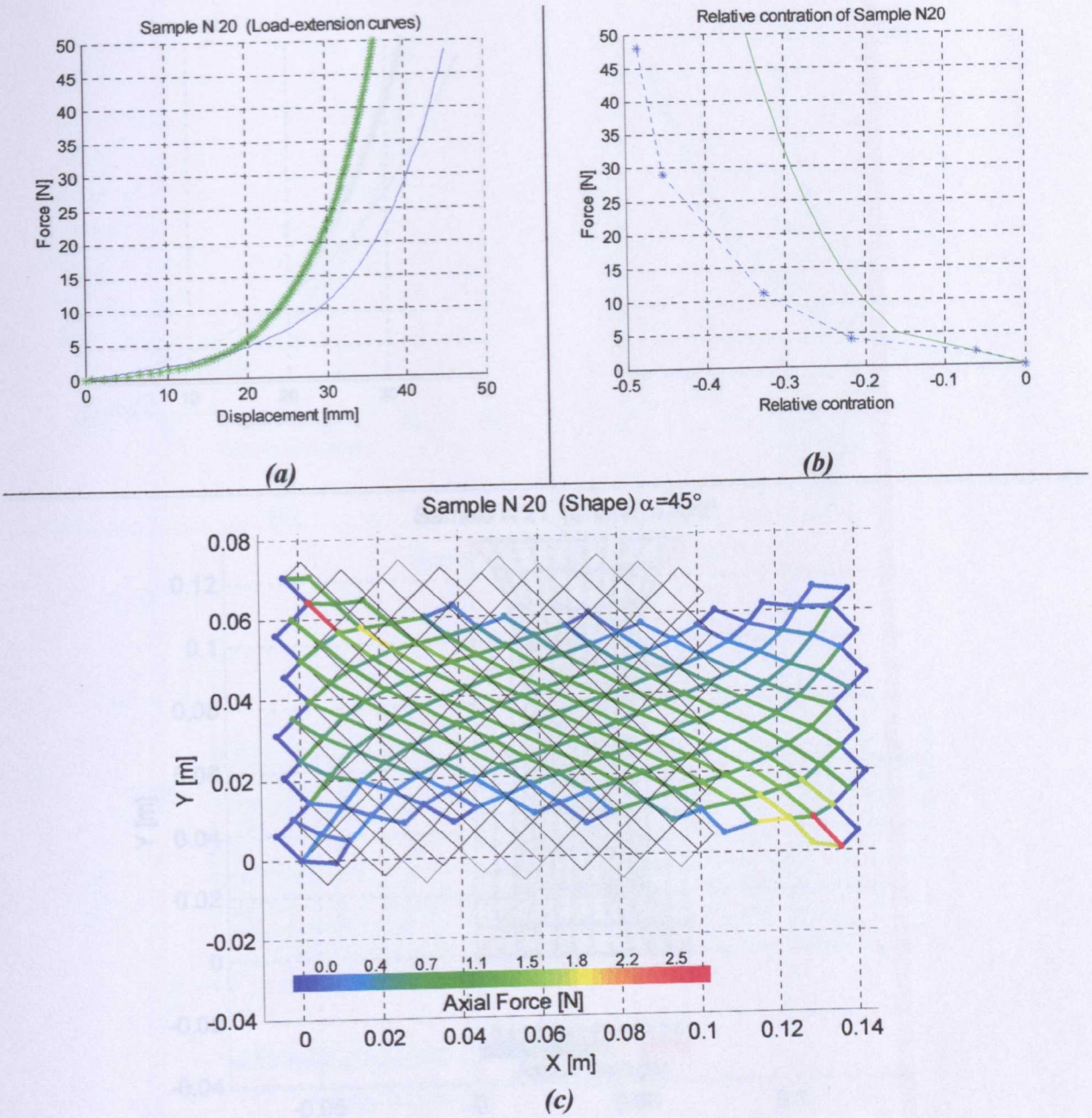

Figure A. 18(a, b, c). ***Sample number 20 (see Table 4.3).***

(a) – load extension curves; numerical model – green, experiment – blue ;
(b) – relative lateral contraction; numerical model – green, experiment – blue;
(c) – Numerically simulated shape; initial state – black

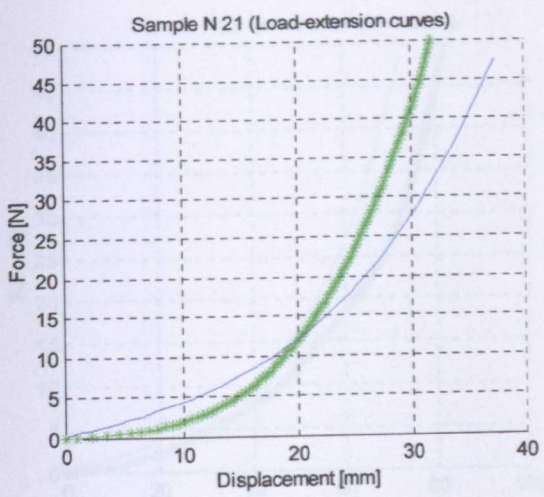

(a)

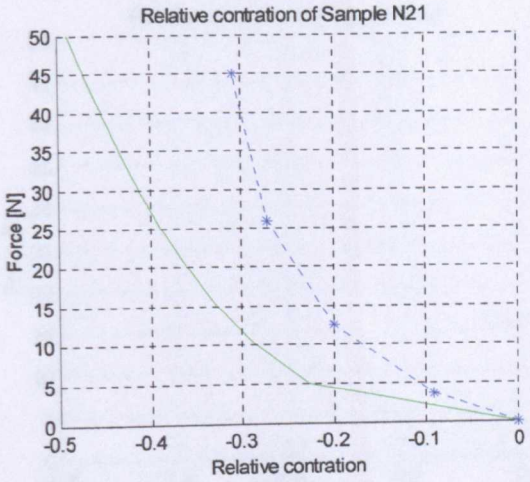

(b)

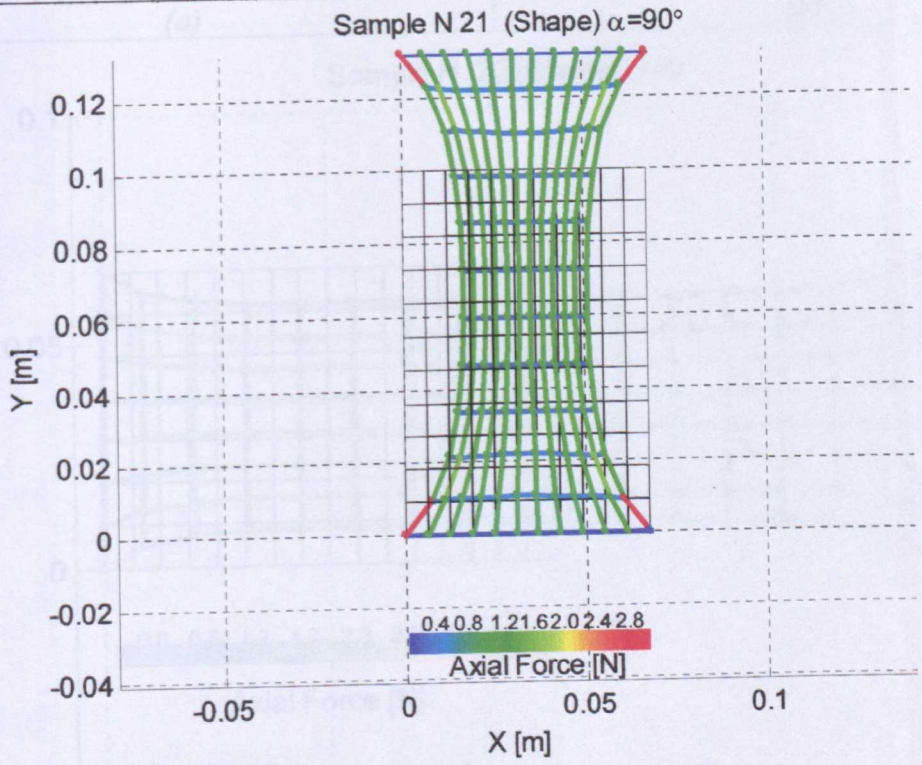

(c)

Figure A. 19(a, b, c). ***Sample number 21 (see Table 4.3).***

(a) – load extension curves; numerical model – green, experiment – blue ;
(b) – relative lateral contraction; numerical model – green, experiment – blue;
(c) – Numerically simulated shape; initial state – black

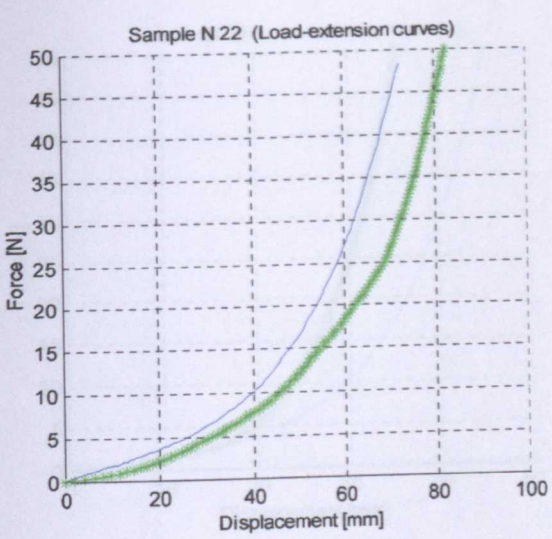

(a)

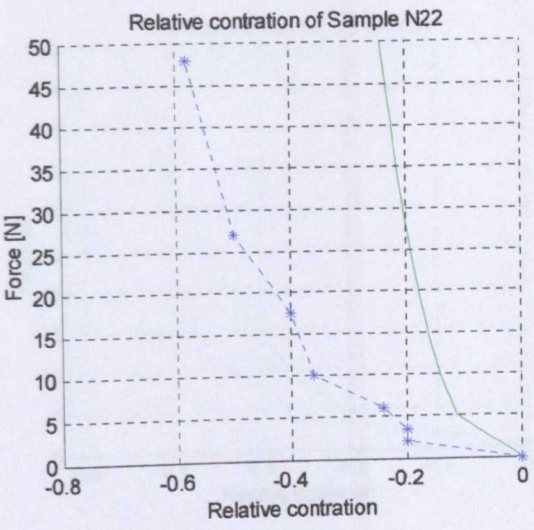

(b)

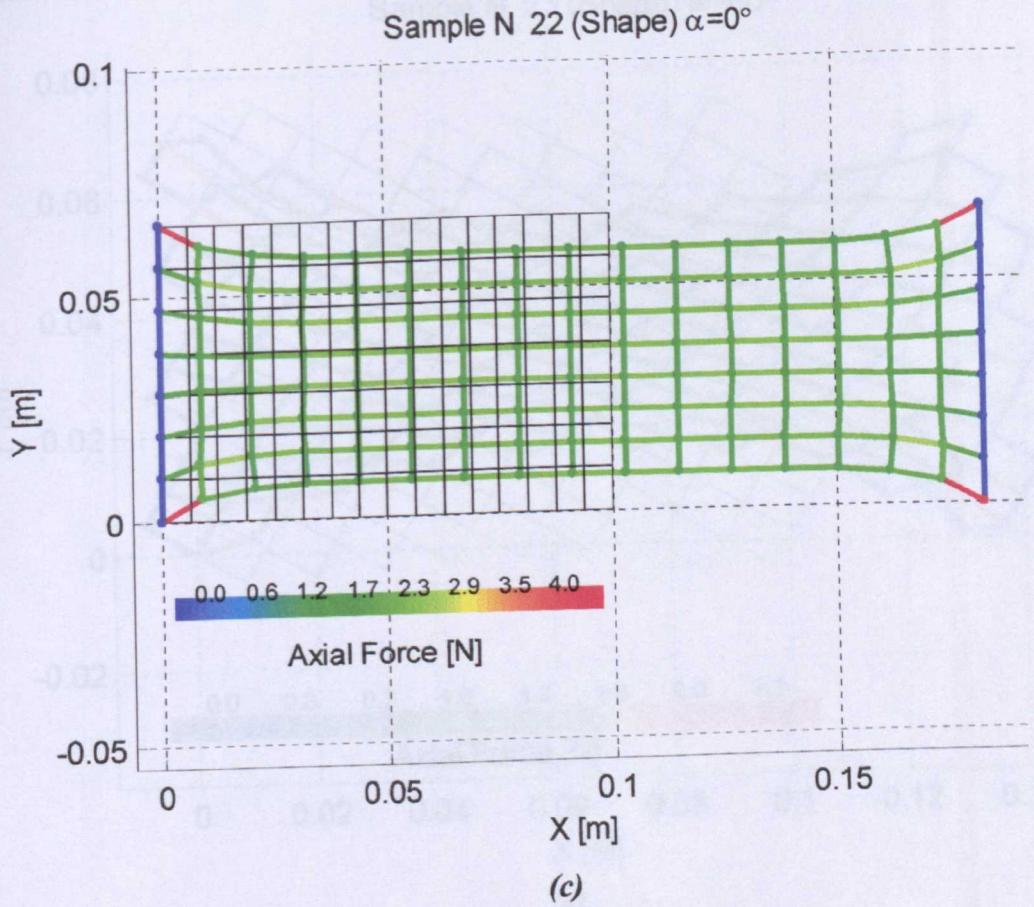

(c)

Figure A. 20(a, b, c). ***Sample number 22 (see Table 4.3).***

(a) – load extension curves; numerical model – green, experiment – blue ;
(b) – relative lateral contraction; numerical model – green, experiment – blue;
(c) – Numerically simulated shape; initial state – black

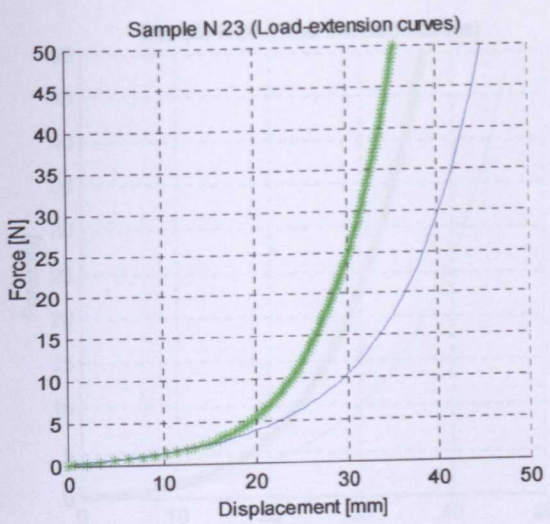

(a)

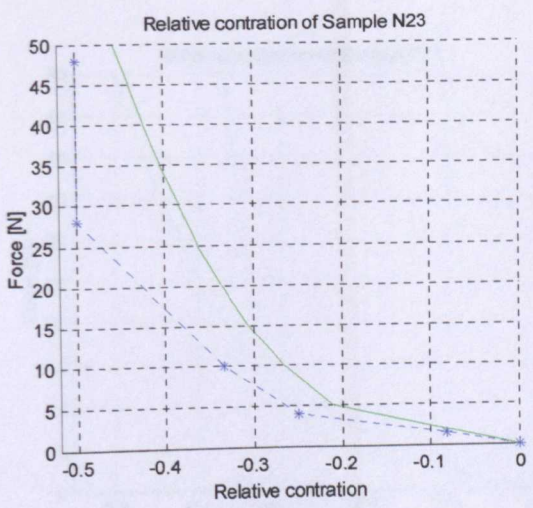

(b)

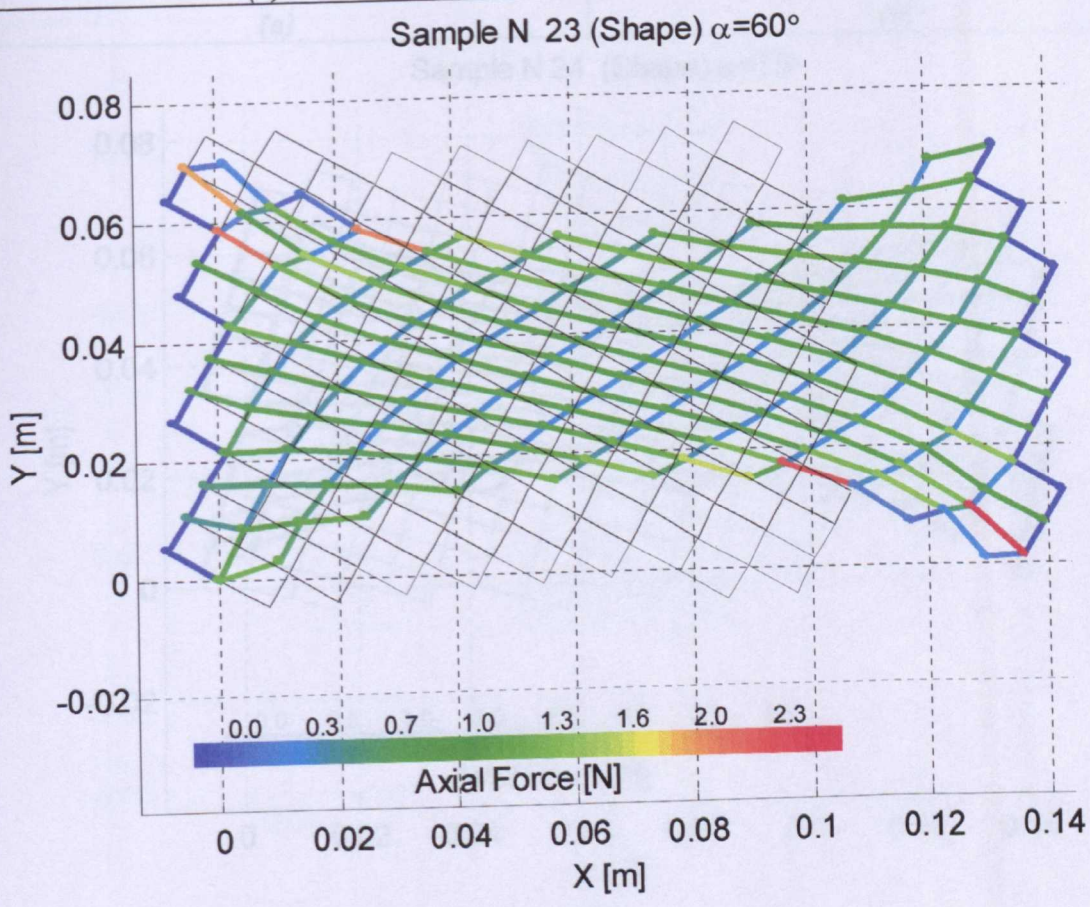

(c)

Figure A. 21(a, b, c). ***Sample number 23 (see Table 4.3).***

(a) – load extension curves; numerical model – green, experiment – blue ;
(b) – relative lateral contraction; numerical model – green, experiment – blue;
(c) – Numerically simulated shape; initial state – black

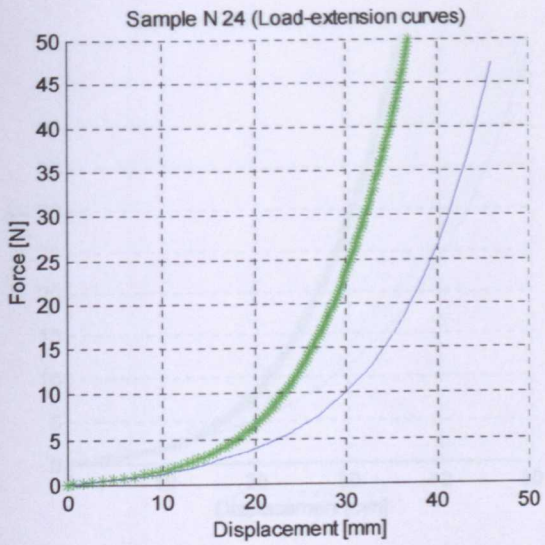

(a)

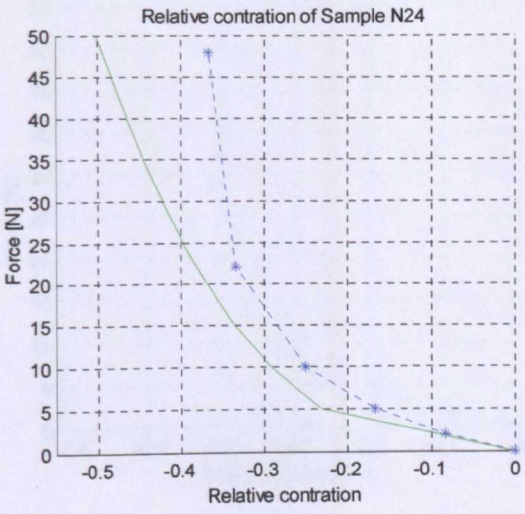

(b)

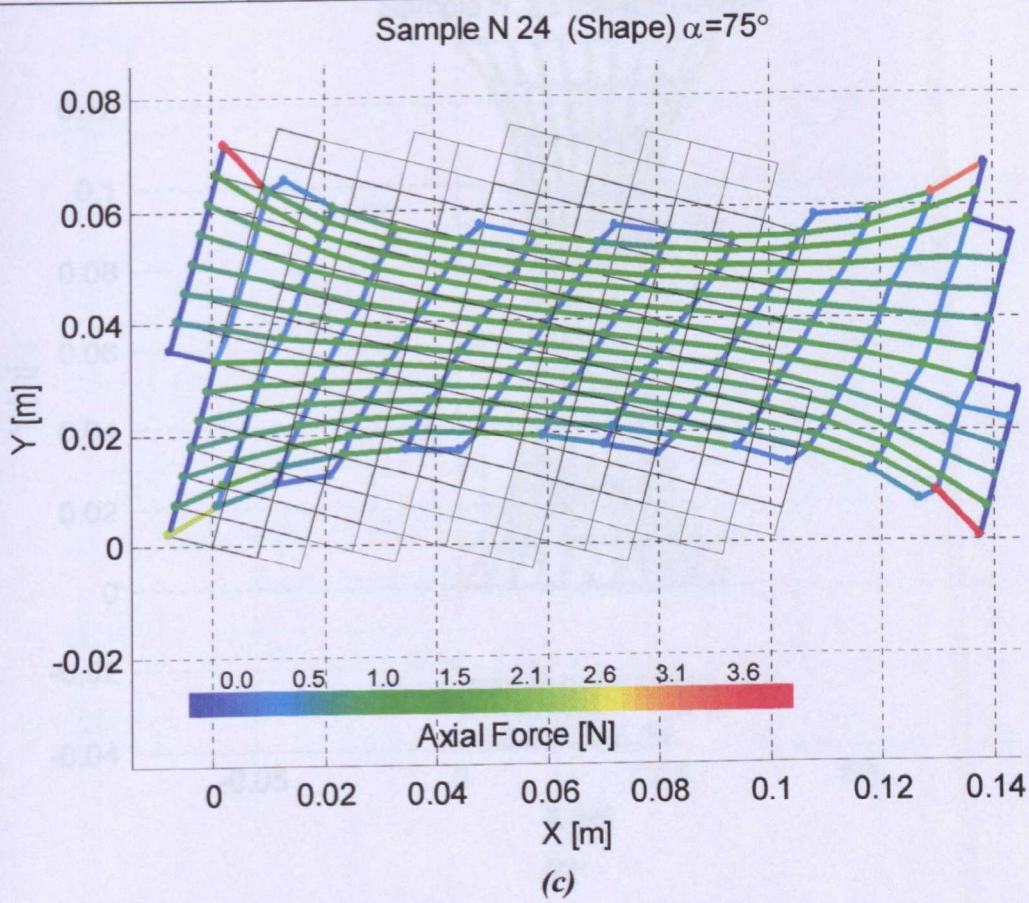

(c)

Figure A. 22(a, b, c). ***Sample number 24 (see Table 4.3).***

(a) – load extension curves; numerical model – green, experiment – blue ;
(b) – relative lateral contraction; numerical model – green, experiment – blue;
(c) – Numerically simulated shape; initial state – black

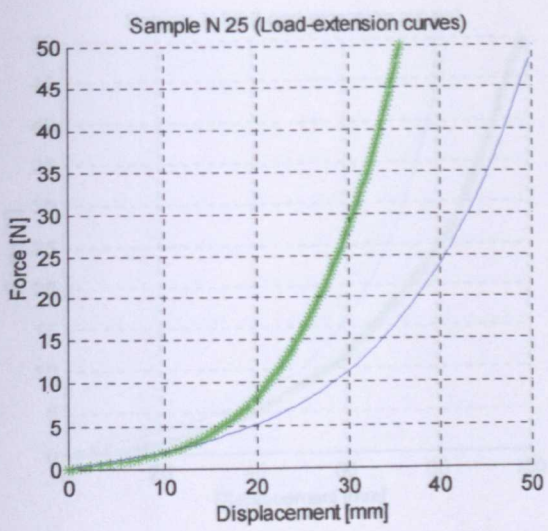

(a)

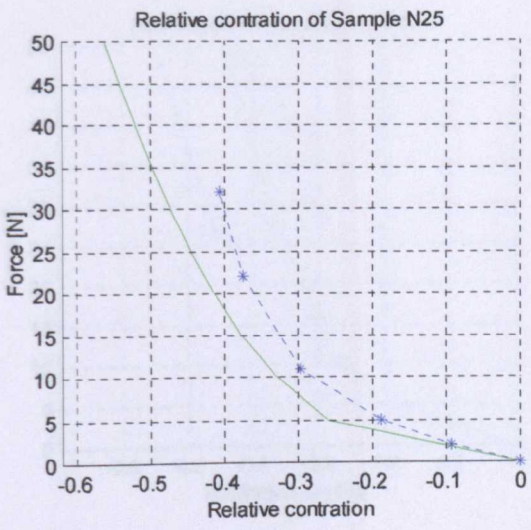

(b)

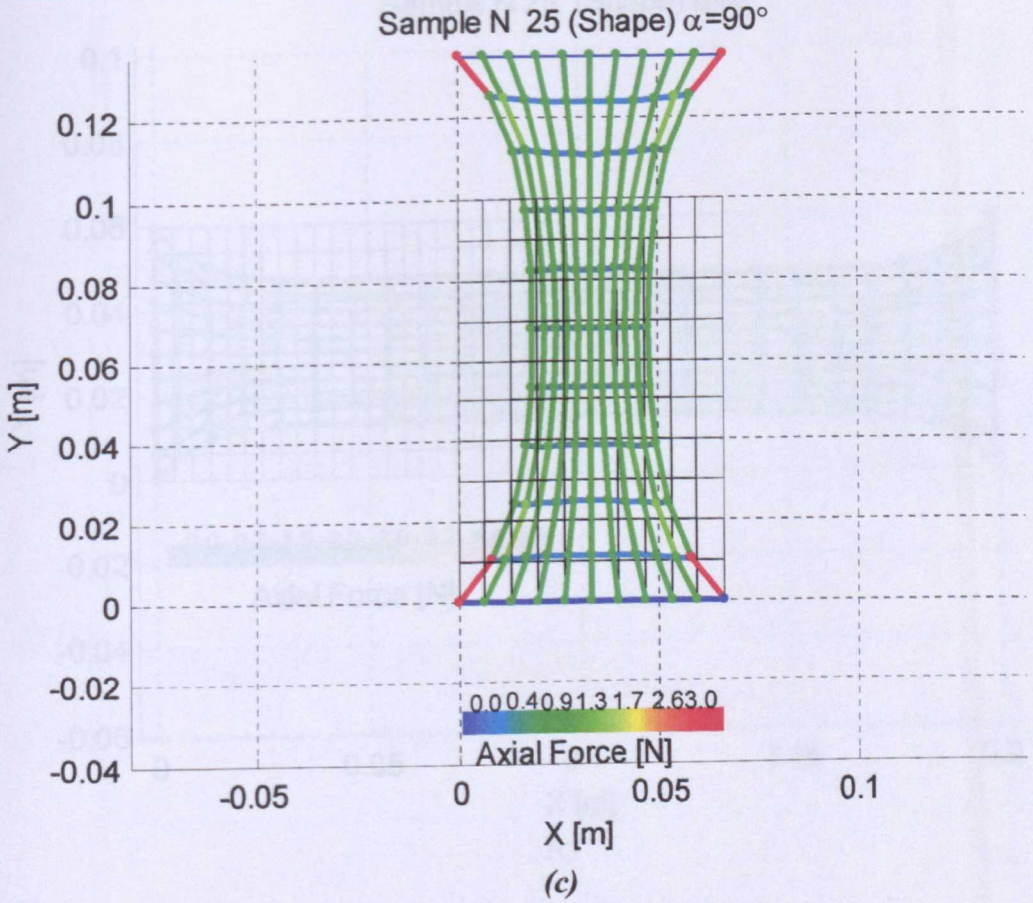

(c)

Figure A. 23(a, b, c). ***Sample number 25 (see Table 4.3).***

(a) – load extension curves; numerical model – green, experiment – blue ;
(b) – relative lateral contraction; numerical model – green, experiment – blue;
(c) – Numerically simulated shape; initial state – black

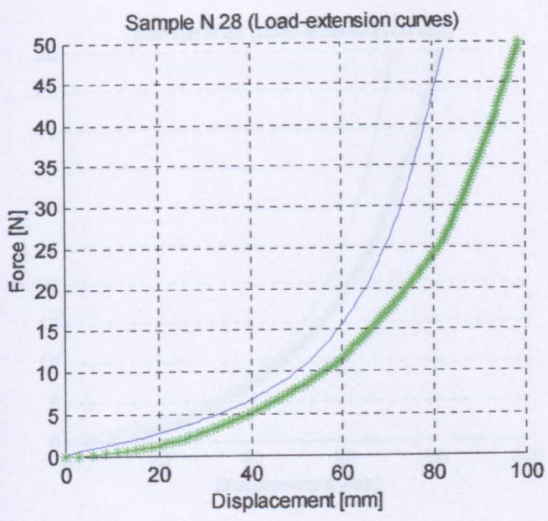

(a)

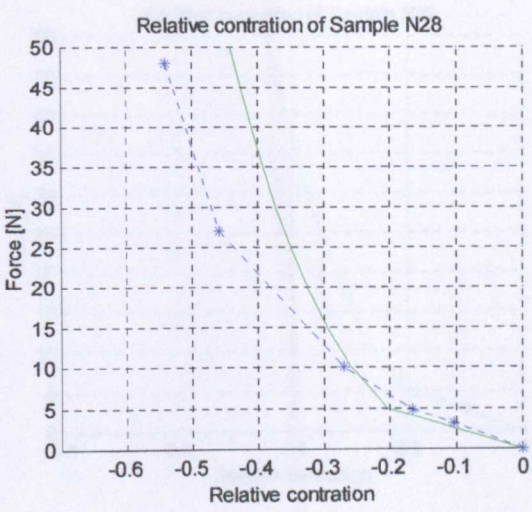

(b)

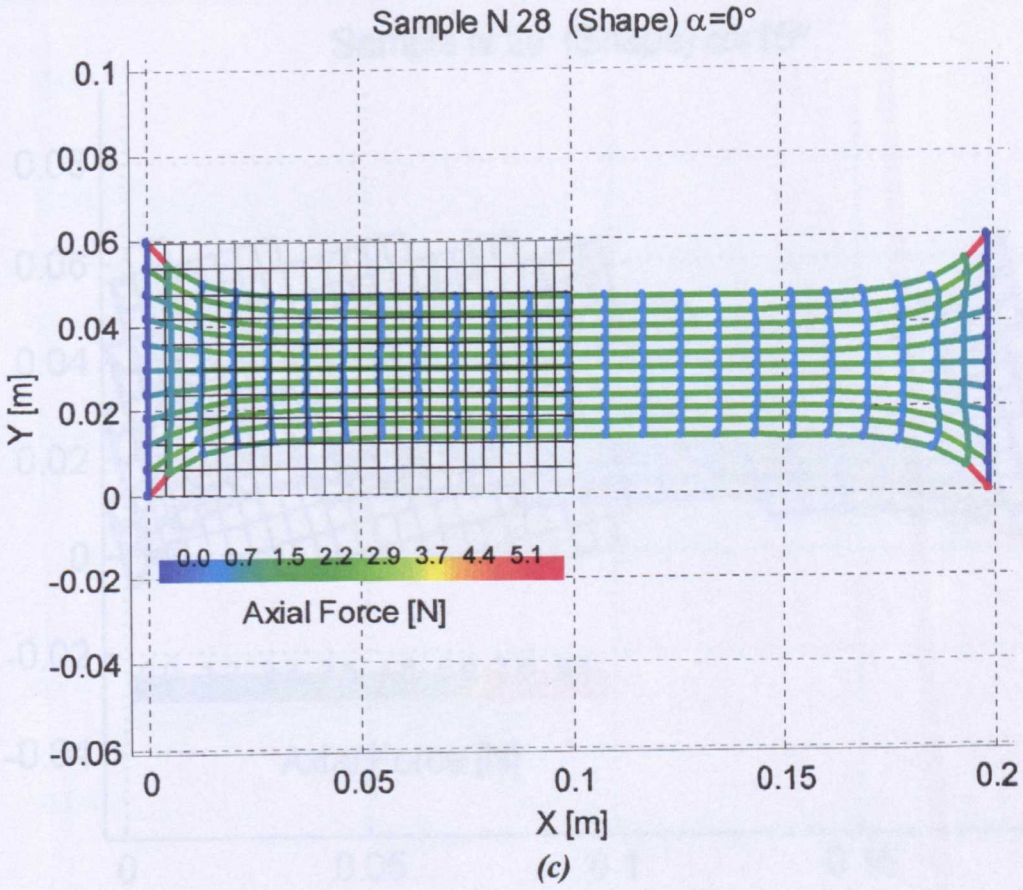

(c)

Figure A. 24(a, b, c). ***Sample number 28 (see Table 4.3).***

(a) – load extension curves; numerical model – green, experiment – blue ;
(b) – relative lateral contraction; numerical model – green, experiment – blue;
(c) – Numerically simulated shape; initial state – black

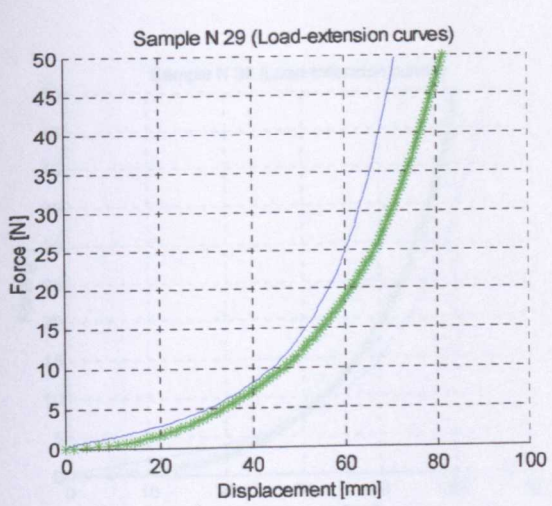

(a)

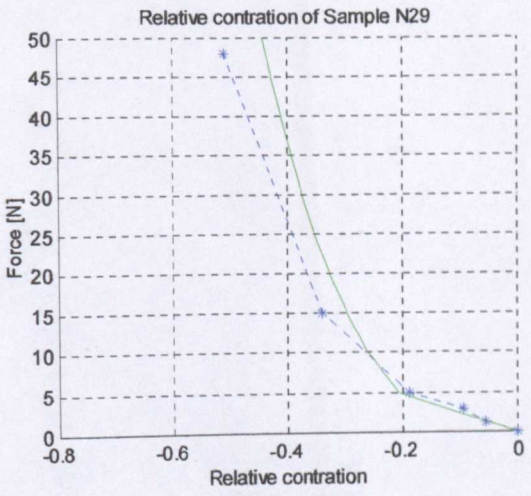

(b)

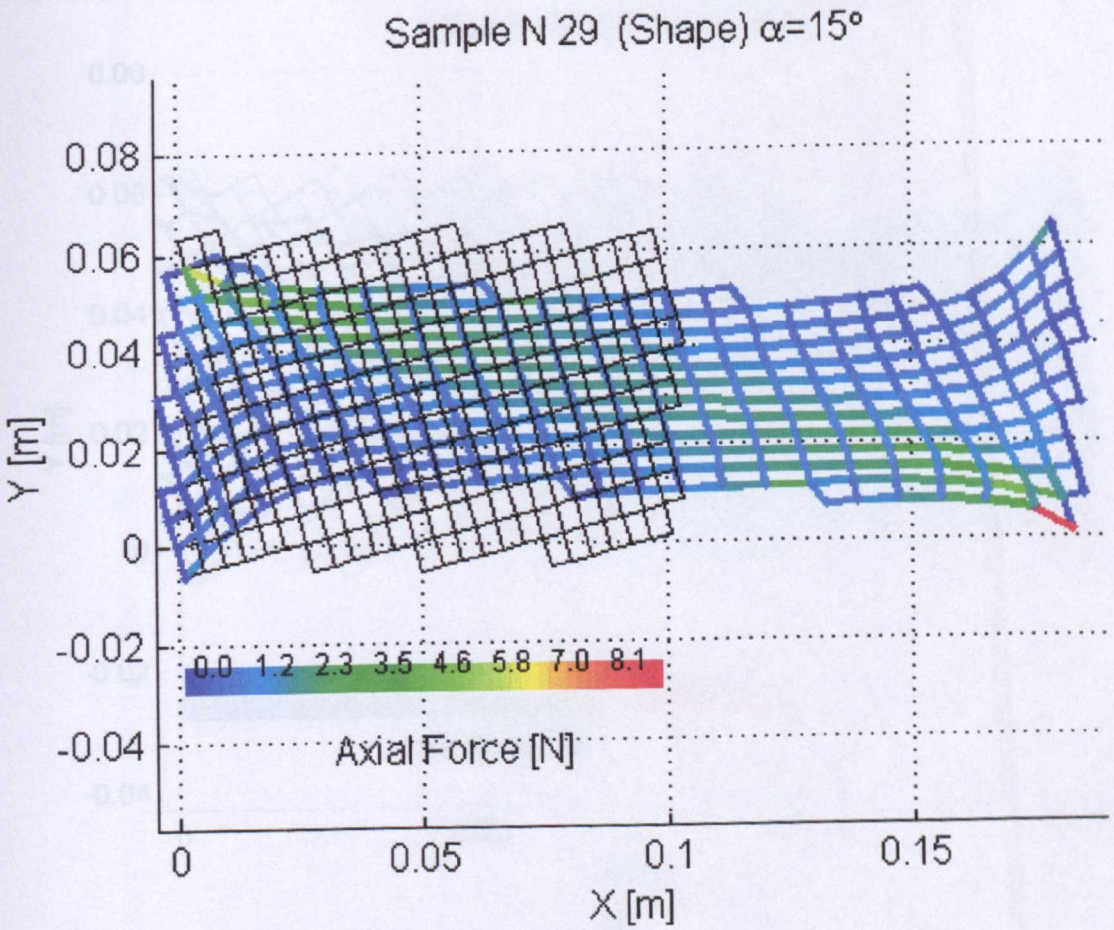

(c)

Figure A. 25(a, b, c). ***Sample number 29 (see Table 4.3).***

(a) – load extension curves; numerical model – green, experiment – blue ;
(b) – relative lateral contraction; numerical model – green, experiment – blue;
(c) – Numerically simulated shape; initial state – black

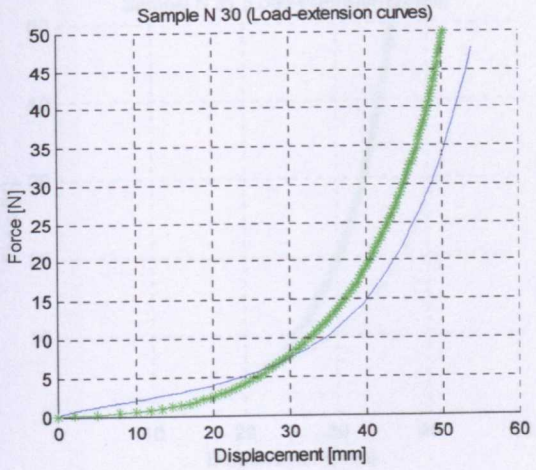

(a)

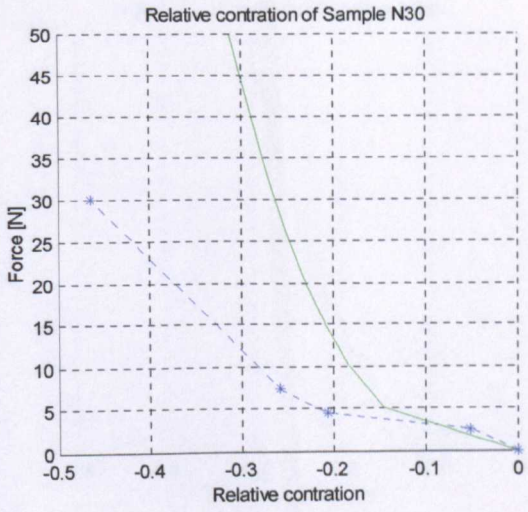

(b)

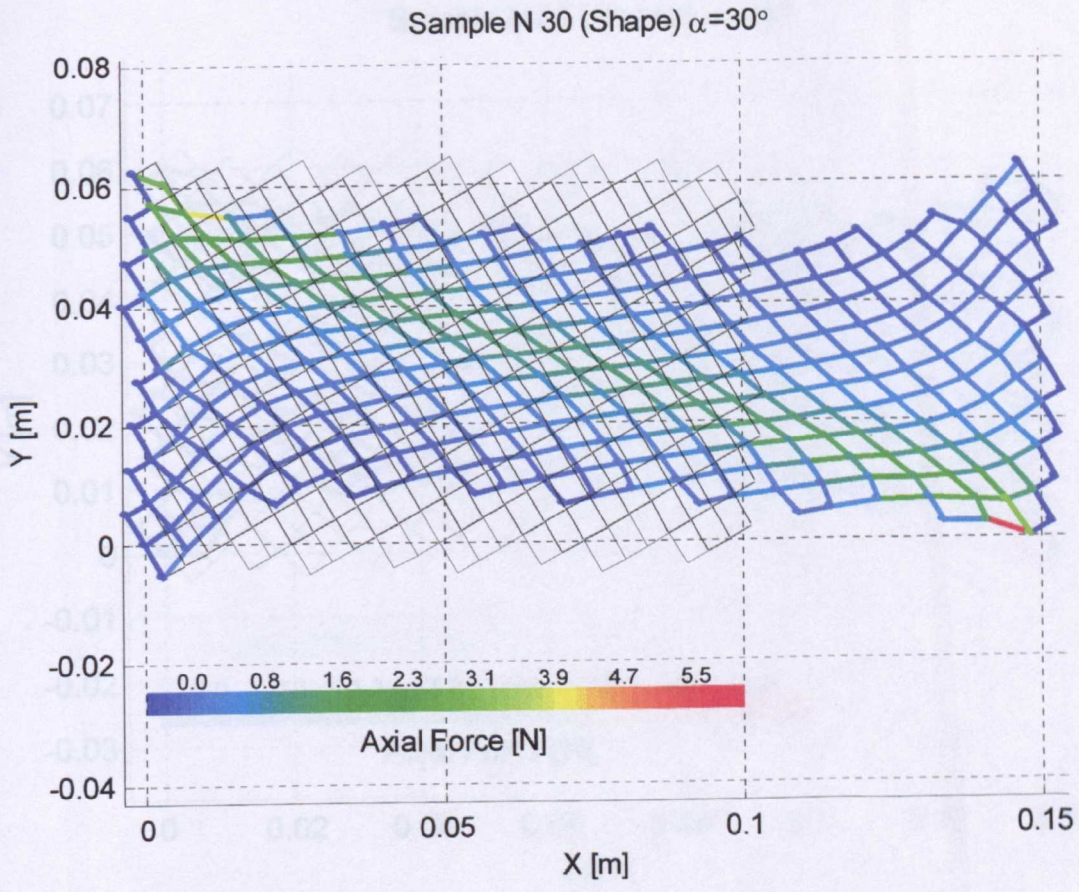

(c)

Figure A. 26(a, b, c). ***Sample number 30 (see Table 4.3).***

(a) – load extension curves; numerical model – green, experiment – blue ;
(b) – relative lateral contraction; numerical model – green, experiment – blue;
(c) – Numerically simulated shape; initial state – black

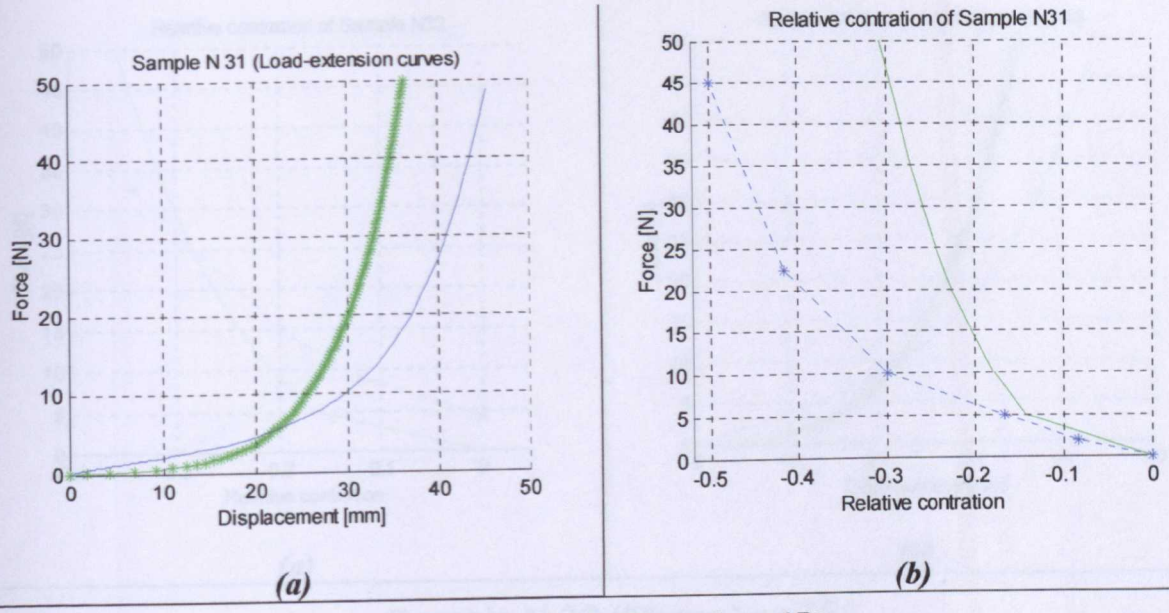

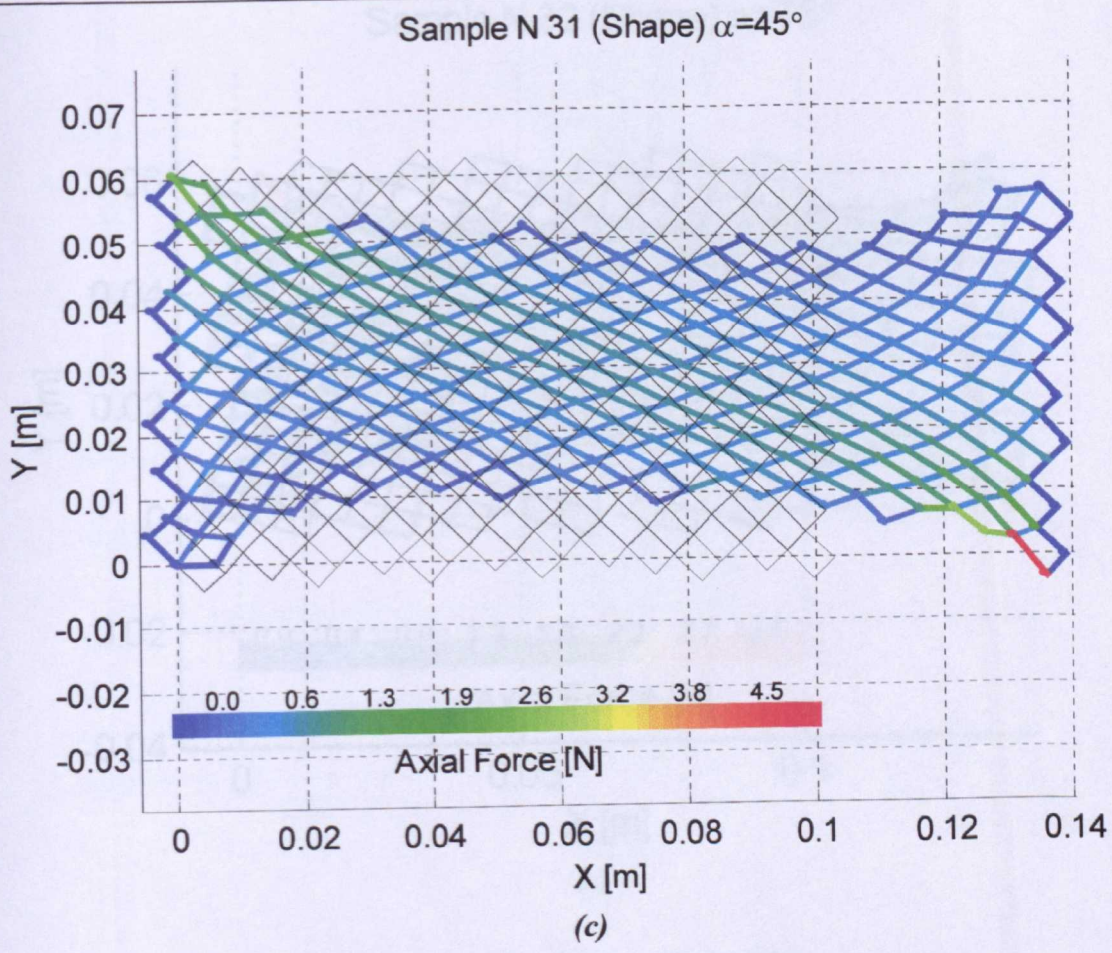

Figure A. 27(a, b, c). ***Sample number 31 (see Table 4.3).***

(a) – load extension curves; numerical model – green, experiment – blue ;
(b) – relative lateral contraction; numerical model – green, experiment – blue;
(c) – Numerically simulated shape; initial state – black

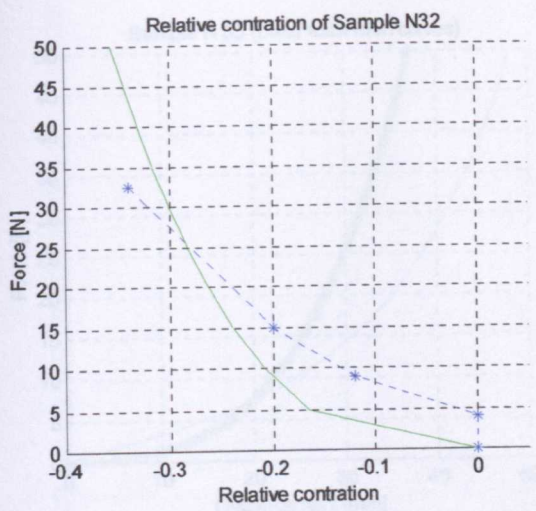

(a)

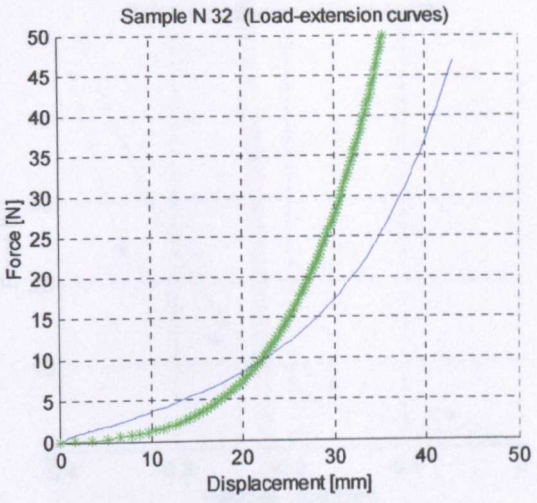

(b)

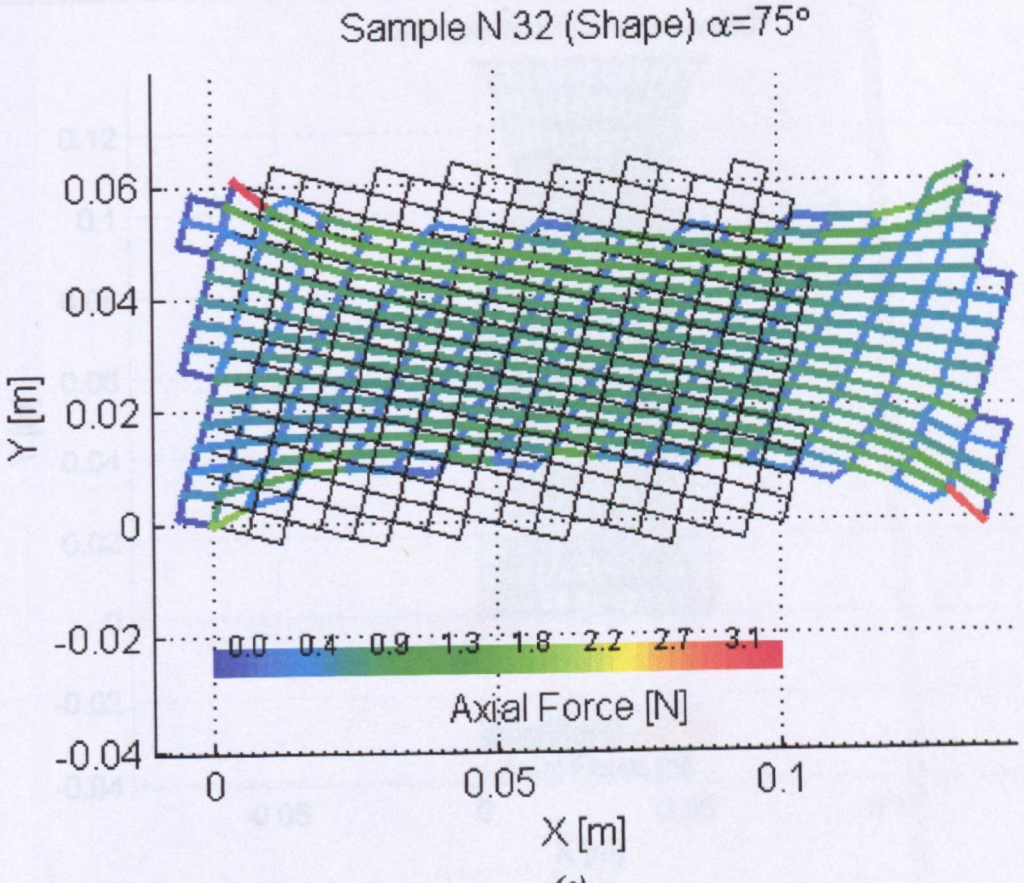

(c)

Figure A. 28(a, b, c). ***Sample number 32 (see Table 4.3).***

(a) – load extension curves; numerical model – green, experiment – blue ;
(b) – relative lateral contraction; numerical model – green, experiment – blue;
(c) – Numerically simulated shape; initial state – black

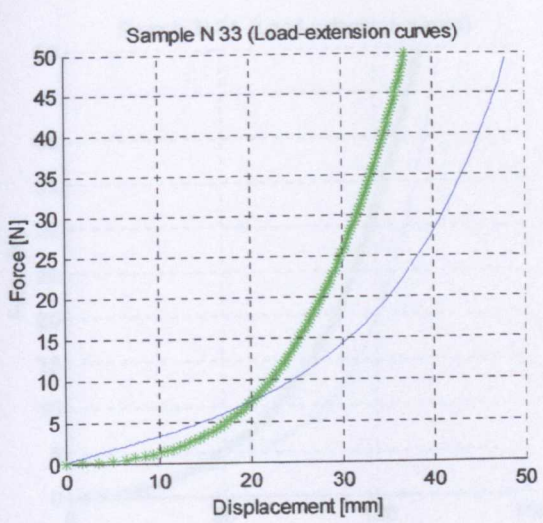

(a)

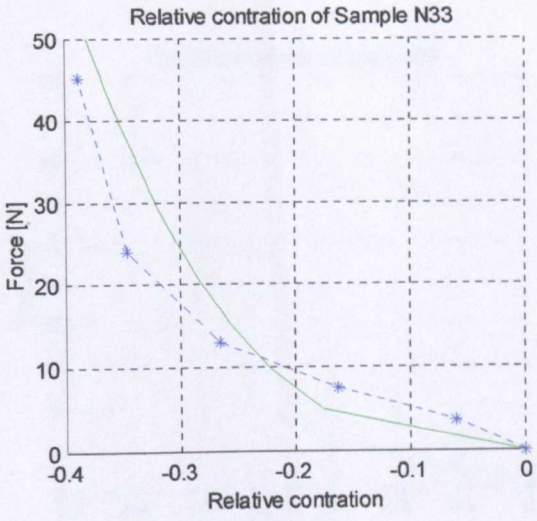

(b)

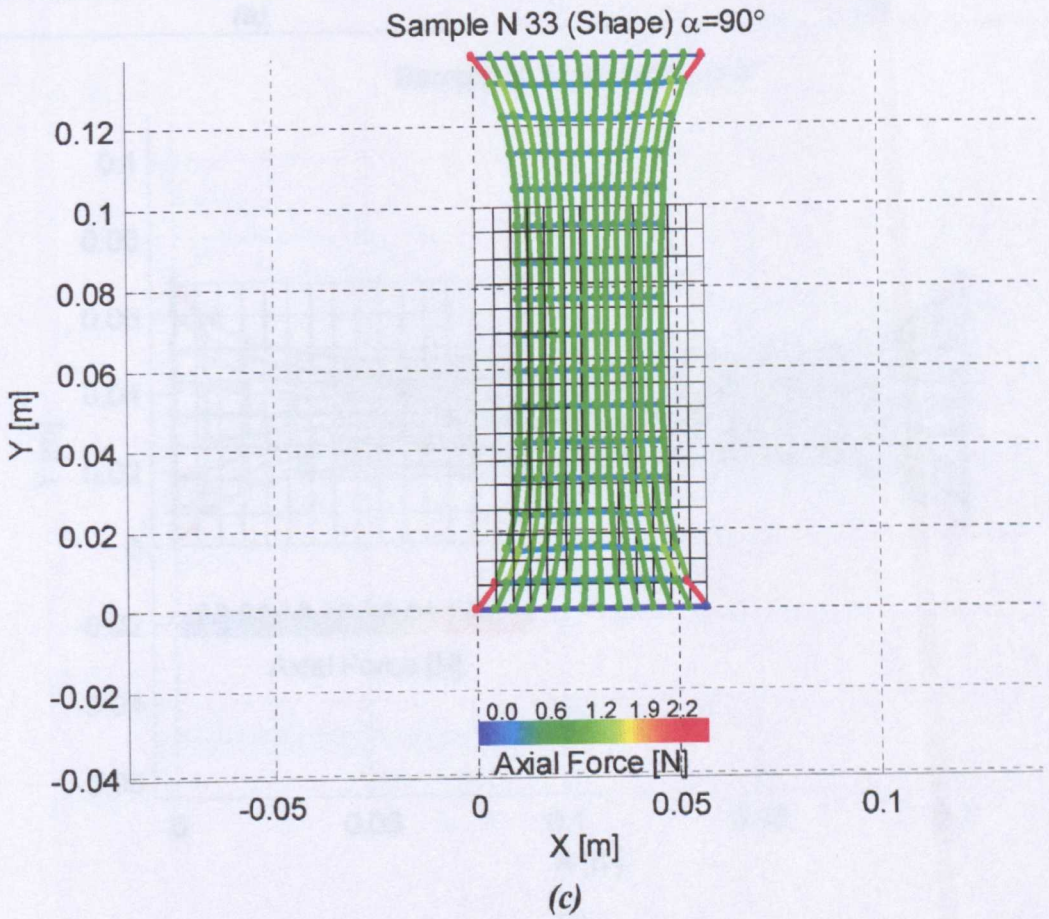

(c)

Figure A. 29(a, b, c). ***Sample number 33 (see Table 4.3).***

(a) – load extension curves; numerical model – green, experiment – blue ;
(b) – relative lateral contraction; numerical model – green, experiment – blue;
(c) – Numerically simulated shape; initial state – black

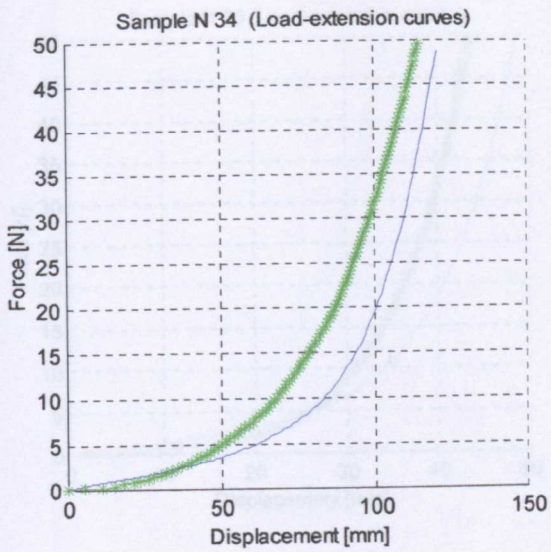

(a)

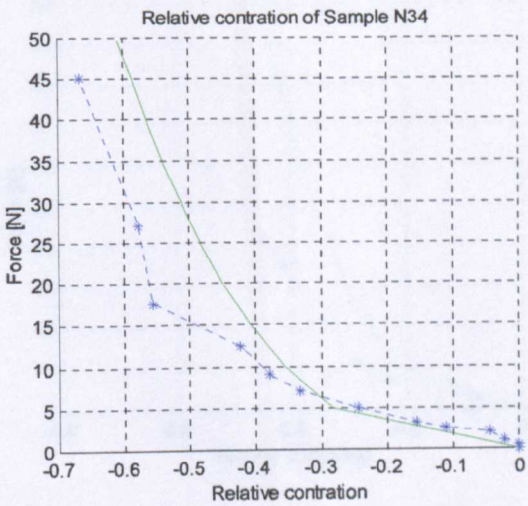

(b)

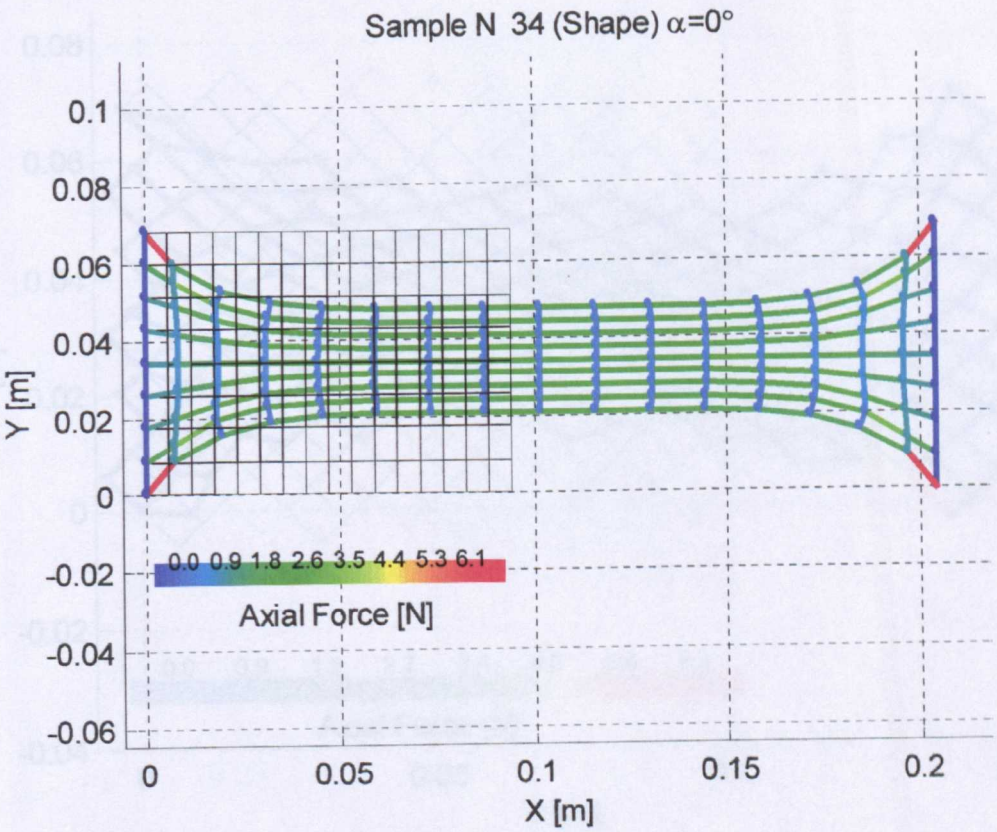

(c)

Figure A. 30(a, b, c). ***Sample number 34 (see Table 4.3).***

(a) – load extension curves; numerical model – green, experiment – blue ;
(b) – relative lateral contraction; numerical model – green, experiment – blue;
(c) – Numerically simulated shape; initial state – black

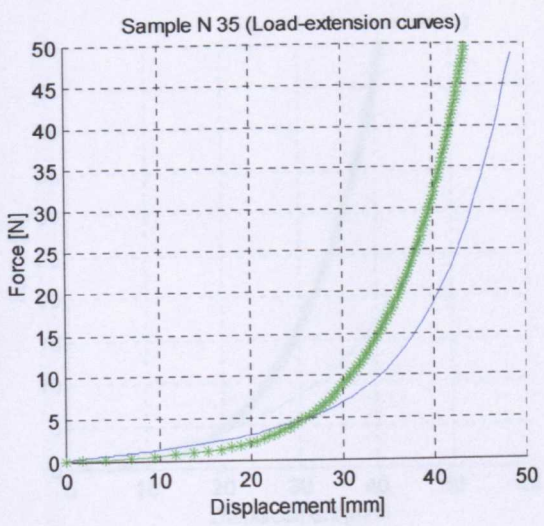

(a)

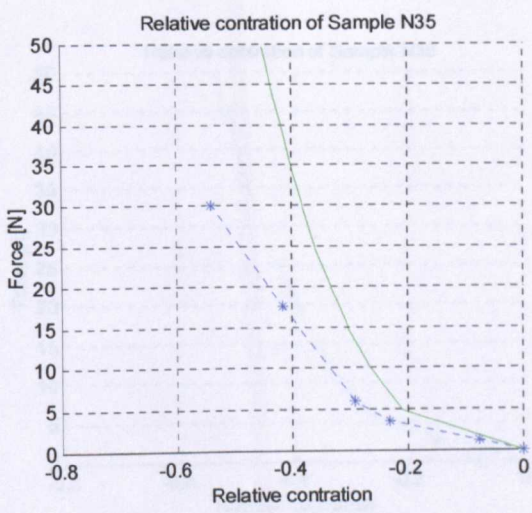

(b)

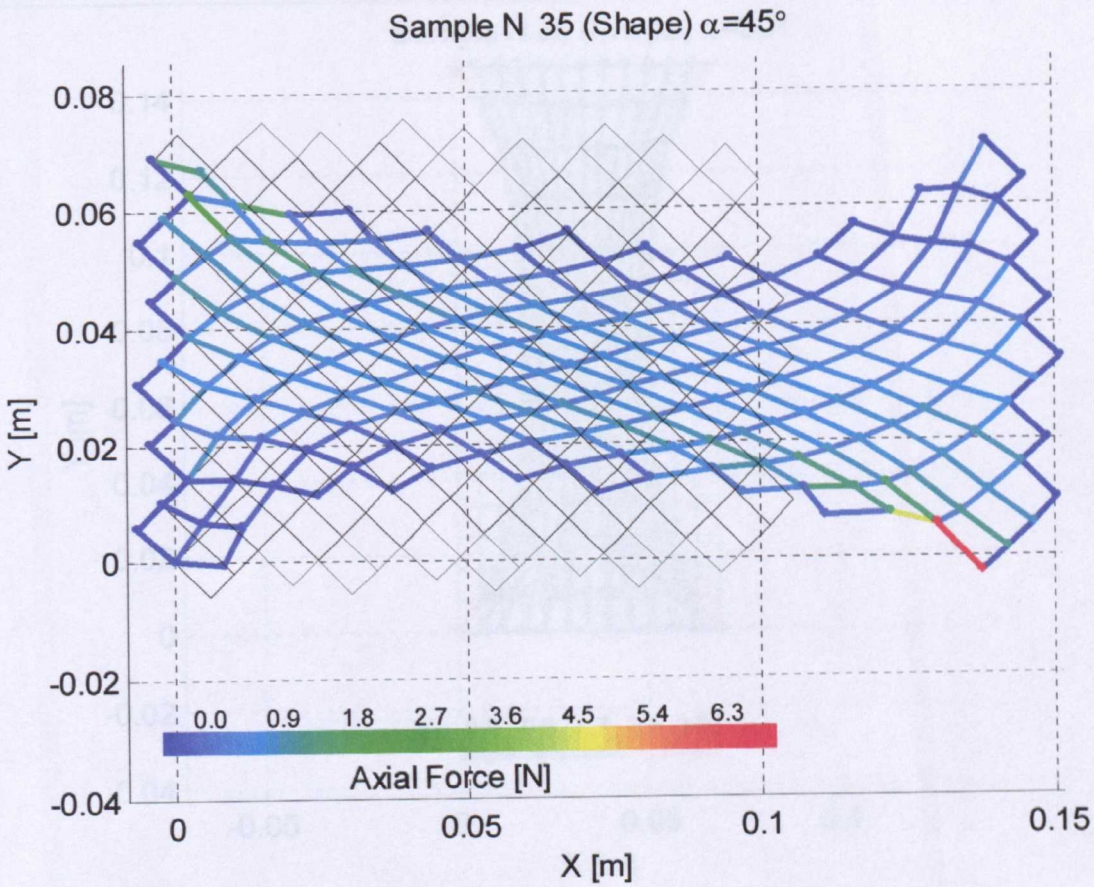

(c)

Figure A. 31(a, b, c). ***Sample number 35 (see Table 4.3).***

(a) – load extension curves; numerical model – green, experiment – blue ;
(b) – relative lateral contraction; numerical model – green, experiment – blue;
(c) – Numerically simulated shape; initial state – black

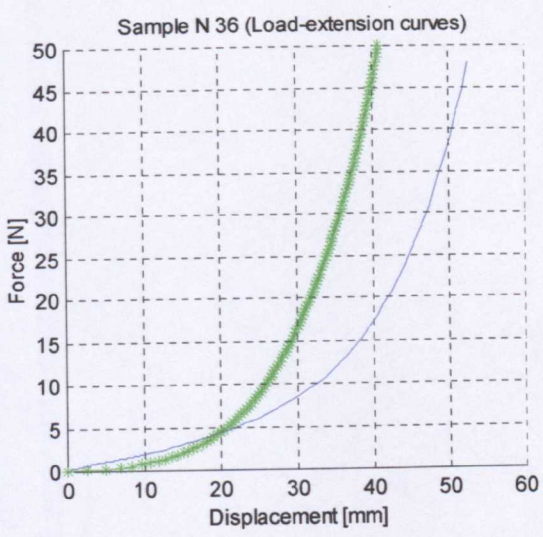

(a)

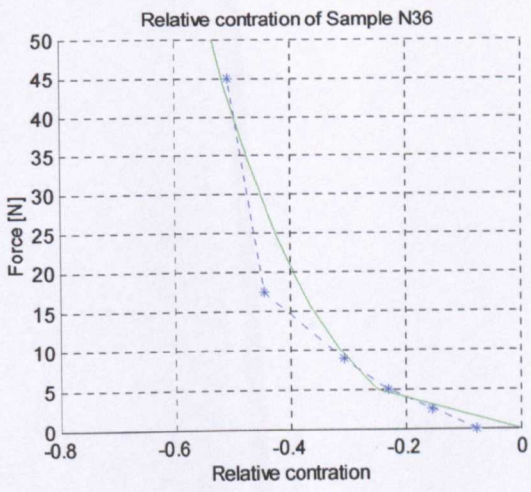

(b)

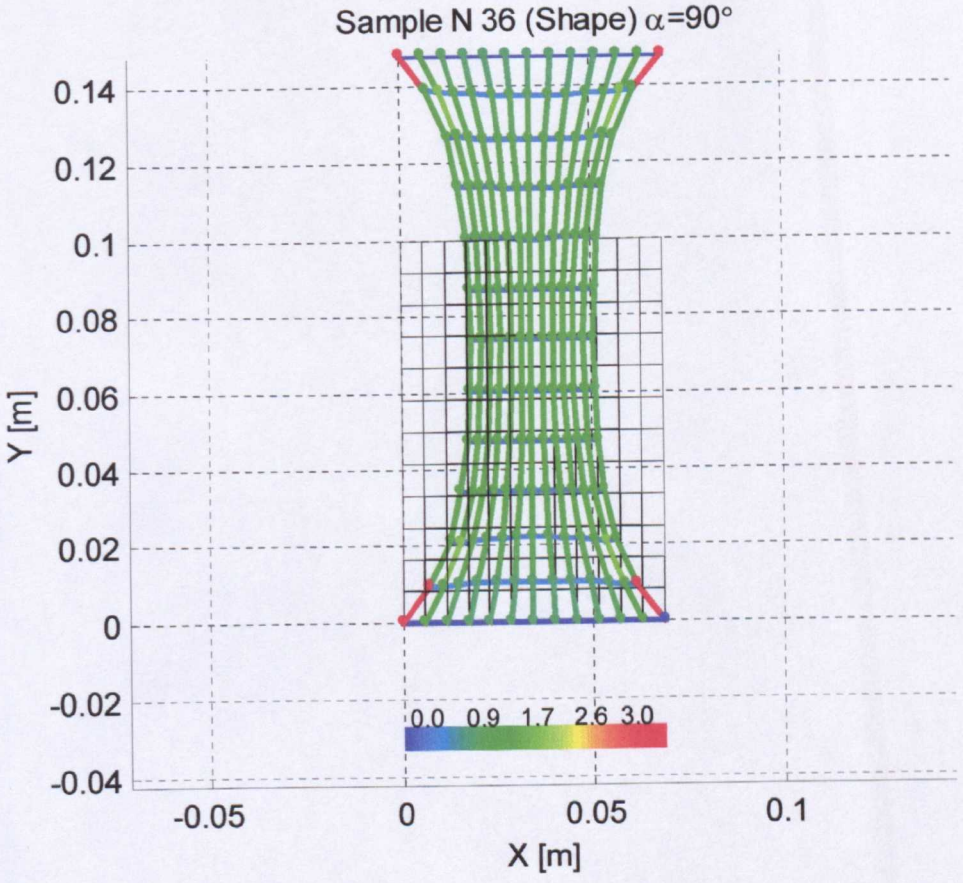

(c)

Figure A. 32(a, b, c). ***Sample number 36 (see Table 4.3).***

(a) – load extension curves; numerical model – green, experiment – blue ;
(b) – relative lateral contraction; numerical model – green, experiment – blue;
(c) – Numerically simulated shape; initial state – black